CHARACTERISATION AND MODELLING OF LOUDSPEAKER CONE RESONANCE

A thesis submitted

for the degree of

Doctor of Philosophy in Physics and Electronic Engineering

by

ANDREW JAMES TABERNER

The
University
of Waikato
*Te Whare Wānanga
o Waikato*

July 1998

ABSTRACT

Loudspeaker cone resonance ("cone break-up") is a fundamental cause of ripple in the electrical impedance and sound pressure responses of electrodynamic loudspeakers. In this thesis, the dependence of the characteristics of loudspeaker cone resonances on the material properties and thickness profile of the cone is extensively determined by creating 2D and 3D finite element models of a 6½-inch polypropylene-cone loudspeaker. Techniques for adjusting the resonant characteristics of loudspeaker cones by varying the material properties and thickness profile of the cone are explored and summarised.

The effect of cutting narrow slots through the surface of a loudspeaker cone is determined using 3D finite element modelling techniques, and cone slots are shown to have a large influence on the characteristics of the loudspeaker cone. A slotted loudspeaker cone with desirable impedance and sound pressure response characteristics is modelled and constructed. The measured response of the slotted loudspeaker is demonstrated to be a significant improvement over the characteristics of an unslotted loudspeaker.

ACKNOWLEDGMENTS

Firstly, my grateful thanks go to Garry Lambert, whose novel ideas provided the initial motivation for this thesis, and whose ongoing technical support was invaluable.

Special thanks are also due to Dale Carnegie for initially arranging this research project, and for providing ongoing supervision, encouragement, and support throughout its duration, and the writing of this thesis. Thanks also to Dr W.H. Round, Dr E.L. Bydder, and Dr P.T. Gaynor for their supervision and support.

Thanks also to the administrative and technical assistance of: Heidi Eschmann, Bruce Rhodes, Dave Bugden, Brian Peach and the other technical staff of the Department of Physics and Electronic Engineering.

Financial support was gratefully received from a University of Waikato Post-graduate Scholarship.

Finally, I would like to thank Louise for her unerring support and patience, and India for providing plenty of motivation.

CONTENTS

LIST OF FIGURES

LIST OF TABLES

CHAPTER 1

INTRODUCTION

The goal of the "ideal" loudspeaker is to accurately reproduce a sound pressure wave from an electrical signal, without adding to or detracting from the signal. Such a loudspeaker would create a pressure wave as a "point source", be uniformly responsive across the audible frequency spectrum, generate no extraneous frequency components, and be perfectly efficient at transforming applied electrical power into radiated sound power. In practice, the typical loudspeaker falls far short of these ideals.

During the last ninety or so years, loudspeaker system designers have employed a variety of methods to pursue these ideals and create the desired sound pressure wave. The very earliest designs [1] utilised an electrodynamic motor system to vibrate a paper cone. Later designs employed electrostatically and electrodynamically driven planar diaphragms, while exotic loudspeaker systems have utilised flame or ion transducers, and, more recently, intermodulated ultrasonic beams. Of all these designs, the electrodynamic loudspeaker has remained the most common, perhaps due to its relative simplicity, and ease of manufacture.

The electrodynamic loudspeaker[1] consists of a radiating surface, (often conical in shape), driven by an electrodynamic motor system. Even the earliest designers and manufacturers of electrodynamic loudspeakers recognised that the magnitude of the sound pressure wave produced by such a loudspeaker varies over its usable frequency range. This undesirable "ripple" in the sound pressure response is audible even to the untrained ear, and, along with other loudspeaker non-idealities, is often described by such terms as "colouration", or "distortion". Further, all electrodynamic loudspeakers produce unwanted harmonics to some extent, and fail to radiate equally in all directions.

---

[1] A detailed explanation of the theory and working principles of the electrodynamic loudspeaker is given in Chapter 2.

Ideally, the radiating surface of an electrodynamic loudspeaker would be perfectly rigid, so that at every driving frequency all parts of the surface move with the same phase and displacement. However, in reality, a loudspeaker's radiating surface is never completely rigid, but flexes with its own series of natural frequencies. Consequently, as the natural frequencies of a non-rigid radiating surface are excited, its motion is far from uniform. When the radiator is vibrated at a natural frequency, a standing wave is excited across the surface, causing adjacent areas to vibrate out of phase with each other. When this occurs, the loudspeaker's radiating surface is said to be undergoing "break-up".

Cone[2] break-up has long been understood as a major (although not exclusive) cause of non-uniformity in the sound pressure frequency response of the electrodynamic loudspeaker [2]. Furthermore, cone break-up can also be a cause of harmonic distortion, as the loudspeaker cone flexes in a non-linear manner.

Consequently, there has always been ample motivation for researchers and designers to develop mathematical models of electrodynamic loudspeakers in order to calculate their surface displacement response and subsequent sound pressure response. Such models are also extremely useful for describing the behaviour of electrodynamic loudspeakers, and exploring the effects of design changes on their characteristics.

1.1 MODELLING LOUDSPEAKER RESONANCE

Models of electrodynamic loudspeakers have usually concentrated on one of two main areas. Firstly, the resonances of the loudspeaker cone itself have been the subject of research for many years, as detailed below. Secondly, other published research has concentrated more on the physical behaviour of the loudspeaker's motor system [33, 34, 43]. Both of these constituent components have a demonstrable effect on the sound radiation of the loudspeaker cone, and both can be the cause of sound pressure "distortion" and "colouration." However, this thesis is essentially concerned with aspects of the resonances of the cone itself, and their effect on the developed sound field of the loudspeaker.

The earliest attempts at modelling loudspeaker sound radiation assumed that the cone vibrated as a rigid body [3, p184]. This idealisation allowed an estimate of the loudspeaker's sound pressure response to be calculated using relatively simple techniques first developed by Lord Rayleigh. Although these techniques accurately predict the sound pressure response of an ideal rigid loudspeaker, they are inadequate for determining the response of realistic loudspeakers. A more accurate calculation of the developed sound pressure response requires the loudspeaker cone's non-uniform surface velocity to be exactly calculated across its usable frequency range.

Calculation of the sound pressure response of a non-uniformly vibrating loudspeaker is typically performed in two steps. Firstly, the velocity distribution across the non-

---

[2] It is usual for the radiating surface to be conical in shape.

uniformly vibrating radiating surface is ascertained. Secondly, the surface velocity distribution is subsequently used to calculate the sound pressure response at points in space around the loudspeaker.

The earliest type of electrodynamic loudspeaker radiating surface consisted of a truncated straight-sided cone driven from its apex. Among the first to attempt to find a numerical solution for such a cone's non-rigid vibration were Goldberg and Bogdannoff [4], who applied the classical theory of thin shells to several straight-sided cones. Goldberg's method involved dividing the cone into a series of adjoining concentric shells, and, using a lumped-parameter technique, numerically solving the differential equations for each shell. By this means, the mode shapes and natural frequencies of straight-sided cones were calculated on a computer, with good accuracy.

Kalnins [5] later expanded on the work of Goldberg to allow the modes and frequencies of rotationally symmetric shells of arbitrary shape to be solved. The computer program written by Kalnins allowed the natural frequencies and mode shapes of concave and convex cones to be determined.

Frankfort's excellent and comprehensive treatise on the vibration and sound radiation of straight-sided loudspeaker diaphragms [6,7] was the first major attempt at determining both the vibration and sound radiation of loudspeaker cones. Like Goldberg, Frankfort also utilised a technique of dividing the loudspeaker cone into a series of abutting annuli, and applied two different shell theories to find the vibration patterns of axisymmetric straight sided cones. The displacement across the surface of the loudspeaker cone was found for a number of different frequencies, and the sound pressure and power responses calculated using a source superposition technique.

Frankfort was able to utilise this technique to determine the frequencies of the natural modes of a straight-sided cone, and their dependence on cone material properties and geometry. The shapes of the natural modes of the cone were compared with measured mode shapes obtained using a holographic interferometry technique.

Bruneau [8] used a similar holographic interferometry method to measure the mode shapes of a loudspeaker. Later, Bruneau and Bruneau [9] combined a shell model with holographic and electrical measurements of a loudspeaker cone to create a more complete and complex mathematical model of loudspeaker vibration and sound radiation. Their model allowed the calculation of the sound pressure response of two straight-sided loudspeakers of different dimensions to upper limits of approximately 900Hz and 3kHz.

Since the early 1980's other authors [10, 11, 12, 13] have utilised a similar, but more generalised discretisation technique to obtain the loudspeaker's cone surface displacement solution. This method became known as the Finite Element Method (FEM), and was first applied to loudspeaker cones by Suzuki and Nomoto [11] in the late 1970's. Suzuki and Nomoto calculated the mode shapes and surface displacement of a concave loudspeaker cone, and using a source superposition method, solved for the

resulting sound radiation.

Concurrently, Kagawa *et al.* [12] used the finite element technique to find the structural vibration of a loudspeaker cone, and coupled these results to an acoustic finite element model of a loudspeaker cabinet. Previously published research had ignored the effect of the mechanical impedance of the air on the resonant behaviour of the loudspeaker; a fully coupled analysis accounts for the air load experienced by the radiating surfaces of the loudspeaker. This approach enabled the authors to determine the sound pressure distribution inside and outside the cabinet, while also calculating the effect of the acoustic field air loading on the frequency and shape of natural modes of the loudspeaker cone.

Kaizer and Leeuwestein [13] also used the finite element method to create a model of a loudspeaker cone and the loudspeaker's radiated acoustic sound field. This allowed the sound pressure field at any point in space to be determined, but first required a "calculation sphere" (over which correct boundary conditions are applied) to be meshed with finite elements. The sound pressure at any point outside the calculation sphere was calculated using the sphere's surface velocity potentials. Thus, the FE method is not ideally suited to modelling free-field loudspeaker sound radiation, as at least part of the sound field must be divided into finite elements. Typically, this requires the use of a large number of finite elements and is computationally expensive.

A more useful technique is the boundary element method (BEM), which allows the pressure at points in a sound field to be calculated by modelling only the field's boundary, including the vibrating surface. This greatly reduces the computational complexity of modelling sound pressure radiation. The BEM was applied to general sound radiation problems in the late 1970's and early 1980's (refer to Kirkup and Jones [14] for a large list of references), and subsequently applied to loudspeaker cone radiation.

During the last 15 years, the BEM has become the favoured technique for modelling loudspeaker sound radiation, when coupled to a finite element model of the loudspeaker cone itself [14, 23, 30]. Commercial FE and BE software packages have become readily available, allowing the loudspeaker designer to create and solve realistic models of loudspeaker cones on a desktop computer, without the need for extensive computer programming.

1.2 REDUCING CONE BREAK-UP

The development of the modelling techniques discussed in Section 1.1 has allowed researchers to explore some of the attributes and characteristics of electrodynamic loudspeakers. These mathematical tools and models allow the researcher to predict the effect of changes in cone design on the behaviour of the loudspeaker, without the expensive inconvenience of constructing the loudspeaker.

As loudspeaker cone break-up is a major source of sound pressure response ripple, some studies have examined techniques for minimising the effects of cone break-up on the sound pressure response. Usually, techniques for minimising the effect of cone break-up fall into one of two categories:

- Maximising the stiffness and/or minimising the mass of the radiating surface.
- Removing the energy of any travelling waves in the cone through cone material damping, or the use of a well-matched surround.

The rationale for increasing the cone stiffness is typically as follows: Since standing waves on the loudspeaker cone are essentially a consequence of cone flexure, by increasing the stiffness of the cone, standing wave formation will be precluded. The justification for decreasing the cone mass is that doing so reduces the inertia of the outer area of the cone, thereby increasing the ability of the cone to maintain rigid-body vibration.

Some published research has focussed on developing new cone materials or geometries that have an inherently greater stiffness, and therefore an increased resistance to cone flexure. Aluminium, Kevlar, and titanium [15], amongst other materials, have found favour with some designers due to their high stiffness:mass ratio. More exotic materials that have been developed for use in loudspeakers include polymer-graphite [16], olefin polymer [17], and glass fibre [18]. Others have used honeycomb [19], laminated [20] and "sandwich" [21,22] structures in order to improve the stiffness of the loudspeaker cone[3]. Some of these authors used numerical modelling techniques to optimise their cone materials and geometries.

Frankfort [6] used his loudspeaker model to determine the effect of cone material properties, thickness, apex angle, and inner and outer radii on the frequencies of the natural modes of straight sided cones. While Frankfort's work was restricted to straight-sided cones, his results identified some broad trends in the dependence of natural modes on material properties and cone geometry.

Geaves [23] used a combined FE/BE model to explore the effect of the properties of the cone and surround material on the cone's sound pressure response. He concluded that

---

[3] Some of these materials also possess a high internal loss factor, which also helps minimise the amplitude of cone standing waves, as discussed later.

the Young's modulus of the surround has the greatest effect on the magnitude of features in the sound pressure response, while the Young's modulus of the cone affects their frequency.

While increasing the stiffness and decreasing the mass of the cone material certainly delays the onset of cone break-up, as all natural resonances are moved to higher frequencies, it does not remove it entirely. Moreover, stiff, light diaphragms often possess a lower internal damping ratio, thus allowing any excited natural modes to ring more freely. Furthermore, perfectly rigid cone motion is not necessarily a desirable outcome, as discussed in Chapter 2.

A second method for minimising cone breakup is to remove standing wave energy from the loudspeaker, and thus minimise the amplitude of cone standing waves. This can be achieved by increasing the mechanical loss factor of the cone material, usually by adding doping agents to the cone material, or coating the cone surface with an absorptive substance. This is the approach adopted by Murata *et al.* [24] in their patent for a pulp paper cone doped with Chitin. Similarly, the loudspeakers used in this thesis are manufactured from mineral-doped polypropylene, which combines a moderate degree of stiffness with a high internal loss factor.

Wave energy can also be removed from the loudspeaker cone by using a well-matched surround. If the mechanical impedance of the surround is a good match with that of the cone, travelling waves reaching the outer edge of the cone will be mostly transmitted into the surround, rather than reflected back down the cone. The importance of a well-matched surround is widely recognised ([25] p44, [26] p29) but there is little published research on the subject.

The loudspeaker design invented by Schreiher [27] combines an innovative surround with a highly damped cone. Cone damping is achieved by extending a rubber damping material down the front surface of the cone in a leaf pattern.

Shindo *et al.* [28] used a finite element model to calculate the effect of the voice coil and surround on straight-sided, convex, and concave loudspeaker cones. Their results indicated that the surround could affect the shapes and frequencies of the natural modes of cones. However, their analysis was limited to paper cones using a felt surround, and conclusions cannot be drawn from their work for cones and surrounds of other materials and geometries.

Heed [29] used a FE model to research the factors that affected the amplitude of standing waves in loudspeakers, and concluded that the cone and surround material damping ratios had the most significant influence. Heed performed an ANOVA analysis, using the elastic modulus and damping ratios of cone and surround, and the cone density, as independent variables. Heed also concluded that a stiff cone with soft surround performs better than a soft cone with stiff surround. However, his results give no insight into the individual contribution that each of these variables makes to the frequency and amplitude of cone standing waves.

In a different approach to smoothing the sound pressure response, Geaves [30] uses a feedback process to optimise the shape and thickness of a loudspeaker cone to a pre-specified "mechanically filtered" sound pressure response criterion. An iterative technique was used to make incremental adjustments to a set of design variables defining the cone shape and thickness, resulting in a modelled loudspeaker design with a sound pressure response that decreased linearly at high frequency.

All of the preceding articles assume that the loudspeaker is symmetric about its driving axis. Thus, the modelling techniques employed are restricted to two-dimensional rather than three-dimensional models. Consequently, there is almost no published research examining the resonant behaviour of non-axisymmetric loudspeakers. An exception is Struck [31], who used a laser velocity transducer to measure the resonant modes of a loudspeaker. Struck briefly considers the effect of adding a mass to a point on the loudspeaker cone, and measures the resulting non-axisymmetric mode shape.

The lack of published research in this area is partly due to the fact that significantly non-axisymmetric loudspeakers are rarely used in expensive loudspeaker systems where sound quality is a major design criteria. Accordingly, published FE analyses all seem to assume axial symmetry, which greatly reduces the size of the FE model. Furthermore, it is only recently that desktop computer power has developed to the extent that 3D FE modelling of non-axisymmetric loudspeakers has become feasible.

In summary, there are many published articles addressing aspects of modelling loudspeaker cone vibration and sound radiation. The majority of these articles examine methods for minimising the effects of cone break-up by increasing cone stiffness and damping, and reducing cone mass.

Although results of FE analyses on loudspeakers are often published, many references to the dependence of break-up resonances on cone material properties and geometry are incidental, rather than specific and explicit. There is little published, comprehensive research into the dependence of standing wave frequency, shape, and amplitude on cone material properties and thickness parameters.

Previous published numerical analyses of loudspeaker cone resonance use two-dimensional modelling techniques, and are thus restricted to the consideration of axially symmetric loudspeakers.

1.3 AIM OF THESIS

The object of this thesis is to contribute to the current understanding of the nature of loudspeaker cone break-up, and explore some specific means of controlling and minimising its adverse effect on a loudspeaker's sound pressure response. The mathematical models developed and employed throughout this thesis are not intended to completely model all aspects of the behaviour of an electrodynamic driver. Rather, the mathematical models are limited to a consideration of the behaviour of the loudspeaker cone itself, and are used as tools for exploring the dependence of cone break-up on aspects of the cone's design.

In particular, the aims of this thesis are as follows:

1. To extensively examine and summarise the resonant behaviour of a mineral-doped polypropylene loudspeaker by using 2D and 3D FE models of the cone and surround.
2. To use 2D FE models to explore the dependence of the frequency and magnitude of natural cone resonant modes on the cone's material properties and thickness parameters.
3. To employ 3D FE models to examine the resonant behaviour of a 6½-inch polypropylene loudspeaker cone with narrow slots cut through its surface.

In the pursuit of all three objectives, the loudspeaker's behaviour is extensively quantified and summarised by the use of FEM and BEM results, expressed in terms of mode shapes, cone displacement patterns, mechanical admittance, and sound pressure response. Extensive use is made of three-dimensional plots, allowing trends in amplitude and frequency to be readily identified.

The first objective is achieved using the novel combination of calibrated two- and three-dimensional FE models. Using these models, the standing wave types excited in a loudspeaker cone are classified and their shapes extracted. The effect of the loudspeaker's surround on the mode shapes and frequencies is systematically identified and summarised. Only the surround used with the polypropylene loudspeakers in question is modelled; no attempt is made to comprehensively explore the attributes and effects of surrounds of different geometries and materials.

By varying the material properties in the 2D FE model one-by-one, the dependence of the frequency, amplitude and shape of the resonant modes of the cone is determined. Furthermore, the effect of changes in material properties on the magnitude and frequency of sound pressure response ripple is calculated, both on and off the loudspeaker's driving axis. The effect of cone thickness and thickness profile on cone resonance is explored and summarised.

The third objective is pursued using a full three-dimensional model of a polypropylene loudspeaker cone. This is a novel approach, and allows the resonant behaviour of non-

axisymmetric cone designs to be modelled. The non-axisymmetric designs of particular interest are those where slots are cut into the cone in various configurations.

As cone break-up is well known to be due to cone standing waves, some loudspeaker designers and manufacturers have intuitively suggested that cutting slots in the cone would preclude the formation of standing waves. As there appears to be no existing published research relating to this type of approach to controlling cone resonance, this thesis examines different slot configurations and determines how cone slots affect the resonance of the loudspeaker. Modelled results are generated and compared to measured results for a real "slotted" loudspeaker cone.

1.4 SYNOPSIS

The thesis is presented as follows:

Firstly, the theory of operation of an electrodynamic loudspeaker is introduced in Chapter 2 with particular reference to a 6½-inch polypropylene loudspeaker. An electromechanical model of the loudspeaker is developed, and an outline of cone vibration and sound radiation is given. This chapter also considers the contributing factors that determine the sound field produced by the loudspeaker, and shows that cone break-up is a significant cause of fluctuations in sound pressure response.

Chapter 3 gives a general overview of the techniques used to model and measure the response of the loudspeakers. An overview of the finite element and boundary element methods is given, and measurement and experimental techniques are summarised.

In Chapter 4, two- and three-dimensional FE models of the loudspeaker cone are developed and calibrated against measured results for two experimental loudspeakers. These models are subsequently used to determine the natural resonances of the loudspeaker, and their effect on the loudspeaker's characteristics. In particular, the loudspeaker's mode shapes, mechanical admittance, and sound pressure response field are calculated.

Chapter 5 uses the calibrated 2D FE model to explore the effect of cone material parameters and cone thickness on the frequency, shape, and magnitude of cone standing waves. Their effect on the developed sound pressure field is also considered and summarised.

In Chapter 6, the calibrated 3D FE model is used to explore the effects of cone slots on the mode shapes and admittance characteristic of the loudspeaker cone. A slotted loudspeaker cone is constructed, and its measured characteristics shown to compare favourably with those predicted by the FE model.

In Chapter 7, the results of the research presented in the previous chapters are outlined and summarised. Limitations of the results are discussed, and recommendations for implementation and further research given.

CHAPTER 2

ELECTRODYNAMIC LOUDSPEAKER THEORY

2.1 OVERVIEW

This chapter introduces the design and theory of operation of the electrodynamic loudspeaker, with particular reference to the loudspeakers modelled and measured throughout this thesis.

The constituent components of a mid-range electrodynamic loudspeaker "driver" are introduced and briefly described. A mathematical model of low-frequency loudspeaker behaviour is derived and developed, initially subject to the assumption that the loudspeaker cone vibrates as a rigid body. The model is subsequently expanded to take into account higher frequency, non-rigid cone vibration.

Some of the common parameters and forms of notation used for describing loudspeaker behaviour are introduced, and employed to describe the response of a typical loudspeaker to a sinusoidal electrical input.

A qualitative introduction to cone standing waves is given, along with a description of their effect on the measurable response of the loudspeaker.

The major contributing factors to the developed sound pressure of a loudspeaker are identified, and the relative contribution of each of these factors to the characteristics of the sound pressure response is explored.

2.2 PHYSICAL DESIGN AND COMPONENTS

An electrodynamic loudspeaker consists of an electromotive motor system connected to a radiating surface, which is usually a straight sided or hyperbolic cone. The motor system is formed by a coil of fine wire (the "voice coil") placed in a stationary magnetic field. An alternating current is passed through the coil, providing a sinusoidal force that vibrates the radiating surface, thereby producing a sound pressure wave.

Figure 2.1 shows an exploded view of one of the electrodynamic loudspeakers used in this thesis.

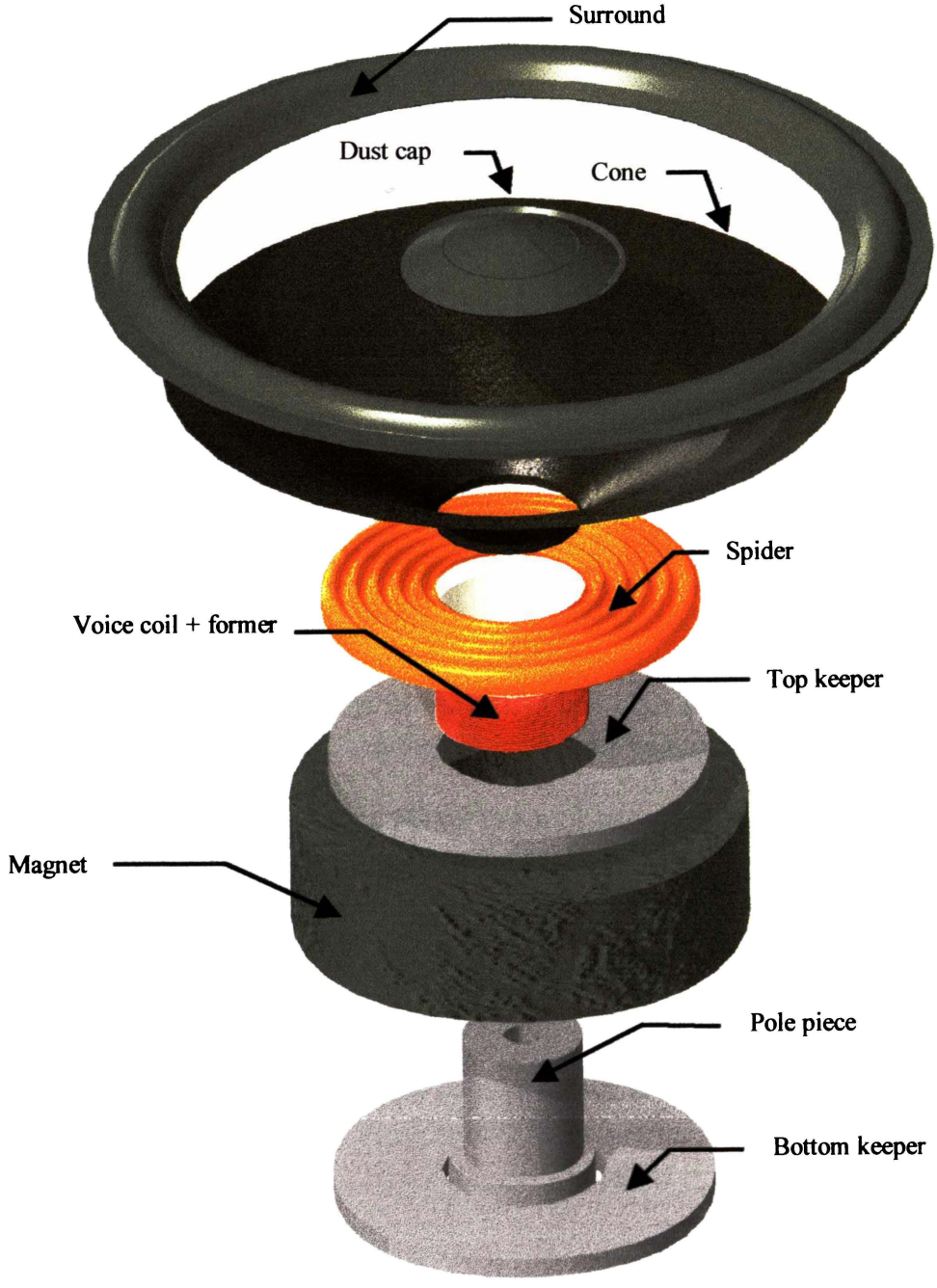

Figure 2.1. Exploded view of the electrodynamic loudspeaker

The keeper/magnet/pole-piece assembly and the outer edges of the spider and surround are attached to a die cast frame (not shown), which allows the loudspeaker to be mounted rigidly into a cabinet.

The main components that constitute an electrodynamic loudspeaker, as shown in Figure 2.1 are the surround, cone, voice coil, spider, and keeper/magnet/pole piece assembly. These components are considered separately in the following sections.

2.2.1 SURROUND

The surround (sometimes called the outer suspension) attaches the outer edge of the cone to the loudspeaker frame, as shown in Figure 2.2.

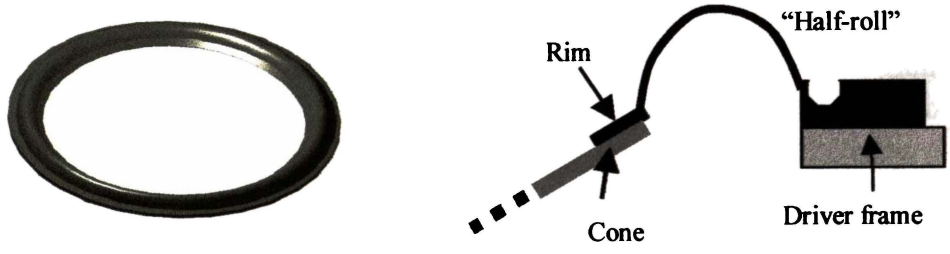

Figure 2.2. a) Surround b) Section view of surround, driver frame, and cone edge

The function of the surround is to ensure that the movement of the cone is restricted to the axial direction, and side to side rocking is prevented. It also provides an air seal to prevent the passage of air from the front of the radiating surface to the rear, as well as providing a small amount of restoring force on the centre of the cone.

A carefully selected surround can also assist in damping travelling waves on the surface of the cone. Good mechanical impedance matching between the outer edge of the cone and the surround results in a large percentage of travelling wave energy propagating from the cone into the surround. As little energy is reflected back from the cone's outside edge, the amplitude of cone standing waves is minimised. A suitably shaped surround constructed from a well-damped material will quickly dissipate any energy transmitted into it.

The surround employed in these loudspeakers consists of an external half-roll (Figure 2.2b), formed from butyl rubber. A rubber rim is attached to the front surface of the cone, which is connected to the loudspeaker frame by means of the half roll. This design and material has good damping characteristics while allowing considerable cone excursion at low frequency.

The surround has a significant effect on the resonant behaviour of the loudspeaker, as shown in Section 4.5.

2.2.2 DUST CAP

The dust cap is a small cup of soft rubber, glued to the front surface of the loudspeaker cone. The role of the dust cap is primarily to prevent dust and dirt entering the motor system of the loudspeaker. It also performs a second role in preventing the passage of air between the front and rear of the loudspeaker. The dust cap has little measurable effect on the measured electrical characteristics of the loudspeaker, apart from slightly raising its moving mass.

Since the dust cap forms a small part of the radiating surface of the loudspeaker, it can have a small effect on the radiated sound pressure response, as shown by Geaves [32]. However, as discussed in Section 2.6, the non-uniform motion of the loudspeaker cone obscures this effect.

For simplicity, all measurements of the loudspeaker (motional impedance, sound pressure) are made with the dust cap removed, precluding the necessity of including the dust cap in analytical and finite element models.

2.2.3 CONE

The loudspeaker's radiating surface is a truncated hyperbolic convex cone, vacuum-formed from mica-doped sheet polypropylene. The outside diameter of the cones used in this thesis is 122mm. While some loudspeakers have been manufactured with straight sided, concave or even flat radiating surfaces, the convex cone is the preferred design for most electrodynamic loudspeaker designers. This shape is more rigid than a truncated straight-sided isometric cone and thus possesses natural resonances of higher frequency.

The process of vacuum forming tends to create a cone that is thin near the apex, but thick at the outer edge, an undesirable scenario from the point of view of resistance to break-up, as demonstrated in Section 5.3.2. However, mica-doped polypropylene possesses a high degree of self-damping which helps to absorb the energy of standing waves on the surface of the cone. The doping agent also helps increase the stiffness of the cone, and thus increase the frequency at which cone break-up begins to occur, extending the upper limit of the loudspeaker's useable frequency range

2.2.4 VOICE COIL AND FORMER

The voice coil consists of a 100-turn coil of thin aluminium wire wound on to one end of a Mylar or aluminium former, as shown in Figure 2.3. The two ends of the voice coil wires are connected to a pair of lugs mounted on the driver frame. The voice coil is arranged such that it is mounted in the middle of the magnetic field of the keeper/magnet/pole-piece assembly when the cone is in its equilibrium position.

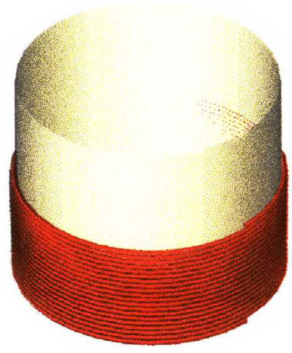

Figure 2.3. Voice coil and former.

The other end of the voice coil is glued to both the cone and the spider, supplying the driving force to the loudspeaker cone. The voice coil is often represented in electrical equivalent circuits as a series resistor and inductor, a convention adopted in this thesis. While this is sufficient for the purpose of broadly explaining the low-frequency resonant behaviour of a loudspeaker, a more accurate representation demands a more complicated equivalent circuit [33,34].

2.2.5 SPIDER

The inner suspension or "spider" has the dual function of centering the voice coil and cone assembly in the motor system, and providing restoring force to return the cone to its equilibrium position in the centre of the magnetic field. The spider is constructed of epoxy impregnated polyester fabric, and is pressed into the shape of an inverted cup. (refer Figure 2.4). The inner edge of the spider is glued to the voice coil, while the outer edge attaches to the loudspeaker frame.

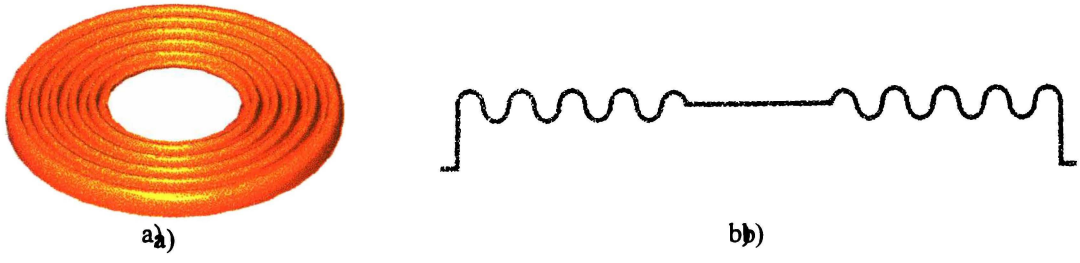

Figure 2.4. a) Spider b) Section view of spider showing cup shape of spider.

This shape is designed to provide a linear restoring force to the cone/voice coil assembly, while allowing considerable cone excursion. The spider's restoring function is quantified in terms of its mechanical compliance C_{spider} (the inverse of the spring constant k_{spider}).

The spider possesses its own resonant frequencies, which can be excited by the voice coil, and cause measurable fluctuations in the electrical impedance of the loudspeaker (refer Section 4.3.3). However, it is usual to consider the spider as a simple spring, and account for its effects by post-processing the results of a mathematical model of the loudspeaker cone. Since the spider is mounted behind the loudspeaker cone, any

radiation from the spider can be neglected.

2.2.6 KEEPERS, MAGNET AND POLE PIECE

The remaining components of the driver create, as nearly as possible, a constant magnetic field between the top former and the pole piece. The top plate forms one pole of the magnet, while the pole piece forms the other pole.

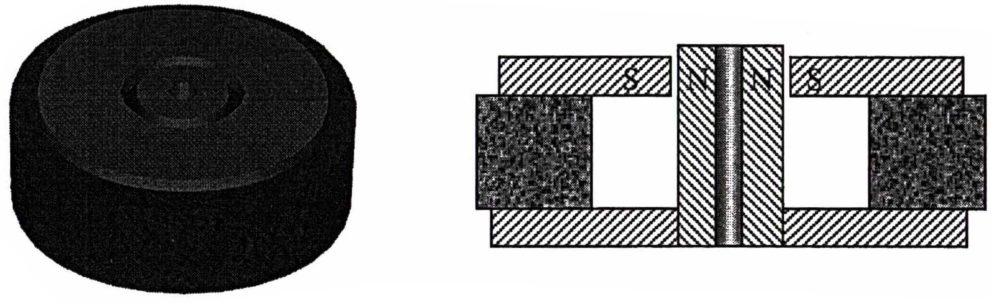

a) b)

Figure 2.5. Keeper/magnet/pole-piece assembly. a) Assembled view b) Cross section

The voice coil is larger than the length of the top keeper, so unless the voice coil excursion is excessively high, the length of voice coil in the magnetic field remains constant. Large magnitude AC currents can cause the coil to travel out of the magnetic field, giving rise to a non-linear displacement response and harmonic distortion. By assuming the excursion of the cone is kept low enough such that the voice coil is at all times entirely within the magnetic field, these effects can be ignored.

B denotes the magnetic flux density, while the length of wire in the magnetic field is denoted by ℓ. As the force produced by the motor is given (in scalar notation, assuming B is perpendicular to I) by $F = B\ell I$, we adopt the convention of expressing the total motor strength in terms of the product $B\ell$.

2.3 ELECTRICAL AND MECHANICAL BEHAVIOUR

In this section, the differential equations governing rigid-body loudspeaker motion are introduced and discussed, allowing the loudspeaker to be described by a simple linear system block diagram, and an electrical equivalent circuit.

All measured results and mathematical models considered in this thesis are for a loudspeaker vibrating in a vacuum or radiating into free space. Thus, the models developed in this section concern the behaviour of the loudspeaker driver itself; the well-known effects of loudspeaker cabinets on the low frequency behaviour of the loudspeakers [35, 36] are not considered.

2.3.1 THE ELECTRODYNAMIC LOUDSPEAKER AS A LINEAR SYSTEM

When a voltage V is applied to the voice coil, a current I flows through the series resistor and inductor formed by the coil, according to Ohm's Law. This current results in a force F being applied to the cone according to $F = B\ell I$. Any motion of the cone is opposed by the spring restoring force provided by the "spider" and outer suspension. A mechanical resistance, that is, a damping force proportional to cone velocity, also opposes motion. Finally, movement of the coil in the magnetic field also generates a back-emf, $\varepsilon = Blv$, reducing the net current experienced by the voice coil.

If the loudspeaker is initially assumed to vibrate as a rigid body, the individual mass, compliance and mechanical resistance contributions of the cone, voice coil, spider and surround can be represented as lumped parameters M_{tot}, C_{tot} and R_{tot}. The electro-mechanical process can then be described mathematically by writing the differential equations:

$$V - B\ell\frac{du}{dt} = IR_{coil} + L_{coil}\frac{dI}{dt} \tag{2.1}$$

$$F = B\ell I = M_{tot}\frac{d^2u}{dt^2} + R_{tot}\frac{du}{dt} + \frac{u}{C_{tot}} \tag{2.2}$$

where:

V = Applied voltage (V)
$B\ell$ = Electromagnetic coupling factor (magnetic field × length of coil wire) (T.m)
u = Displacement of piston-like cone (m)
R_{coil} = Resistance of coil (Ω)
L_{coil} = Inductance of coil (H)
M_{tot} = Total moving mass of loudspeaker (kg)
R_{tot} = Total mechanical resistance of speaker (N.s/m)
C_{tot} = Total mechanical compliance of spider + surround (m/N)

Taking the Laplace transforms of equations (2.1) and (2.2) gives:

$$V(s) - B\ell sU(s) = (R_{coil} + L_{coil}s)I(s) \tag{2.3}$$

$$F(s) = B\ell I(s) = \left(M_{tot}s^2 + R_{tot}s + \frac{1}{C_{tot}} \right) U(s) \tag{2.4}$$

These equations can be combined graphically to give an overall system diagram for the electrodynamic loudspeaker, with voltage as input, and displacement as output:

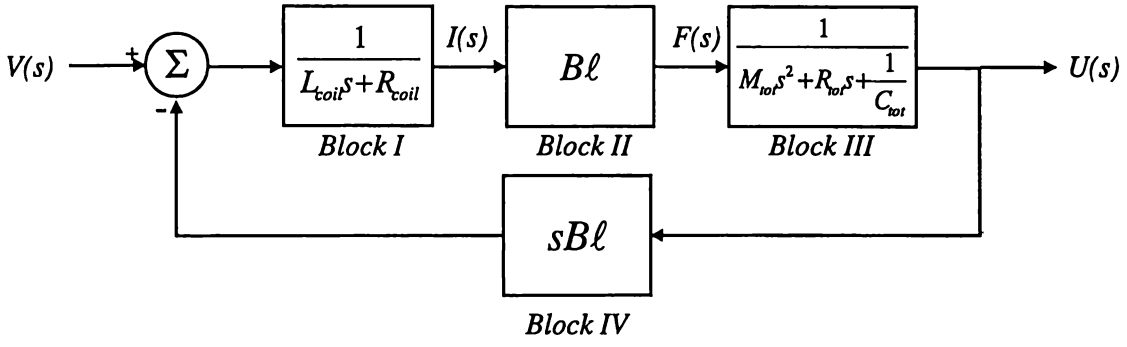

Figure 2.6. Block diagram of Electrodynamic loudspeaker system.

Block I of Figure 2.6 represents the transformation between voltage and current performed by the electrical admittance of the voice coil. This current is multiplied by the coupling factor (Block II) of the voice coil/magnet system to produce a force according to $F = BI\ell$.

Block III represents the transformation of the voice coil force into the displacement of the voice coil and the cone, spider and suspension. Finally, Block IV represents the back-emf generated by the motor system of the loudspeaker. The net voltage across the voice coil is the applied voltage less the back-emf generated by voice coil motion.

2.3.2 AN ELECTRICAL EQUIVALENT CIRCUIT

It is common to describe the behaviour of the electrodynamic loudspeaker system of Figure 2.6 by means of an electromechanical equivalent circuit [3, Ch.3], whereby the mechanical properties of the loudspeaker system are represented by electrical components.

The use of electrical circuits to represent mechanical systems is justified upon comparison of the differential relationships governing the behaviour of electrical circuits and mechanical systems. In particular, the current equation for a parallel LCR resonant circuit and the equation of motion for a spring-mass-damper system can be written as:

$$I = C\frac{dV}{dt} + \frac{V}{R} + \frac{1}{L}\int V dt \qquad (2.5)$$

$$F = M_{tot}\frac{dv}{dt} + R_{tot}v + \frac{1}{C_{tot}}\int v dt \qquad (2.6)$$

Comparison of these two equations suggests that a parallel LCR circuit can be used to describe a simple spring-mass-damper system. Specifically, Equations 2.5 and 2.6 imply that in such an equivalent circuit, force is equivalent to current, velocity to voltage, mass to capacitance, mechanical admittance to electrical resistance, and mechanical compliance to inductance. This form of electrical equivalent circuit is known as a mobility-type circuit.

A convenient form of mobility-type circuit is the transformer circuit shown in Figure 2.7. The equivalent circuit of Figure 2.7 consists of a primary and secondary electrical circuit coupled by an ideal transformer (zero primary and secondary coil impedance).

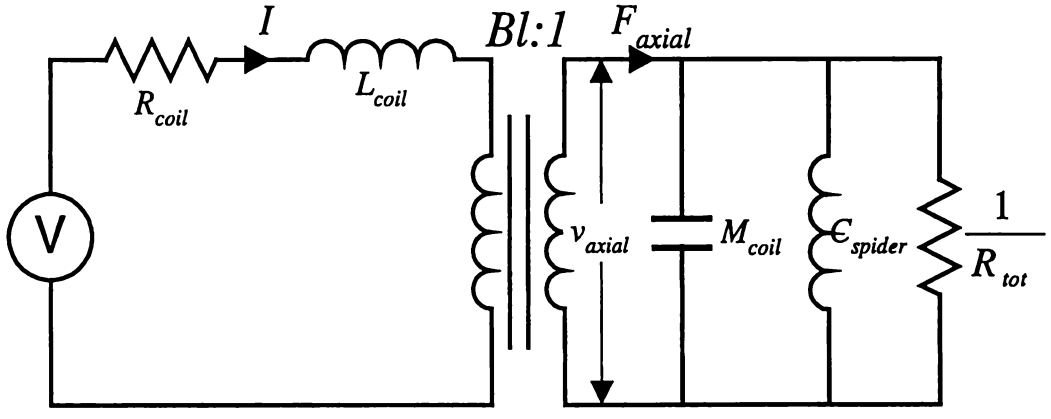

Figure 2.7. Mobility-type electrical equivalent circuit of loudspeaker.

The primary side of the circuit is used to represent the electrical properties of the voice coil, depicted here as a series resistance and inductance. An "ideal" transformer, of turns ratio $B\ell:1$, represents the transformation between current in the voice coil and mechanical force on the loudspeaker cone. Thus, current in the primary circuit is transformed to force in the secondary circuit according to $F = BI\ell$. Further, voltage in

the primary circuit is converted to velocity in the secondary circuit and is denoted by v_{axial}.

The three lumped parameters describing the mechanical characteristics of the spring-mass-damper system formed by the total cone/voice-coil/spider/surround appear in the secondary circuit of the transformer as a parallel LCR resonant circuit. Thus, the driving force, represented as a current, is distributed amongst the mechanical impedances of the secondary resistance, inductance and capacitance, according to Newton's second law.

Since the velocity of the cone generates a back-emf in the primary circuit according to $\varepsilon = Blv$, the mechanical vibration of the loudspeaker cone affects the electrical properties of the loudspeaker.

This electrical equivalent circuit provides a valid description of the behaviour of the loudspeaker for low frequencies when the cone vibrates as a rigid body; at higher frequencies, this model requires modifications, as discussed in Section 2.3.5

2.3.3 Coil, Motional, and Total Impedance

The total electrical impedance experienced by the driving voltage in the electromechanical equivalent circuit of Figure 2.7 is comprised of the sum of the primary and effective-secondary impedances. Since the primary circuit represents the electrical properties of the voice coil, the primary impedance is denoted as Z_{coil}. The secondary circuit represents the mechanical properties of the loudspeaker that govern the motion of the cone, and its contribution to the total electrical load is denoted Z_{mot}, the motional impedance.

The motional impedance arises in the primary circuit due to the back-emf induced by motion of the voice coil in the magnetic field. Thus, Z_{mot} is the component of the total electrical impedance that reflects the mechanical behaviour of the loudspeaker.

The total electrical impedance of the loudspeaker can then be written:

$$Z_{tot} = Z_{coil} + Z_{mot} \tag{2.7}$$

with:

$$Z_{coil} = R_{coil} + j\omega L_{coil} \tag{2.8}$$

$$Z_{mot} = \frac{(B\ell)^2}{R_{tot} + j\omega M_{tot} + 1/j\omega C_{tot}} \tag{2.9}$$

Substituting equations 2.8 and 2.9 into 2.7 allows the total electrical impedance of a loudspeaker to be written as:

$$Z_{tot} = R_{coil} + j\omega L_{coil} + \frac{(B\ell)^2}{R_{tot} + j\omega M_{tot} + 1/j\omega C_{tot}} \tag{2.10}$$

Consider, for example, a loudspeaker with the following parameters:

Parameter	Value	Parameter	Value
R_{coil}:	7 Ω	M_{tot}:	10 g
L_{coil}:	0.3 mH	C_{tot}:	0.002 m/N
$B\ell$:	6.2 T.m	R_{tot}:	1 Ns/m

Table 1.1 Example values of rigid-body loudspeaker parameters

The following electrical, motional and total impedance characteristics for this loudspeaker can be calculated from equations 2.8, 2.9, 2.10:

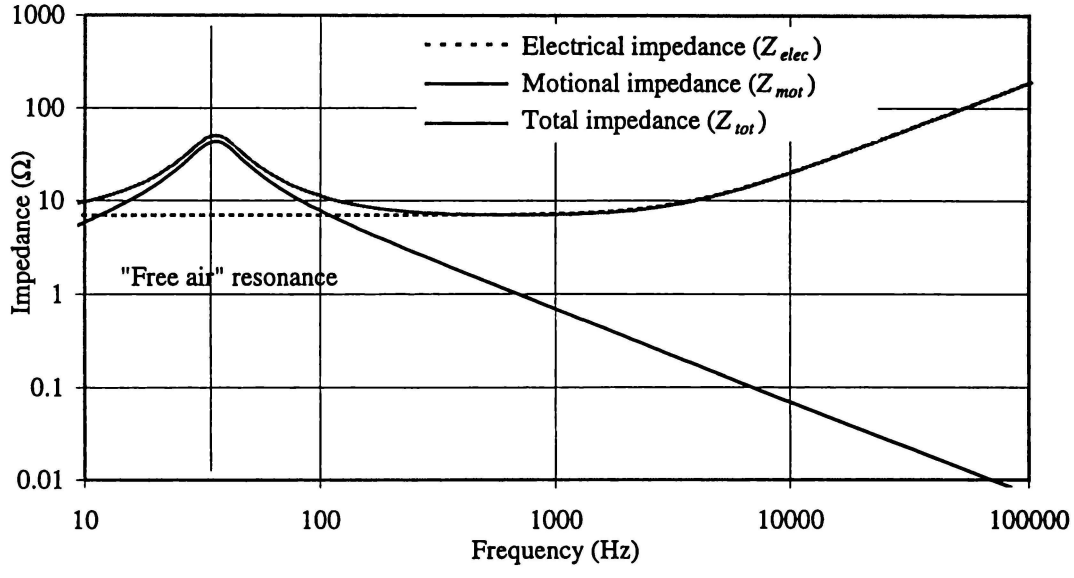

Figure 2.8. Electrical, motional, and total impedances of example loudspeaker.

Figure 2.8 shows that at low frequency the motional impedance dominates the total electrical impedance. The motional impedance, formed by the spring-mass-damper system has the characteristic impedance curve of a first order LCR bandpass filter, with

$$f_0 = \frac{1}{2\pi\sqrt{C_{tot}M_{tot}}} \tag{2.11}$$

This frequency, known as the "*free air resonance*", decreases with increasing total mass and/or compliance, and in this example is approximately 36Hz. The "sharpness" of the motional and total impedance responses near the free air resonance is described by the Q factor:

$$Q = 2\pi f_0 \frac{M_{tot}}{R_{tot}} \tag{2.12}$$

Systems with higher mechanical resistance possess a lower Q and exhibit a broader peak near free air resonance. Conversely, a system with low mechanical resistance possesses a more undamped free-air-resonance, and thus a higher Q, resulting in a pronounced peak at f_0.

Above f_0, the total electrical impedance begins to be dominated by the electrical impedance of the voice coil. The voice coil can be modelled as an electrical first-order low-pass filter of cut-off frequency:

$$f_c = \frac{R_{coil}}{2\pi L_{coil}} \tag{2.13}$$

Accordingly, above the cut-off frequency of the voice coil (≈3700Hz in this example) the total electrical impedance of the loudspeaker increases at a rate of 20 dB/decade.

2.3.4 FREQUENCY DEPENDENCE OF CONE VELOCITY

The total mechanical admittance ($Y_{tot(mech)}$) of a uniformly vibrating body is defined as the body's velocity per unit of applied force:

$$Y_{tot(mech)} = v/F \tag{2.14}$$

The total mechanical admittance of a uniformly vibrating loudspeaker can be described by manipulating equation 2.6 to give:

$$Y_{tot(mech)} = \frac{v_{axial}}{F} = \frac{1}{R_{tot} + j\omega M_{tot} + 1/j\omega C_{tot}} \tag{2.15}$$

Comparing equation 2.15 with equation 2.9, it follows that:

$$Z_{mot} = (B\ell)^2 Y_{tot(mech)} \tag{2.16}$$

Thus, the motional impedance of a loudspeaker, (measured in electrical ohms), is directly proportional to its mechanical admittance. It also follows that the motional impedance is directly proportional to v_{axial}, the axial velocity of the loudspeaker cone, when a constant magnitude driving force is applied.

Accordingly, a measurement of the motional impedance of a loudspeaker gives a direct indication of the velocity of the voice coil as a function of driving frequency. As v_{axial} is directly proportional to $Y_{tot(mech)}$, which in turn is directly proportional to Z_{mot}, it follows that the axial velocity of a loudspeaker with a perfectly rigid cone driven by a frequency independent force follows the shape of the $Y_{tot(mech)}$ characteristic described by equation 2.15, as shown in Figure 2.9.

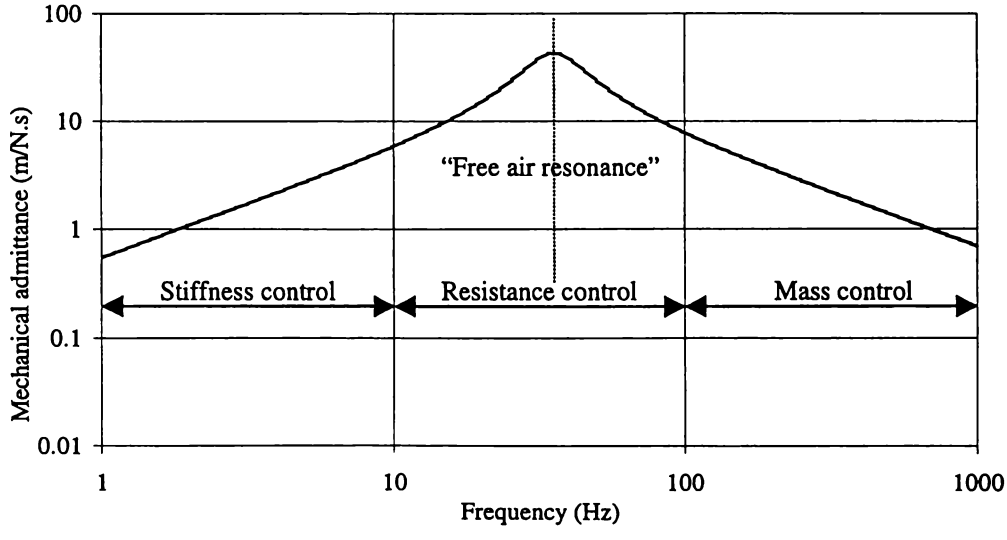

Figure 2.9. $Y_{tot(mech)}$ characteristic for example speaker

For frequencies less than f_0, equation 2.15 is dominated by the compliance term, and thus:

$$Y_{tot(mech)} \approx j\omega C_{tot} \tag{2.17}$$

Under constant current driving conditions, the axial velocity rises proportionally with frequency. In this frequency range, the motion of the loudspeaker is said to be stiffness controlled.

At frequencies close to the free air resonance, the behaviour of the loudspeaker is dominated by the resistance term, the axial velocity reaching its peak at free air resonance. At the free air resonance, the mass and compliance terms cancel.

When $f > f_0$, the mass term dominates the $Y_{tot(mech)}$ response, and:

$$Y_{tot(mech)} \approx \frac{1}{j\omega M_{tot}} \tag{2.18}$$

Thus, above free air resonance, the axial velocity decreases proportionally with frequency. The cone motion is then said to be mass controlled, and the cone velocity, being proportional to $Y_{tot(mech)}$, decreases with increasing frequency.

When modelling loudspeakers, it is common to assume that the loudspeaker's voice coil is driven by a constant amplitude current, resulting in a frequency independent voice coil force that can be simply modelled.

However, under usual listening conditions, loudspeakers are driven with amplifiers which (neglecting the output impedance of the amplifier) provide a constant voltage rather than constant current output. This results in the axial force experienced by the speaker cone varying with frequency, reaching a local minimum at f_0, and a maximum above f_0, but below f_c, as shown in Figure 2.10.

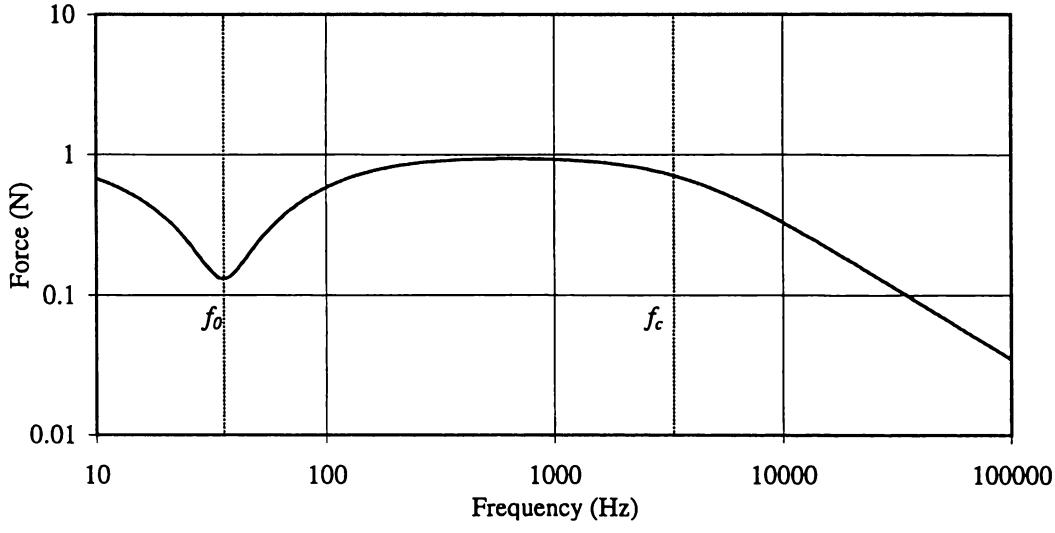

Figure 2.10. Voice coil force for a loudspeaker driven from a constant voltage source.

Consequently, although cone velocity is at its maximum at f_0, for both constant voltage and constant current situations, the velocity response for constant voltage driving conditions exhibits a far broader and less pronounced peak near free air resonance, as shown below:

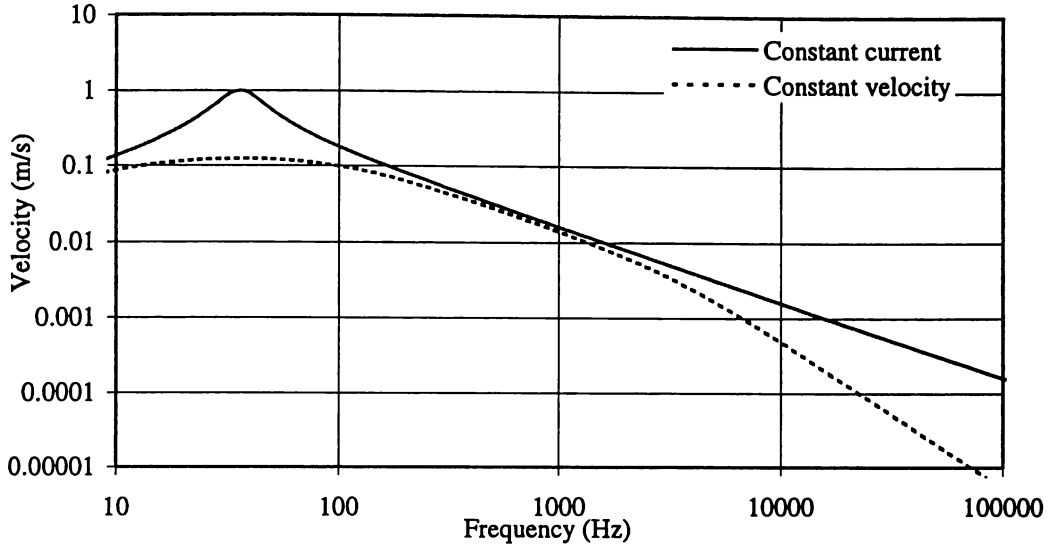

Figure 2.11. Cone velocity as a function of frequency when driven by a) constant current amplifier b) constant voltage amplifier.

Figure 2.11 demonstrates that the cone velocity decreases at a greater rate at high frequency when the constant voltage amplifier experiences the greater load of the loudspeaker due to the rising inductive impedance of the voice coil. Thus, in the region of particular interest from 1kHz to 20kHz, the constant force/constant current assumption results in a somewhat higher velocity than would be expected under more usual constant voltage conditions. Correspondingly, a loudspeaker's measured sound pressure response has a greater magnitude in this range when the loudspeaker is driven with a constant current amplifier.

If the sound radiation response of a loudspeaker is to be modelled precisely, the variation of voice coil force with frequency (Figure 2.10) must be carefully taken into account. This is commonly achieved by post-processing the displacement results from a constant-force driven FE model [30,37].

However, for simplicity, all calculations and measurements of sound pressure presented in this thesis are made using constant force/current conditions, an approach adopted by Frankfort [6] and Shindo [28], among others. Adopting this simplification reduces the overall processing time, but requires the use of a constant-current amplifier when making loudspeaker sound pressure measurements. As the sound pressure response is measured and modelled under the same constant force conditions, a good match between measured and modelled results is achieved.

2.3.5 NON-UNIFORM CONE MOTION

The preceding discussion was based upon the assumption that the loudspeaker's mechanical behaviour can be modelled by a simple driven spring-mass-damper system. At high frequency, this is not the case, and the motional impedance characteristic is more complicated than the simplified "bandpass" model presented in Figure 2.7.

A real loudspeaker cone is not perfectly rigid, but possesses its own natural resonant frequencies. As cone break-up occurs (f > 1-2 kHz), and the diaphragm begins to flex (as natural frequencies of the cone are excited), modulations in the magnitude of the motional impedance appear. This necessitates the modification of the electromechanical equivalent circuit as follows:

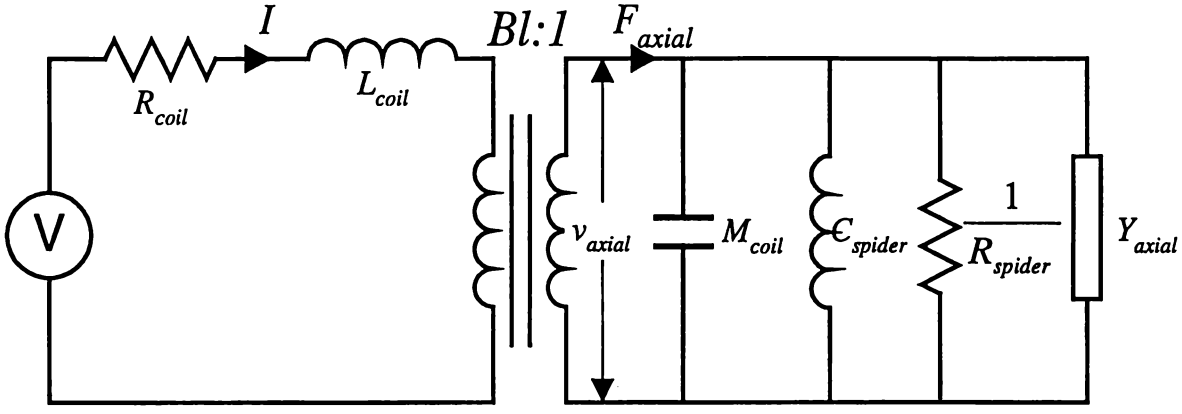

Figure 2.12. Equivalent circuit of a speaker "breaking up"

where:

M_{coil} = Mass of voice coil + spider + surround
C_{spider} = Compliance of spider + surround
R_{spider} = Mechanical resistance of spider + surround
Y_{axial} = Axial admittance of cone (v/F)

The mechanical properties of the voice coil, spider, and surround are now described separately to those of the loudspeaker cone itself, which is represented here by its axial admittance, Y_{axial}. The axial admittance of the loudspeaker is defined as the axial velocity of the centre of the cone (where the voice coil is attached) per unit force applied in the axial direction. Although the velocity distribution across the cone is no longer uniform, the movement of the centre of the cone determines the axial admittance of the loudspeaker, and thus the total electrical impedance experienced by the driving voltage.

Y_{axial} is dependent on the resonant behaviour of the loudspeaker cone itself, which cannot be described by a simple analytical formula, but must be calculated numerically. Y_{axial} is dependent on the cone material properties (mass density ρ, Young's modulus E, Poisson's ratio ν), and the geometry (shape, size etc) of the loudspeaker cone. The

material properties and geometry of the cone are used to calculate Y_{axial} numerically, using the Finite Element (FE) method, as discussed in Chapter 3. However, at low frequency, the cone behaves as a rigid body, and its behaviour can be defined by its total mass M_{cone}.

The total electrical impedance of the loudspeaker is now written:

$$Z_{tot} = R_{coil} + j\omega L_{coil} + \frac{(B\ell)^2}{R_{spider} + j\omega M_{coil} + 1/j\omega C_{spider} + 1/Y_{axial}} \tag{2.19}$$

The motional impedance of a loudspeaker with a breaking up cone is given by:

$$Z_{mot} = \frac{(B\ell)^2}{R_{spider} + j\omega M_{coil} + 1/j\omega C_{spider} + 1/Y_{axial}} \tag{2.20}$$

The total admittance is given by:

$$Y_{tot} = \frac{1}{R_{spider} + j\omega M_{coil} + 1/j\omega C_{spider} + 1/Y_{axial}} \tag{2.21}$$

At low frequency, the motional impedance response follows the same trend as for a rigid cone. However, once cone break-up begins to occur, the Y_{axial} term begins to dominate equation 2.20, and the motional impedance response begins to deviate from the rigid-cone approximation. The effect of the natural frequencies of the loudspeaker cone on a typical Z_{mot} response is shown in Figure 2.13:

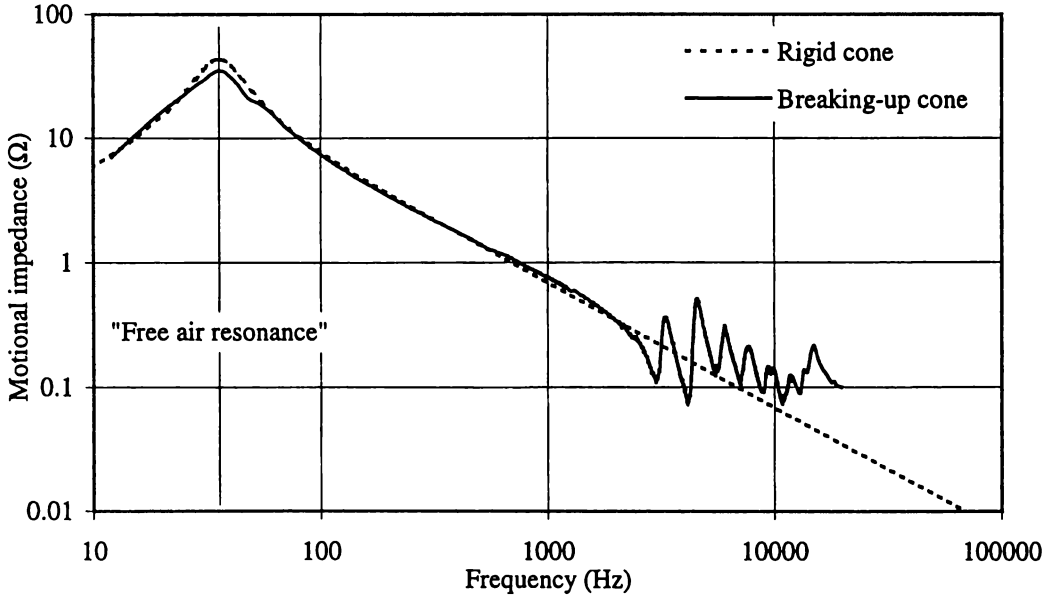

Figure 2.13. Motional impedance of: rigid cone; cone undergoing break-up.

The natural resonances of the loudspeaker cone have a considerable affect on the axial admittance of the loudspeaker, and consequently on its motional impedance. The nature of these resonances is explained qualitatively in Section 2.4, and quantitatively for a specific loudspeaker in Section 4.4.

The ratio M_{cone}:M_{coil} has a large influence on the magnitude and frequency of the resonant features in the Z_{mot} response. If the mass of the voice coil is large in comparison to that of the cone, the increase in motional impedance caused by the voice coil mass will diminish the resonant features in the Z_{mot} response. This effect can be seen in Figure 2.14 where the total admittance response is plotted as a function of voice coil mass.

The upper plot of Figure 2.14 is a 3D view of the change in the Y_{tot} response as the voice-coil mass is increased. The vertical axis is the $|Y_{tot}|$, the horizontal axis is the driving frequency, and the Y-axis (out of the page) is the mass of the voice coil in kg. The cone used in this loudspeaker has a mass of approximately 6.5g, so a voice coil mass of 25g approximates to $4M_{cone}$.

The lower plot of Figure 2.14 is a birds-eye view of the upper plot, in order to clearly show the change in frequency of the resonances of the cone with increasing coil mass.

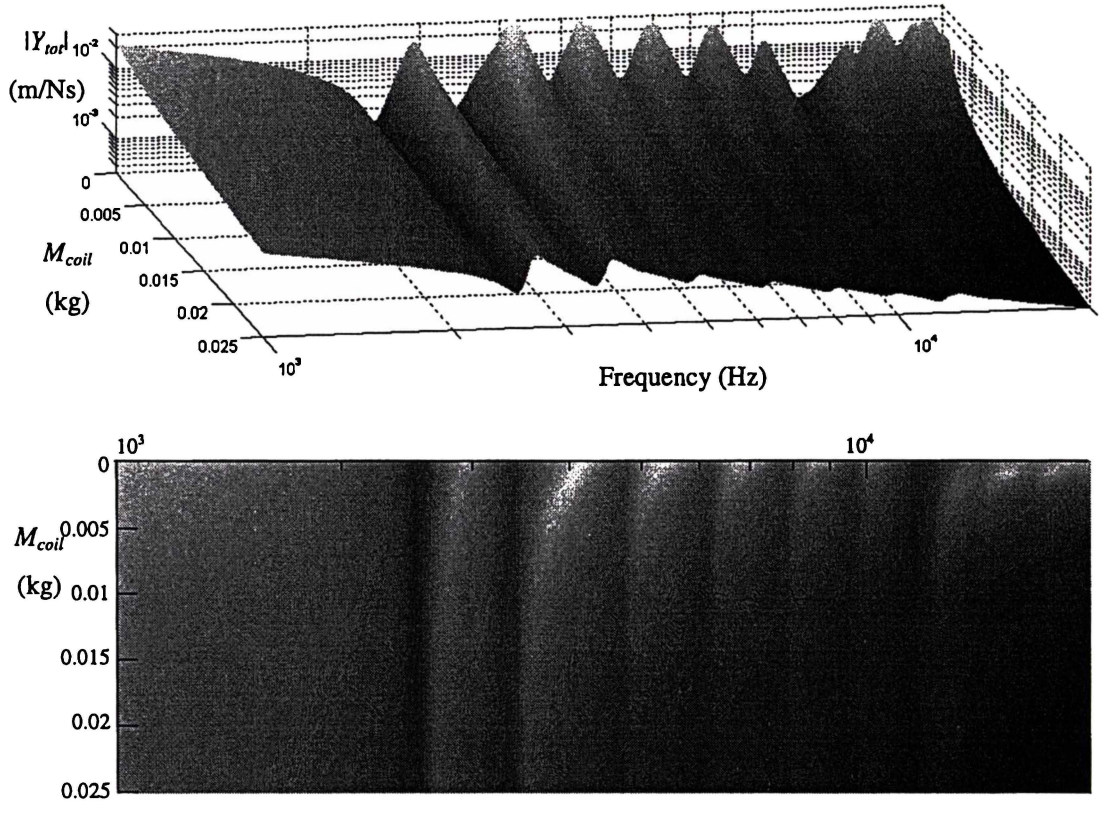

Figure 2.14. 3D plot of Y_{total} as M_{coil} is varied from $0 \rightarrow \approx 4M_{cone}$ (25g)

Figure 2.14 indicates that increasing the voice coil mass has the effect of diminishing the magnitude and frequency of the natural resonances of the cone. Also, f_0, the loudspeaker efficiency, and the loudspeaker bandwidth are decreased by a reduction in

M_{cone}:M_{coil}, as discussed in Section 2.5.4.

2.4 LOUDSPEAKER CONE RESONANCE

If a perfectly rigid loudspeaker cone were excited by a frequency independent force, the displacement and velocity of the cone would be constant across its entire surface, with velocity inversely proportional to driving frequency (for $f > f_0$). Thus, the displacement of the outer edge of the cone would always have the same amplitude and phase as the inner edge, the energy applied at the inner edge being effectively instantaneously distributed over the entire surface of the cone (refer Figure 2.15.)

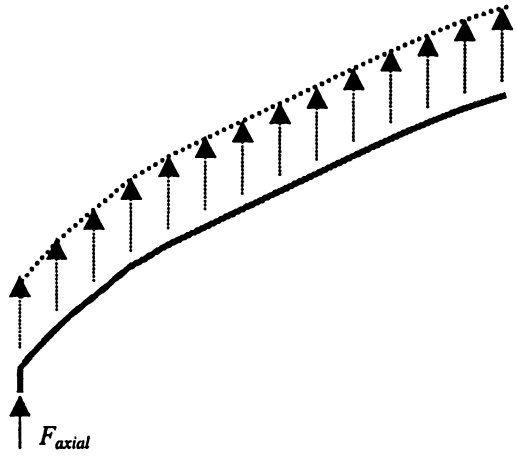

Figure 2.15. Edge cross section of axially driven cone

This idealisation of piston-like motion is true for very low driving frequencies, but as the driving frequency is increased, the inertia of the outer parts of the cone begins to overcome the stiffness of the cone material. Once the cone begins to flex, cone motion is far from uniform, and standing waves begin to form.

2.4.1 FORMATION OF STANDING WAVES:

Any real object possesses its own resonant frequencies, which are related to the physical dimensions of the object and the properties of the materials from which the object is constructed. In a real loudspeaker system, the axial driving force provided by the voice coil can excite the natural resonances of the loudspeaker cone itself, forming standing waves in the cone and measurably affecting both the motional impedance and sound radiation of the loudspeaker. Such natural resonances are a direct consequence of the finite propagation time for waves and wave energy in the loudspeaker cone.

At low driving frequencies, the real loudspeaker cone moves approximately as a rigid body with piston-like motion, all parts of the loudspeaker cone moving in phase with each other. Although the energy applied at the centre of the cone radiates outwards in the form of a mechanical wave and takes a non-zero amount of time to reach the outer edge of the cone, the time delay between inner and outer edge movement is insignificant

in comparison with the period of the driving force.

As the wave propagates through the structure, the energy contained in the wave diminishes at a rate dependent on the self-damping properties of the cone material. Unless the outer edge of the cone is perfectly terminated with a surround of mechanical impedance exactly equal to that of the cone itself, a certain amount of energy will be reflected back from the outer edge towards the centre of the cone.

As the driving frequency increases, the propagation time for energy to travel up the meridian of the cone becomes significant, and the outer edge of the cone begins to exhibit significant phase lag with respect to the inner edge. Eventually a frequency is reached at which the energy reflected from the outer edge of the cone arrives back at the centre of the cone 180° out of phase with the driving force, forming a standing wave with minimum cone displacement at the inner edge. Such a frequency is known as an antiresonant frequency, and is marked by a local minimum in the v_{axial}, Y_{axial}, or Z_{mot} responses. At antiresonant frequencies, an odd number of quarter wavelengths fit along the cone meridian.

There are other frequencies at which the reflected wave will arrive back at the cone centre in phase with the driving force, forming a resonant mode. Resonant modes occur when an integral number of half wavelengths fits along the cone meridian and are identified as occurring when the v_{axial}, Y_{axial}, or Z_{mot} responses reach a local maximum.

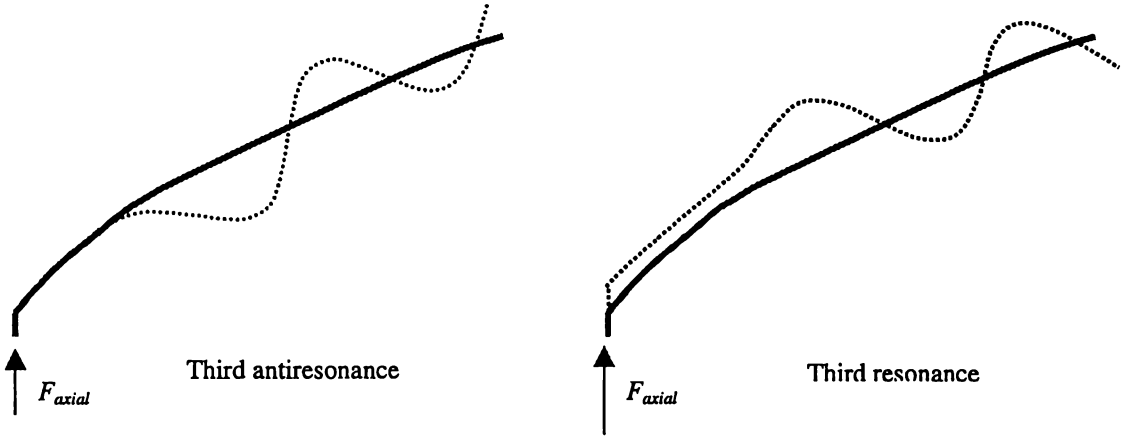

Figure 2.16. Mode shape of a) third antiresonance b) third resonance.

For example, Figure 2.16 shows an edge profile view of the third bending antiresonance and resonance of an axially driven loudspeaker cone.

2.4.2 TYPES OF STANDING WAVE

As the standing waves described in Section 2.4.1 are set up between the inner and outer edges of a homogeneous axially symmetric loudspeaker cone, they display rotational symmetry about the central axis of the loudspeaker. Consequently, they are known as *axisymmetric* or *concentric* modes, and are the most important7 standing wave type in a loudspeaker cone. Their nodal and antinodal lines form around the centre of the loudspeaker in the radial, or azimuthal direction (refer Figure 2.17).

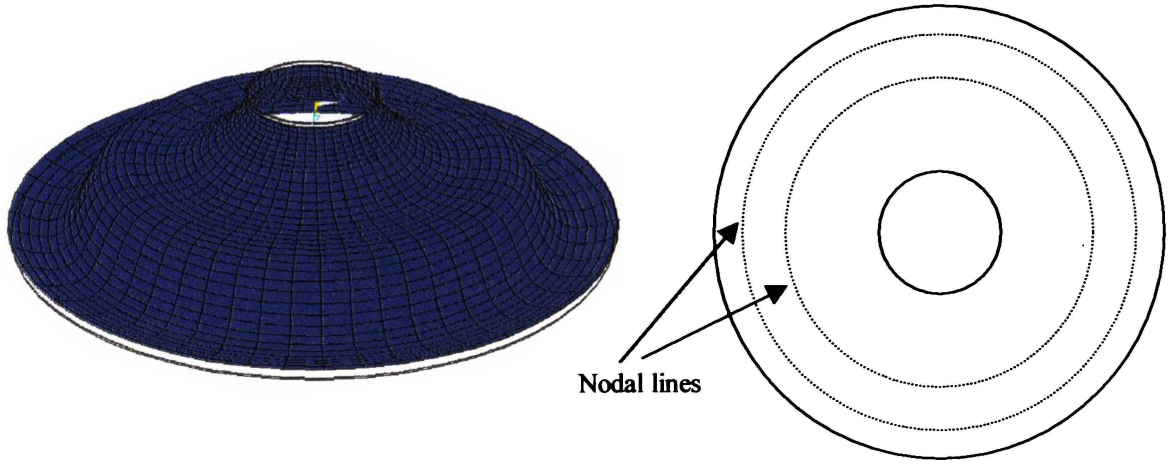

Figure 2.17. "Axisymmetric" or "concentric" modes.

Other standing waves can be set up as multiples of wavelengths fit around the outer edge of the loudspeaker cone. Such modes form nodal lines running in a meridional direction, (from inner to outer edge), and are known as "bell", "radial" or "asymmetric" modes (refer Figure 2.18).

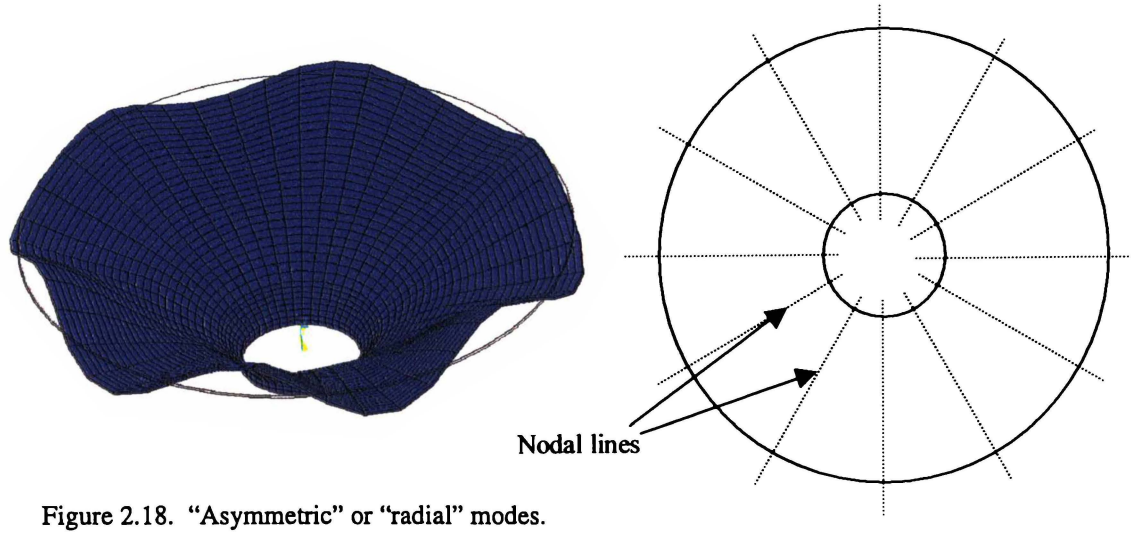

Figure 2.18. "Asymmetric" or "radial" modes.

Since the bending stiffness of a loudspeaker cone in the azimuthal direction is far less than that in the radial direction, asymmetric modes tend to occur at much lower frequencies than axisymmetric modes. Typically, the lowest order asymmetric modes of

a 12cm diameter loudspeaker occur at frequencies of between 100-500Hz. At these frequencies, the wavelength in air is far greater than the bending wavelength of the waves on the cone, and thus the waves are said to be "acoustically short-circuited", radiating very little sound power. Standing waves of the radial type are not usually excited in axially symmetric cones that are subject to purely axial driving forces and symmetric boundary conditions.

Torsional or twisting modes about the central axis of the loudspeaker also exist, but again are not normally excited by the driving force of the voice coil. In any case, these modes would radiate little or no sound radiation, as cone motion would be largely in the azimuthal direction, with little transverse component.

Non axisymmetric cones, such as those considered in Chapter 6, and cones subject to slightly off-axis driving forces can sometimes exhibit a combination of asymmetric bending and torsional wave motion. In some cases, the bending wavelength of the waves on the cone can be considerably greater than the wavelength of the waves in air, in which case these modes can create significant sound radiation.

The axisymmetric and asymmetric standing waves considered thus far are of the bending type, where the displacement energy of the cone is primarily transverse. At high frequency, the voice coil force can also excite longitudinal wave motion, where the displacement of parts of the cone is primarily in the meridional direction. As the velocity of longitudinal waves is much higher than that for bending waves, longitudinal standing waves occur at much higher frequencies (>10kHz) than bending standing waves. As the transverse motion of the cone is minimal, little sound radiation occurs at these frequencies.

2.5 SOUND PRESSURE RESPONSE

The sound pressure level developed by the electrodynamic loudspeaker is primarily determined by the velocity distribution across the area of the radiating surface, the shape of the radiating surface and the characteristics of the baffle or cabinet in which the radiating surface is enclosed.

The loudspeaker cabinet has an important but well-understood effect on the radiated sound pressure response at low frequency [35]. Diffraction effects around the edges of the loudspeaker cabinet are also known to affect the radiated sound pressure at higher frequencies [25, p301, 26, p101]. The consideration of these effects is outside the scope of this thesis; for simplicity the loudspeakers are assumed to be infinitely baffled, and to radiate into an unbounded volume.

In this section, the sound pressure response generated by a rigid flat plate, a rigid cone, and a cone undergoing break-up are determined and compared. This allows the relative contributions of the shape of the radiating surface and the surface velocity distribution to overall sound pressure to be determined. The mathematical technique that allows the calculation of the sound pressure response of loudspeakers is outlined in Chapter 3.

2.5.1 THE RIGID PLATE RADIATOR

A completely rigid radiating surface has a constant velocity response across its surface, as all areas of the surface move with equal displacement and equal phase. Consider a perfectly rigid flat plate of radius R_p set in axial motion by a frequency independent axial force. The force is supplied by a motor system with a voice coil of negligible mass.

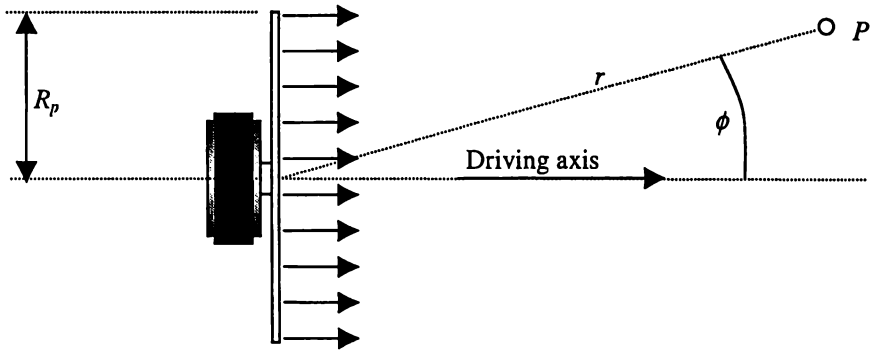

Figure 2.19. The rigid plate radiator

For frequencies above the free air resonance of the loudspeaker, the velocity of the plate decreases with increasing frequency. Assuming the plate radiates into free space, the sound pressure at point P, (distance r from the centre of the plate, angle ϕ from the driving axis) can be calculated using the mathematical process summarised in Section 3.2.

It is convenient to examine the magnitude of the sound pressure radiated by the rigid plate by means of a 3D polar frequency response plot, as in Figure 2.20. Figure 2.20 shows the polar frequency response plot of a vibrating flat plate (R_p = 0.0605m) determined at a distance of r=10m over the frequency range 0-20kHz. The sound pressure scale is referred to the pressure generated by the rigid plate for ϕ=0, f=20kHz.

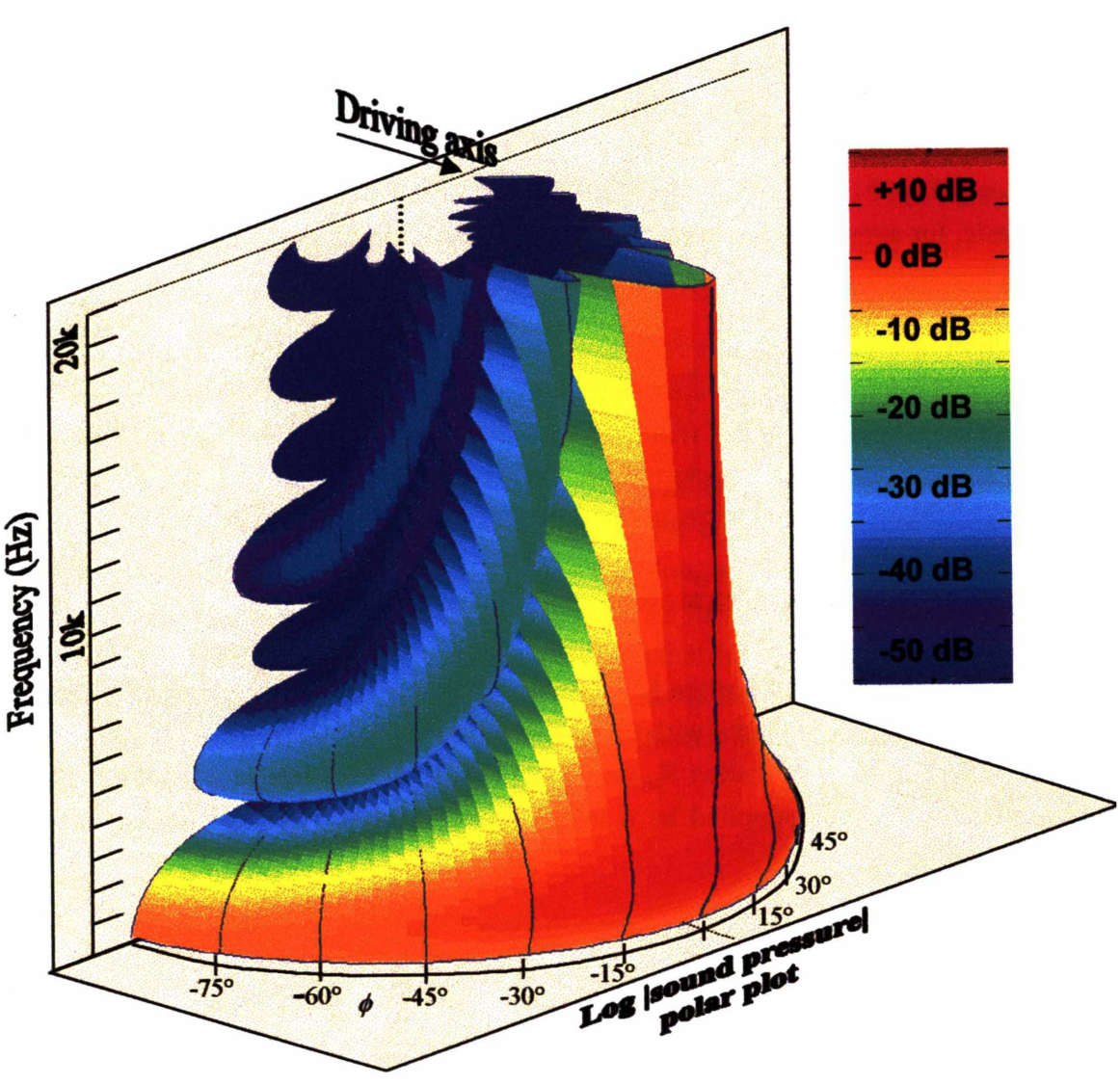

Figure 2.20. 3D Polar frequency sound pressure response of rigid plate radiator.

Figure 2.20 shows that the on-axis frequency response (ϕ=0) of an axially vibrating rigid flat plate is frequency independent. At low frequencies, where the wavelength of sound is greater than the diameter of the piston, the sound radiation is approximately spherical with only a slight decrease in sound pressure for large values of ϕ.

At higher frequencies, the sound wavelength decreases until it becomes comparable to the diameter of the radiating surface. At these frequencies, the wavefronts emitted from different areas of the radiating surface arrive at the measurement point (off-axis) with a significant phase difference. Consequently, at higher frequencies the sound pressure response is more directional and focussed, to the extent that at 20kHz the sound

pressure decreases by 20dB as ϕ approaches ±10°. A number of pressure dips and peaks also are evident as side-lobes form around the semicircle of radius 10m.

In summary, a rigid-plate radiator produces a desirably smooth on-axis sound pressure response across the entire frequency spectrum, but "beams" at high frequency.

2.5.2 THE RIGID CONE RADIATOR

Plane radiators such as the rigid plate considered in the previous section are rare, and are far from rigid. Usually the radiating surface of an electrodynamic loudspeaker consists of a straight sided or hyperbolic cone, as in Figure 2.21:

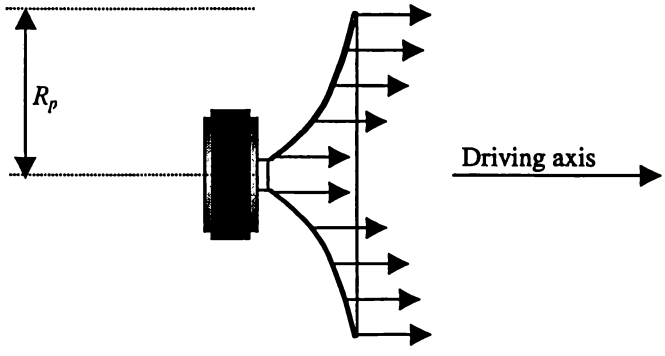

Figure 2.21. The rigid cone radiator

Assuming the radiating surface maintains perfect rigidity, the surface velocity is constant, as it was for the rigid plate. However, the shape of the radiating surface has a considerable effect on the polar frequency response of the system, particularly on-axis, as shown in Figure 2.22.

Figure 2.22 reveals that the on-axis sound pressure response of the rigid cone radiator significantly diminishes with increasing frequency. The on-axis sound pressure response at 20kHz is more than 20dB less than that at 1kHz, due to phase cancellation between the wavefronts emitted from the inner and outer edges of the cone.

Further, the 3D polar frequency response pattern, particularly at high frequencies, substantially differs from that of a rigid flat plate. Broader side-lobes exist at 20kHz, resulting in a diminished, yet more uniform polar response at high frequency.

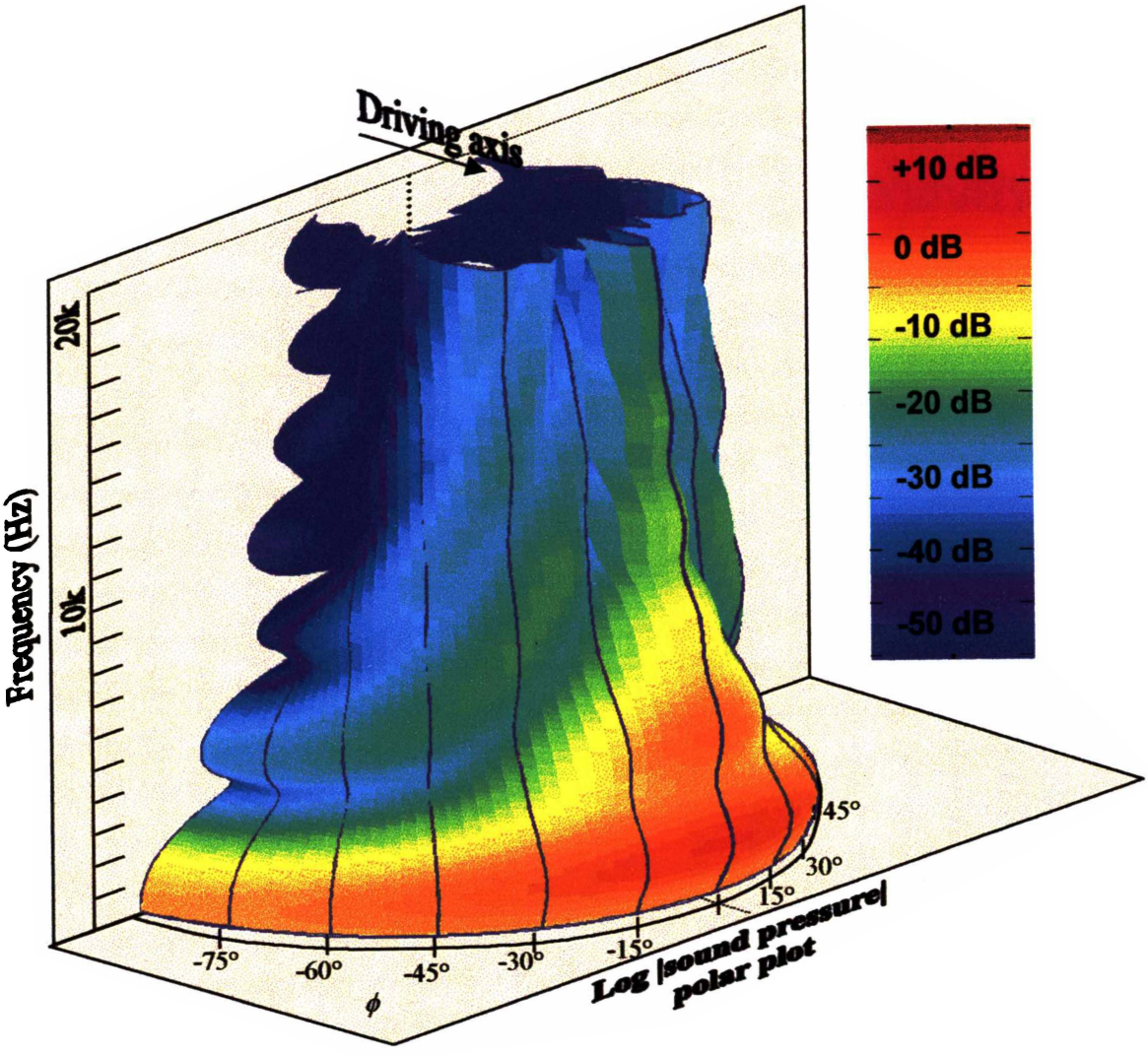

Figure 2.22. 3D Polar sound pressure frequency response of rigid cone radiator.

2.5.3 THE NON-RIGID CONE RADIATOR

In practice, a loudspeaker cone driven by an axial force does not vibrate as a rigid body but begins to break-up as the natural resonances of the cone are excited. Thus, the surface velocity of an axially driven cone is far from uniform, with different parts of the loudspeaker cone surface vibrating out of phase with each other, as shown in Figure 2.23.

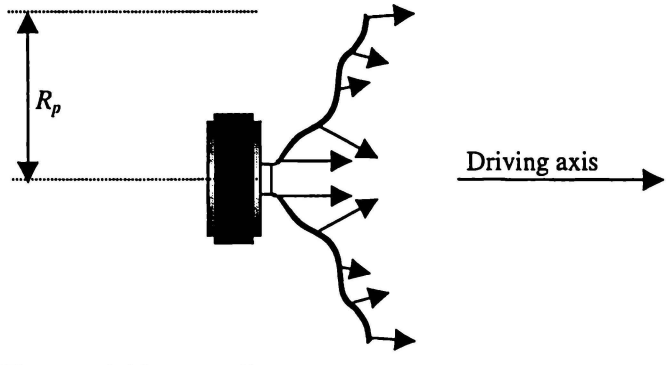

Figure 2.23. The non-rigid cone radiator.

The degree of non-uniform cone motion is strongly dependent on the self-damping property (ξ) of the cone material (refer Section 5.2.4). The polar sound pressure response of a comparatively undamped, non-rigid loudspeaker cone, (ξ=0.1, Figure 2.24) exhibits not only phase cancellation effects due to the shape of the cone, but also effects caused by the cone's phase-varying surface velocity response.

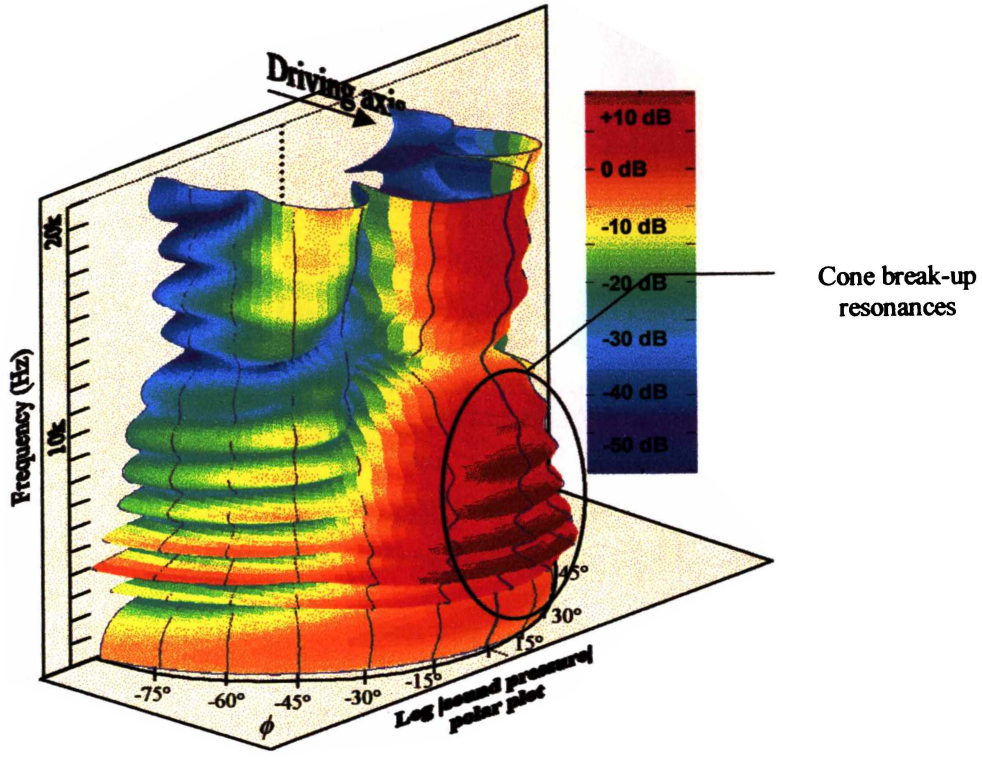

Figure 2.24. 3D Polar sound pressure frequency response of a non-rigid cone radiator with ξ=0.1.

Comparing Figure 2.24 with Figure 2.22 reveals that the 3D polar sound pressure response of a non-rigid cone is notably different from that of a rigid cone. The phase cancellation effects due to cone profile are masked largely by the resonances caused by cone break-up. In particular, the on-axis response no longer exhibits the sound pressure roll-off with frequency that is exhibited by a rigid cone. On the contrary, the developed sound pressure of a breaking-up cone at ~20kHz is of a similar level to that at ~1kHz.

In the frequency range of 2kHz-10kHz, standing waves on the surface of the cone cause peaks and dips in the on-axis sound pressure response of the loudspeaker. These standing waves are of the bending type, and consequently emit considerable sound radiation. At ~12kHz there is a significant decrease in the on-axis sound pressure, due to the onset of the first longitudinal antiresonance. Above this frequency, bending waves begin to re-emerge on the cone, and the sound pressure increases accordingly.

While standing waves on the surface of the cone can result in measurable fluctuations in the sound pressure frequency response, they can be controlled by increasing the self-damping of the cone material. Figure 2.25 shows the 3D polar-frequency response of a loudspeaker cone identical to that of Figure 2.24, but with ξ increased to 0.3.

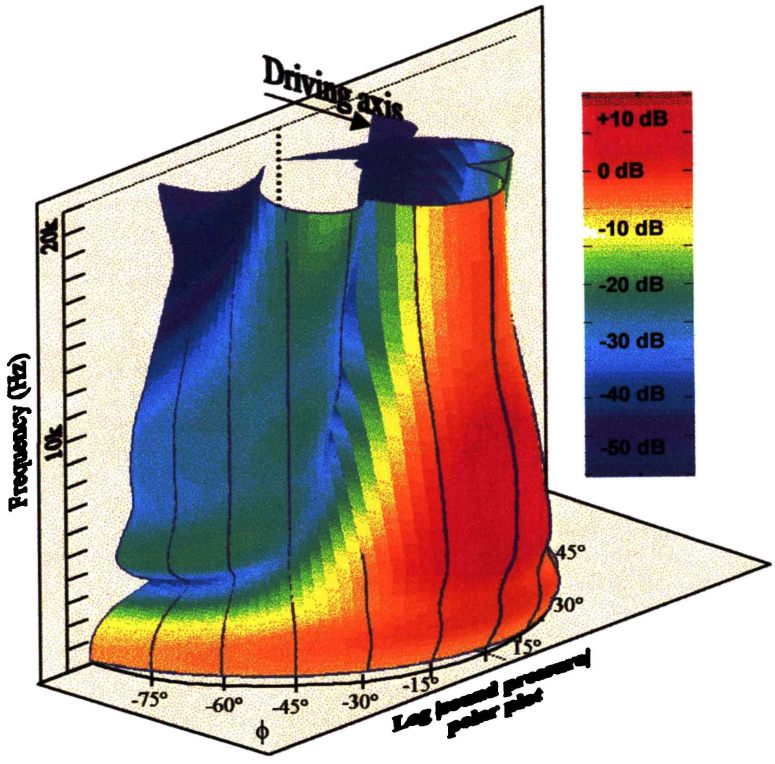

Figure 2.25. 3D Polar sound pressure frequency response of non-rigid cone radiator with ξ=0.3.

Figure 2.25 shows that increasing the cone material's self-damping ratio results in the bending resonances and antiresonances of the cone being damped to the extent that they no longer dominate the polar frequency response. Thus, the sound pressure radiation of a well-damped yet non-rigid loudspeaker cone extends to higher frequency, and is more uniform over the range 1kHz-10kHz than is the case for a completely rigid cone (Figure 2.22). Thus, if a high bandwidth is required for a given loudspeaker cone, highly damped cone flexure is preferable to no cone flexure at all.

2.5.4 Effect of Voice Coil mass

The results of Sections 2.5.1 – 2.5.3 are calculated on the assumption that the mass of the voice coil used in the motor system is negligible in comparison with the mass of the radiating surface. In practice, this assumption is often invalid, as the voice coil mass, and the moving mass contribution of the spider and surround can be equal to, or greater than the mass of the cone.

When M_{coil} is large in comparison to M_{cone}, the denominator of equation 2.20 becomes dominated by the term $j\omega M_{coil}$. Consequently, the motional impedance, total admittance, cone velocity, and sound pressure all decrease at –20dB/decade at high frequency. Increasing the mass of the voice coil increases the effect of this mass term in the denominator of equation 2.20, and thus reduces the bandwidth of the loudspeaker. Maximising the ratio $\frac{M_{cone}}{M_{coil}}$ helps achieve a high loudspeaker bandwidth [6, 28].

The effect of the voice coil mass is demonstrated in Figure 2.26 where the 3D polar sound pressure response for a breaking up cone is calculated for $M_{coil} = 2M_{cone}$[4].

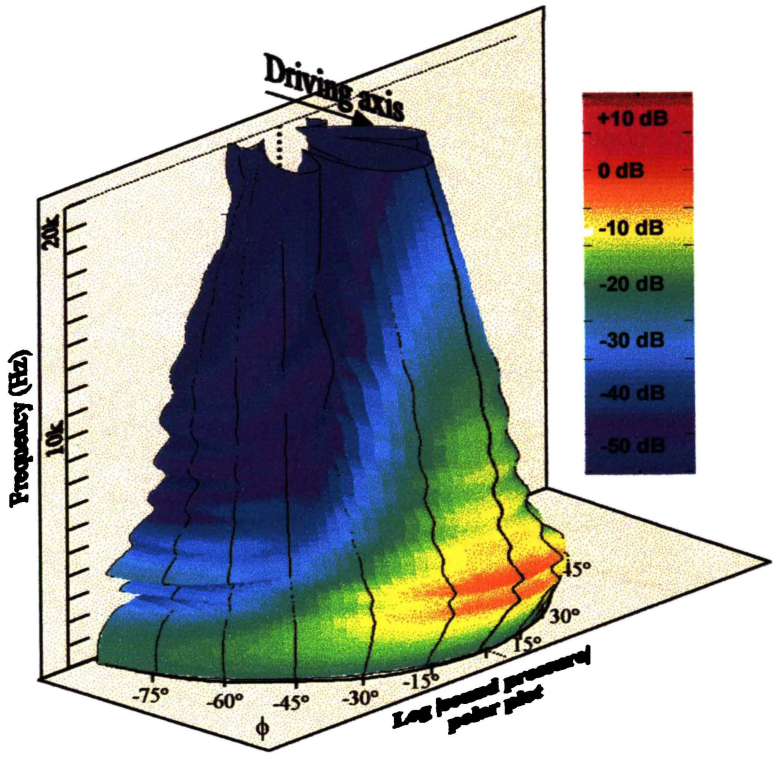

Figure 2.26. 3D Polar sound pressure frequency response of non-rigid cone radiator with $M_{coil} \approx 2M_{cone}$. The damping ratio used is identical to that used in Figure 2.24.

Figure 2.26 shows that the effect of the additional mass of the voice coil is to diminish the high frequency sound pressure response, both on- and off-axis. The shape of the on-axis sound pressure response is also significantly changed, as the peaks and dips in the response are slightly lowered in frequency. Peaks caused by higher order resonances are diminished in comparison to lower order modes. The efficiency of the loudspeaker is also reduced resulting in lower overall radiated sound power.

[4] A cone to coil mass ratio of ½ is typical for the loudspeakers considered in this thesis.

2.5.5 SUMMARY.

The mid- to high-frequency sound pressure level developed by a loudspeaker is dependent on several factors: the shape of the radiating surface, the flexing motion of the cone, and the ratio of cone mass to voice coil mass. Figure 2.27 shows a comparison of the on-axis sound pressure p_{ax} developed by a rigid plate, rigid cone and breaking-up cone.

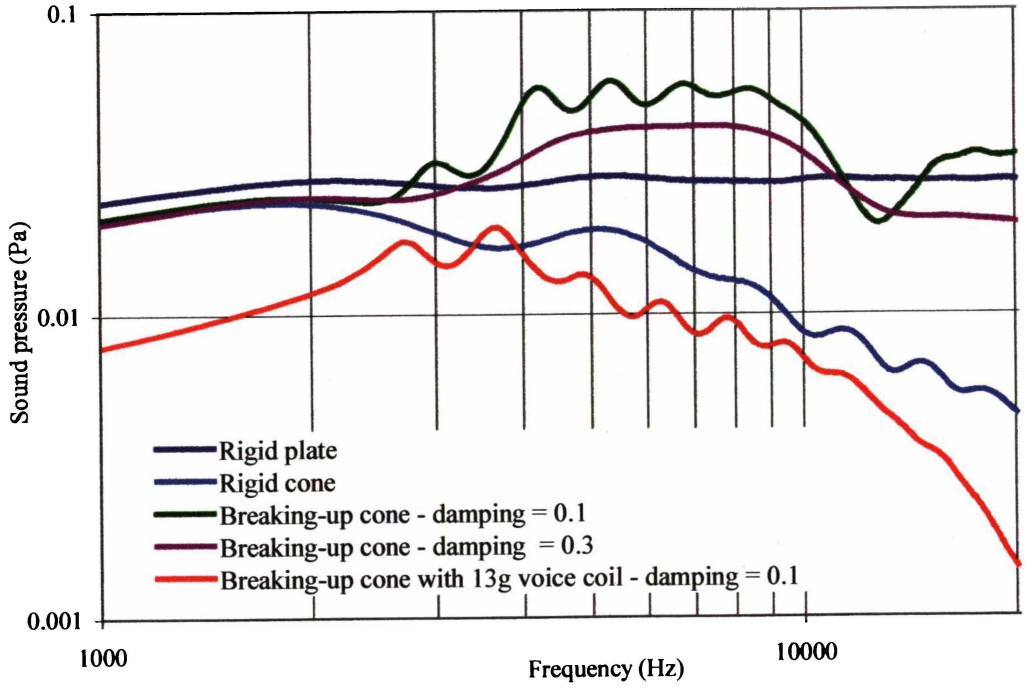

Figure 2.27. On-axis sound pressure responses (p_{ax}) of radiators considered in Sections 2.5.1 – 2.5.4.

In the frequency range 1kHz-10kHz cone break-up is the dominant factor that determines the "smoothness" of the sound pressure response of the loudspeaker, obscuring the phase cancellation effects of the shape of the radiating surface.

The mass of the voice coil also has an important influence on the overall shape of the sound pressure response, causing a roll-off in sound pressure above $f \approx 4$kHz.

2.6 CONCLUSION

The electrodynamic loudspeaker can be modelled as a simple linear system, which converts applied electrical energy into a velocity distribution across the radiating surface. This electromechanical system can be described by means of a simple electrical transformer equivalent circuit.

By writing electrical equations for the equivalent circuit, the mechanical behaviour of the loudspeaker can be summarised in terms of its motional impedance, Z_{mot}. Z_{mot} can be measured by making impedance measurements of the loudspeaker, as detailed in Chapter 3, and can be calculated from the axial admittance results of a finite element model.

The natural resonant frequencies of the loudspeaker cone have an effect on the mechanical admittance of the loudspeaker, and thus on its motional impedance. Further, these resonant frequencies are the major cause of ripple in the sound pressure response of the loudspeaker. Although the cone shape and voice coil mass both have an affect on the overall shape of the sound pressure response, cone break-up is the major factor which determines the "smoothness" of both the on- and off-axis frequency response. Thus, the overall smoothness of the axial admittance and/or motional impedance response can be used as an indicator of the smoothness of the loudspeaker's sound pressure response.

CHAPTER 3

MODELLING AND MEASUREMENT TECHNIQUES

3.1 OVERVIEW

This chapter gives an overview of the modelling and experimental techniques that are used to model and measure some of the characteristics of the loudspeaker cones considered in this thesis.

In order to understand better the behaviour and characteristics of loudspeaker cones, it is useful to develop a mathematical model of both cone vibration and subsequent sound radiation. The finite element and boundary element methods are two numerical techniques that are utilised to produce the modelled results presented in this thesis. A summary of these two numerical methods is given in Section 3.2.

In order to calibrate the mathematical models presented in Section 3.2, several reference measurements must be performed on real loudspeaker cones. In the course of this thesis, four loudspeaker cones, A, B, C and D were used to obtain experimental results. Section 3.3 summarises the measurements made on these loudspeakers and the methods and equipment used to perform them.

3.2 NUMERICAL MODELLING TECHNIQUES

The earliest attempts at predicting the sound radiation of loudspeaker cones were limited by the requisite assumption that the loudspeaker cone vibrated as a rigid body. As discussed previously, this assumption is valid for very low frequencies, but for frequencies above the order of 1kHz cone motion is far from uniform. Accurately modelling loudspeaker sound pressure response for frequencies at and above this range requires the non-uniform surface velocity response of the cone to be determined.

In this thesis, the ANSYS™ finite element software package is utilised to create and solve several different finite element models of loudspeaker cones. The ANSYS software allows axisymmetric and non-axisymmetric cones to be modelled, and the structural response of the cone to transient or steady state sinusoidal forces to be determined.

In this thesis, the surface displacement results from ANSYS finite element analyses of axisymmetric loudspeaker cones are used as inputs to a boundary-element model, which is subsequently employed to calculate the sound pressure at specific field points. The commercial boundary element software chosen to perform this calculation is the SYSNOISE™ package.

These numerical modelling tools can be used to calculate the characteristics of a loudspeaker and quantify them in terms of its mode shapes, and axial admittance, motional impedance and sound pressure responses. Other parameters, such as cone stress and strain may also be modelled using the FEM, but are not considered in this thesis, as they yield little additional insight of the behaviour of the loudspeaker.

The following sections give a brief overview of the finite element and boundary element techniques and their application to finding the mechanical behaviour of a vibrating loudspeaker cone and the resulting sound radiation. A more detailed mathematical consideration can be found in any good introductory finite element analysis text [38,39, 40] as well as the ANSYS 5.2 theory manual [41], and SYSNOISE theoretical manual [42].

3.2.1 THE FINITE ELEMENT METHOD

The finite element method is a numerical technique that enables the partial differential equations describing the behaviour of a system to be solved by creating a discretised model of the continuous system they describe. In order to calculate the motion of a loudspeaker cone of arbitrary shape, the cone is divided into a series of "elements" of small size, connected at points called "nodes".

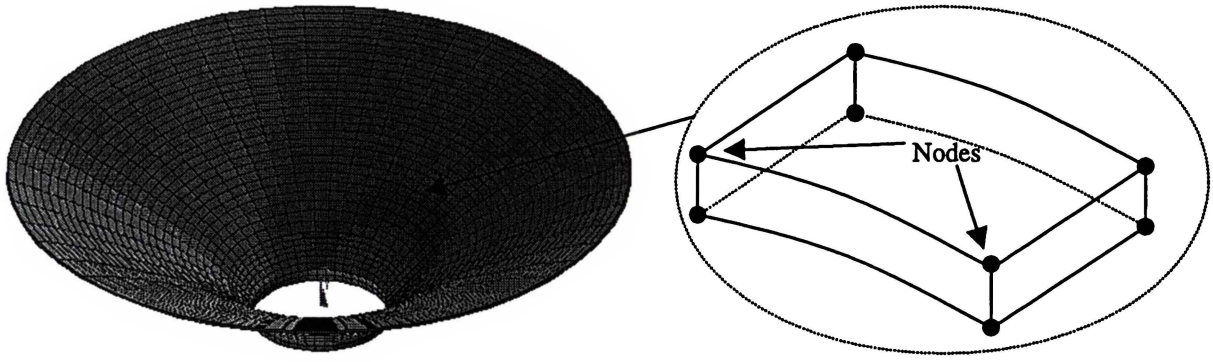

Figure 3.1. 3D model of a loudspeaker cone using 8-node structural elements.

Elements of various shapes having different numbers of nodes are selected depending on the particular type of analysis required. Figure 3.1 shows a finite element model of a loudspeaker cone consisting of 1680 8-node solid elements.

Having created a "mesh" of finite elements, the equations governing the structural vibration of the loudspeaker cone can be formulated by considering the stresses and strains of each element comprising the finite element model. This can be summarised as follows:

For any given element of volume V, defined in a Cartesian coordinate system $\{x,y,z\}$ the state of stress in the element can be described by means of a vector containing the direct and shear stresses in each dimension. The stress vector $\{\sigma\}$ is written as:

$$\{\sigma\} = [\sigma_x \ \sigma_y \ \sigma_z \ \sigma_{xy} \ \sigma_{yz} \ \sigma_{xz}] \tag{3.1}$$

where σ_x, σ_y and σ_z are the normal components of stress, and σ_{xy},σ_{yz} and σ_{xz} are the components of shear stress, as shown in Figure 3.2:

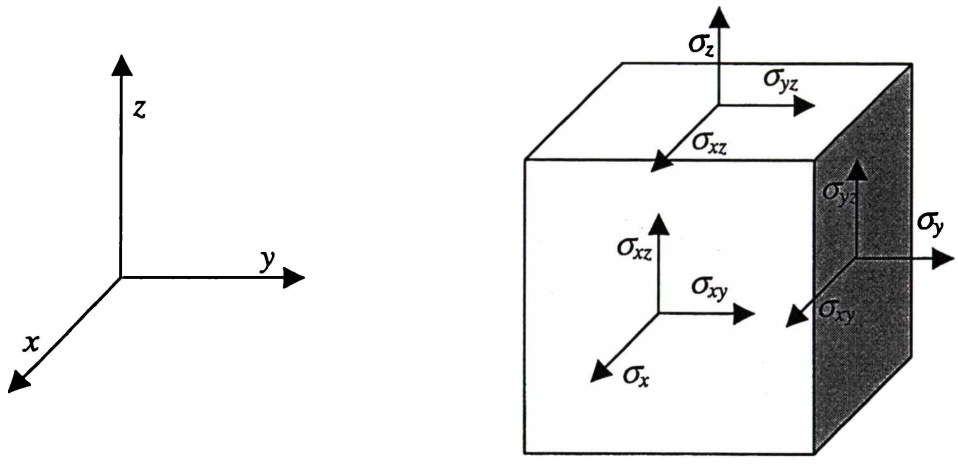

Figure 3.2. Element coordinate system and stress components.

If the material from which the loudspeaker cone is constructed is linear and elastic, the stress-strain relationship for each element can be written as:

$$\{\sigma\} = \mathbf{D}\{\varepsilon\} \tag{3.2}$$

where **D** is a 6×6 elasticity matrix calculated from the user-defined Young's modulus (E) and Poisson's ratio (ν) of the cone material, and $\{\varepsilon\}$ is the 6×1 vector of x, y, and z direct and shear strains for the element.

If the displacement of the nodes of an element is denoted by a displacement vector $\{u_n\}$, the displacement of any point in the element $\{u\}$ can be interpolated from $\{u_n\}$ by means of a matrix of shape functions **N**, which depend on the element type and geometry. Thus, we write:

$$\{u\} = \mathbf{N}\{u_n\} \tag{3.3}$$

The six strain components forming the strain vector $\{\varepsilon\} = [\varepsilon_x \ \varepsilon_y \ \varepsilon_z \ \varepsilon_{xy} \ \varepsilon_{yz} \ \varepsilon_{xz}]$ are calculated from:

$$\{\varepsilon\} = \mathbf{B}\{u_n\} \tag{3.4}$$

where **B** is known as the strain-displacement matrix and is generally composed of derivatives of the shape functions **N**.

The governing equilibrium equations can be derived for the finite element by applying the principle of virtual work [41, Section 2.2] and equating virtual changes in the internal strain energy of the element with the external work done on the element. This results in an equilibrium equation of the form:

$$\mathbf{M}_e\{\ddot{u}_n\} + \mathbf{K}_e\{u_n\} = \{F_n\} \tag{3.5}$$

where:

$\mathbf{K}_e = \int_V \mathbf{B}^T \mathbf{D}\, \mathbf{B}\, dV$ = Element stiffness matrix

$\mathbf{M}_e = \rho \int_V \mathbf{N}^T \mathbf{N}\, dV$ = Element mass matrix (ρ = mass density of the element.)

$\{\ddot{u}_n\} = \frac{\delta^2}{\delta t^2}\{u_n\}$ = vector of nodal accelerations

$\{F_n\}$ = vector of nodal forces

The corresponding equilibrium equation for the entire FE model can now be written as:

$$\mathbf{M}\{\ddot{u}\} + \mathbf{K}\{u\} = \{F\} \tag{3.6}$$

where $\mathbf{K}$ and $\mathbf{M}$ are the global stiffness and mass matrices for all the finite elements, and $\{F\}$, $\{u\}$ and $\{\ddot{u}\}$ are the global nodal force, displacement and acceleration vectors.

3.2.2 Modal Analysis

Modal analysis is the technique used to determine the frequencies and shapes of the natural modes of loudspeaker cones.

For an undamped cone in free, unforced vibration, equation 3.6 can be written:

$$\mathbf{M}\{\ddot{u}\} + \mathbf{K}\{u\} = \{0\} \tag{3.7}$$

The free vibration of the surface of a loudspeaker cone will be harmonic in nature, and can be written:

$$\{u\} = \{\phi\}_i \cos \omega_i t \tag{3.8}$$

where $\{\phi\}_i$ is the eigenvector representing the mode shape of the i^{th} natural frequency (ω_i) of the cone.

Substituting for $\{u\}$ and ignoring the oscillatory component, equation 3.7 becomes:

$$\left(-\omega_i^2 \mathbf{M} + \mathbf{K}\right)\{\phi\}_i = \{0\} \tag{3.9}$$

The non-trivial solution of this equation is:

$$\left|-\omega^2 \mathbf{M} + \mathbf{K}\right| = 0 \tag{3.10}$$

which constitutes an eigenvalue problem of the form:

$$\mathbf{K}\{\phi\}_i = \lambda_i \mathbf{M}\{\phi\}_i \tag{3.11}$$

Eigenvalue (λ_i) and eigenvector calculation and extraction is performed using the ANSYS SUBSPACE solver, as detailed in the ANSYS Theory Manual [41, Section

15.10.2]. Once the eigenvectors are calculated the mode shapes can be plotted, as shown in Figures 2.17, 2.18, and 4.14.

3.2.3 HARMONIC ANALYSIS

It is very often desirable to solve the time-dependent equations of motion of the loudspeaker cone in order to determine the frequency-dependent nature of its steady-state vibration. A harmonic analysis is performed by subjecting the FE model of the loudspeaker to a combination of forces and boundary conditions, and calculating the steady-state vibration at a number of frequencies.

The degree of energy loss in the vibrating cone material is modelled through the use of a viscous damping matrix **C**. The damping matrix is specified using a constant damping ratio ξ, which is defined as the ratio of actual damping to critical damping. The damping ratio is calibrated experimentally by comparing the magnitude of ripples in the measured and modelled Z_{mot} responses (refer Section 4.3.3). Having specified a value for ξ, the damping matrix is calculated from:

$$\{u\}^T[\mathbf{C}]\{u\} = 4\pi f\xi \tag{3.12}$$

The equations of motion for the finite element model of a loudspeaker cone subject to a sinusoidal force become:

$$\mathbf{M}\{\ddot{u}\} + \mathbf{C}\{\dot{u}\} + \mathbf{K}\{u\} = \{F\} \tag{3.13}$$

where **M**,**C**, and **K** are the mass, damping and stiffness matrices respectively, and $\{F\}$ is the applied force vector. In general, the only boundary conditions of harmonic analyses are that the nodes on the inner edge of the cone are constrained to pure axial movement while an axial force of 1N is applied to them. If the applied force is purely sinusoidal in nature, we may write:

$$\{F\} = \{F_{\max}\}e^{j\omega t} \tag{3.14}$$

The steady-state harmonic displacements of the cone will now be given by:

$$\{u\} = \{u_{\max}\}e^{j\phi}e^{j\omega t} \tag{3.15}$$

where $\{u_{max}\}$ is the displacement magnitude and ϕ is the displacement phase shift, which can be different for each point of calculated displacement.

Thus, equation 3.13 may be written (omitting the $e^{j\omega t}$ factor):

$$\left(-\omega^2\mathbf{M} + j\omega\mathbf{C} + \mathbf{K}\right)\{u\} = \{F\} \tag{3.16}$$

All harmonic analyses in this thesis utilise the ANSYS "full solution" ([41], Section

17.4) method that solves equation 3.16 directly for $\{u\}$ over a number of different frequencies. The total displacement vector $\{u\}$ allows the displacement shape of the cone to be visualised at every calculated excitation frequency. However, the axial displacement of the node at the inner neck of the cone, denoted u_{ax}, is of particular importance, as the axial admittance Y_{ax} is given by:

$$Y_{ax} = \frac{j\omega u_{ax}}{F_{ax}} \tag{3.17}$$

where F_{ax} is the applied axial force.

The modelled Z_{mot} response can be calculated from Y_{ax} using Equation 2.14. By comparing the calculated motional impedance response with the measured Z_{mot} response of the loudspeaker being modelled (Section 3.3.1), the FE model can be validated, and fine-tuned if necessary.

3.2.4 2D Axisymmetric Models

It is often convenient to take advantage of axial symmetry when creating the finite element model of a loudspeaker cone. Two-dimensional finite element models of loudspeaker cones are much simpler to mesh and quicker to solve than their full three-dimensional counterparts as they require only the section profile of the speaker to be described and meshed. The section profile of an axisymmetric loudspeaker is shown in Figure 3.3:

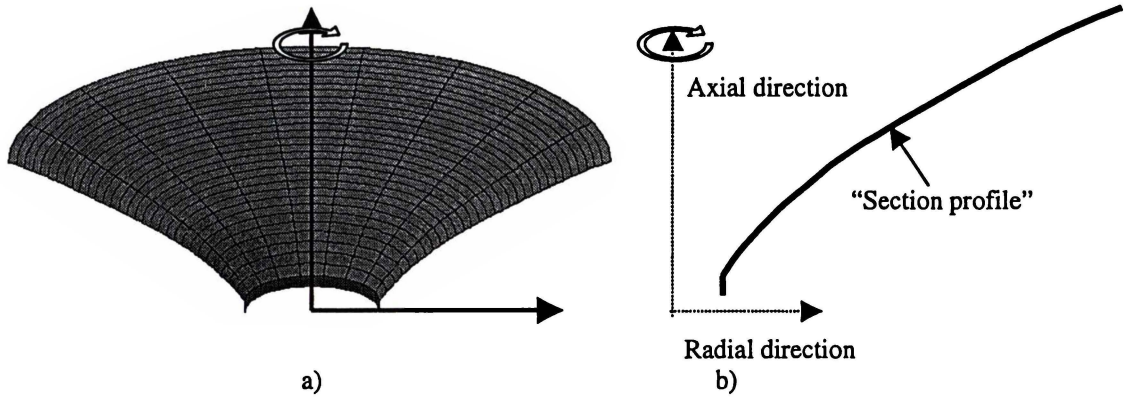

Figure 3.3. a) Cutaway view and b) section profile of axisymmetric loudspeaker.

The section profile of the cone is typically divided into 31 elements, with element 1 at the inner edge of the cone and element 31 at the outer edge of the cone. As discussed in Section 4.3.1, the choice of 31 elements is a compromise between the requirements of determining the mode shapes and frequencies with sufficient accuracy, and minimising the processing time.

Two-dimensional models are generated by explicitly defining the positions of the nodes in terms of x and y coordinates. The nodes are then connected by elements of either two

or four nodes, as described in Sections 3.2.4.1 and 3.2.4.2.

3.2.4.1 2 NODE 2D SHELL ELEMENTS

The simplest axisymmetric element used to characterise the loudspeaker cone is the SHELL61 2D axisymmetric-harmonic shell element provided by ANSYS. This element is characterised by two nodes (I, J) and two thicknesses (TK(I), TK(J)) as follows:

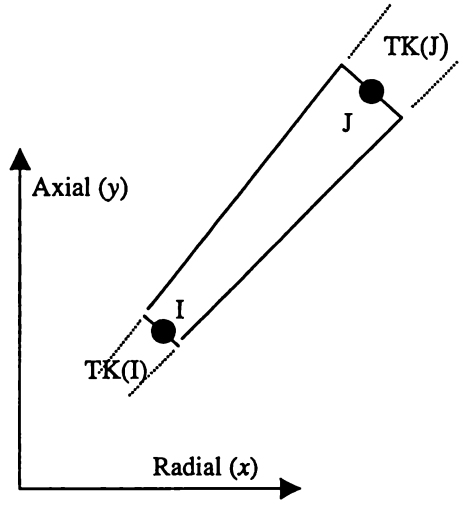

Figure 3.4. Geometry of a SHELL61 element.

A series of 32 nodes connected by 31 SHELL61 elements is used to describe the edge profile of the cone. The thickness at each end of the element is user-defined, while the thickness between the nodes of an element is determined by a linear interpolation between the element's two end thicknesses. This allows cones of differing "thickness profiles" to be defined. The thickness profile of the cone has an important effect on mode shapes and frequencies, as discussed in Section 5.3.

SHELL61 has four degrees of freedom, allowing displacement in the radial and axial directions, and also rotation of the nodes around the z (radial-axial) axis.

In 2D models the motion of nodes 1 and 2 is constrained to the axial direction only, while all other nodes are free to move in radial or axial directions and rotate about their nodal positions in the radial-axial plane. A force of 1N is applied to node 1 in the positive axial direction.

This 2D model is used to calculate the natural axisymmetric mode shapes and frequencies (in 2D) of a normal loudspeaker cone, and their dependence on material properties, cone thickness, and thickness profile, as discussed in Chapter 5.

3.2.4.2 4 NODE 2D SOLID ELEMENTS

A 2D 4 node element, PLANE42 is utilised to model the cone and surround when the surround was attached to the outer edge of the cone as in Section 4.5.3. In contrast to the SHELL61 element, the thickness of a PLANE42 element is defined implicitly by means of four nodes I,J,K,L. A PLANE42 element is shown in Figure 3.5.

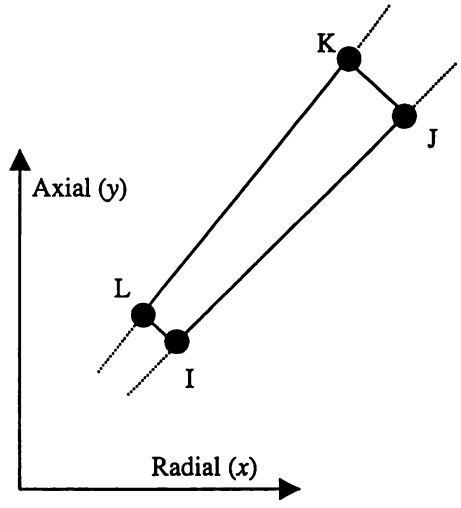

Figure 3.5. Geometry of PLANE42 element.

The finite element model of the loudspeaker cone using four-node 2D solid element consists of 64 nodes connected by 32 elements, as illustrated in Figure 3.6:

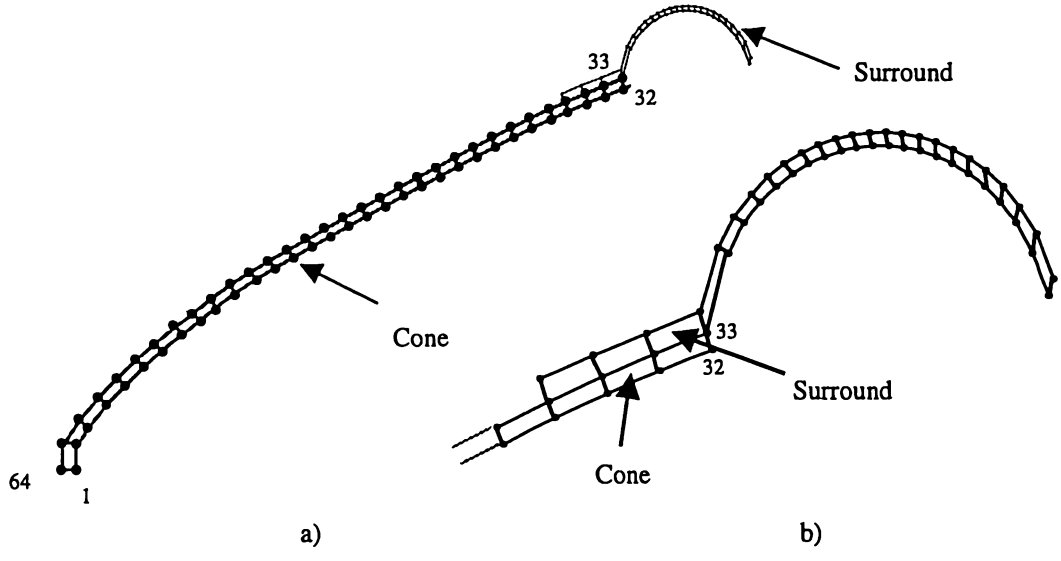

Figure 3.6. FE model of a) cone section profile and b) surround using PLANE42 elements

The butyl-rubber surround is modelled by 24 elements, arranged as in Figure 3.6b). PLANE42 models readily allow the finite element model of the surround to be attached to the outer edge of the cone by "gluing" the upper nodes of the three outermost elements of the cone to the lower nodes of the three innermost elements of the surround.

The nodes of PLANE42 elements are free to move in both x and y directions. For harmonic analyses of PLANE42 models, an axial force of 0.5N is defined on nodes 1 and 64, while nodes 1,2,63,64 are constrained to have no movement in the radial direction. When this element is used to model the cone and surround, the outermost nodes of the surround are constrained from any movement, while the axial force is divided equally over nodes 1 and 64.

3.2.5 3D MODELS

In order to model non-axisymmetric loudspeaker cones, such as those considered in Chapter 6, a full three dimensional finite element model is required. The 3D models employed to model "slotted" loudspeaker cones utilise 4 node 3D SHELL63 elements. Nodal positions are not defined explicitly when 3D elements are used; rather, the geometry of the cone is defined using solid modelling techniques, and the model meshed using the ANSYS meshing algorithms.

Meshed models of 3D axisymmetric cones are rotationally symmetric and uniform, while meshes for "slotted" cones are less uniform, particularly near slot edges.

The SHELL63 elastic shell element provided by ANSYS is used to create a 3D model of axisymmetric and slotted loudspeaker cones. The SHELL63 element is defined in Cartesian space by its four nodes I, J, K and L, and the thickness at each node. Each node of SHELL63 elements has translational and rotational degrees of freedom in x, y, and z directions.

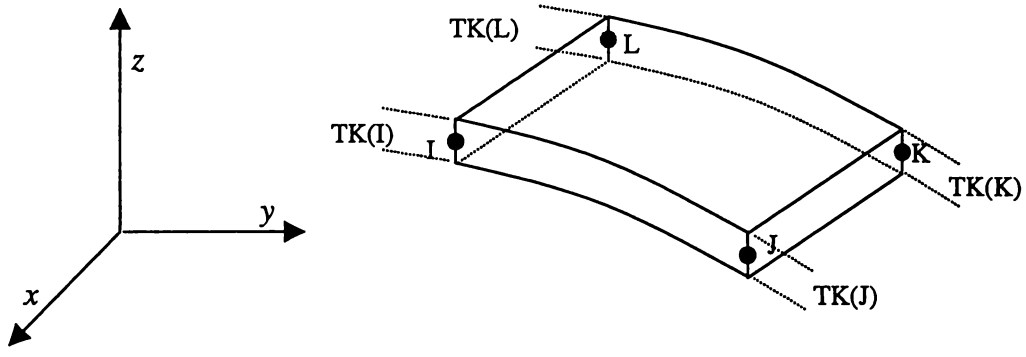

Figure 3.7. Geometry of SHELL63 element.

Although this element allows for a different thickness at each node, we assume that the loudspeaker's thickness profile is uniform, and the loudspeaker can be approximated as a 3D shell of constant thickness. This slightly reduces the accuracy of the FE model (refer Figure 4.9), but greatly simplifies the process of meshing slotted cones.

3.2.6 MODELLING SOUND RADIATION

The previous sections outlined the Finite Element technique that is used to calculate the displacement and velocity response of all points on the loudspeaker's surface. The surface vibration of the loudspeaker cone subsequently sets in motion a sound wave that propagates out into the air. This section gives a brief overview of the boundary element method that is used by the SYSNOISE software to calculate the sound pressure response of the loudspeaker, using the ANSYS structural results as inputs. A more detailed mathematical description can be found in the SYSNOISE theoretical manual.

In general, wave propagation through a linear homogeneous media such as air, is governed by the 3D wave equation:

$$\nabla^2 p(r,t) = \frac{1}{c^2}\frac{\partial^2 p(r,t)}{\partial t^2} \tag{3.18}$$

where ∇^2 is the Laplacian operator, c is the speed of sound in the media, and $p(r,t)$ is the pressure field at the point defined by vector r at time t. If the surface velocity distribution of the vibrating object is purely sinusoidal in nature, equation 3.18 will describe sinusoidal pressure solutions of the form $p(r,t) = p(r)e^{i\omega t}$, and reduces to the Helmholtz equation:

$$\nabla^2 p + k^2 p = 0 \tag{3.19}$$

where k is the wavenumber $\left(\frac{\omega}{c}\right)$ and p is the complex pressure amplitude.

Sound radiation problems can be solved by considering the surface of the vibrating object to be made up of a series of infinitesimally small point sources of spherical sound waves. The sound pressure field can then be calculated by summing the contributions of each of these point sources, along with appropriate boundary conditions, to the total pressure throughout the fluid. An acoustic point source is defined as the limit as r→0 from a uniform pulsating sphere of radius r and finite source strength q:

$$q = \rho_{air} \cdot S \cdot v \tag{3.20}$$

where ρ_{air} = fluid density

S = surface area of sphere

v = surface velocity

The pressure field around the point source has to satisfy equation 3.19, while at the position of the point source itself (Y):

$$\nabla^2 p + k^2 p = -q \cdot \delta(X - Y) \tag{3.21}$$

In equation 3.21, X is the measurement point, Y is the position of the point source, and $\delta(X-Y)$ is the 3D Dirac function. The pressure field at point X due to the source at point Y that satisfies equation 3.21 is written:

$$p(X,Y) = q\frac{e^{jkr(X,Y)}}{4\pi r(X,Y)} \tag{3.22}$$

In equation 3.22, $r(X,Y)$ denotes the distance between point X and source location Y.

Green's third theorem (Equation 3.23) relates a surface integral S to a volume integral over V bounded by S for any two functions ψ and ϕ that are smooth and non-singular in V. (∂_n is the derivative in the outward normal of S.)

$$\int_S (\phi \cdot \partial_n \psi - \psi \cdot \partial_n \phi) dS = \int_V (\phi \cdot \nabla^2 \psi - \psi \cdot \nabla^2 \phi) dV \tag{3.23}$$

If ψ is defined to be a Green's function $G(X,Y)$ equal to the pressure due to a point source of strength 1 and ϕ is defined to be the sound pressure p, equation 3.23 can be used to relate the pressure at a point X in volume V to an integral across the surface of the vibrating loudspeaker.

$$\psi = G(X,Y) = \frac{e^{jkr(X,Y)}}{4\pi r(X,Y)} \tag{3.24a}$$

$$\phi = p \tag{3.24b}$$

After substituting equations 3.24 into equation 3.23, and considerable rearrangement and simplification [42, p29], the following integral relationship is attained:

$$p(X) = \int_S (p(Y) \cdot \partial_n G(X,Y) - G(X,Y) \cdot \partial_n p(Y)) dS(Y) \tag{3.25}$$

Equation 3.25 relates the pressure at point X enclosed by volume V to an integral of the pressure and pressure gradient across the radiating surface S. The pressure gradient follows directly from the normal velocity of the radiating surface, according to:

$$\partial_n p(Y) = -j\omega\rho v_n \tag{3.26}$$

The value of $p(Y)$ at the radiating surface is calculated by solving a series of m simultaneous equations, where m is the number of FE nodes. Once the pressure and pressure gradient at the radiating surface are calculated from the FE results, the pressure at any point in the (unbounded) radiating volume follows from a discretised form of equation 3.25.

The process of applying this boundary element technique and calculating the sound pressure response at points in the sound field was performed by the SYSNOISE software package. The SYSNOISE version used was limited to 200 nodes, which prohibited the calculation of sound pressure from full 3D ANSYS models, as such models require at least 1200 nodes to be used. Further, the time taken to calculate the sound pressure response even at just one frequency is prohibitive for such a large model. Thus, the calculation of sound pressure results was restricted to 2D axisymmetric loudspeaker cones such as those considered in Chapters 4 and 5.

The process of calculating the sound pressure field developed by a non-rigid vibrating loudspeaker cone is summarised in Figure 3.8.

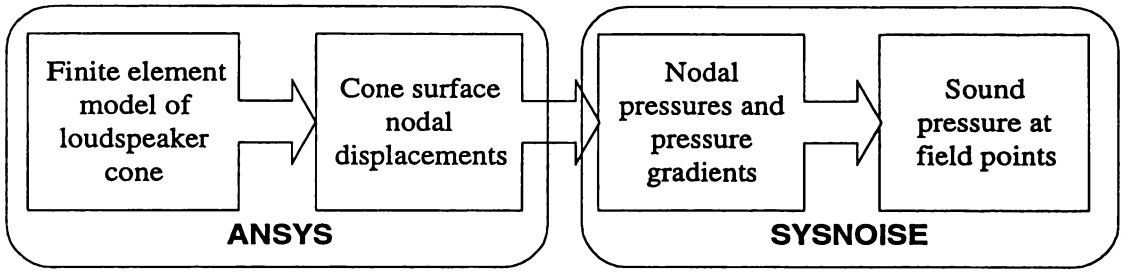

Figure 3.8. Flow chart for calculating sound pressure results using a coupled ANSYS-SYSNOISE model.

The process of Figure 3.8 is *uncoupled*; that is, the nodal displacements of the loudspeaker cone are assumed to be unaffected by the radiation impedance offered by the air in which the loudspeaker cone vibrates. The ANSYS FE model itself does not account for radiation impedance since this requires a sound field to be meshed with acoustic finite elements, at considerable processing expense.

Although SYSNOISE does allow the radiation impedance to be accounted for at extra processing expense, we choose to not utilise this feature. This commonly adopted approach [6, 30] simplifies and speeds up the solving process with no appreciable decrease in modelling accuracy. Since the measured motional impedance response of the loudspeakers is substantially identical whether measured in air or in a vacuum chamber, and the modelled and measured sound pressure responses show good correlation, this assumption seems justified.

Further, the loudspeaker is assumed to be baffled, and to radiate into an unbounded (and therefore anechoic) volume. In practice, all sound pressure measurements were made in an anechoic chamber with the loudspeaker mounted in a baffle, but with the loudspeaker's outer surround removed. This resulted in a small gap between the edge of the cone and the baffle, but since the baffle has negligible effect on frequencies above 1kHz, measured and modelled results still show a good correlation.

In general, the finite element model consisted of a total of 31 elements and 32 nodes. The sound pressure response was calculated at field points directly in front of the

loudspeaker at a distance of 1m and 10m. The sound pressure at a further 36 points placed at 2.5° increments around a 90° arc of radius 10m were calculated and used to generate the polar response plot of the loudspeaker (refer Figure 2.20).

3.3 MEASUREMENTS

The finite element and boundary element methods discussed in Section 3.2 allow the surface displacement of the loudspeaker cone, and the resulting sound pressure response to be calculated. The surface displacement response is used to calculate the theoretical motional impedance response Z_{mot} of the loudspeaker cone, while the BEM is used to calculate the sound pressure on axis, p_{ax} at a distance of 1m. As both of these parameters can be readily measured for a real loudspeaker, they are useful tools to aid the calibration and validation of the FE and BE models.

This section gives an overview of the techniques and equipment used to measure the motional impedance and on-axis sound pressure responses of the loudspeaker cone.

3.3.1 MOTIONAL IMPEDANCE

As shown in Chapter 2, the resonant and antiresonant frequencies of an axially driven loudspeaker cone have a profound effect on the measured Z_{mot} response of the loudspeaker. Since Z_{mot} can easily be calculated by post-processing FE displacement results, the measured motional impedance response is a convenient tool for calibrating FE models.

In order to measure the motional impedance of a speaker we employ the "blocked voice coil" method [6, 9]. A constant magnitude current I (Appendix IIa) is passed through the speaker under test (Z_{test}). As shown in Chapter 2, Z_{test} can be expressed as the sum of an electrical and motional impedance and so we write:

$$Z_{tot(test)} = Z_{elec(test)} + Z_{mot(test)} \tag{3.27}$$

The same current I then passes through a reference loudspeaker (Z_{ref}) which is simply an identical loudspeaker with its voice coil glued in place so that no movement can occur. Thus, the total impedance of the reference loudspeaker has no motional dependence:

$$Z_{ref} = Z_{elec(ref)} \tag{3.28}$$

By using a difference amplifier (Appendix IIb) to instantaneously subtract the voltage across the reference loudspeaker from the voltage across the test loudspeaker, and assuming that $Z_{elec(ref)} = Z_{elec(test)}$, the voltage across the test loudspeaker due to motional impedance alone is measured (refer Figure 3.9):

$$V_{mot} = V_{test} - V_{ref} \tag{3.29}$$

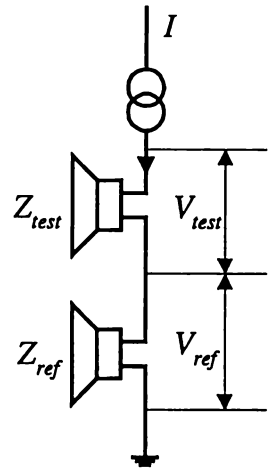

Figure 3.9. Measurement of motional impedance using a constant current amplifier and reference voice coil.

Z_{mot} is determined from $Z_{mot} = V_{mot}/I$, allowing the motional impedance to be measured as a function of frequency.

In practice, measurements of Z_{mot} were carried out using a swept-spectrum method, with V_{mot} measured using a HP3478A digital multimeter, and the excitation signal applied in frequency steps by a HP3314A programmable function generator. Equipment control and data collection was performed by custom LabView software using the General Purpose Interface Bus (GPIB) protocol. In general, 50 measurements were taken in both 10-100Hz and 100Hz-1kHz ranges, with a further 500 in the range 1kHz–20kHz.

All Z_{mot} measurements were made with the loudspeaker mounted in a vacuum chamber in order to conveniently preclude any sound radiation. The measured motional impedance response was identical when the loudspeaker was mounted in an anechoic chamber.

Once the Z_{mot} curve has been measured, the break-up frequencies of the loudspeaker can be accurately determined, and compared to the frequencies predicted by FE model modal analyses. Further, the overall shape of the Z_{mot} response is a useful tool for calibrating the FE model, and characterising the behaviour of the loudspeaker.

3.3.2 MOTOR PARAMETERS

Before calculating the motional impedance response from the Y_{ax} response predicted by the FE model of the cone, the loudspeaker's motor parameters must first be determined. The motor system parameters: total compliance, moving mass, mechanical resistance and motor strength are particularly important for matching the Z_{mot} response at low frequency, when the loudspeaker is under stiffness and resistance control.

Motor compliance is determined by the spring resistance force provided by the spider, and, to a lesser extent, that of the outer surround. Compliance can be measured by adding known masses ($0 < m < 250$g) to the centre of the loudspeaker, which is laid flat on its magnet. The added mass provides a force on the centre of the cone, which acts against the restoring force of the spider and surround, and causes the cone to lower. The displacement of the lowered cone is subsequently measured to within 10 microns using a laser range finder. The compliance can then be calculated by finding the inverse slope of a graph of the applied force versus the cone displacement, as shown in Figure 3.10.

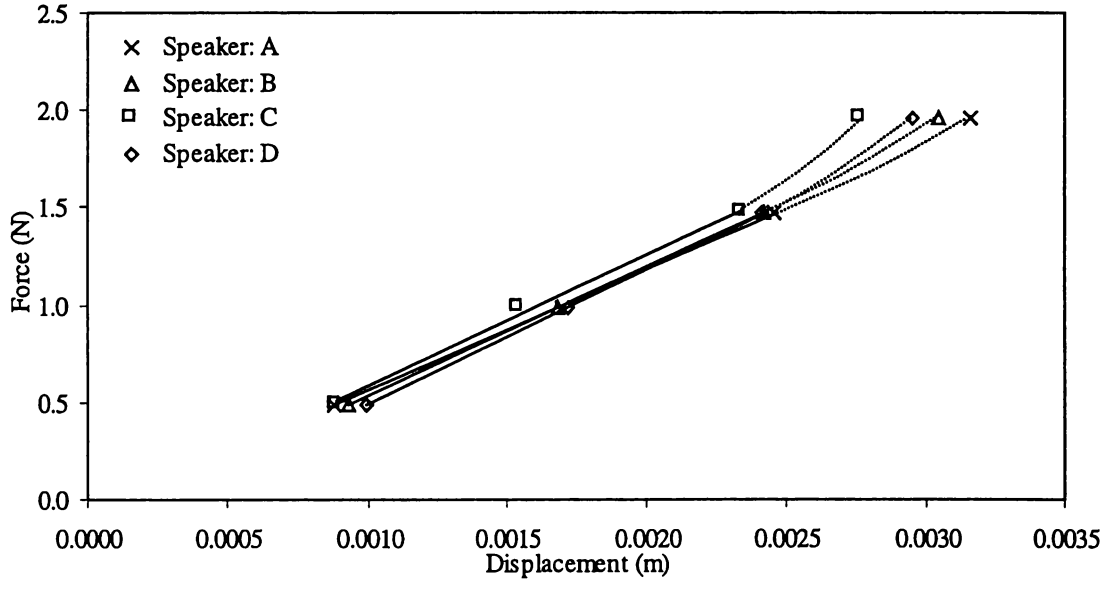

Figure 3.10. Graphs of cone force versus displacement for loudspeakers A-D

Figure 3.10 shows that the force displacement-relationship is linear for displacements of less than $\leq$ 2.5mm and approximately the same for all four motor systems measured. The slope of each of the above plots gives the spring constant k for that particular motor system, while the inverse of the slope gives the compliance. The spring constants and compliances are summarised in Table 3.1.

Speaker	Spring constant (N/m)	Compliance (m/N)
A	620	1.61×10^{-3}
B	660	1.52×10^{-3}
C	670	1.50×10^{-3}
D	690	1.45×10^{-3}

Table 3.1. Spring constants and compliances for loudspeakers A-D.

The electromechanical coupling factor $B\ell$ is also found by applying forces to the cone by means of added weights. As previously, a known weight is added to the cone by means of small masses, and then the cone restored to its equilibrium position by passing a DC current through the voice coil. The cone displacement is measured using a laser range finder to ensure that the cone is accurately restored to equilibrium. Since $F = BI\ell$, the slope of a graph of applied force versus voice coil current (Figure 3.11) yields the motor constant $B\ell$.

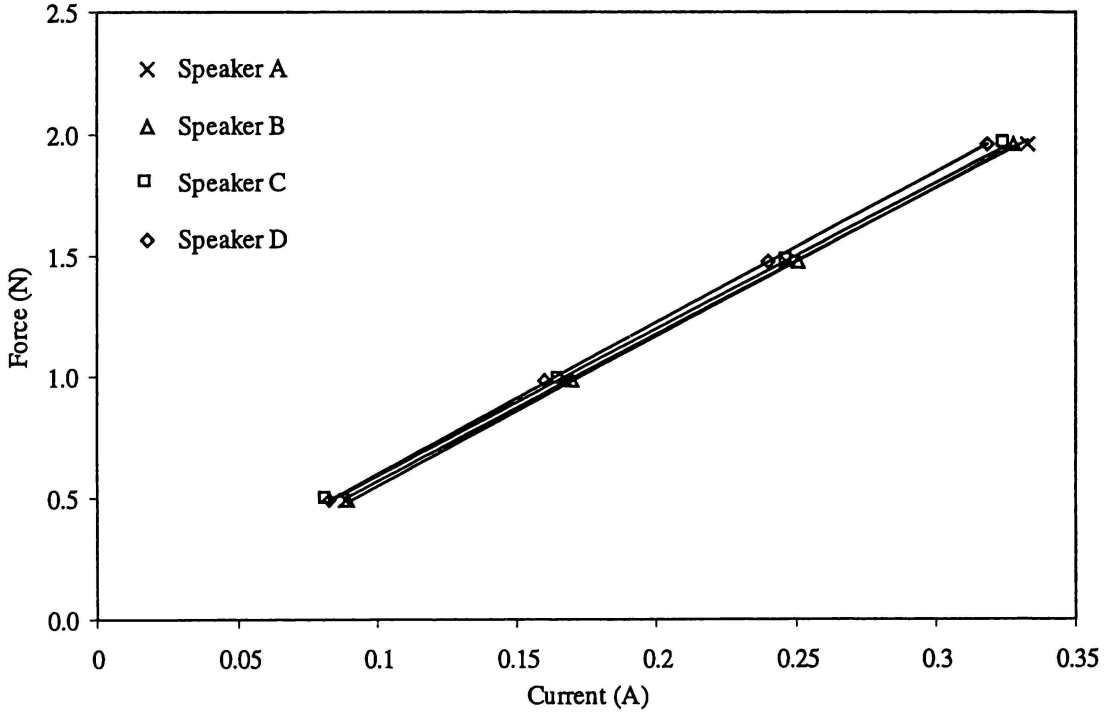

Figure 3.11. Graphs of cone force versus voice coil current for loudspeakers A-D.

The slopes of all four plots in Figure 3.11 are approximately identical, and give a value of $B\ell \approx 6.2$.

Once the compliance of each loudspeaker system has been calculated, its moving mass can also be found by experimentally determining the free-air-resonance f_0. The mass of the loudspeaker then follows by rearranging equation 2.11 to give:

$$M_{tot} = \frac{1}{4\pi^2 f_0^2 C_{tot}} \tag{3.29}$$

The free air resonant frequencies of all four loudspeakers were measured and are shown with the calculated loudspeaker moving masses in Table 3.2.

Speaker	Free air resonance f_0 (Hz)	Total mass M_{tot} (g)
A	35	12.8
B	36	12.9
C	35	13.8
D	36	13.5

Table 3.2. Free air resonance and total moving mass of loudspeakers A-D.

The mechanical resistance of the loudspeaker motor system determines the system's "Q" near f_0. While the mechanical resistance can be measured accurately, its exact value is not critical, and choosing a value of R = 0.1 yields an appropriately shaped Z_{mot} response near free air resonance for all four loudspeakers.

3.3.3 Sound Pressure

All sound pressure measurements were made in an anechoic chamber using a B&K precision microphone and an HP3561A audio spectrum analyser. The B&K microphone is specified accurate to ±0.5dB across the audio spectrum. The spectrum analyser's standard FFT measurement technique was used, with the transformed measurements averaged 500 times.

Measurements were made with the microphone at a distance of approximately one metre, with the loudspeaker driver mounted in a standard IEC baffle. In general, the sound pressure response was measured using 400 frequency bins linearly spaced at 50Hz intervals over the range 10Hz – 20kHz.

CHAPTER 4

CHARACTERISATION OF LOUDSPEAKER CONE RESONANCE

4.1 OVERVIEW

In this chapter a finite element (FE) model of an axisymmetric loudspeaker cone is developed. Modelled Z_{mot} responses are used to calibrate the FE model to the measured responses of two particular loudspeaker cones, A and C. The measured and modelled sound pressure responses are also used as a final check of model validity. The FE model for cone C is subsequently employed to fully characterise the natural resonant behaviour of an axisymmetric loudspeaker cone.

The Y_{ax} and Z_{mot} responses are calculated from the finite element model of cone C, allowing significant resonant and antiresonant modal frequencies to be identified. Subsequently, the displacement patterns of these modes are extracted in order to characterise the nature of cone resonance.

The FE model is then extended to include the outer surround, which is an integral part of an electrodynamic loudspeaker. The effect of the outer surround on the axial admittance characteristic and modes shapes of the loudspeaker is determined and discussed.

4.2 INTRODUCTION

In Chapter 3, the necessary tools and techniques for creating a FE model of a loudspeaker cone were outlined. These tools allow the mathematical equations describing the physical behaviour of a loudspeaker cone to be numerically solved, resulting in a detailed description of the nature of loudspeaker cone resonance. This

description can be utilised to predict the effects of changes in the loudspeaker cone design on the measured characteristics of a real loudspeaker.

However, for any FE model to be of any practical use, it must first be calibrated and validated. By comparing the characteristics predicted by the FE model with the measured characteristics of a real loudspeaker cone, the validity of the model can be confirmed.

Two characteristics of a loudspeaker driver that closely reflect the loudspeaker cone's resonant behaviour are the motional impedance (Z_{mot}) and on-axis sound pressure (p_{ax}). Of these, the motional impedance is the simplest to measure repeatably and accurately, using the method described in Section 3.3.1. Since the motional impedance of a vibrating loudspeaker can also be calculated easily from the FE model, the Z_{mot} response is a convenient calibration criterion.

Measured characteristics such as motional impedance and sound pressure can differ significantly between nominally identical loudspeakers (even between those from the same batch), due to differences in cone thickness and/or material properties. Consider for example, the measured motional impedance responses for two loudspeaker cones, A and C, shown in Figure 4.1. Loudspeakers A and C are nominally identical 6½-inch polypropylene loudspeakers of the type described in Chapter 2, selected from different batches manufactured almost a year apart:

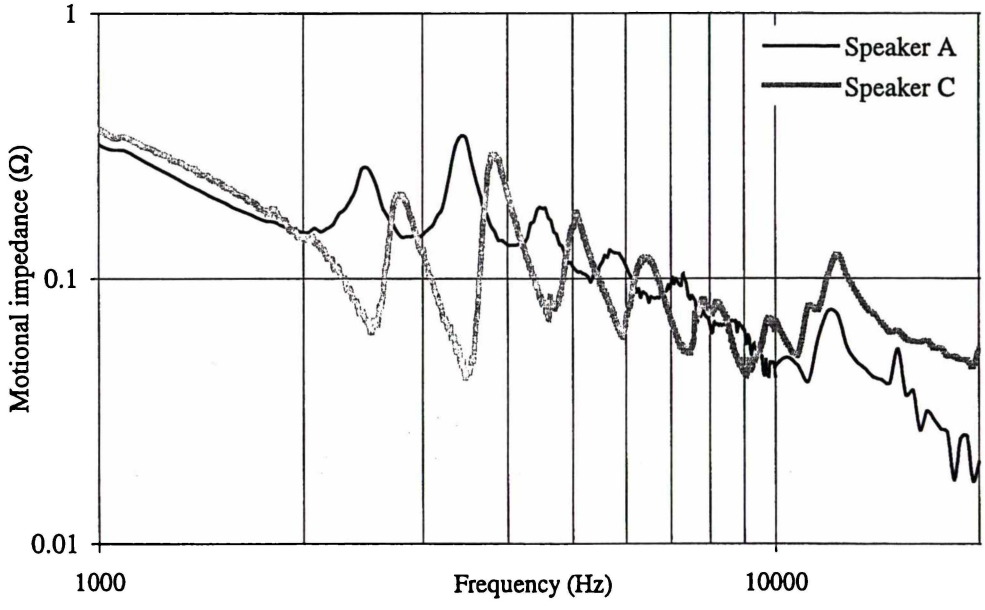

Figure 4.1. Measured Z_{mot} response for loudspeakers A and C

The results of Figure 4.1 highlight the considerable variations that can exist even between nominally identical loudspeakers. Not only do the natural frequencies of these two loudspeakers differ considerably, but also the shape of the motional impedance responses near each resonance and antiresonance. Further, the measured motional impedance response for a loudspeaker is sometimes found to change over time, perhaps because of changes in the properties of the cone material. The effects of variations in

loudspeaker cone material properties, and aspects of cone geometry are considered in detail in Chapter 5.

Consequently, if a FE model is required to represent any particular loudspeaker of a given geometry and cone material to a very high degree of accuracy, calibration to that particular loudspeaker's measured characteristics is necessary. This is achieved by adjusting the material properties used to create the FE model until acceptable agreement between measured and modelled results is attained. While this procedure can be carried out for each loudspeaker if necessary, much useful information can still be gained from the FE model by selecting material properties that are typical for the loudspeakers being modelled.

In Section 4.3, the FE model is calibrated to the measured characteristics of cones A and C, in order to demonstrate the degree of correlation between measured and modelled results. The calibrated material properties for cone C are then assumed to be representative of polypropylene cones of these dimensions, and are used in subsequent FE models.

4.3 MODEL GENERATION AND VALIDATION

The generation of the finite element model progressed in two main stages. Firstly, a two dimensional axisymmetric model was generated and calibrated using the measured Z_{mot} response of cones A and C. Secondly, the FE model was extended to three dimensions, in order to allow the full 3D mode shapes to be extracted, and non-axisymmetric loudspeakers to be considered. All three dimensional cone models considered herein are based on the calibrated material properties for loudspeaker cone C.

The steps taken to generate and calibrate the 2D axisymmetric cone model are summarised in Figure 4.2.

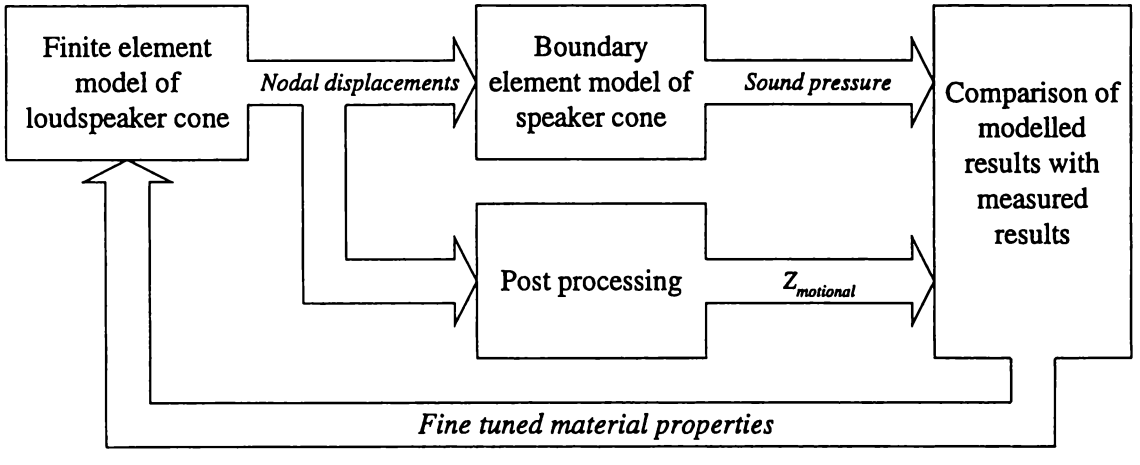

Figure 4.2 Procedure followed in calibration of FE models

This procedure can be summarised as follows:

1. Using the manufacturer's specified material properties, and the measured cone

geometry, develop a two-dimensional ANSYS model of a loudspeaker cone with no surround. (Initially the effect of the surround is neglected allowing the natural resonances of the cone itself to be modelled.)

2. Solve the model for the displacement response of each node along the edge profile of the cone for the frequency range 100Hz – 20kHz.

3. Use the nodal displacement results from ANSYS as boundary condition inputs to a SYSNOISE model of the cone in order to solve for the sound pressure field; by post-processing the nodal displacement results, calculate the motional impedance of the cone.

4. Validate the FE model by comparing modelled motional impedance results and modelled sound pressure results with the measured characteristics of cone with no surround.

5. Fine tune the material properties (Young's modulus, damping ratio, Poisson's ratio, and mass density) and repeat steps 2-5 as necessary.

By following this process, material properties were calibrated for loudspeakers A and C.

4.3.1 Cone Geometry and Physical Properties

In order to define accurately the shape of the loudspeaker cone in the FE model, the cone's meridional (from inner to outer edge) profile was measured to a resolution of 10-micron using a laser range finder. The resulting section profile is shown in Figure 4.3.

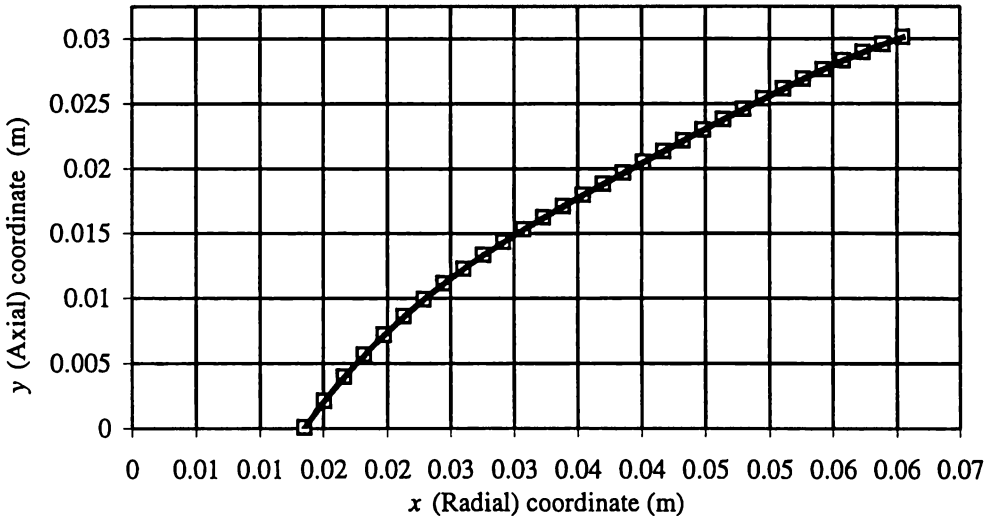

Figure 4.3. Section profile of loudspeaker cone, interpolated with 5th order polynomial function

A polynomial curve was fitted to the measured cone edge profile data resulting in a function describing y, the axial component of the cone shape in terms of the x, the radial coordinate.

The n nodal positions were explicitly defined by dividing the x coordinate range into n-1 equally spaced sections and calculating the corresponding y coordinate for each value of x. In addition, a further node was placed 2.25mm below the innermost node defined by the curve of Figure 4.3 in order to model the inner "neck" of the cone.

Thirty-two nodes were used to define the edge profile of the loudspeaker cone itself. The designers of SYSNOISE recommend that at least six elements be used to discretise each acoustic wavelength in air. At 20kHz, the acoustic wavelength is ≈1.7cm; using thirty-two nodes results in an element density of ~10 elements per acoustic wavelength at this frequency. In practice the minor improvement in modelling accuracy afforded by exceeding the number of nodes recommended by this rule of thumb was found to be more than offset by the increased expense in processing time.

Of considerable importance to the accuracy of the finite element model of the cone is the variation of cone thickness from inner to outer edge – the cone thickness profile. A typical vacuum-formed cone's thickness can vary by up 20% from its nominal value, and is usually thinner at the inner and outer edges than in the middle. In order to account for this manufacturing anomaly, the thickness profile for cone C was measured using a micrometer, and is shown in Figure 4.4.

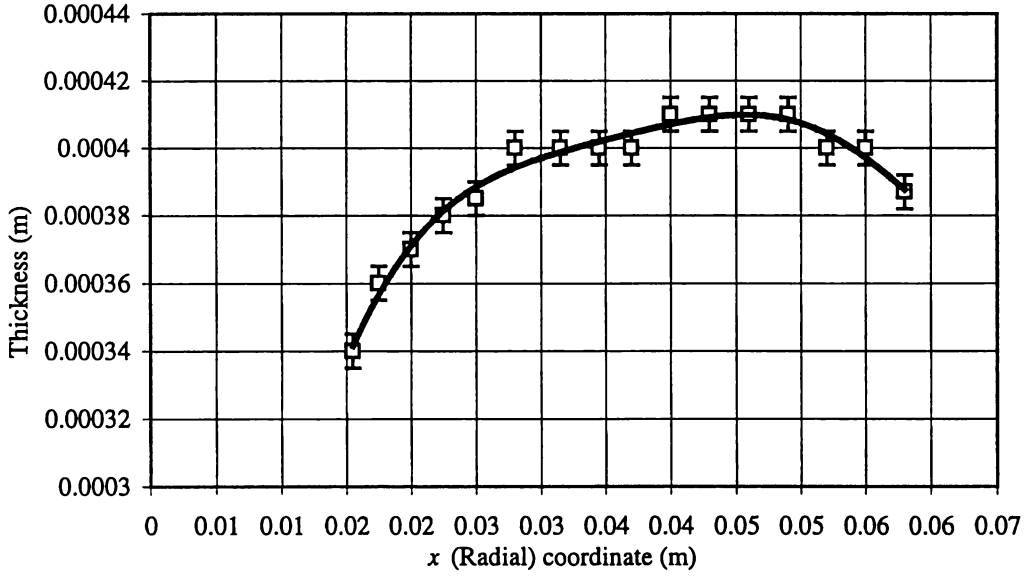

Figure 4.4. Cone C thickness profile as measured by micrometer; interpolated by a 6th order polynomial.

As before, a polynomial was fitted to the measured thickness variation and subsequently used to explicitly define the thickness of the cone t_x in terms of the radial coordinate. This function is then used to explicitly define the thickness at each node in the FE model.

Although the exact thickness and thickness profile varies slightly from cone to cone, and batch to batch, the results shown in Figure 4.4 (taken from loudspeaker C) are typical of the thickness variation trend from inner to outer edges.

As mentioned in Chapter 3, it is also important to model the total moving mass of the loudspeaker. This includes not only the mass of the cone and voice coil/former, but also the mass of the glue used to attach the voice coil to the cone neck. Furthermore, there is an additional component of moving mass contributed by the spider and external voice coil connection wires.

In general, the additional moving mass contributed by the voice coil, spider and glue can be accounted for by adding in an additional term while post-processing, and need not be included in the FE model. However, this becomes impractical if the sound pressure response is to be calculated from the FE model results.

In order to expand the FE model to include the extra moving mass, a 1cm long element of the same thickness as the inner neck of the loudspeaker cone was attached to the innermost node (node1). By defining an extremely large Young's modulus for this material, and choosing an appropriate mass density, the element simulates an almost infinitely stiff ring mass.

The actual total moving mass of the assembled loudspeaker is easily determined from the free-air resonant frequency, and the previously measured compliance of the speaker's motor system. By subtracting from this the mass of the loudspeaker cone (determined from the ANSYS model), an appropriate value for the mass density of the additional moving mass ring was determined.

The loudspeaker cone material is mica-loaded polypropylene sheet, and has the following manufacturer-supplied characteristics:

Property:	Value:
Mass density:	1100 kg/m^3
Young's modulus:	3×10^9 N/m^2
Poisson's ratio:	0.25

Table 4.1. Polypropylene loudspeaker cone properties as supplied by loudspeaker cone manufacturer

These material properties, while approximate, allow an initial finite element model to be generated and compared with measured results.

4.3.2 INITIAL 2D FE MODEL

A simple two-dimensional axisymmetric model consisting of 33 explicitly defined nodes was generated using SHELL51 elements, as shown in Figure 4.5. The inner edge of the cone was constrained to purely axial motion by means of a zero displacement boundary condition, while all other nodes were unrestricted. Further, a 1N frequency independent axial force was applied to the innermost node (Node 1) to simulate the force generated by a constant-current driven voice coil.

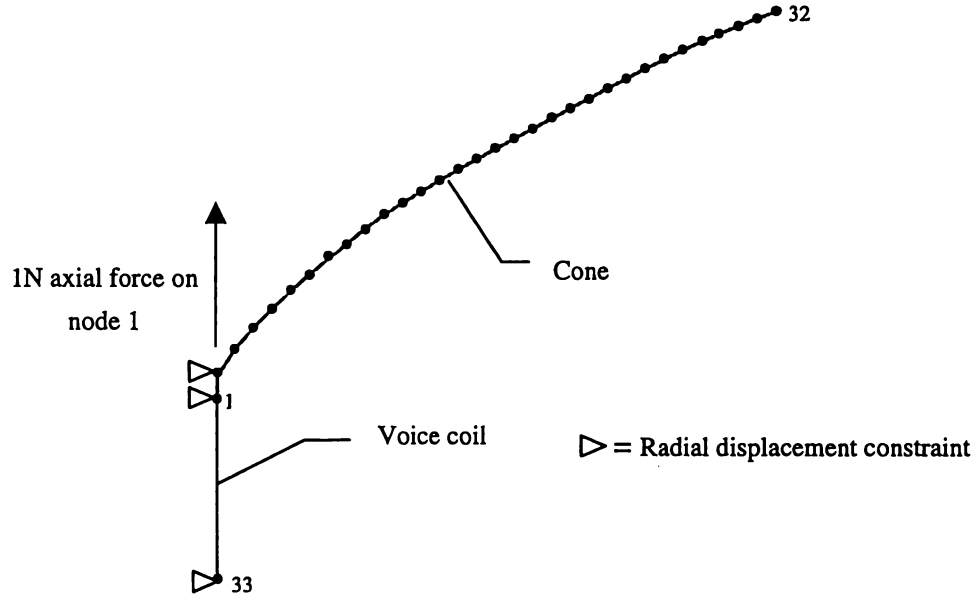

Figure 4.5. Finite element model of loudspeaker cone and voice coil.

A harmonic analysis was performed over the frequency range 10Hz – 20kHz yielding the displacement response of every node. Subsequently, the axial displacement results for node 1 were post-processed (via spreadsheet) to yield the axial admittance response of the cone and voice coil. The properties of the motor system were used along with the calculated axial admittance to calculate the total motional impedance response of the loudspeaker.

The initial modelled motional impedance response was subsequently compared to the measured motional impedance response of cones A and C, and the material properties fine tuned for each speaker, according to the procedure detailed in Section 4.3.3

4.3.3 CALIBRATION

Each of the three isotropic material properties (Young's modulus, Poisson's ratio and mass density) has an effect on the absolute and relative frequencies of the natural modes of the loudspeaker cone. Additionally, the choice of damping ratio affects the shape of the motional impedance response near each resonance and antiresonance. The damping ratio can also slightly shift the frequencies of the natural modes, although this shift is insignificant for realistic damping ratios (ξ <0.1). The values of some of these material properties can be fine-tuned to improve the accuracy of match between measured and modelled results.

In general, the mass density of the loudspeaker cones can be assumed to be constant from cone to cone, at least for loudspeakers manufactured from the same batch. Batches manufactured some time apart may show some variance in mass density, but this is likely to be minimal in comparison to variations in other properties such as Young's modulus.

By adjusting the value of Young's modulus for the cone material, it is possible to shift all the predicted resonant and antiresonant frequencies to closely match those measured in the motional impedance response of a real cone. This is achieved by the following method [6]

1. Using an initial estimate for Young's modulus, E', calculate an estimate of the frequency of the first bending antiresonance, f'_{ba1}. (Refer Figure 4.10)

2. Measure the actual frequency of the first bending antiresonance f_{ba1}.

3. Since all resonant and antiresonant frequencies are proportional to the square root of Young's modulus (refer Chapter 5), a better estimate for Young's modulus, E, is given by:

$$E = \left(\frac{f_{ba1}}{f'_{ba1}} \right) E' \tag{4.1}$$

The value of Poisson's ratio has no effect on the frequency or shape of bending resonances and antiresonances but does affect the longitudinal resonant frequencies (refer Section 5.2.3). Thus, by slightly adjusting the value of Poisson's ratio we may adjust the position of the first longitudinal resonance relative to the bending modes.

Lastly, the damping ratio was initially set to a value of 0.1, and subsequently adjusted in order to provide the best match between the height of resonant features on the measured and modelled motional impedance responses.

The modelled and measured on-axis sound pressure (p_{ax}) is used as a final test of model validity. The sound pressure predicted by the SYSNOISE software is compared to the

on-axis sound pressure of the speaker, as measured in an anechoic chamber at a distance of 1m. When measured, the loudspeaker consisted of a cone and voice coil mounted in a motor assembly with no outer surround or dust-cap attached, allowing the cone to resonate freely, and all resonant frequencies to be readily identified. As is common practice, the loudspeaker was mounted in a standard IEC baffle, although there was a space of ≈1cm between the outer edge of the cone and the start of the baffle owing to the removal of the surround. The sound pressure response for frequencies below 1kHz is not considered as it is well below the onset of cone break-up.

A reasonable match between the frequencies of features in both measured and modelled sound pressure responses is looked for. In general, calibrating material properties with the use of motional impedance measurements results in a satisfactorily representative model, and no further calibration is necessary upon calculation of the sound pressure response. The final material properties chosen for cones A and C after calibration are shown in Table 4.2.

Property:	Value:	
	Cone A	**Cone C**
Mass density:	1113 kg/m^3	1113 kg/m^3
Young's modulus:	5.0×10^9 N/m^2	6.4×10^9 N/m^2
Poisson's ratio:	0.30	0.22
Damping ratio (ξ):	0.025	0.020

Table 4.2. Calibrated material properties for loudspeaker cones A and C

Figures 4.6 and 4.7 show the final calibrated Z_{mot} and p_{ax} results for cones A and C.

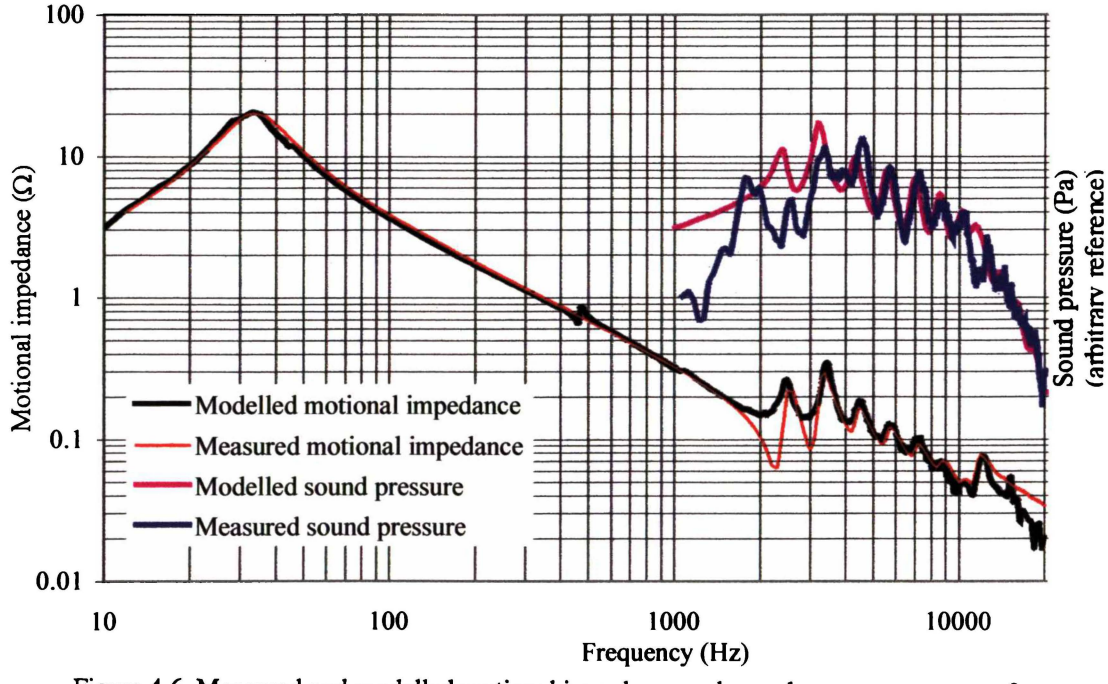

Figure 4.6. Measured and modelled motional impedance and sound pressure responses for cone A

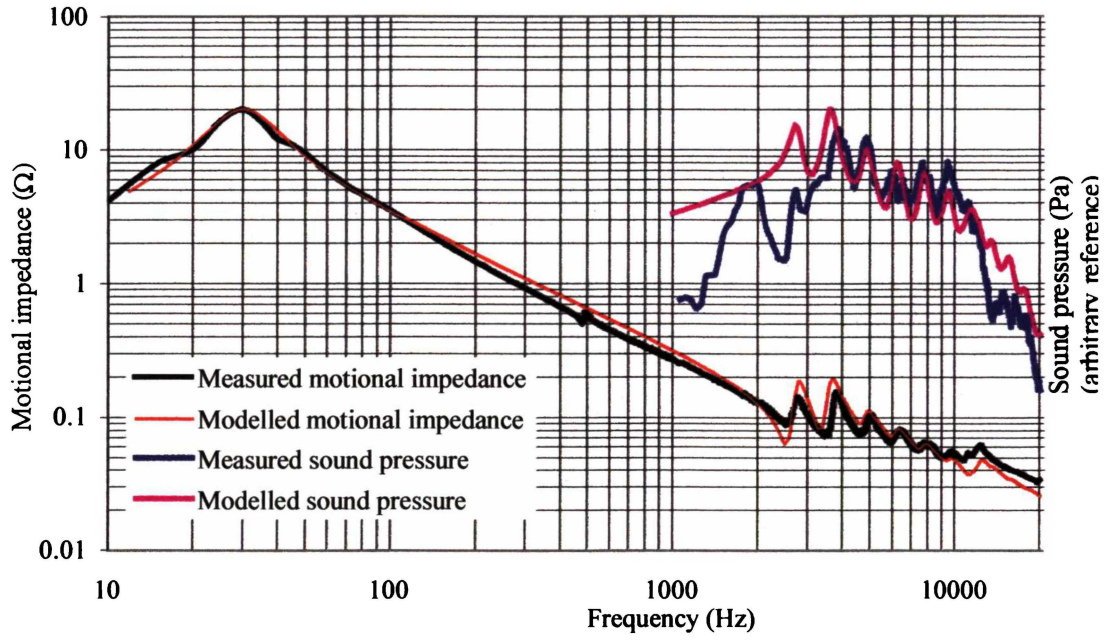

Figure 4.7. Measured and modelled motional impedance and sound pressure responses for cone C

The modelled and measured motional impedance responses of Figure 4.6 and Figure 4.7 exhibit good frequency matching between their major features. On average, the first six modelled and measured bending resonant frequencies in the Z_{mot} response of Figure 4.6 (Cone A) agree within 1%, while the sound pressure response resonances agree within 4%. In Figure 4.7 (Cone C), the first six measured Z_{mot} resonances lie (on average) within 2% of their modelled counterparts, while for the sound pressure response, the agreement is 1%.

However, there is inevitably some degree of compromise in the calibration procedure, as it is essentially a manual process. Often, calibration to one particular feature, such as the shape of the motional impedance curve near the first resonance and antiresonance, requires a compromise in another feature, such as the sound pressure response. Nevertheless, the overall shapes of the modelled motional impedance and sound pressure responses are sufficiently similar to the measured responses.

The small resonance evident in the motional impedance curves of both loudspeakers A and C at $f \approx 500$Hz has been identified as the first resonant frequency of the spider. The mode shape was clearly visible when the spider was illuminated by strobe light while being driven at a frequency of 500Hz. Although the effect of the spider is not taken into account in the FE model, its role as the supplier of the spring restoring force to the centre of the cone is taken into account during post-processing. As the spider is sealed behind the driver cone, it produces negligible sound radiation, even when vibrating at resonance. The spider has a second resonant frequency at f≈1000Hz, and a third at f≈1800Hz.

Some features of the sound pressure curve warrant particular comment. Both measured sound pressure curves exhibit a significant peak at just below 2kHz. No such feature is

evident in the measured motional impedance, nor in the modelled sound pressure response. At least two factors have been identified which demonstrably contribute to this measured sound pressure peak.

1. This frequency approximately corresponds to the first resonant frequency of the frame (1950Hz) which normally supports the outer suspension. As the outer suspension had been removed from these drivers, the driver frame was able to ring, and contribute to the sound pressure near these frequencies. However, in normal circumstances, the driver frame is heavily damped by the suspension and tightly screwed into a cabinet, thereby practically removing the contribution of the driver frame resonance.

2. There appears to be a significant sound pressure contribution from the small resonant cavity formed by the space between the end of the pole piece and the inner edge of the cone. Further, there is a resonant cavity formed by the vent down the centre of the pole piece. It has been noted that sealing the back end of the pole-piece vent causes a decrease in the frequency of this resonance. It is perhaps possible that with some further careful modelling these resonant effects could be taken account of in the FE model. A third resonant cavity is formed by the volume of air enclosed by the spider and the magnet assembly.

Since the FE model does not attempt to model the structural resonances of the loudspeaker motor system and frame, these resonances are absent from the modelled sound pressure response.

Apart from the driver frame and pole piece resonances, the measured sound pressure response is somewhat less than the modelled response for frequencies below the second bending resonance (~3kHz). The first bending resonance is predicted at approximately the same frequency at which it is measured, albeit with a lower sound pressure. Above this frequency, there is good matching between measured and modelled sound pressures.

The minor discrepancies between measured and modelled sound pressure may be attributable in part to the difference between the baffle conditions of the test and modelled loudspeakers. The measured loudspeaker is mounted in a large baffle, which is standard practice when measuring a loudspeaker driver's sound pressure response. However, as the outer surround of the loudspeaker was removed, there was a gap of 1cm between the outer edge of the cone and the start of the baffle. The removal of the surround may also have caused further minor discrepancies by allowing the test loudspeaker's voice coil to twist more than usual and make contact with the magnet system.

These relatively minor disparities aside, the degree of agreement between measured and modelled motional impedance and sound pressure responses suggests that the developed FE model sufficiently predicts the characteristics of cones A and C. The results also imply that the FE model is quite adequate for the purposes of exploring the effect of

material properties and cone geometry on the natural frequencies of a nominal loudspeaker.

4.3.4 3D MODEL

Having calibrated the 2D model and determined realistic material parameters, a 3D model of loudspeaker C was created using ≈1100 SHELL63 elements. This 3D model was developed to assist in generating the mode shapes and characteristics of unslotted loudspeakers. It was also used as a starting design for exploring the effects of cone slots on the resonant behaviour of loudspeaker cones (Chapter 6). A cutaway view of this model is shown below in Figure 4.8.

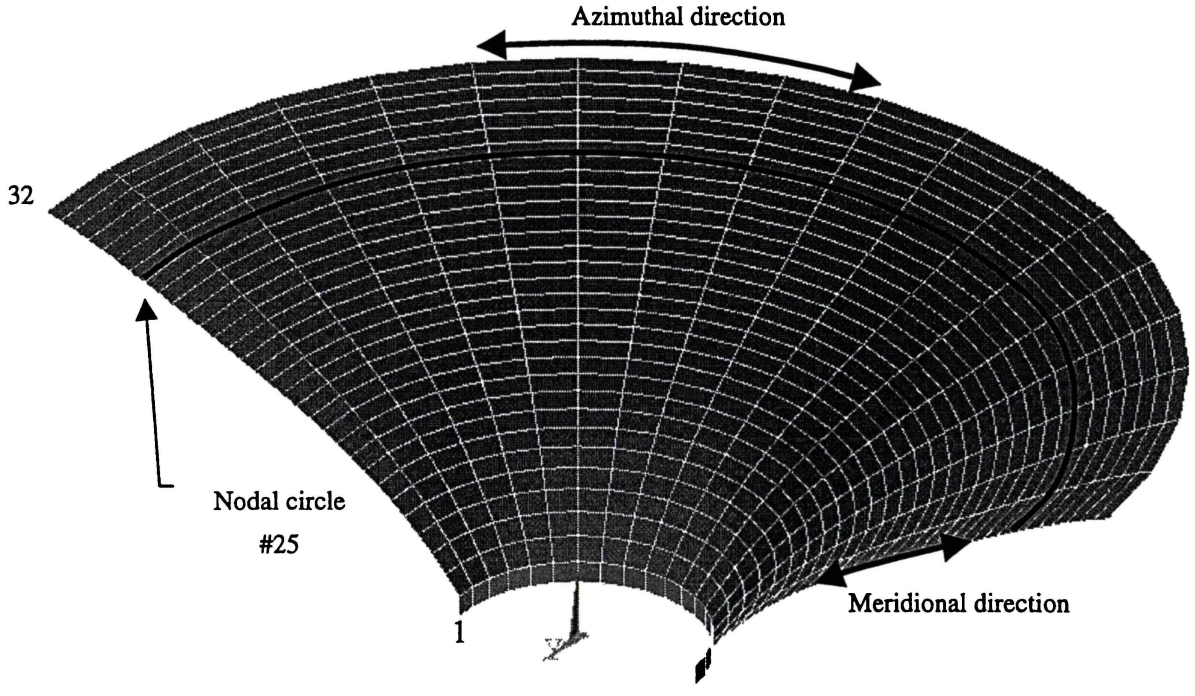

Figure 4.8. Cutaway view of 3D cone model.

Nodes lying along meridional and azimuthal lines define the shape of the loudspeaker cone. In general, we refer to different parts of an axisymmetric loudspeaker cone in terms of the nodal circle number, where the innermost circle is nodal circle 1 and the outermost nodal circle 32. (Nodal circle 25 is highlighted in Figure 4.8 as an example.)

As for the 2D model, degree of freedom constraints are applied to nodal circles 1 and 2 in order to constrain the inner neck of the cone to purely axial motion. All other nodes are unconstrained. The 1N driving force applied to the inner nodal circle is distributed across the 36 nodes around the circle; each of these nodes experiences a force of 1/36 N.

The motional impedance response calculated using this FE model is shown in Figure 4.9:

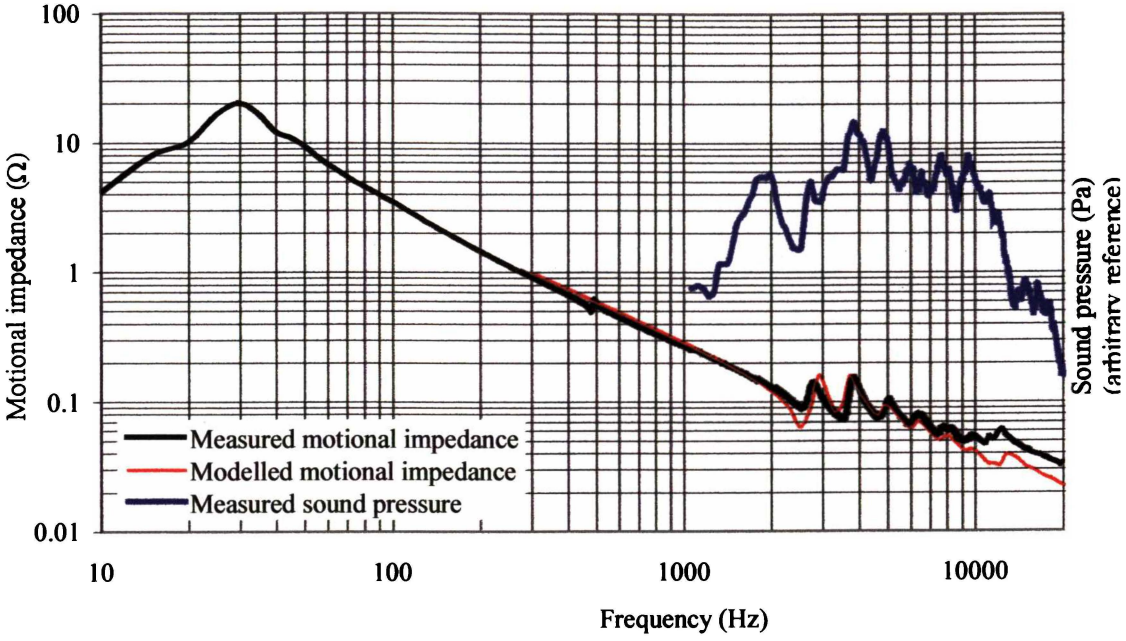

Figure 4.9. Measured and modelled Z_{mot} response for cone C. Generated from 3D model.

On average, the first six bending resonances of the Z_{mot} response generated by the 3D axisymmetric model lie within ±2% of the measured Z_{mot} resonant frequencies.

As 2D models are necessarily axisymmetric, a full 3D model is the only means by which asymmetric loudspeakers can be modelled. Unfortunately, the 3D model of Figure 4.8 consists of approximately 1100 elements as opposed to the 32 elements of Figure 4.5, resulting in considerably greater processing expense. The calculation time required for a 200-frequency step harmonic response analysis of a 2D model is of the order of 1 minute while the same calculation on a 3D model requires up to 12 hours. It was not feasible to calculate sound pressure response results for any of the 3D models considered herein, as the SYSNOISE software being used was limited to 200 nodes only. Further, the cost in processing time for such a large design using the BE method would be severe, and impractical in view of the large number of different 3D models considered.

However, the smoothness of the modelled Y_{ax} response of a 3D loudspeaker provides a very good indication of the smoothness of the resulting sound pressure response.

4.4 AXISYMMETRIC LOUDSPEAKER CHARACTERISTICS

In this section, the calibrated FE model of loudspeaker C is used to determine the exact nature of the resonant behaviour of a typical axisymmetric 6½-inch polypropylene loudspeaker. The loudspeaker is characterised by means of its axial admittance response, sound pressure response, natural frequencies and mode shapes. Asymmetric modes are generally not excited in an untreated loudspeaker and are therefore not considered.

4.4.1 AXIAL ADMITTANCE RESPONSE

As the measured sound pressure response created by a loudspeaker is closely related to its axial and total admittance responses, it is convenient to use the admittance characteristic as a tool for describing the resonant behaviour of the loudspeaker. Plotting the axial admittance of the cone itself and ignoring the effect of the added mass of the voice coil allows the cone's resonant and antiresonant frequencies to be readily identified, as shown in Figure 4.10:

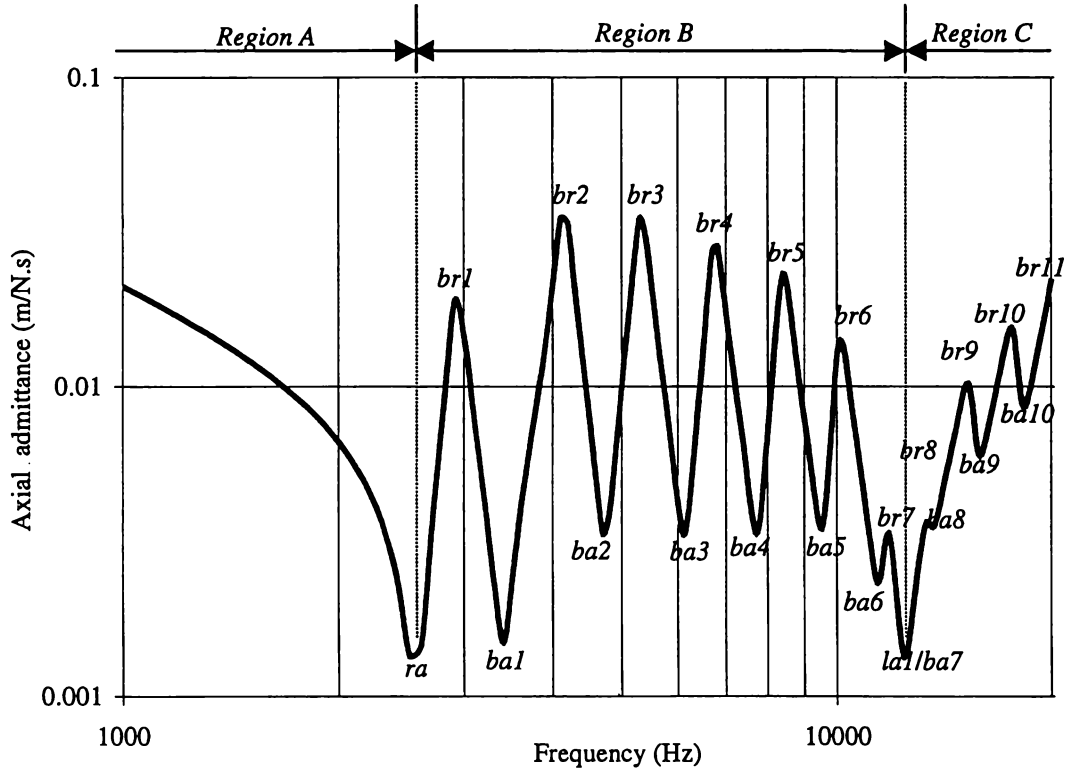

Figure 4.10. Modelled axial admittance response for loudspeaker cone C

The ring antiresonance is denoted *ra,* the first ten bending antiresonances are denoted *ba1-ba10,* the first eleven bending resonances *br1-11,* and the first longitudinal resonance *la1.* Thus, loudspeaker C enters cone break-up at a frequency of approximately 2.5 kHz, with the ring antiresonance occurring at 2575Hz. The first longitudinal antiresonance occurs at ~12500Hz, and is evident as a pronounced minimum in axial admittance.

4.4.2 SOUND PRESSURE RESPONSE

It is useful to consider the far-field sound pressure response of cone C by means of a 3D polar sound pressure radiation plot as shown in Figure 4.11. The polar sound pressure response is generated from SYSNOISE, by defining a 180° arc, 10m in front of the loudspeaker cone. Seventy-two measurement points are defined around this arc, and the sound pressure response is derived for each point at 200 driving frequencies in the range 100Hz-20kHz.

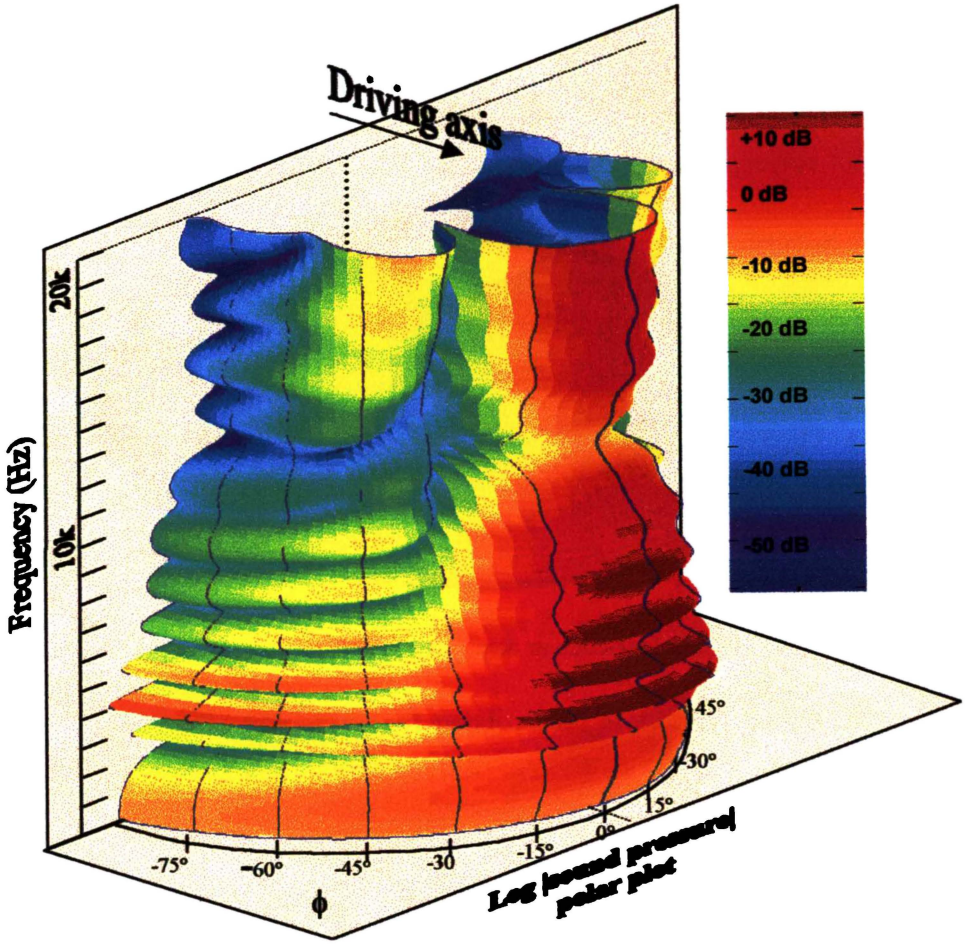

Figure 4.11. 3D Polar sound pressure frequency response plot for cone C with no voice coil and no surround.

Figure 4.11 shows the predicted polar sound pressure response of cone C with a zero mass voice coil. The effect of the bending resonances is clearly seen in the region 1000Hz – 10kHz, both in the on and off-axis response. A considerable reduction in sound pressure is evident at the onset of longitudinal antiresonance (≈12.5kHz).

In general, the off-axis response of an axisymmetric loudspeaker can be estimated by superimposing the shape of the total admittance characteristic on the polar response plot of Figure 2.25.

4.4.3 MODE SHAPES

Having identified the natural frequencies of the cone itself, it is useful to consider the modal shapes of each resonant and antiresonant mode. This is achieved by means of two different types of plot: the colour contour displacement plot and the colour vector plot.

The colour-contour displacement plot shows the deformed shape of the cone at a particular frequency, using colour to represent the displacement of each area of the cone from its undeformed position. The colour scale ranges from blue→red, blue representing small displacements and red large displacements. An example of a colour-contour displacement plot is shown below where the shape of cone vibration at 1075Hz (which does not correspond to a cone resonant frequency):

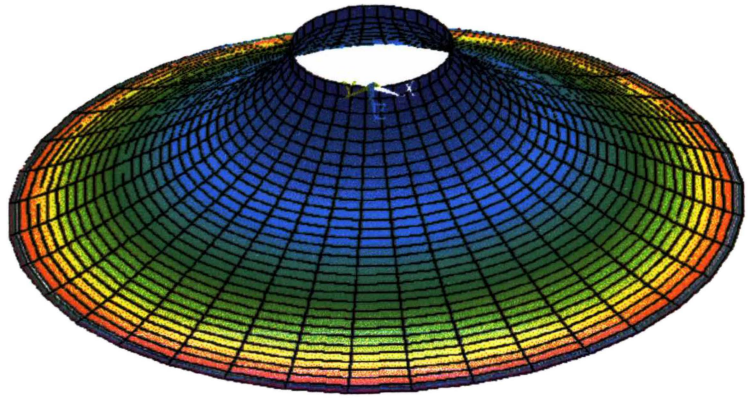

Figure 4.12. Colour-contour displacement plot for cone C for $f = 1075$ Hz.

The displacement colour scale is recalculated for each plot generated, and thus these plots should be taken as indicative of mode shape alone and not absolute cone displacement. In order to more clearly show the phase relationship of different parts of the cone, and the relative amounts of transverse and longitudinal displacement, the colour vector displacement plot is also used:

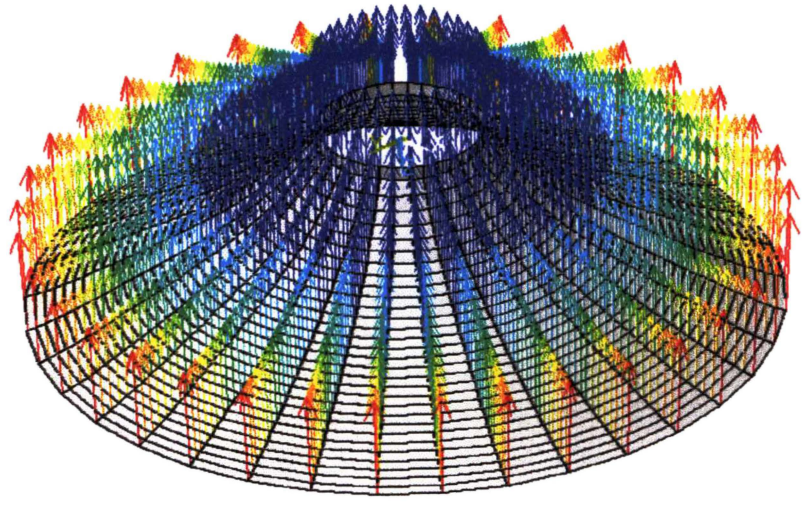

Figure 4.13. Colour vector displacement plot for loudspeaker cone C for $f = 1075$ Hz.

The natural frequencies of Figure 4.10 are characterised in Figure 4.14 by means of displacement and vector plots. All plots are observed from a viewpoint behind the rear surface of the cone.

Displacement plot **Vector plot**

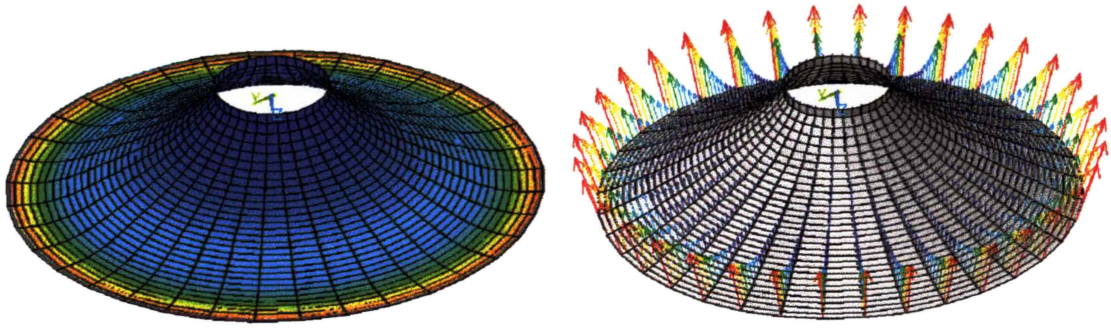

a) Ring antiresonance $f_{ra} \approx 2600$ Hz

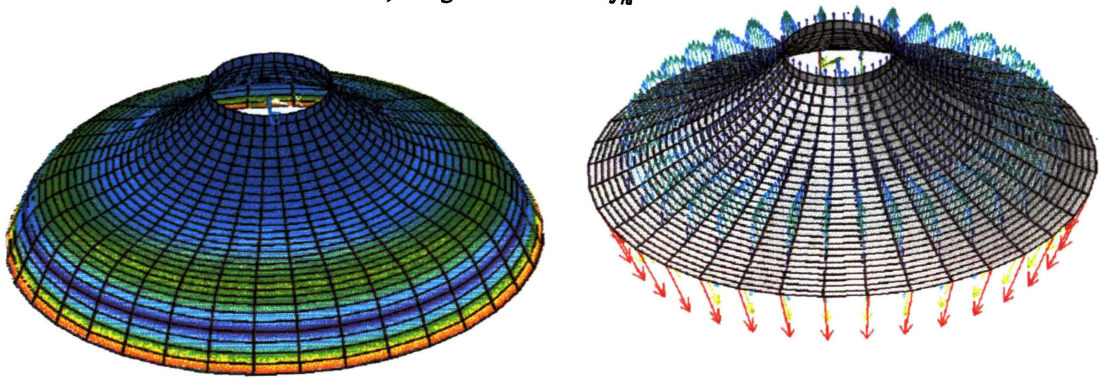

b) First bending resonance $f_{br1} \approx 3000$ Hz

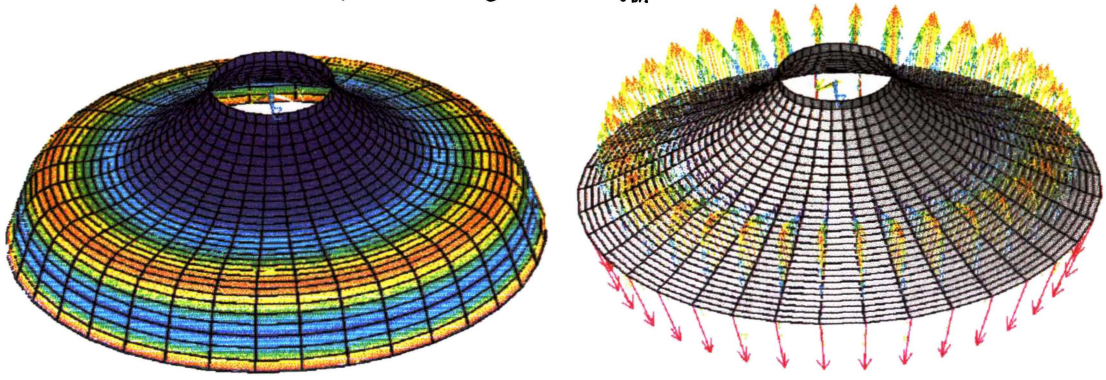

c) First bending antiresonance $f_{ba1} \approx 3500$ Hz

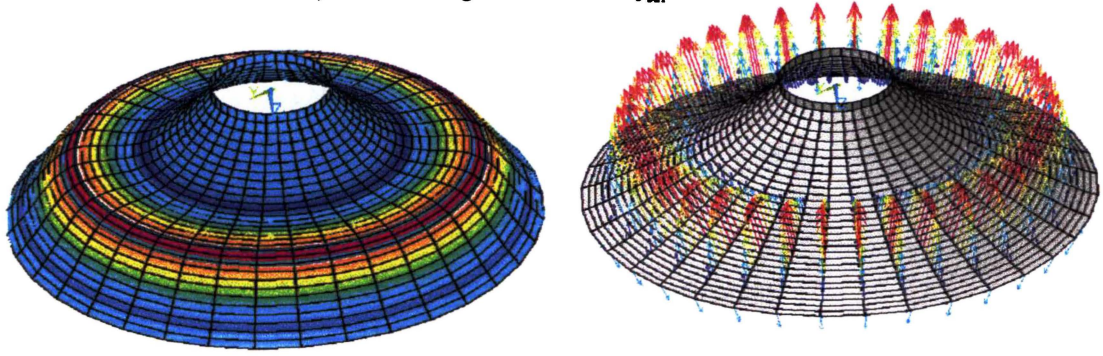

d) Second bending resonance $f_{br2} \approx 4150$ Hz

Figure 4.14. Colour displacement and vector plots for a) ring antiresonance, b) first bending resonance, c) first bending antiresonance, d) second bending resonance.

Displacement plot **Vector plot**

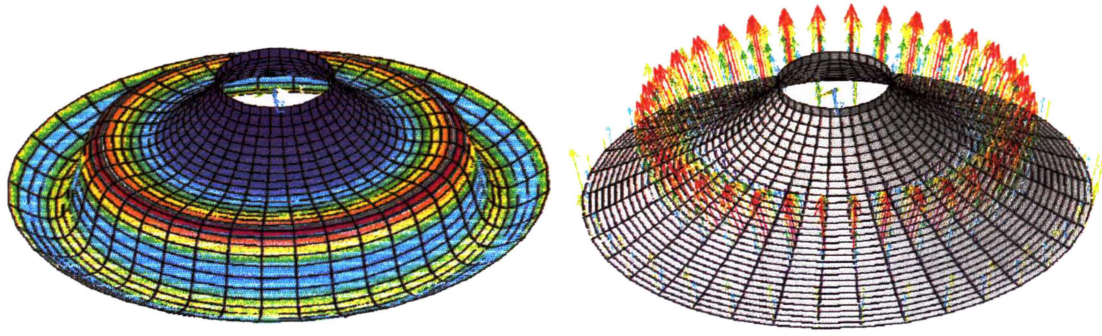

e) Second bending antiresonance $f_{ba2} \approx 4750$ Hz

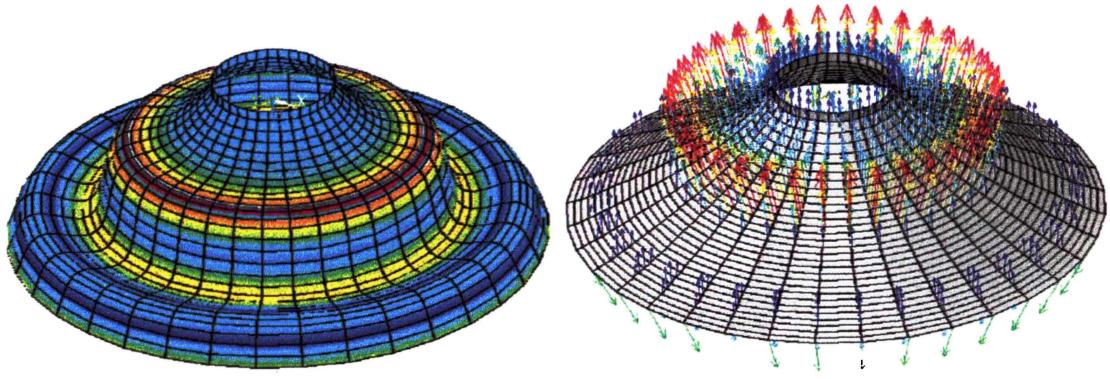

f) Third bending resonance $f_{br3} \approx 5350$ Hz

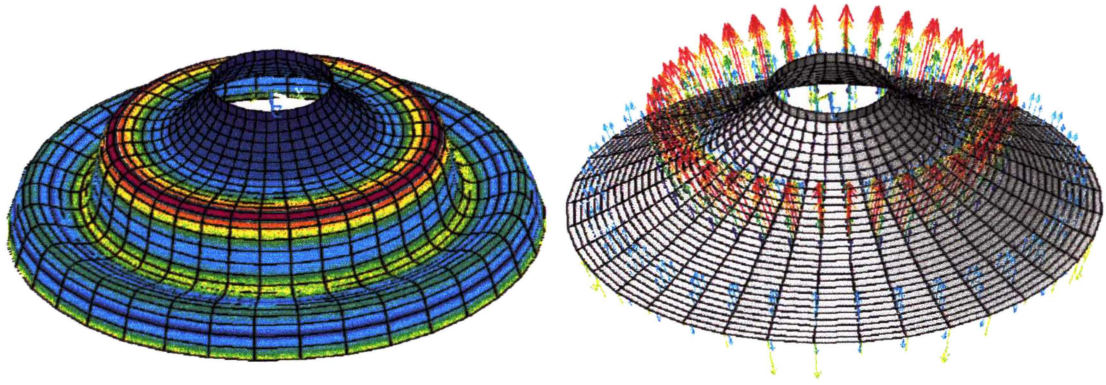

g) Third bending antiresonance $f_{ba3} \approx 6100$ Hz

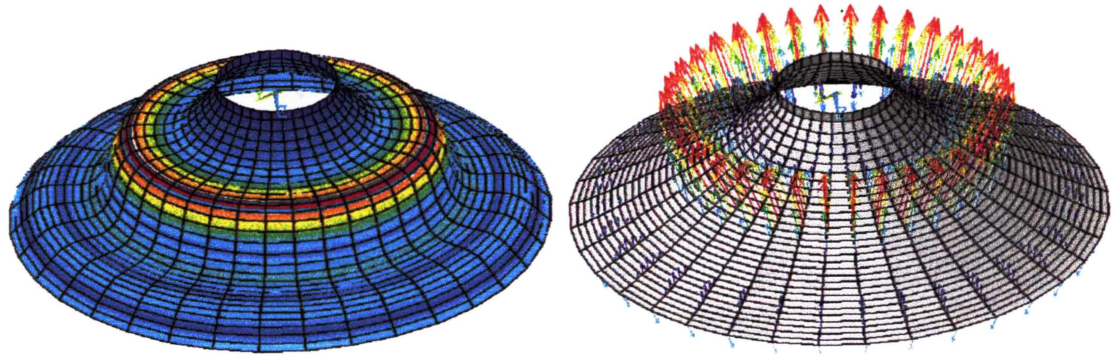

h) Fourth bending resonance $f_{br4} \approx 6700$ Hz

Figure 4.14 (cont.). Colour displacement and vector plots for e) Second bending antiresonance, f) Third bending resonance, g) Third bending antiresonance, and h) Fourth bending resonance.

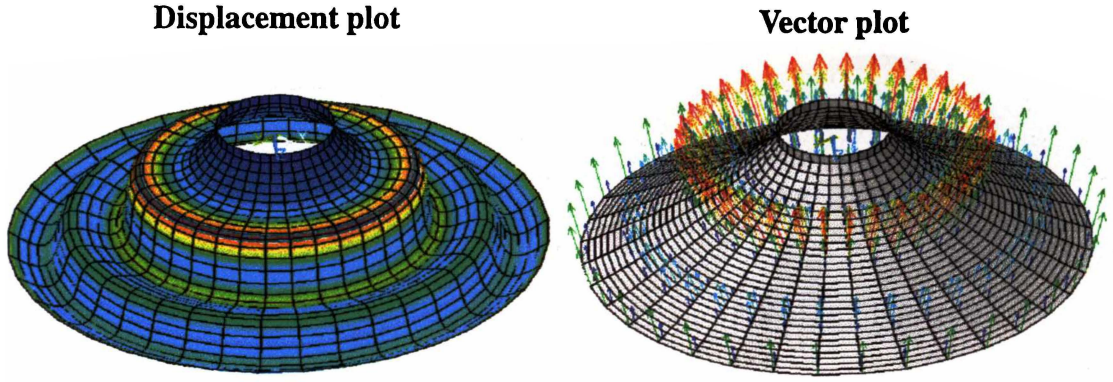

i) Fourth bending antiresonance $f_{ba4} \approx 7700$ Hz

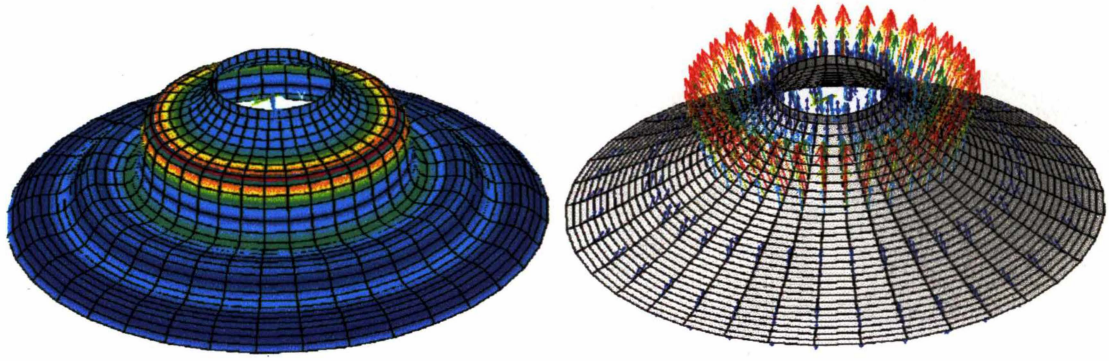

j) Fifth bending resonance $f_{br5} \approx 8350$ Hz

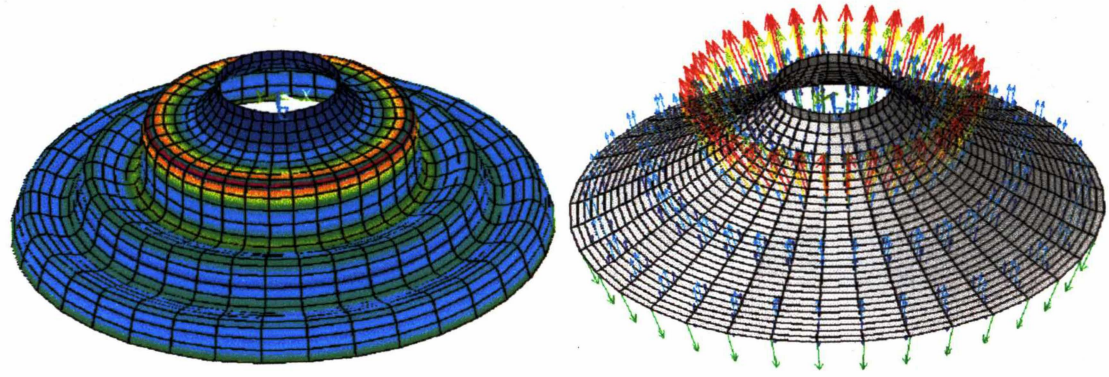

k) Fifth bending antiresonance $f_{ba5} \approx 9400$ Hz

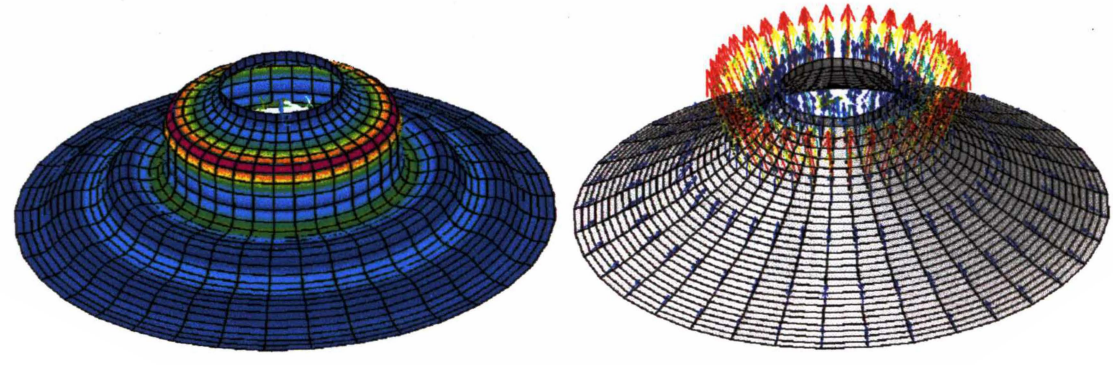

l) Sixth bending resonance $f_{br6} \approx 10000$ Hz

Figure 4.14 (cont.). Colour displacement and vector plots for i) Fourth bending antiresonance, j) Fifth bending resonance, k) Fifth bending antiresonance, and i) Sixth bending resonance.

Displacement plot **Vector plot**

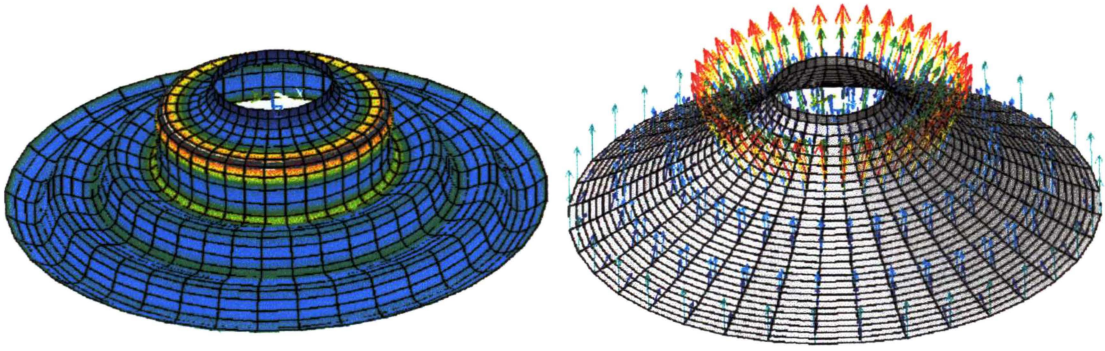

m) Sixth bending antiresonance $f_{ba6} \approx 11250$ Hz

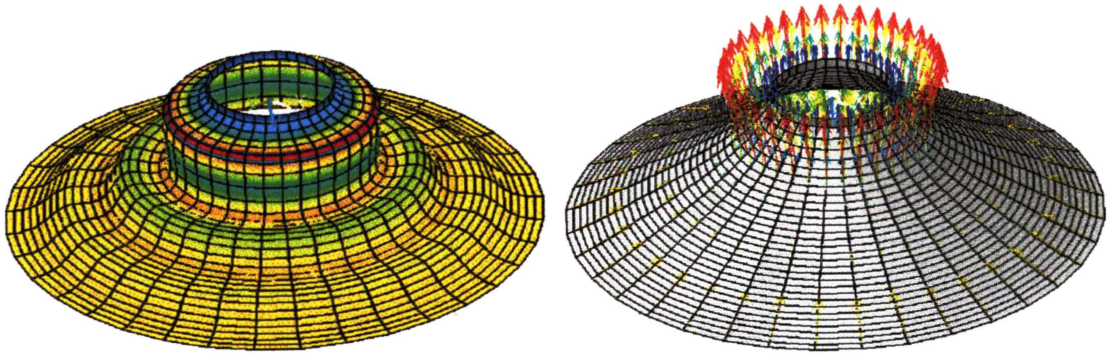

n) Seventh bending resonance $f_{br7} \approx 11700$ Hz

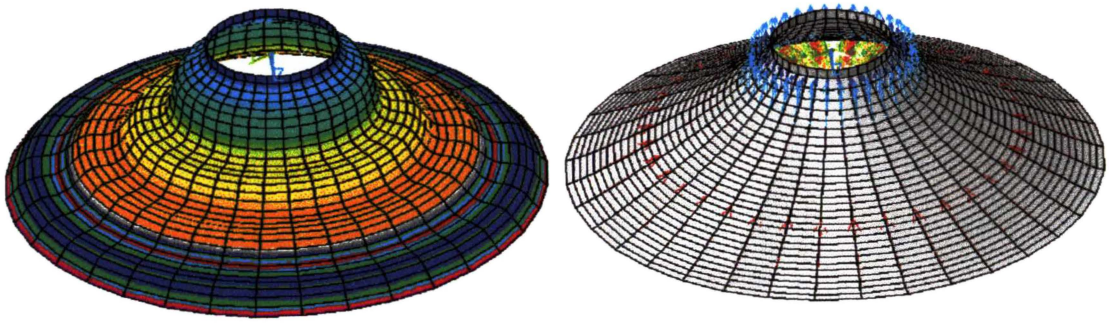

o) First longitudinal antiresonance f_{la1}, Seventh bending antiresonance $f_{ba7} \approx 12500$ Hz

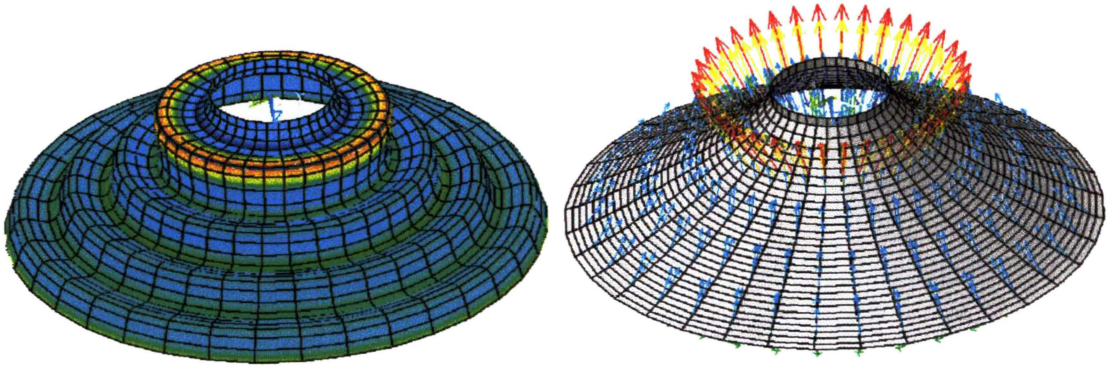

p) Eighth bending resonance f_{br8}, Eight bending antiresonance $f_{ba8} \approx 13500$ Hz

Figure 4.14 (cont.). Colour displacement and vector plots for m) Sixth bending antiresonance, n) Seventh bending resonance, o) First longitudinal antiresonance and Seventh bending antiresonance, p) Eight bending resonance and antiresonance.

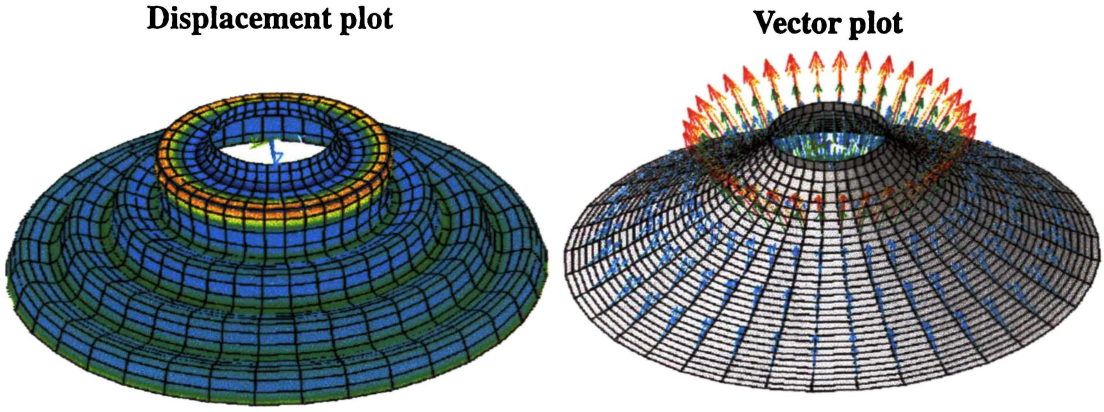

q) Ninth bending resonance $f_{br9} \approx 15000$ Hz

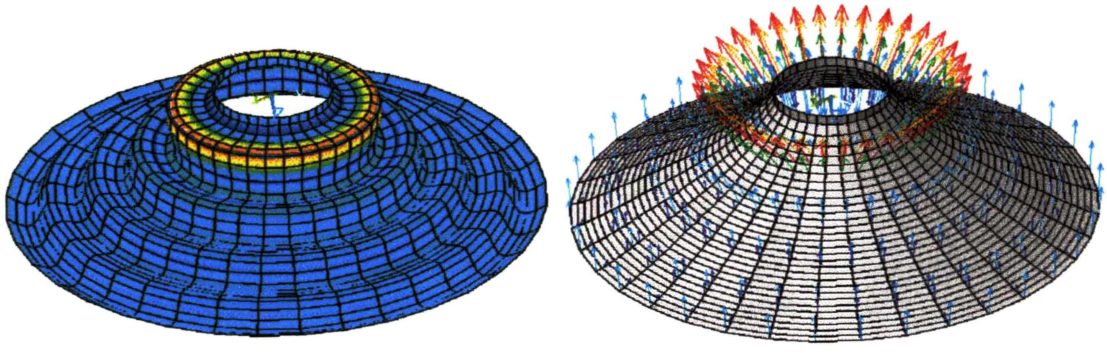

r) Ninth bending antiresonance $f_{ba9} \approx 15500$ Hz

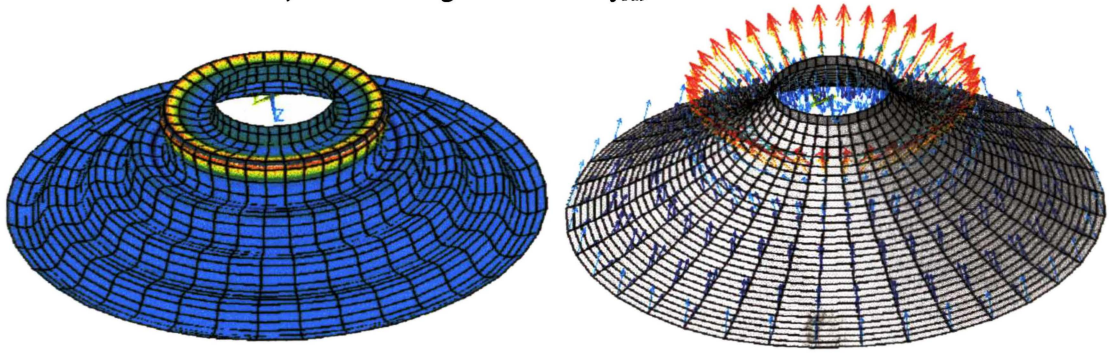

s) Tenth bending resonance $f_{br10} \approx 17000$ Hz

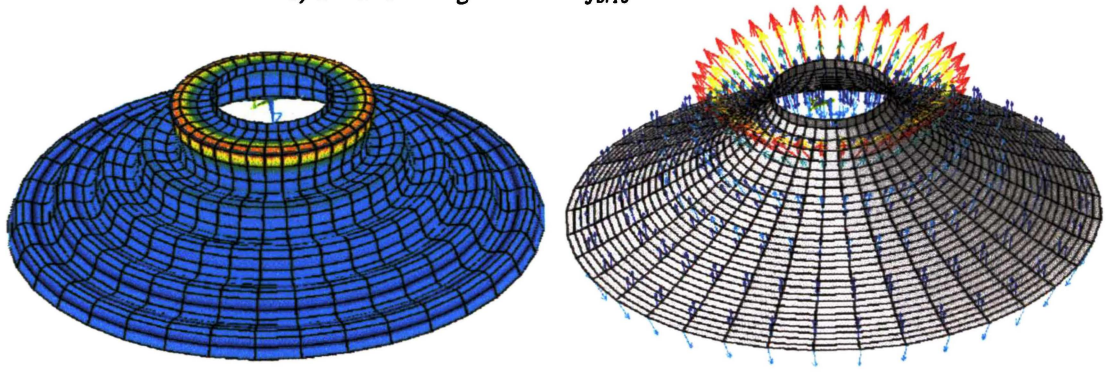

t) Tenth bending antiresonance $f_{ba10} \approx 17750$ Hz

Figure 4.14 (cont.). Colour displacement and vector plots for q) Ninth bending resonance, r) Ninth bending antiresonance, s) Tenth bending resonance, t) Tenth bending antiresonance.

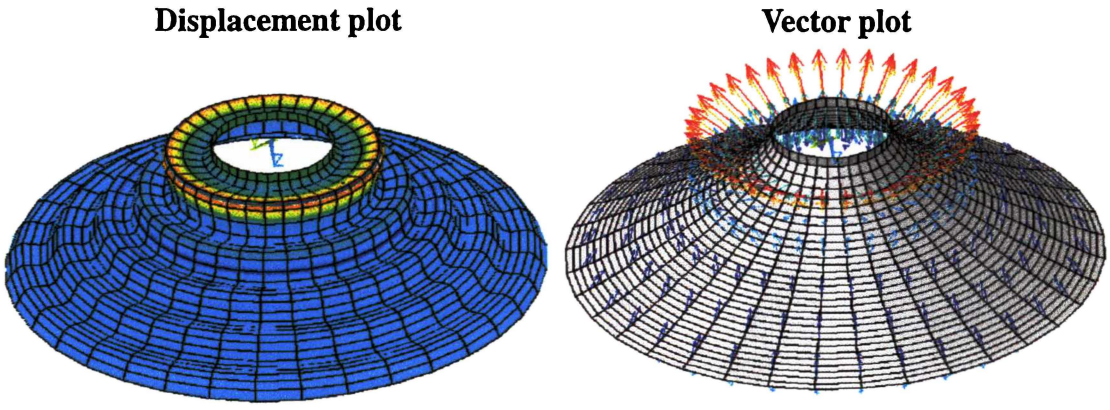

u) Eleventh bending resonance $f_{br11} \approx 19500$ Hz

Figure 4.14 (cont.). Colour displacement and vector plots for u) Eleventh bending resonance.

The cone motion described by Figure 4.14 can be classified into three main frequency ranges as follows:

Region A. $f < f_{ra}$

At low frequency, the loudspeaker vibrates in an approximately piston-like manner, the displacement of the outer edge lagging slightly in phase behind the inner edge. In this region, the axial admittance is principally imaginary; the cone vibrates as an almost-rigid body. The displacement of the inner edge is less than that at the outer edge, as shown in Figure 4.12 and Figure 4.13.

When the driving frequency is increased to ≈2575Hz, the so-called ring antiresonant frequency f_{ra} is reached, marking the onset of cone break-up. At this point, the real component of the axial admittance is of comparable magnitude to the imaginary component, and the cone begins to behave like a spring.

Region B. $f_{ra} < f < f_{la1}$

At the ring antiresonant frequency, cone motion is at a minimum at the inner edge of the cone, and maximum at the outer edge. The motion of the cone at the outer edge is purely transverse, as shown by the vector displacement plot of Figure 4.14 a). The ring antiresonant frequency arises from azimuthal stretching that occurs at the circumference of the cone as it expands and contracts. Expansion of the circumference of the cone results in a component of the resulting azimuthal stress being directed in towards the axis of the cone.

The ring antiresonance can be thought of as a simple spring-mass resonance between the transverse component of the stiffness experienced by the outer edge of the cone and the cone mass. Consequently, f_{ra} is strongly dependent on the outside radius of the cone; to a first approximation, it is independent of its meridional length.

As the driving frequency is increased above f_{ra}, bending wave motion begins to appear on the surface of the cone. At 3025 Hz, the first bending resonant mode ($f = f_{br1}$) of the cone is excited. This mode is characterised by an antinode at nodal line #23 and a node at nodal line #28 (Figure 4.14b)). The portion of the cone inside nodal line #23 retains an almost piston like motion, and is the part of the cone that moves with maximum displacement. This results in a local maximum in the sound pressure response for this speaker. The outer sections of the cone, although vibrating with much greater amplitude, vibrate antiphase, and thus do not greatly contribute to the developed on-axis sound pressure.

f = 3475Hz corresponds to the excitation of the first bending antiresonance. The mode shape at this frequency is almost identical to that at f_{ba1}, except the inner piston-like portion of the cone exhibits almost zero displacement; only the outer portions of the cone vibrate. This is a characteristic of all bending antiresonances in this region, and consequently all bending antiresonances cause a minimum in the radiation sound pressure response.

As the driving frequency is further increased, higher order resonances are excited, with the innermost antinode moving in towards the centre of the cone with higher frequency. In region B, the n_{th} bending resonant frequency is characterised by n nodal lines, and $n+1$ antinodal lines (including the outside edge). The area of the cone inside the innermost antinodal line moves almost uniformly, maintaining an approximately piston-like motion, while the outer areas of the cone exhibit bending wave motion.

The loudspeaker cone always vibrates with greatest displacement amplitude at the position of the innermost antinode, except during longitudinal antiresonance.

As higher order resonances are excited (Figure 4.14, j), l), n)), the cone begins to exhibit a significant degree of longitudinal motion, particularly towards the outer edge of the cone. This longitudinal motion becomes predominant at 12500Hz (Figure 4.14 o)), as the first longitudinal antiresonant frequency is reached.

Region C. $f > f_{la1}$

At the first longitudinal antiresonant frequency, f_{la1}, a very small inner region of the cone vibrates axially, with all other sections of the cone vibrating in a longitudinal manner along the cone's meridional line. As there is very little transverse component to the cone's vibration, the onset of longitudinal resonance corresponds to a pronounced dip in sound pressure as seen in Figure 4.11. The longitudinal nature of the cone's vibration at this frequency is quite evident in Figure 4.14 o).

Above, f_{la1}, further bending resonances and antiresonances occur. At all these modal frequencies, the innermost part of the cone vibrates in a transverse manner, with high displacement amplitude in comparison to outer parts of the cone. Cone displacement is far lower at the outer edge of the cone than near its centre. Here the wave type is a combination of transverse and longitudinal motion, as shown in the vector plots of

Figure 4.14 p) → u).

It is convenient to summarise the modal shapes of Figure 4.14 by means of a "displacement pattern versus frequency" plot. Figure 4.15 shows the displacement pattern of a line of nodes up the meridian of an axisymmetric loudspeaker as a function of frequency. The frequency axis is linear rather than logarithmic, thereby revealing the displacement results at high frequency more distinctly. Displacements are all normalised to be relative to the displacement of the innermost node. Consequently, the colour scale indicates the deformation of the cone from its equilibrium shape, and not the overall displacement of the cone.

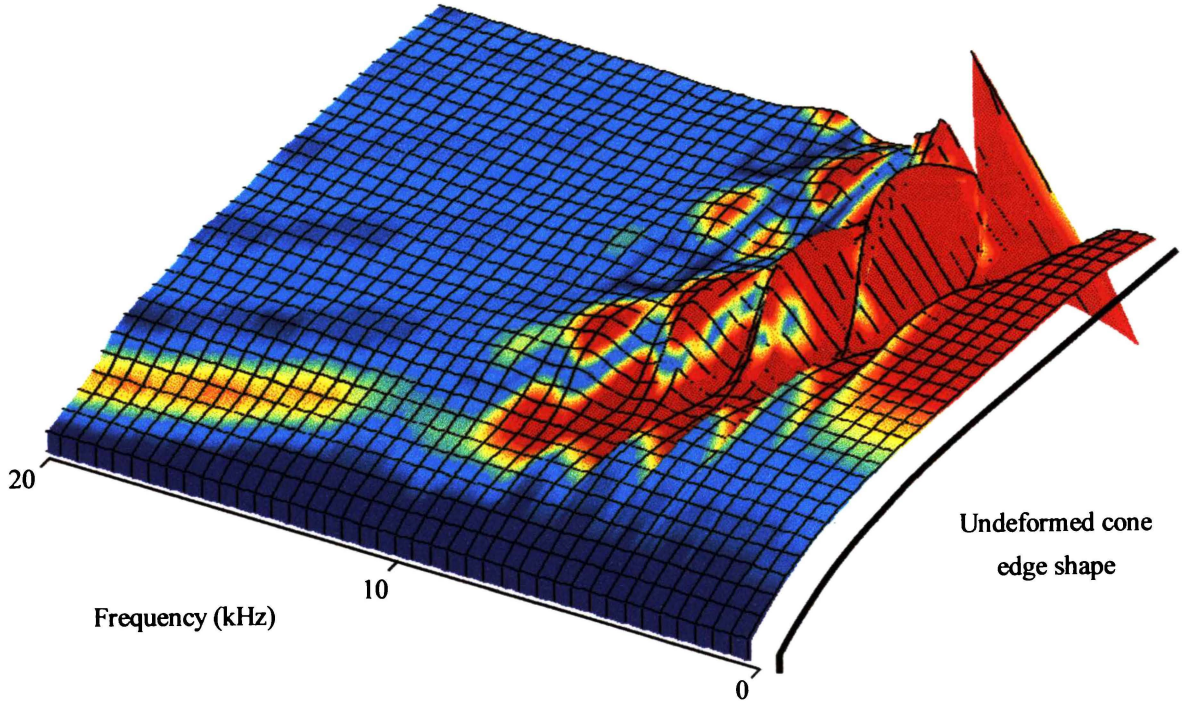

Figure 4.15. Displacement plot of loudspeaker cone edge as a function of frequency.

Figure 4.15 demonstrates that the innermost antinode vibrates with maximum amplitude and moves in towards the centre of the cone with increasing frequency. The onset of longitudinal antiresonance is also evident at $f \approx 12500$Hz, as the cone displacement becomes primarily longitudinal.

The Y_{ax} plot of Figure 4.10, the 3D polar sound pressure frequency response plot of Figure 4.11, the vector and displacement plots of Figure 4.14, and the displacement pattern plot of Figure 4.15 form a set of tools which adequately summarise the resonant behaviour of the loudspeaker. Varying the properties of the loudspeaker will result in changes to some or all of these characteristics.

4.5 EFFECT OF OUTER SURROUND ON LOUDSPEAKER CHARACTERISTICS

In this section the effect of the outer surround on cone behaviour is measured and characterised by means of a finite element model.

4.5.1 INTRODUCTION

The previous sections have considered the resonant behaviour of a loudspeaker cone with no outer surround, allowing the natural resonances of the cone itself to be characterised. However, in practice, all electrodynamic loudspeaker drivers are manufactured with an outer surround, which attaches from the outer edge of the loudspeaker cone to the driver frame. The outer surround serves a threefold purpose:

- Prevention of side to side rocking of the cone
- Prevention of passage of air between front and rear cone surfaces
- Termination and absorption of travelling wave energy in the cone

Additionally, the surround supports the role of the spider by supplying a small measure of restoring force to the cone. It must also be able to withstand the high excursion of the cone that occurs at low frequencies.

Traditionally, paper loudspeaker cones have been manufactured with an outer surround consisting of a series of concentric corrugated rings attached to the cone edge. This has usually been formed by extending the cone material itself, although sometimes an extra felt or cloth extension has been used. Frankfort [6] ignored the outer surround when numerically modelling cone resonance, arguing that a slightly increased cone damping sufficiently models the surround's effect. This may be the case when the surround is manufactured of the same material as the cone itself and is of similar thickness. However, other studies have shown that the outer surround can have a significant effect on the resonant behaviour of loudspeaker cone [28]. In particular, Shindo *et al.* consider the effect of a cloth surround on the behaviour of a conical paper cone and find that the effect of the outer surround cannot be ignored.

Paper or felt loudspeaker cones have been partly superceded by modern cones manufactured from such materials as polypropylene, polyester, and aluminium. These loudspeaker cones are often terminated with surrounds moulded from materials such as plastic foams, neoprene, p.v.c. and nitrile rubber.

It is beyond the scope of this thesis to undertake an exhaustive examination of the relative merits and demerits of different surround designs and materials. Nevertheless, it is appropriate to briefly examine the surround design utilised in the loudspeaker drivers used herein, and determine its effect on the resonant behaviour of an "unterminated" loudspeaker cone.

4.5.2 MEASURED RESPONSE

In order to determine the effect of the outer surround on cone resonance, the Z_{mot} responses of cones A and C were measured with and without their outer surrounds attached. Figure 4.16 compares the measured motional impedance responses.

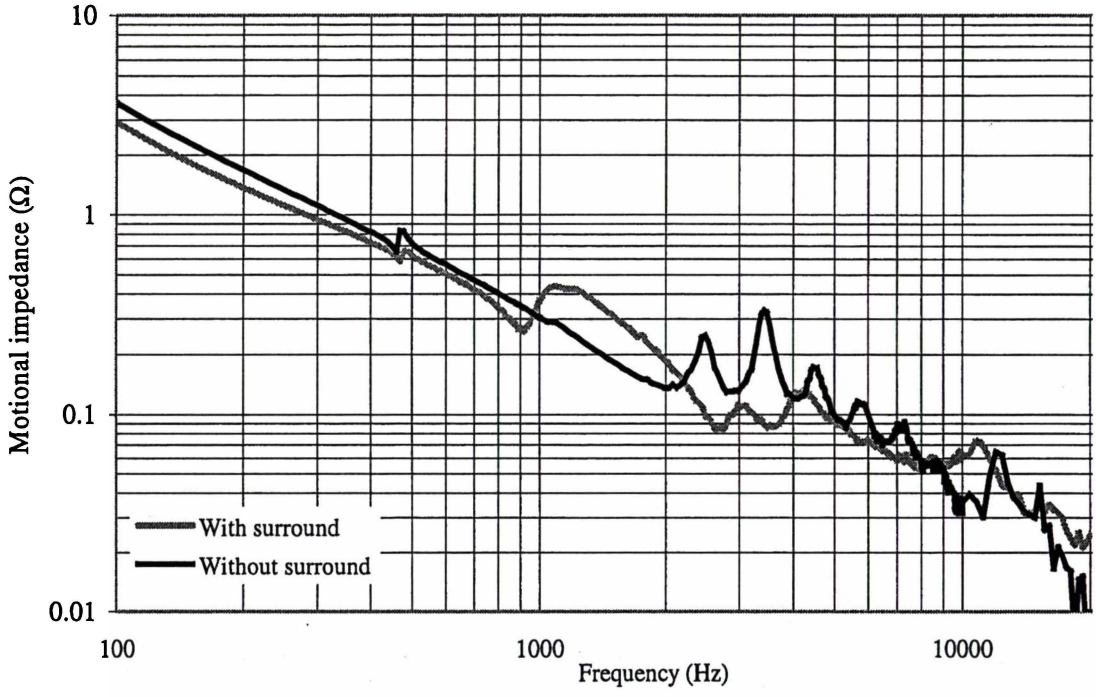

Figure 4.16. Measured Z_{mot} response for loudspeaker cone A with and without surround attached.

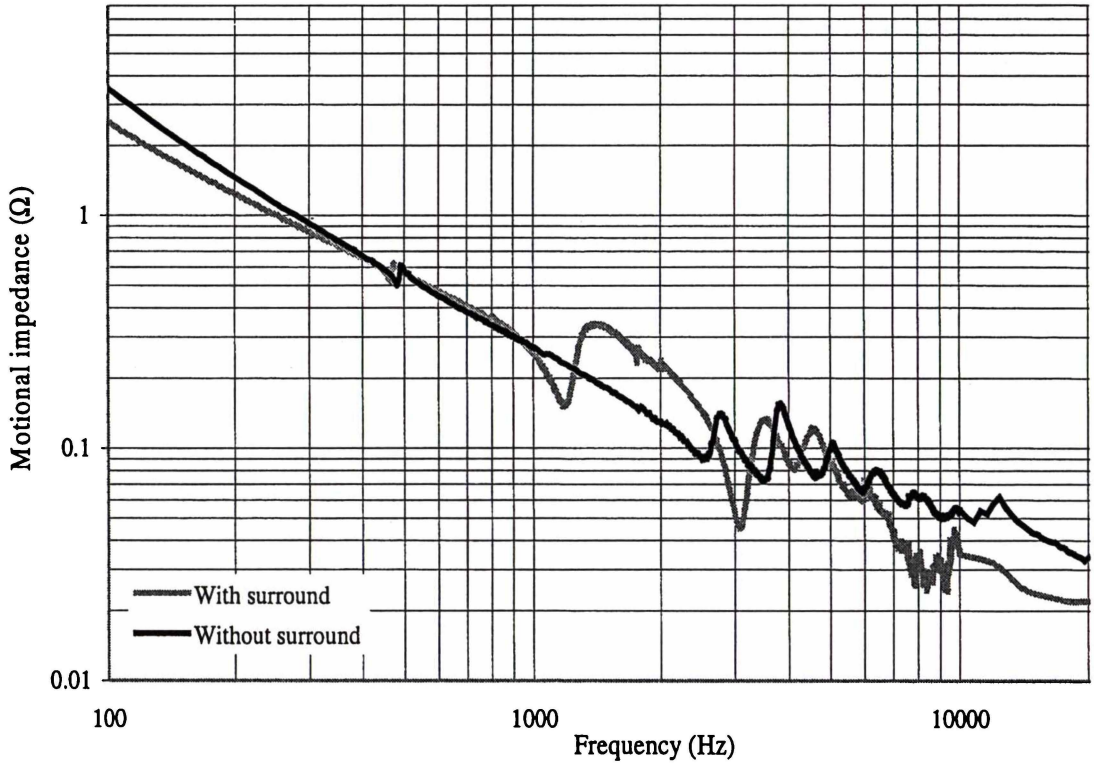

Figure 4.17. Measured Z_{mot} response for loudspeaker cone C with and without surround attached.

From Figure 4.17 it is evident that the outer surround has several significant effects on the resonant behaviour of the loudspeaker:

1. The ring antiresonance feature is significantly decreased in shape and frequency.

2. All bending modes are decreased slightly in frequency and considerably in amplitude.

3. The first longitudinal resonance is lowered in frequency.

(The free-air resonance (not shown) was also shifted upwards slightly for cone A due to the additional spring force provided by the surround.)

These same trends were also noted by Shindo *et al.* [28] in their consideration of the effect of a felt surround on a convex paper loudspeaker.

These results confirm that the rubber surround used with a polypropylene loudspeaker of this type has a considerable effect on its measured motional impedance response, particularly in the frequency range 1-10kHz. Thus, it is appropriate to extend the FE model of this loudspeaker used in the previous sections to include the addition of a surround. This will allow the finite element model to be used to determine the exact effect of the surround on the resonant behaviour of the loudspeaker cone.

4.5.3 FE MODEL EXTENSION

The surround employed by the loudspeakers being considered is of the external half-roll type (Figure 4.18), and is moulded from butyl rubber. A rubber rim extends 4mm down the front face of the loudspeaker, and is joined at the outer edge to an external half-roll (5mm radius, 0.35mm thickness). The outer end of the half roll attaches to another rim, which is firmly glued to the driver frame.

A finite element model of the surround was created using 25 PLANE42 (4 node, 2D) elements. The outermost nodes of the surround were constrained from movement in all directions in order to simulate the connection of the external half roll to the driver frame. This model was connected to a 64-node PLANE42 model of the loudspeaker cone itself, as shown in Figure 4.18.

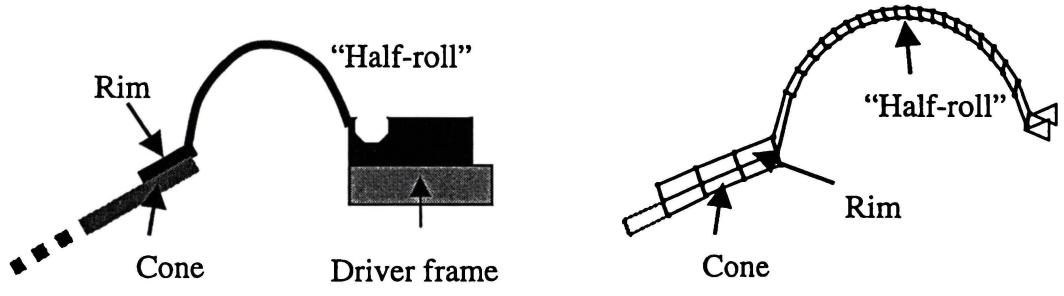

Figure 4.18. Section diagram of the outer surround showing its attachment to the loudspeaker cone and driver frame; corresponding finite element model.

The butyl rubber used to form the surround has a mass density of $\approx$ 1200 kg/m^3, and a Young's modulus of $\approx 2\times10^8$ N/m^2. The Poisson's ratio of the surround was estimated to be ~0.3.

The motional impedance response of Figure 4.19 was calculated using the above properties for the surround material and the calibrated material properties for cone C.

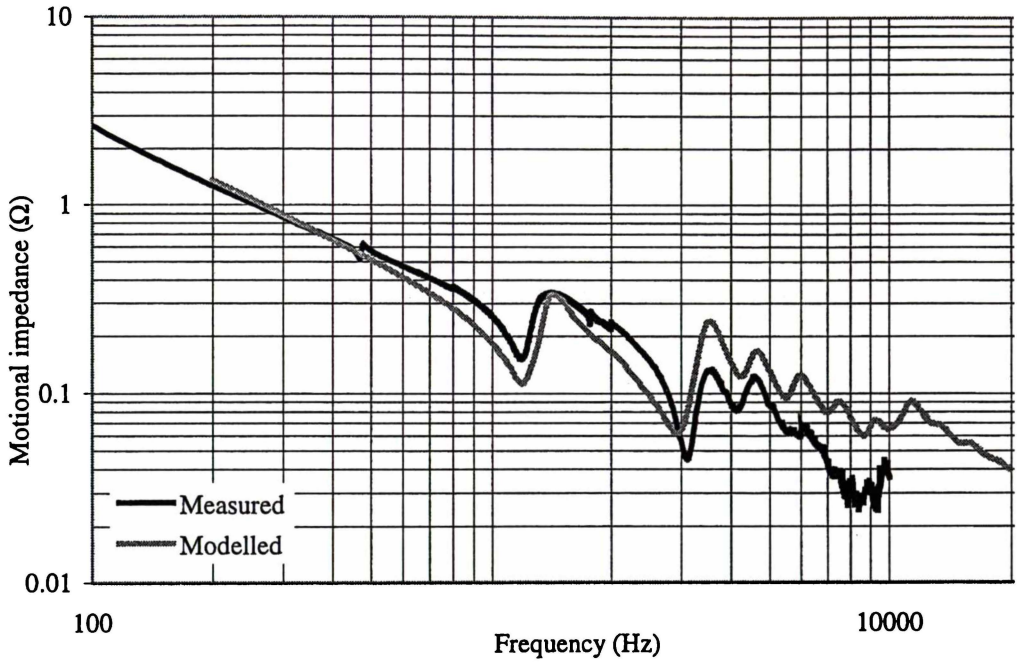

Figure 4.19. Comparison of measured and modelled Z_{mot} responses for cone C, with surround attached.

Figure 4.19 shows that the frequency and shape of the ring antiresonance and the first bending resonance matches well with that measured for cone C. The second and third bending resonances also closely match the measured response. Higher orders modes are indistinguishable in the measured Z_{mot} response curve, and are similarly diminished in the modelled Z_{mot} response.

As this FE model produces a sufficiently accurate representation of the measured response of cone C, the effect of the surround can be characterised in detail by considering the calculated Y_{ax} frequency response and mode shapes.

4.5.4 Effect of Surround on Axial Admittance Response

The effect of the surround on cone resonance can be attributed to two separate components of the surround – the surround rim, and the external half roll.

Firstly, the addition of the rubber rim to the outer edge of the cone lowers the resonant frequencies of the cone, particularly affecting the ring antiresonance and the first resonant frequency. These first modes are the most effected by the added mass at the outer edge, as it is the outer edge of the loudspeaker cone that flexes with maximum amplitude at f_{ra}, f_{brl}.

Secondly, the external half roll adds extra moving mass, and further lowers the first bending resonant and antiresonant frequencies. However, a more significant effect of the external half roll is to provide considerable damping for travelling waves in the cone, thereby diminishing the amplitude of resonant features in the Y_{ax} response.

The first of these effects is best demonstrated by limiting the FE model of the surround to the cone rim alone, and considering the effect of rim density on the axial admittance response. The upper plot of Figure 4.20 shows the Y_{ax} response of cone C with surround rim (no external half-roll) as the density of the cone rim is varied from 0-1200 kg/m^3. The lower plot of Figure 4.20 shows the birds-eye view of the upper plot in order to highlight the density dependence of the resonant modes.

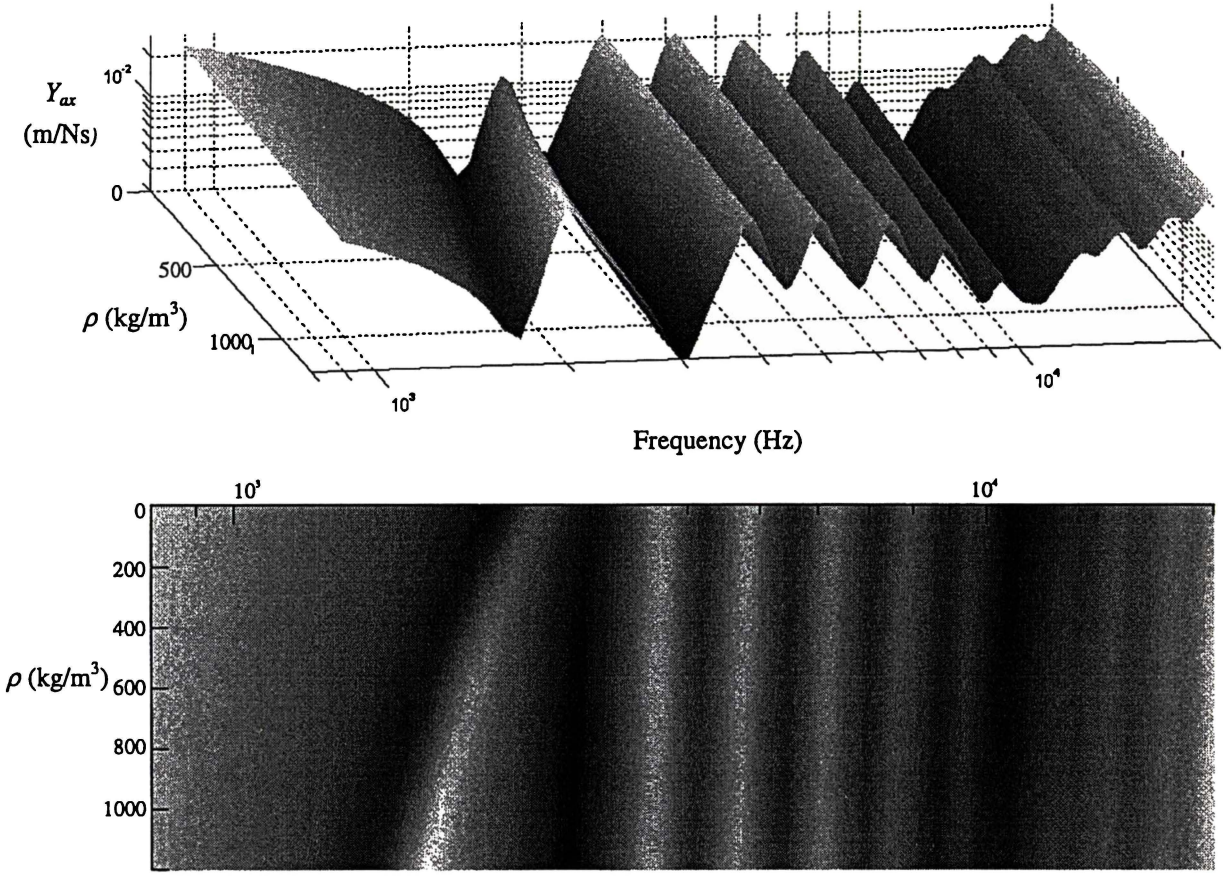

Figure 4.20. Y_{ax} frequency response for cone C with a rubber rim attached to outer edge; the rim density is varied from 0 – 1200 kg/m^3

Figure 4.20 indicates that the primary effect of adding mass in the form of a rubber surround rim is to significantly lower the ring antiresonance of the cone. All other bending modes are also lowered in frequency with increasing surround density, but to a far lesser extent. In contrast, the amplitude of the first resonant feature is increased as a result of the addition of the surround rim.

The effect of the external half roll on the axial admittance response can be clearly demonstrated by removing the cone rim from the FE model and modelling only the half roll component of the surround. In this case, the surround does not overlap the outer edge of the loudspeaker, but simply butts against it. The resulting Y_{ax} frequency response profile is shown below as a function of roll mass density in Figure 4.21.

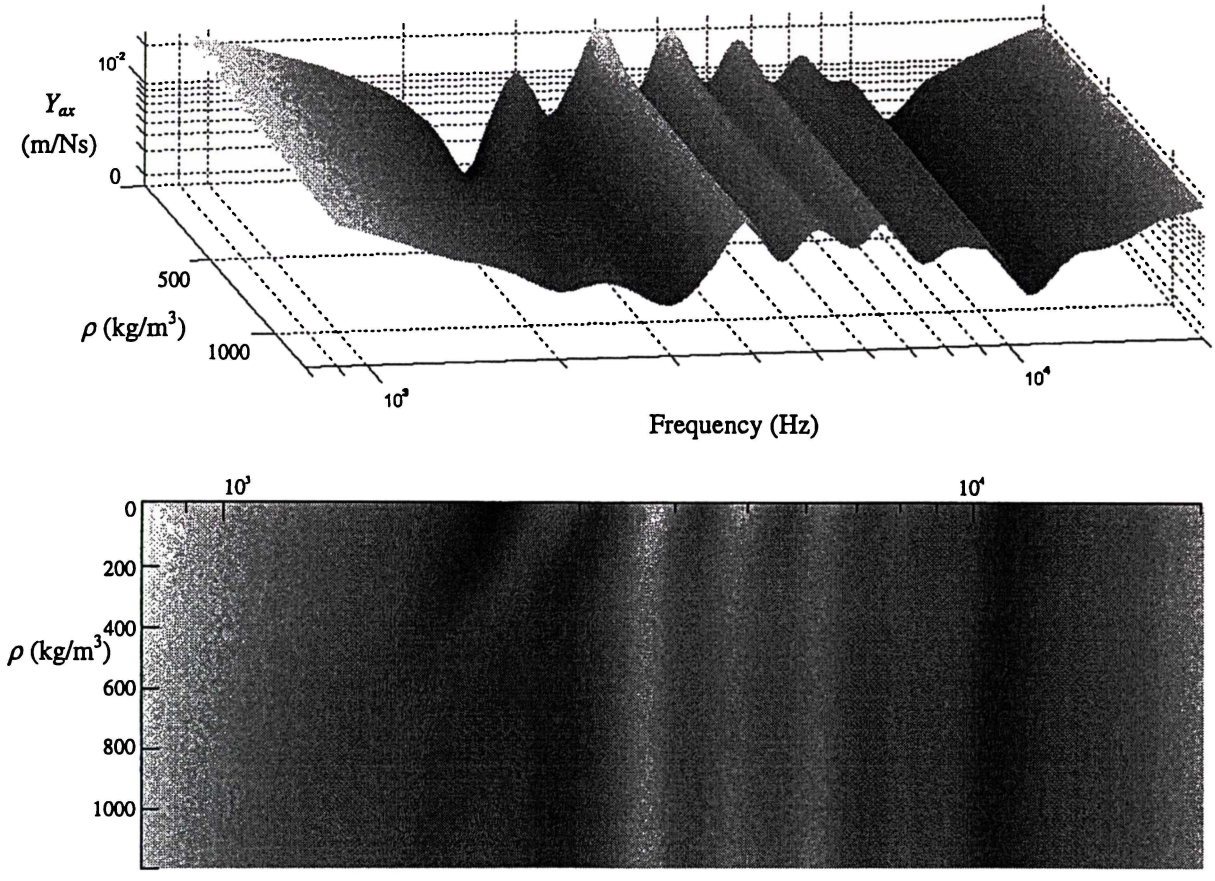

Figure 4.21. Y_{ax} frequency response profile for cone C with an external half roll of rubber attached to the outer edge, as the roll density is varied from 0 – 1200 kg/m^3.

Figure 4.21 confirms that the external half-roll of the surround has a significant damping effect on all the bending resonances, particularly the first bending mode. While the surround also possesses its own resonant modes, they are minimised by the high self-damping properties of the butyl rubber, and are inevident in Figure 4.21.

Combining the surround rim with the external half roll, the density of the entire surround can be varied to demonstrate its overall effect on the cone axial admittance response.

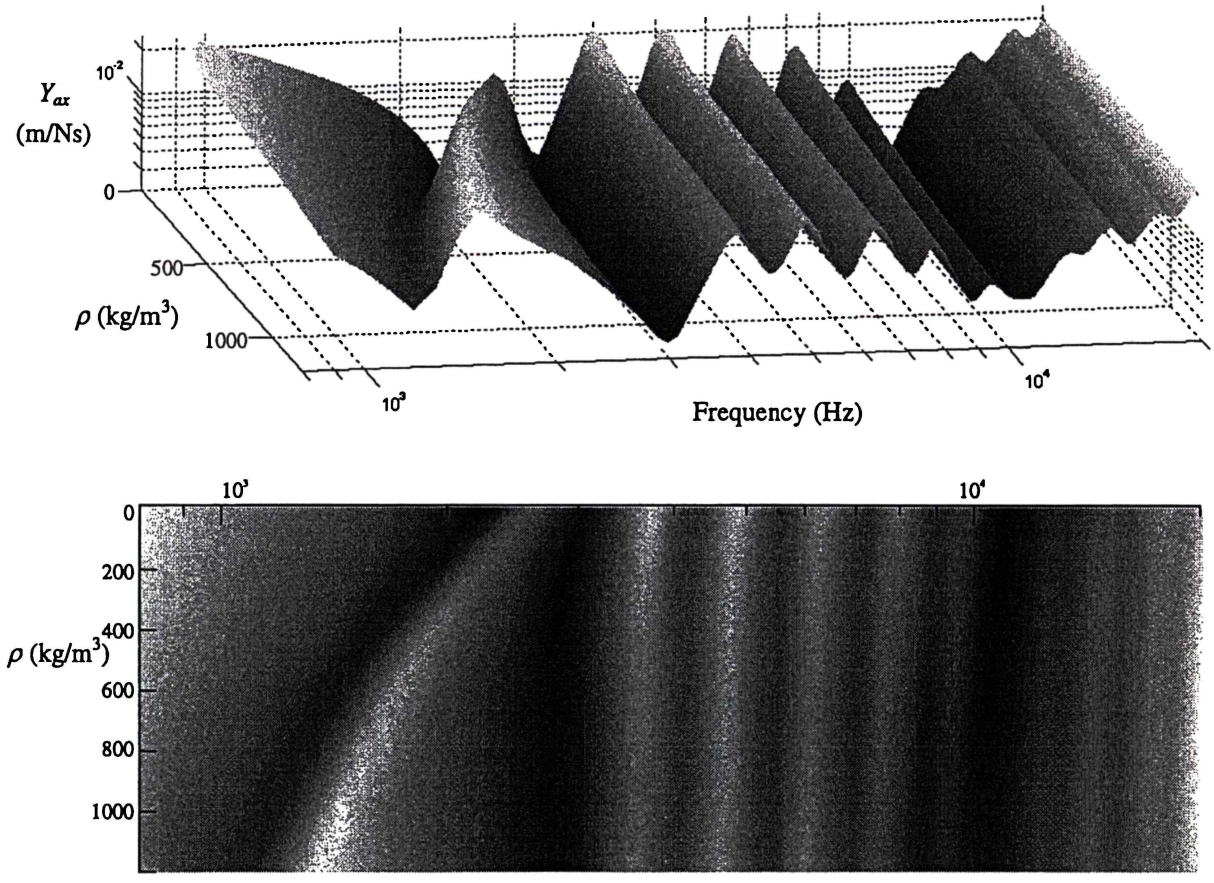

Figure 4.22. Y_{ax} frequency response profile for cone C with entire surround attached to the outer edge, as the surround density is varied from 0 – 1200 kg/m^3.

Figure 4.22 shows that the combination of cone rim and external half roll results in a downward shift in all modal frequencies, particularly the first bending antiresonance, and a diminished amplitude for all resonant modes.

The sound pressure response of the loudspeaker will be similarly affected by the addition of the surround, with the speaker exhibiting a smoother sound pressure response through region B. This will be accompanied by a general lowering of all resonant frequencies, particularly f_{br1}

4.5.5 Effect of Surround on Mode Shapes

Shindo *et al.* [28] noted that the nodal lines and cone displacement pattern of the convex loudspeaker cone they considered were also affected by the addition of an outer surround. Given that the modelled axial admittance response of the speaker is demonstrably altered by the addition of a cone rim and external half roll, it seems reasonable to assume that the cone mode shape would also be affected.

Figure 4.23 shows the modelled cone displacement patterns for cone C with no surround, rubber rim, and external half roll. Figure 4.23 a) is a reproduction of Figure 4.15 and is included here as a reference mode shape.

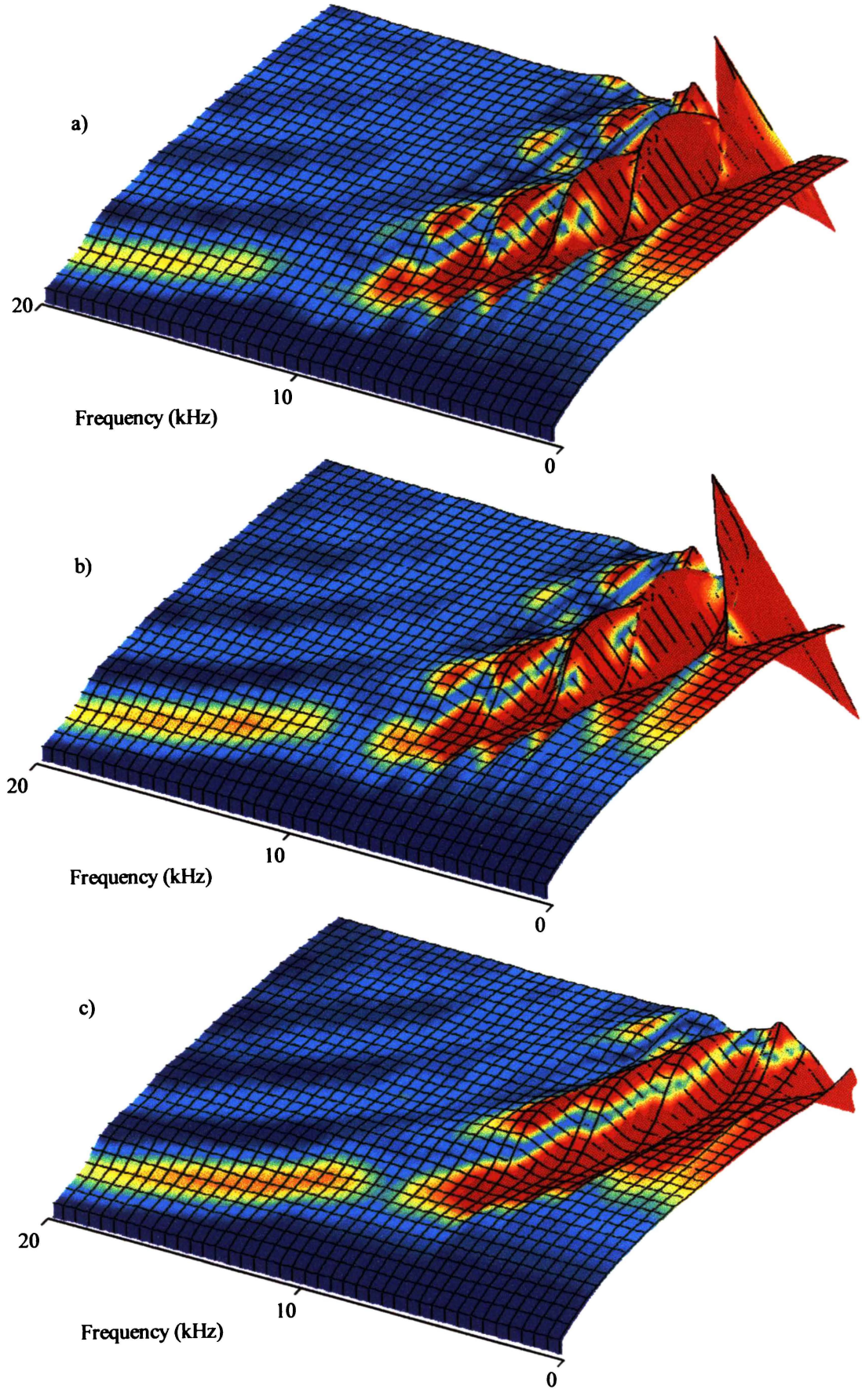

Figure 4.23. Cone displacement patterns for a) Cone with no surround, b) Cone with rim, c) Cone with rim and external half roll.

Figure 4.23 b) shows the displacement pattern for cone C with a rubber rim attached to the outside edge. The inclusion of the rubber rim in the cone model increases the moving mass at the outer edge of the cone, thereby lowering significantly the frequency of the first bending resonant frequency. The nodal line of this resonant mode is moved out slightly towards the outer edge of the cone. The outer edge of the cone vibrates with a greater amplitude displacement than a cone with no surround.

When the external half roll is added to the cone model (Figure 4.23c), the overall cone displacement is reduced notably, particularly at lower frequencies. The extra damping provided by the surround results in the cone motion being more piston-like.

All nodal and antinodal lines are shifted slightly towards the outer edge of the cone by the addition of the surround, due to the cone meridional length being effectively increased.

Summary

The addition of an external half roll butyl rubber surround with a 5mm cone rim has the effect of:

1. Significantly lowering the frequency of the first bending resonant and antiresonant modes.

2. Slightly lowering the frequencies of all other bending and longitudinal modes.

3. Slightly moving all nodal and antinodal lines outwards.

4. Decreasing the variation in cone displacement across the surface of the cone and thus smoothing the sound pressure response.

In general, subsequent FE models do not include the surround, in order keep the number of elements and nodes to a minimum. When necessary, the effect of the surround on the response of any of the 2D or 3D modelled cones can be estimated using points 1-4 as a general guide.

4.6 CONCLUSION

In this chapter, a finite element model of an axisymmetric loudspeaker cone has been designed and calibrated against measured results for two loudspeakers, A and C. Subsequently, the natural frequencies, characteristics, and mode shapes of loudspeaker cone C have been derived and can be taken to be generally indicative of those of a typical 6½" polypropylene driver. Also, the effect of the surround on the axial admittance response and mode shapes of cone C has been established and summarised.

Having derived the characteristics of a typical loudspeaker cone using a calibrated FE model, the effect of various parameters on loudspeaker cone resonance may be ascertained. In particular, Chapter 5 examines the effect of changes in material properties, cone thickness, and cone thickness profile on the natural resonances of the cone and shows how these resonances may be tuned.

Chapter 6 demonstrates the manner in which cone resonance is affected by introducing slots into the surface of the cone. The 3D model calibrated in this chapter is used as the starting point for Chapter 6.

CHAPTER 5

REGULATING LOUDSPEAKER CONE RESONANCE

5.1 OVERVIEW

In Chapter 4, the resonant characteristics of an axisymmetric loudspeaker were quantified in terms of its axial admittance response (Y_{ax}), mode shapes, cone deformation pattern, and radiated sound pressure response. In this chapter, the dependence of these loudspeaker characteristics on the properties of the cone is considered.

The calibrated material properties for cone C are used as a common starting point for all analyses in this chapter. The properties of the cone material are varied independently and the effect of each variation of the resonant behaviour of the cone quantified in terms of the axial admittance, cone deformation pattern, and sound pressure response. The effect of variations in material properties on mode shape is also considered.

The extent to which the thickness and thickness profile of the loudspeaker cone affects cone resonance is explored in Section 5.3. Constant thickness and graduated thickness loudspeaker cones are examined and the effect of cone thickness on the resonant characteristics of the loudspeaker is defined. Consequently, a technique for altering the frequencies and magnitudes of specific bending modes by selectively thinning or thickening parts of the loudspeaker cone is examined and summarised.

5.2 EFFECT OF CONE MATERIAL PARAMETERS ON LOUDSPEAKER CHARACTERISTICS

The loudspeaker cone is described in the FE model by means of three isotropic material properties: Young's modulus, mass density and Poisson's ratio. The frequencies of the natural modes of the loudspeaker cone are strongly dependent on the value of each of these. Further, the specified damping ratio can have an influence on the shape of the axial admittance response, and consequently the sound pressure response. Thus, the resonant behaviour of a loudspeaker cone of given dimensions can be adjusted by selecting materials of appropriate properties.

In this section, the effect of each of the three isotropic material properties on the resonant behaviour of the loudspeaker is considered, with a particular emphasis on bending waves. This is achieved by individually perturbing the material properties of the FE model of cone C over a realistic range, and expressing the characteristics of the loudspeaker in terms of its Y_{ax} response, cone deformation pattern, and p_{ax} response.

Frankfort [6,7] develops a numerical model of a straight-sided loudspeaker cone, and uses it to characterise the cone's resonant behaviour in terms of its on-axis sound pressure, radiated sound power and directivity. His results focus mainly on the effects of geometrical factors (thickness, inner and outer radii, meridional length of cone, and apex angle), but also briefly consider the effect of mass density and Young's modulus on cone resonance.

However, Frankfort's results and conclusions are mainly concerned with the behaviour of the longitudinal modes of the cone. As the peaks and dips in the useable sound pressure range of a loudspeaker cone are largely due to bending wave motion, a greater understanding of the dependence of bending wave behaviour on cone material properties and geometry is required.

Geaves [23] briefly examines the effect of changing the Young's modulus of both the cone and surround material in order to calibrate a FE model. The dependence of the resonances in the developed sound pressure response on the value of Young's modulus is noted, but no further significant conclusions are reached.

Heed [29] uses a combination of lumped parameter and finite element techniques to consider the effect of damping on loudspeaker cone resonance. He argues that the damping ratio of the cone and surround has a very significant effect on the amplitude of transverse standing waves on the loudspeaker cone. The results of Section 5.2.4 provide support for his claims, while explicitly defining the effect of damping on the loudspeaker's characteristics.

In practice, material properties are not independent, and it is difficult to change one property of a material without affecting others. For example, a material of high density will often possess a large Young's modulus, while a material with high self-damping

may also possess a different mass density to an undamped material. However, it is still useful to develop a clear understanding of the individual effect of each material property on the resonant characteristics of the loudspeaker cone. Although the results considered in this section are generated for the specific geometry and design of loudspeaker C, they can be applied in a general manner to loudspeakers of different shapes and sizes.

This consideration is restricted to linear, isotropic, and homogeneous materials. Some loudspeakers are manufactured from materials such as Kevlar and honeycomb-type structures [19], which are not isotropic. Other materials, such as paper or felt, can be moderately inhomogeneous, resulting in the excitation of non-axisymmetric modes. While the developed FE model allows for the possibility of simulating loudspeakers manufactured from anisotropic, non-linear, and inhomogeneous media, it is beyond the scope of this thesis to discuss such materials.

The following sections examine in detail the effect of each material property on the natural resonances of cone C. In each section, the FE model is defined using the calibrated material properties for cone C (Table 4.2), and the material property under investigation is independently varied. Each material property is varied over a realistic range that allows the change in frequency and amplitude of the resonant modes to be readily identified. The behaviour of the loudspeaker cone is quantified in terms of its axial admittance and sound pressure response (both on and off-axis). Cone deformation plots are included for reference.

In general, axial admittance results are shown for the cone itself, (without the added mass of the voice coil) allowing the shift in the natural frequencies of the cone to be clearly seen. However, all modelled sound pressure results are calculated from a FE/BE model which accounts for the voice coil mass. The same voice coil mass (10 g) is used for each plot.

All cone deformation plots are in response to a 1N axial force, and are scaled by the same factor from plot to plot, in order to clearly show the mode shapes. All cone displacements are relative to that of the innermost node.

All directivity versus frequency plots are drawn to the same scale, with colour representing the magnitude of the sound pressure response.

5.2.1 DENSITY

To examine the effect of variations in cone material density ρ, the modelled Y_{ax} response was calculated for ρ ranging between 800 and 1400 kg/m^3. Each Y_{ax} response is calculated for 200 frequencies in the range 1kHz-20kHz.

The uppermost plot of Figure 5.1 displays these results by means of a 3D log-log-log plot. The vertical axis is the axial admittance value Y_{ax} with frequency as the horizontal axis. The cone density ρ forms the third (out of the page) axis. The lower plot of Figure 5.1 shows the bird's-eye view of the upper plot in order to reveal the density dependence of the axial admittance frequency response.

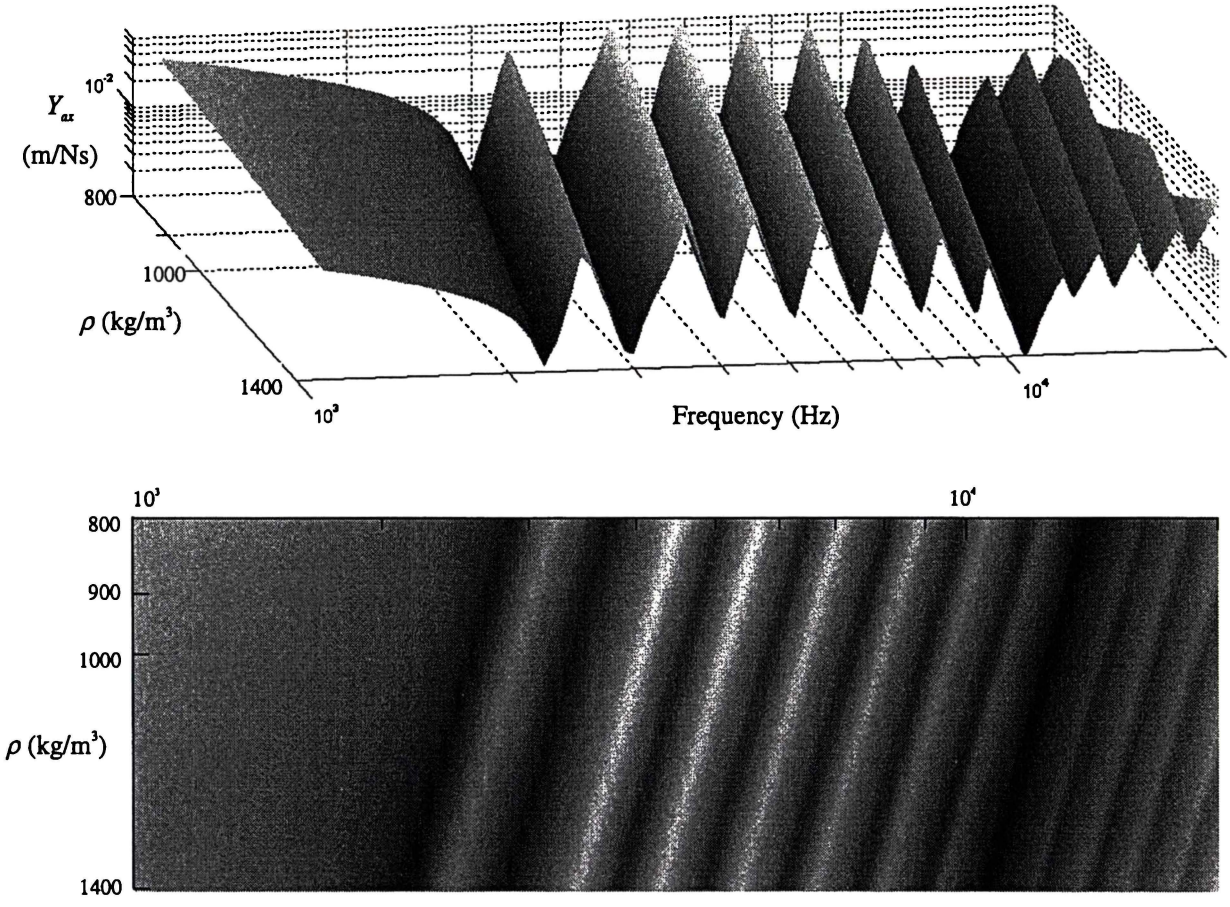

Figure 5.1. Calculated Y_{ax} frequency response of axisymmetric cone as cone density is varied from 800kg/m^3 to 1400 kg/m^3.

Figure 5.1 illustrates that the frequencies of bending and longitudinal resonances and antiresonances decrease with increasing cone density. Moreover, all resonant frequencies f_n can be shown to be proportional to the inverse square root of the cone density:

$$f_n \propto \frac{1}{\sqrt{\rho}} \tag{5.1}$$

Consequently, if a cone of mass density ρ has resonant frequencies denoted f_n, the same

cone of density ρ' will have resonant frequencies given by:

$$f_n' = \frac{\sqrt{\rho}}{\sqrt{\rho'}} f_n \tag{5.2}$$

This relationship could be utilised to calibrate material properties in the FE models so that modelled modal frequencies match well with measured modal frequencies. However, it is preferable to adjust the value for Young's modulus instead, since Young's modulus is more likely to be the factor that varies from speaker to speaker, particularly as the cone material ages.

While the frequencies of all the modes are lowered by an increase in cone mass density in accordance with the relationship of equation (5.2), the overall shape of the axial admittance response is unaffected. The mean value of the axial admittance is decreased with increasing mass density due to the increased total moving mass of the loudspeaker. This is shown in Figure 5.2, where the axial admittance is plotted for ρ = 800 kg/m^3 ρ = 1400 kg/m^3.

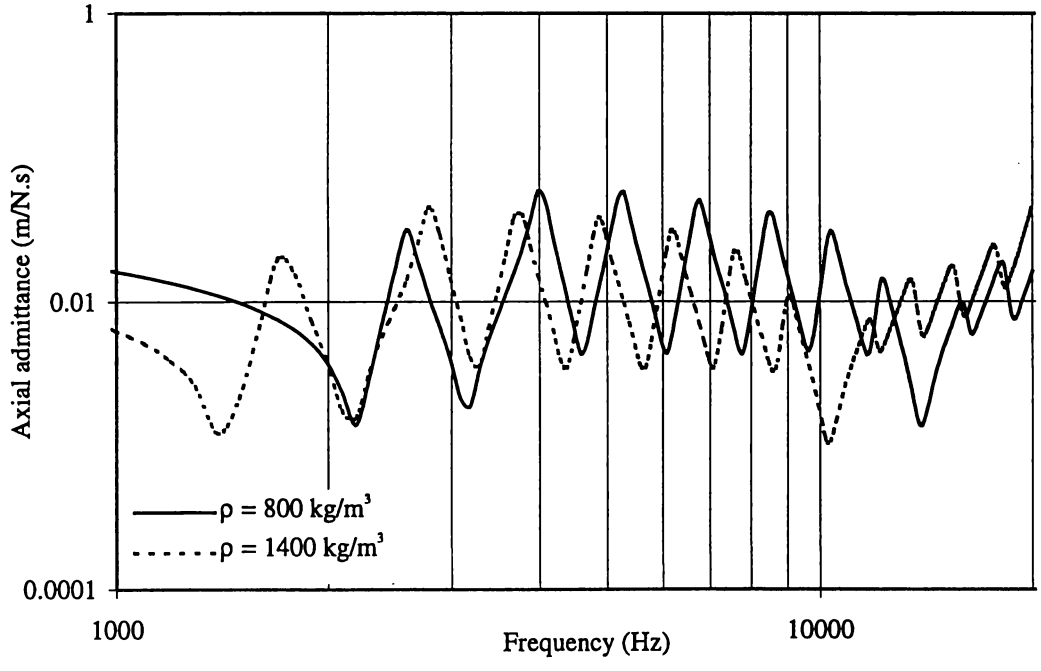

Figure 5.2. Y_{ax} response of cone C for ρ = 800 kg/m^3, ρ = 1400 kg/m^3

Figure 5.2 illustrates that the magnitudes of the peaks and troughs in the axial admittance response are almost unaffected by the mass density of the cone, while the mean axial admittance of the denser cone is lower.

The cone deformation patterns for ρ = 800 kg/m^3 and ρ = 1400 kg/m^3 were also calculated, and are shown in Figure 5.3.

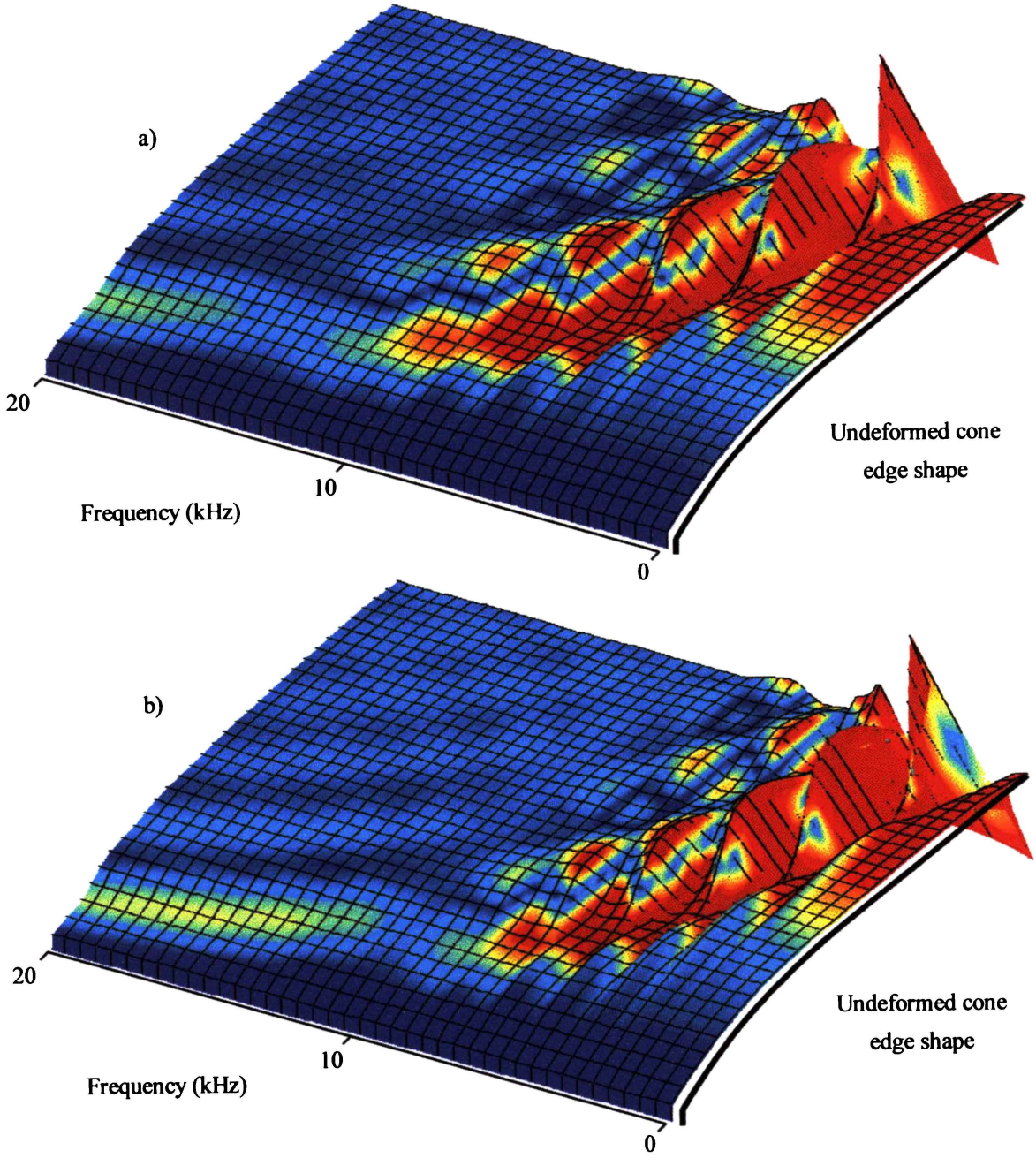

Figure 5.3. Cone deformation pattern for a) $\rho = 800$ kg/m^3, b) $\rho = 1400$ kg/m^3

Figure 5.3 demonstrates that although the frequencies of the natural modes of the cone decrease with increasing cone density, the mode shapes (that is, the positions of nodal and antinodal lines) are unaffected.

The lower total mass of a less dense cone implies a higher radiated sound pressure, and hence higher efficiency. Assuming a voice coil mass of 10 g, the on-axis sound pressure response for $\rho = 800$ kg/m^3, $\rho = 1400$ kg/m^3 was calculated and is shown in Figure 5.4.

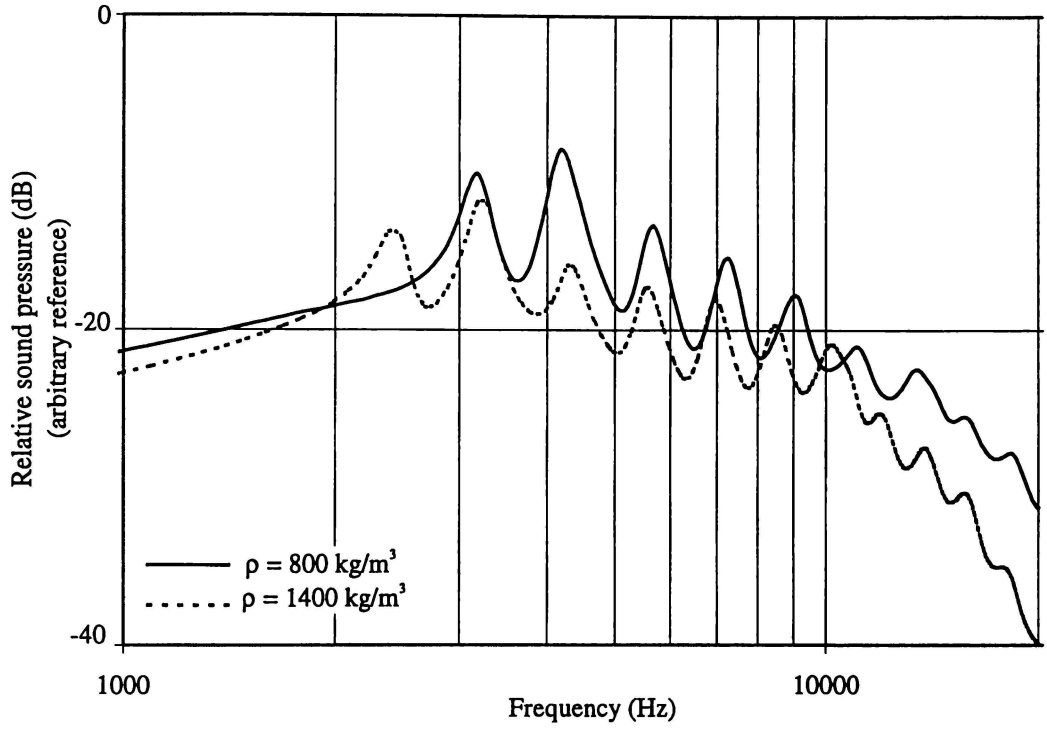

Figure 5.4. On-axis far-field sound pressure responses for $\rho = 800$ kg/m^3, $\rho = 1400$ kg/m^3.

Figure 5.4 confirms that the mean value of the sound pressure response decreases with increasing cone density. The magnitude of ripple in the sound pressure response also slightly diminishes with increasing cone density. Similar trends are evident in the off-axis response, shown in Figure 5.5 by means of a 3D polar sound pressure response plot.

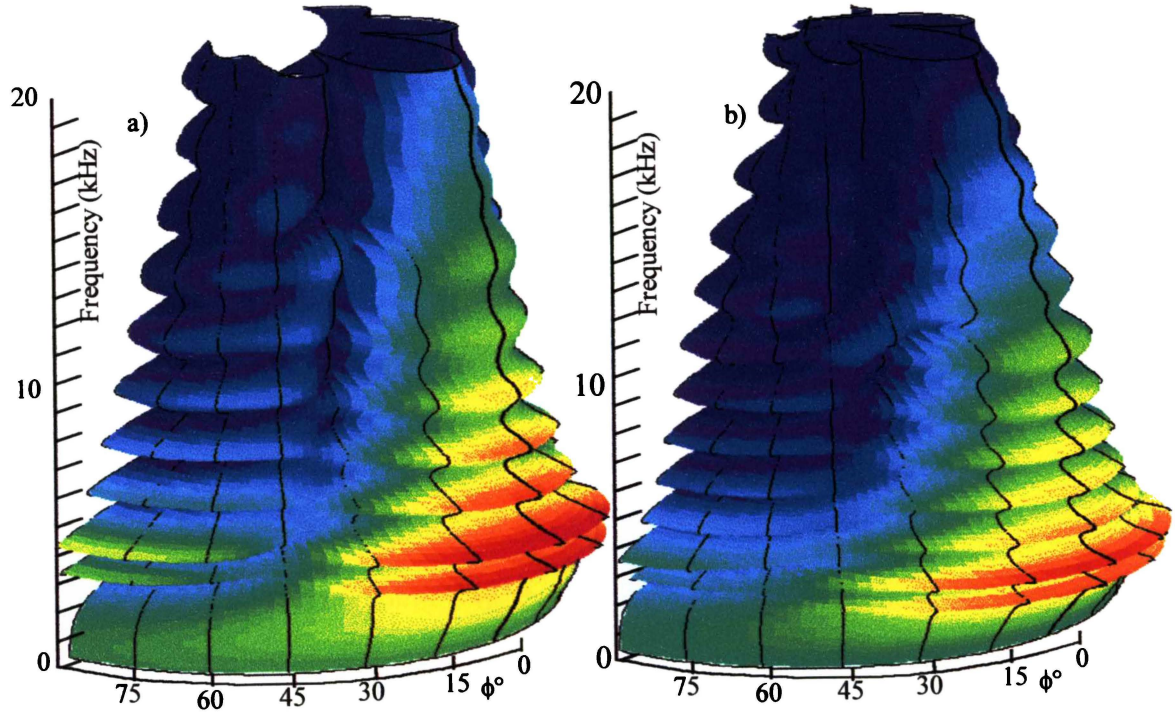

Figure 5.5. 3D Polar sound pressure frequency response plots for a) $\rho = 800$ kg/m^3 b) $\rho = 1400$ kg/m^3

Figure 5.5 indicates that the off-axis response for ρ = 800 kg/m^3 is considerably greater than that for ρ = 1400 kg/m^3 at any given frequency. This is due to the higher longitudinal resonant frequency of the less dense cone. This effect aside, the overall shape of the 3D polar response characteristic is independent of cone density.

Summary

Increasing the cone material density:

- Decreases all bending resonant frequencies according to equation 5.2.
- Shifts the first longitudinal antiresonance to a lower frequency, thereby reducing the bandwidth of the loudspeaker.
- Decreases the overall efficiency of the loudspeaker, and thus the developed sound pressure.
- Slightly decreases the ripple of the sound pressure frequency response, both on and off-axis.

5.2.2 YOUNG'S MODULUS

As the Young's modulus E effectively defines the stiffness of the cone material, it has a considerable effect on the frequency of resonant and antiresonant modes. To illustrate this effect, the Young's modulus of cone C was varied from 4×10^9 to 7×10^9 N/m^2, which is a realistic range for polypropylene. The results are displayed in Figure 5.6 as a 3D log-log-log plot of the axial admittance frequency response versus Young's modulus.

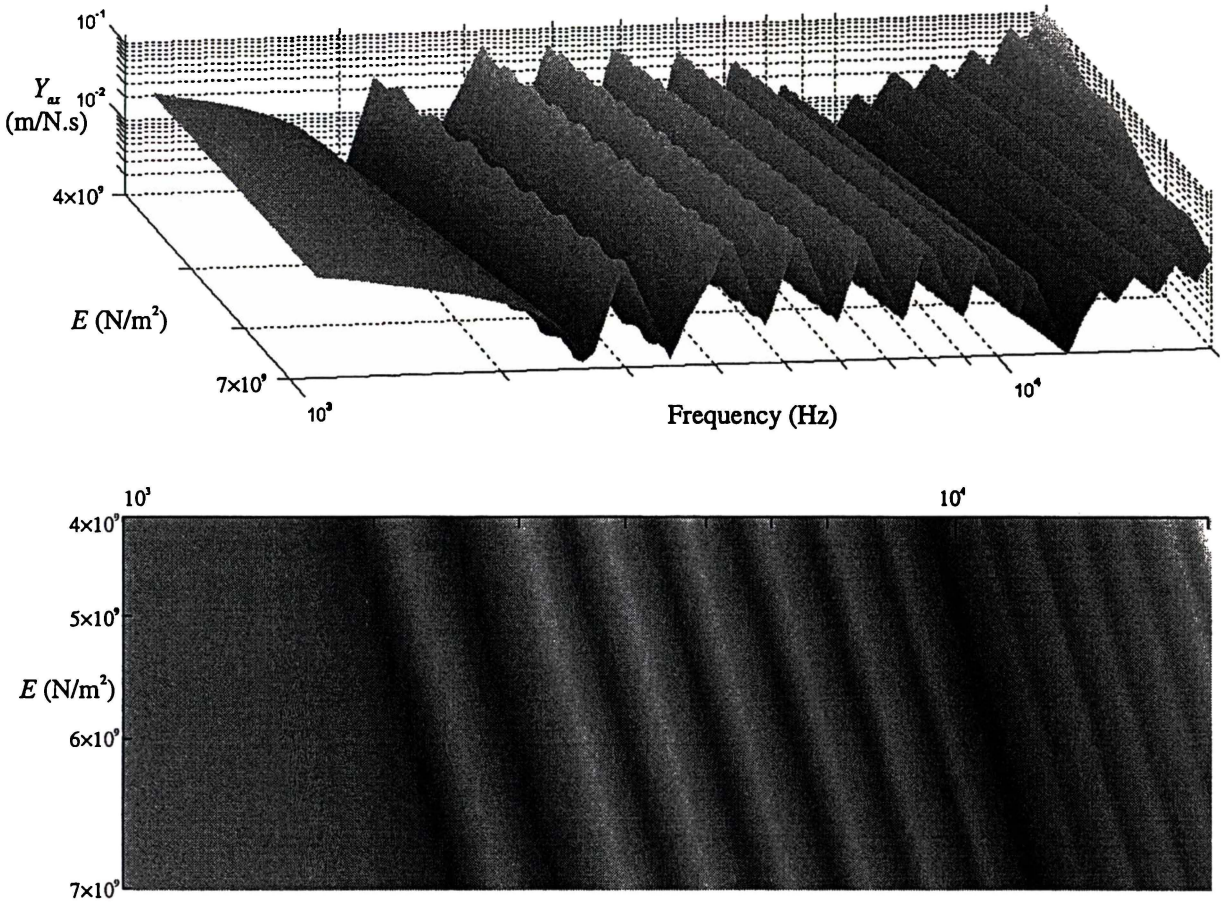

Figure 5.6. Calculated Y_{ax} frequency response of axisymmetric cone as Young's modulus E is varied from 4×10^9 N/m^2 → 7×10^9 N/m^2.

Figure 5.6 demonstrates that the frequencies of bending and longitudinal resonances and antiresonances increase with increasing Young's modulus[5]. All resonant frequencies f_n are proportional to the square root of Young's modulus, E:

$$f_n \propto \sqrt{E} \tag{5.3}$$

Consequently, if a cone of Young's modulus E has resonant frequencies denoted f_n, the

[5] The small ripples evident in the resonant peaks of Figure 5.6 are due to the discrete values of E used to generate the figure, and unfortunately cannot be disguised by the interpolated shading routine utilised by the graphing software. A similar effect can be seen in Figures 5.21 and 5.26.

same cone of Young's modulus E' will have resonant frequencies given by:

$$f_n' = \frac{\sqrt{E'}}{\sqrt{E}} f_n \tag{5.4}$$

This relationship was used to calibrate the FE model as detailed in Chapter 4.

While the resonant frequencies increase with increasing Young's modulus, and the axial admittance response moves to higher frequency, the overall shape of the axial admittance response is unaffected by the Young's modulus of the cone material. This is shown in Figure 5.7 where the Y_{ax} response is plotted for $E = 4\times10^9$ N/m^2 and $E = 7\times10^9$ N/m^2.

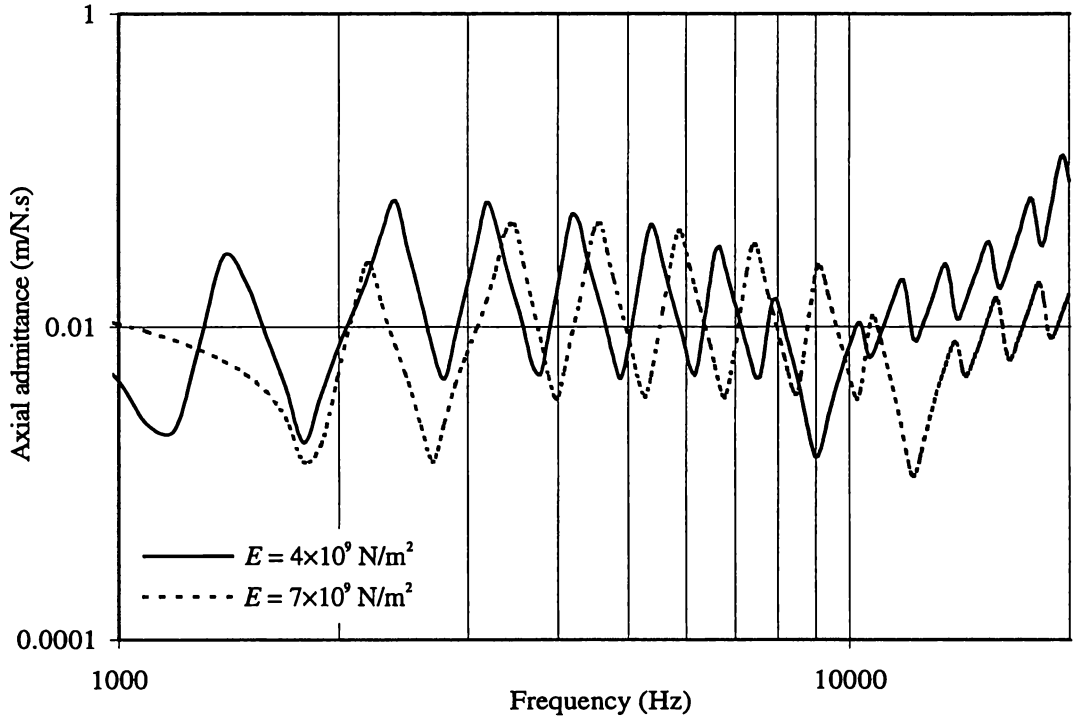

Figure 5.7. Modelled Y_{ax} response for $E = 4\times10^9$ N/m^2 , $E = 7\times10^9$ N/m^2

The two axial admittance responses of Figure 5.7, although differing in frequency, are very similar in magnitude and shape.

However, the cone deformation plots for $E = 4\times10^9$ N/m^2, $E = 7\times10^9$ N/m^2, (Figure 5.8) show that increasing the stiffness of the cone material not only increases the frequencies of the natural resonances of the cone, but also decreases the magnitude of the standing waves on the cone. This is to be expected, as the increased bending stiffness opposes the transverse displacement of the surface of the cone. In the limit, an infinitely stiff loudspeaker cone will exhibit no standing wave behaviour at all, but vibrate as a rigid body. Thus, increasing the Young's modulus of the loudspeaker material results in higher frequency, lower amplitude standing waves.

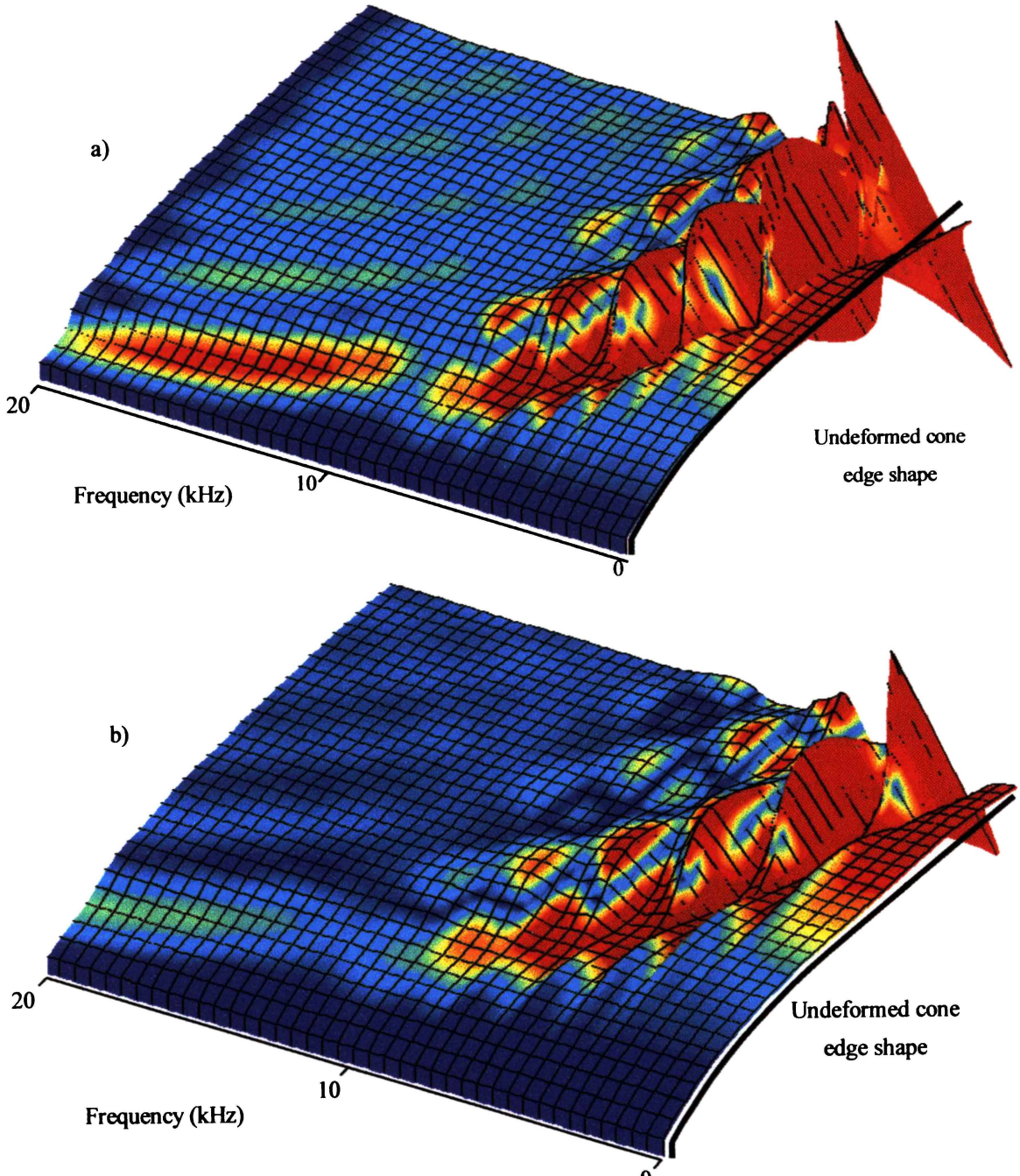

Figure 5.8. Cone deformation pattern for a) $E = 4\times10^9$ N/m^2 b) $E = 7\times10^9$ N/m^2

The effect of this resonant behaviour on the on-axis sound pressure response is shown in Figure 5.9. Although the greater stiffness of the cone with larger Young's modulus results in a lower amplitude of cone deformation, the magnitude of the ripple in the sound pressure response is slightly increased in magnitude with increasing Young's modulus. Thus, when the cone stiffness is increased, all resonant frequencies are similarly increased, but the magnitude of the sound pressure created at each resonant frequency is more pronounced. This results in higher magnitude ripple in the on- and off-axis sound pressure response.

Further, the increased stiffness of a cone with higher Young's modulus increases the first longitudinal antiresonant frequency, thereby extending the bandwidth of the

loudspeaker, both on- and off-axis. This is shown in Figure 5.10, where the directivity of the sound radiation is shown in a 3D polar sound pressure frequency response plot.

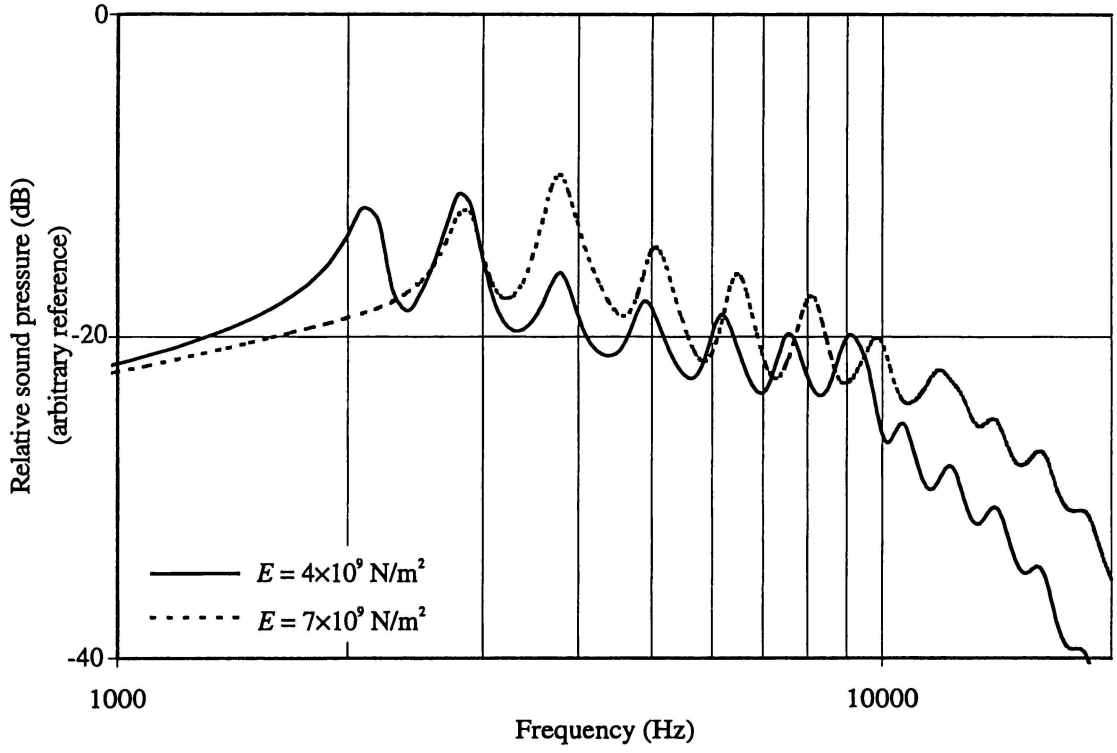

Figure 5.9. On-axis far-field sound pressure responses for $E = 4\times10^9$ N/m², $E = 7\times10^9$ N/m²

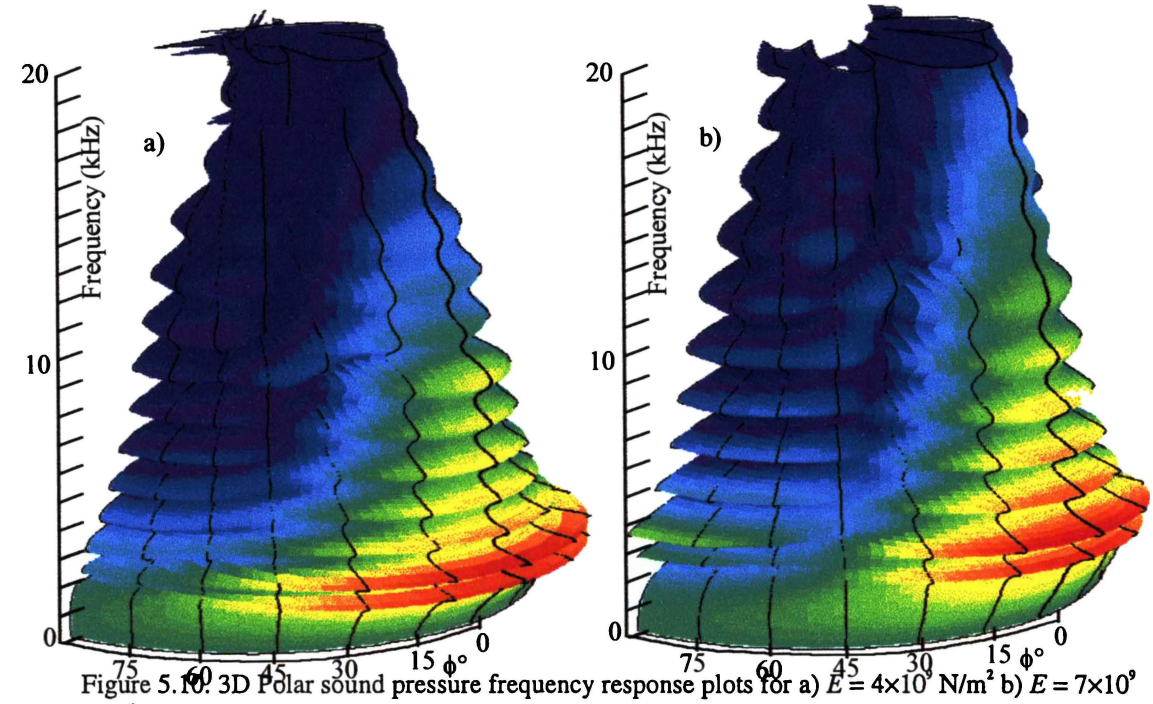

Figure 5.10. 3D Polar sound pressure frequency response plots for a) $E = 4\times10^9$ N/m² b) $E = 7\times10^9$ N/m²

As increasing the stiffness of the cone material has a very similar effect as decreasing its density, loudspeaker cones manufactured from light, stiff materials possess higher resonant frequencies and a higher bandwidth than dense, floppy cones. Consequently, a

light, stiff loudspeaker cone (large value of E/ρ) can be used to higher frequencies before it begins to break up. However, once break-up begins to occur, the magnitudes of the undesirable resonant peaks in the axial admittance and sound pressure responses become more pronounced. For this reason, light, stiff materials often require considerable additional damping in order to absorb some of the resonant energy and diminish the effect of the high frequency, high Q resonant peaks.

Materials such as Kevlar, carbon fibre, and aluminium all posses a high value of E/ρ, and a high degree of flexural rigidity. Although cone drivers manufactured from such materials vibrate in a piston-like motion to relatively high frequencies, they commonly require a sharp electrical crossover or notch filter to reduce the effect of resonant peaks once breakup begins to occur.

Summary

Increasing Young's modulus:

- Shifts all bending resonant frequencies to a higher frequency according to equation 5.4.
- Shifts the first longitudinal antiresonance to a higher frequency, thereby extending the bandwidth of the loudspeaker.
- Slightly increases the magnitude of the ripple in the sound pressure frequency response.

5.2.3 POISSON'S RATIO

The value chosen for Poisson's ratio, ν, also has an effect on the shape of the Y_{ax} frequency response. The value of Poisson's ratio was varied from 0.1 to 0.4 and the following axial admittance response derived:

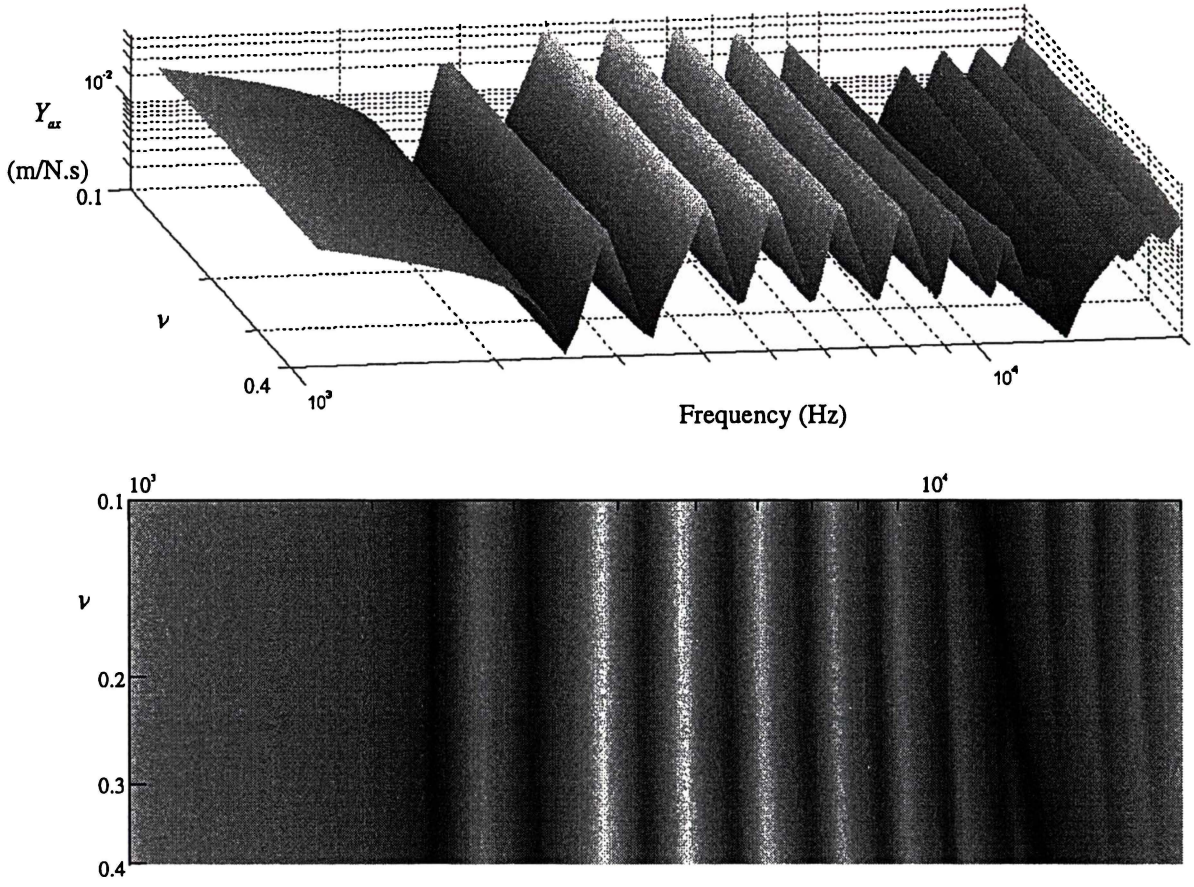

Figure 5.11. Calculated Y_{ax} frequency response of axisymmetric cone as Poisson's ratio ν is varied from 0.1 → 0.4.

Figure 5.11 indicates that the value of Poisson's ratio has only a slight effect on the frequency of bending modes, but a considerable effect on the frequency of longitudinal modes. The longitudinal mode frequency dependence is of the form:

$$f_{longitudinal} \propto \frac{1}{\sqrt{1-\nu^2}} \tag{5.5}$$

By altering the value of Poisson's ratio, the position of the longitudinal mode relative to the bending modes can be specified. Thus by observing the shape of the motional impedance response near the onset of longitudinal resonance, the best value of Poisson's ratio can be determined.

The frequency dependence of the first longitudinal antiresonance on Poisson's ratio also implies that the upper limit of the sound pressure response will be affected by the value of ν. However, the increased value of Poisson's ratio also causes a more pronounced dip at the onset of longitudinal resonance. This becomes more evident if the axial

admittance response at $\nu = 0.1$ and ν=0.4 are plotted together, as in Figure 5.12.

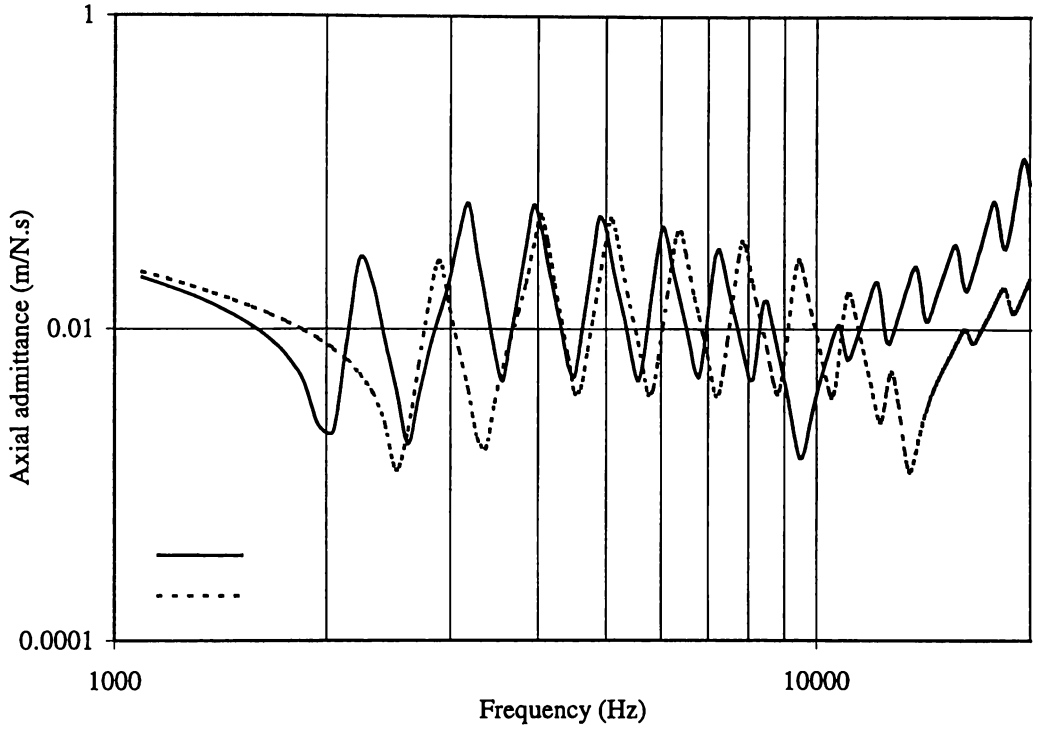

Figure 5.12. Modelled Y_{ax} response for $\nu = 0.1$, $\nu = 0.4$

Increasing the value of ν shifts the longitudinal antiresonance to a higher frequency, and thus would seem to imply an increased bandwidth for the loudspeaker. Conversely, the magnitude of bending resonances in the axial admittance curve at high frequency is diminished for large ν, implying a smoother radiated sound pressure above f_{la1}.

The cone deformation patterns (Figure 5.13) similarly show that the shapes of cone bending modes are unchanged by the value of Poisson's ratio. Figure 5.13 also illustrates that the onset of longitudinal resonance results in a greater longitudinal motion of the cone above f_{la1}. This is depicted in Figure 5.13 b) by the overall lighter colour of the displacement pattern at high frequency. Again, this increased longitudinal motion above f_{la1} implies a rapid high frequency drop off in sound pressure.

The modelled on- and off-axis sound pressure responses for $\nu = 0.1$ and 0.4, shown in Figure 5.14 and Figure 5.15 confirm these assumptions.

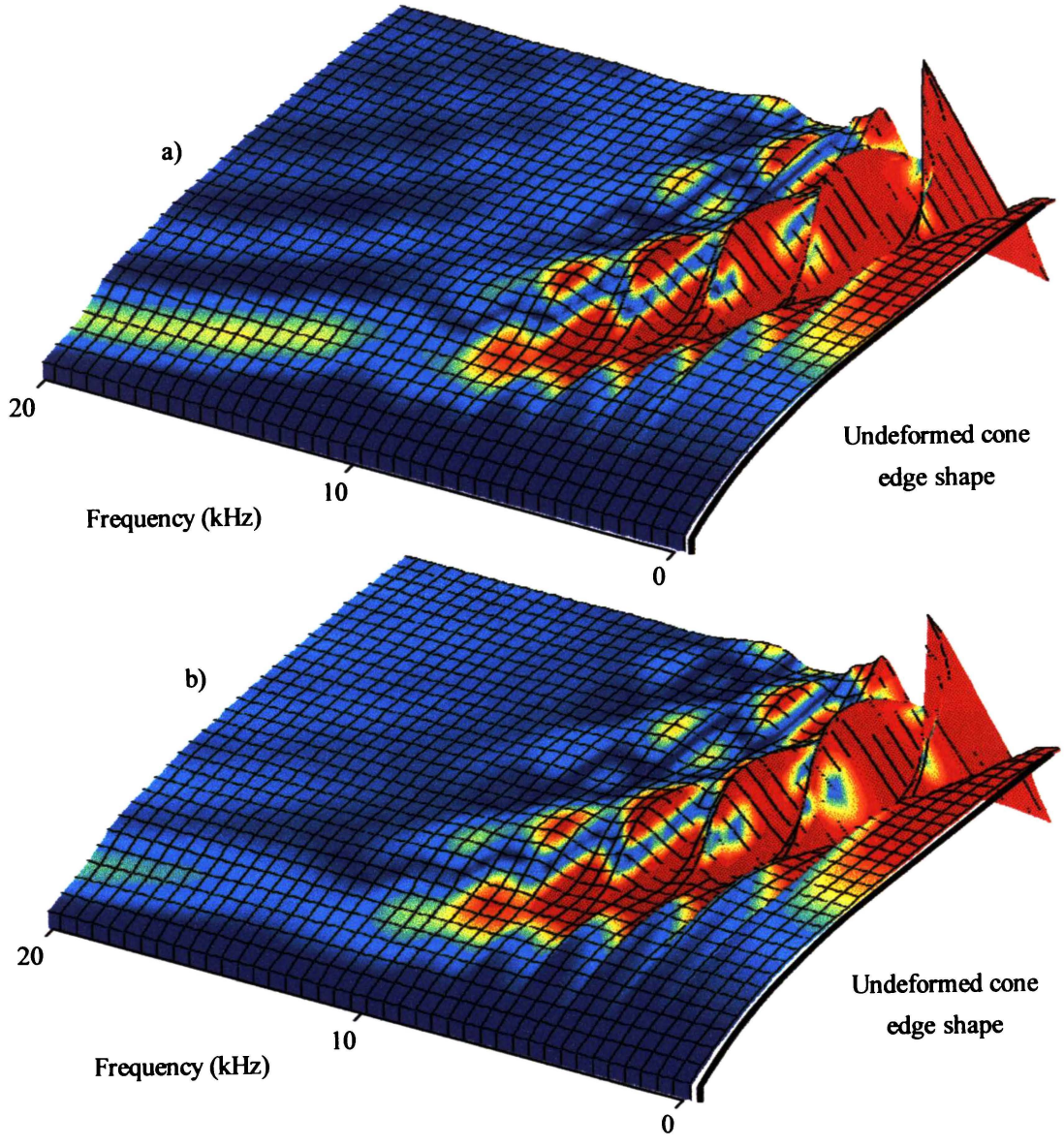

Figure 5.13. Cone deformation patterns for a) $\nu = 0.1$, b) $\nu = 0.4$

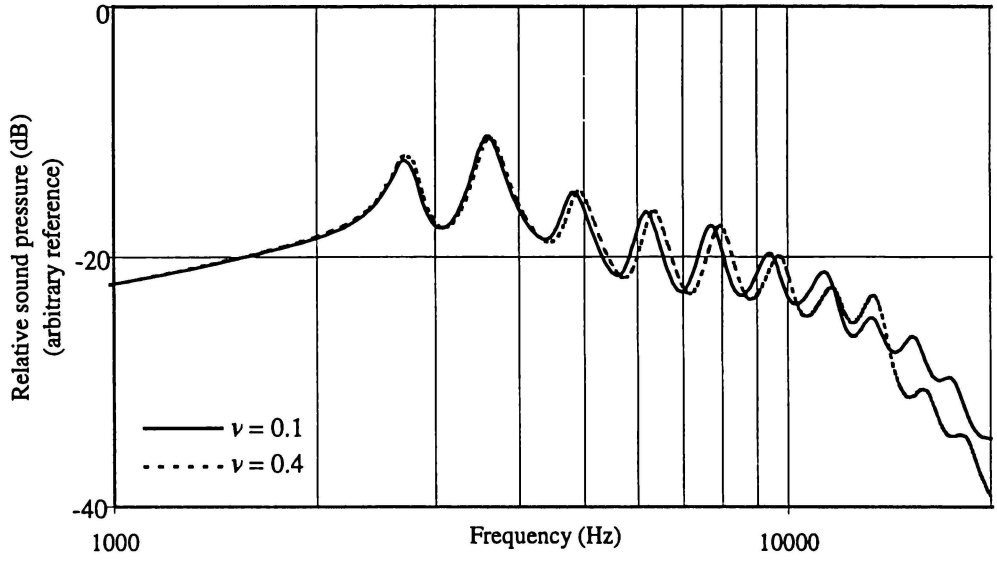

Figure 5.14. On-axis far-field sound pressure responses for $\nu = 0.1$, $\nu = 0.4$

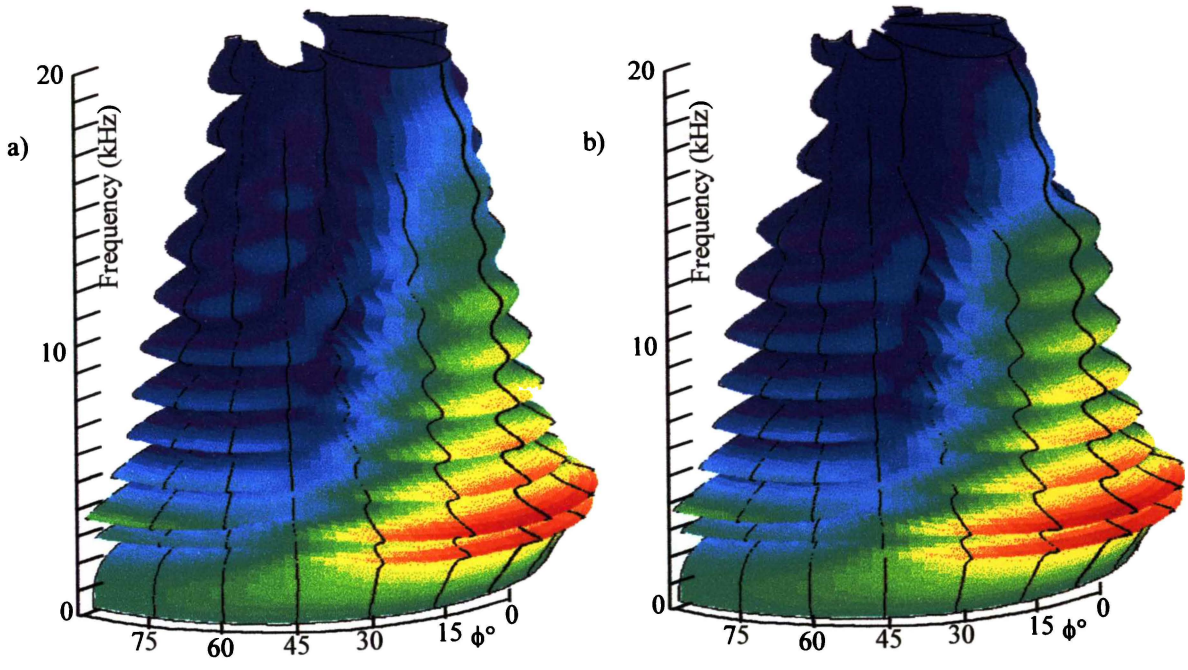

Figure 5.15. 3D Polar sound pressure frequency response plots for a) $\nu = 0.1$ b) $\nu = 0.4$

Figures 5.14 and 5.15 indicate that the features in the sound pressure response caused by bending modes are only slightly dependent on the value of ν. Moreover, the high frequency decrease in sound pressure due to the excitation of the first longitudinal antiresonant mode is greater, and shifted to a higher frequency. Thus, a large Poisson's ratio leads to an increased bandwidth for the loudspeaker, but greatly diminished output above the onset of longitudinal antiresonance.

Summary

Increasing Poisson's ratio:

- Moves bending modes to a slightly higher frequency
- Slightly extends the bandwidth of the loudspeaker
- Diminishes output above the onset of longitudinal antiresonance

5.2.4 DAMPING

As the cone material damping ratio ξ determines the degree to which travelling wave energy is absorbed by the cone material (refer Chapter 3), cone behaviour should be strongly dependent on the choice of ξ. In this section, we consider the effect of the overall material damping ratio on the resonant behaviour of the loudspeaker cone.

By varying ξ from 0.001 $\rightarrow$ 1, the following 3D axial admittance frequency response versus damping ratio plot was generated.

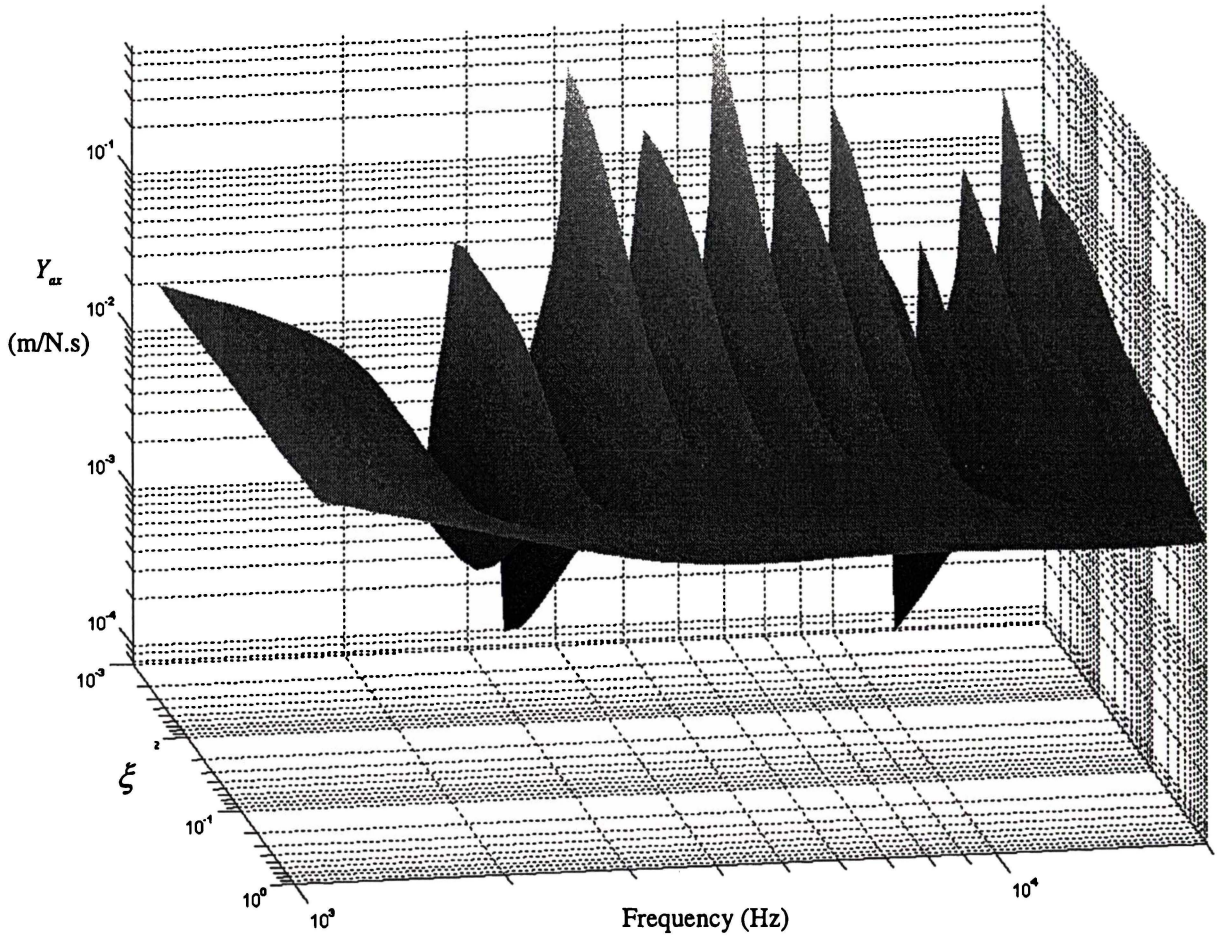

Figure 5.16. Calculated Y_{ax} frequency response of axisymmetric cone as damping ratio is varied from 0.001 – 1.

Figure 5.16 demonstrates that frequencies of all bending and longitudinal standing waves are independent of the damping ratio. Clearly, a highly damped loudspeaker cone material is extremely desirable, from the point of view of achieving a smooth axial admittance response, and consequently a smooth sound pressure response. If the loudspeaker cone were completely damped (an impossibility in practice), the cone would behave as a point mass, and the Y_{ax} response would consist of a steady -20db/decade slope.

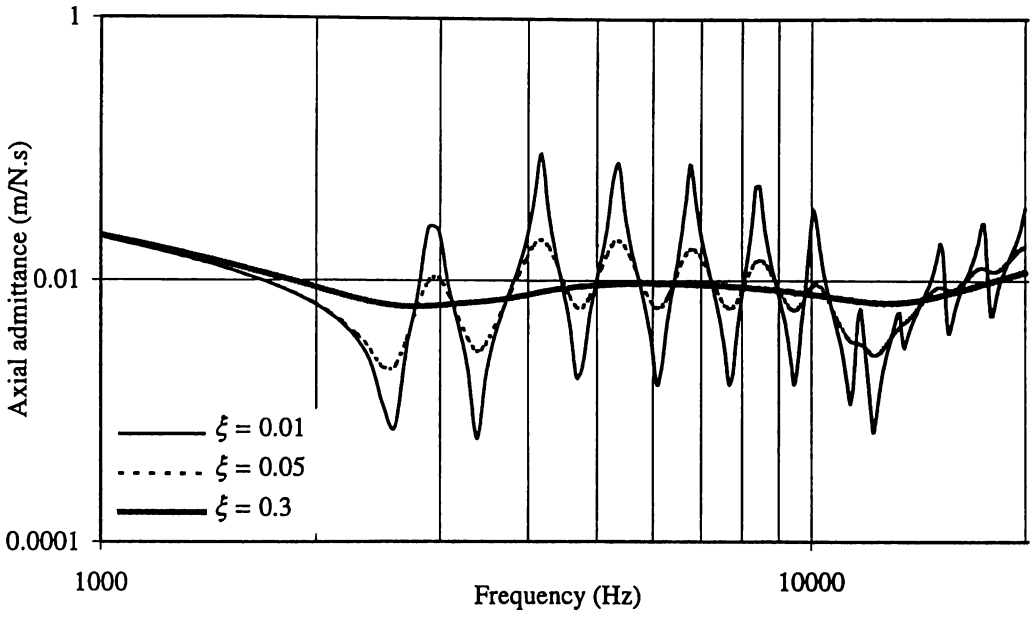

Figure 5.17. Modelled Y_{ax} response for $\xi = 0.01$, $\xi = 0.05$, $\xi = 0.3$

Figure 5.17 verifies that increasing the damping ratio has the principal effect of diminishing the amplitude of bending resonances and antiresonances. At $\xi = 0.05$, the amplitudes of bending features in the Y_{ax} response are greatly diminished in comparison to $\xi = 0.01$. However, the frequencies of the natural modes of the loudspeaker cone are independent of the value of ξ.

Increasing ξ further essentially removes all bending resonant features from the Y_{ax} response. Yet, the cone still undergoes some flexing motion, as the displacement of the outer edge lags that of the inner edge. The cone deformation plots for $\xi = 0.01$, 0.05 and 0.3 are illustrated in Figure 5.18.

When $\xi = 0.01$, (Figure 5.18a) the bending mode shapes are clearly visible. The onset of longitudinal antiresonance is apparent at $f \approx 12500$ Hz. When the damping ratio is increased to 0.05 (Figure 5.18b), the standing wave amplitude is significantly diminished, but the positions of nodes and antinodes for each resonant mode are unaffected. Although increasing the damping ratio further to $\xi = 0.3$ results in the cone motion being almost uniform, even this very highly damped cone exhibits a little flexing motion.

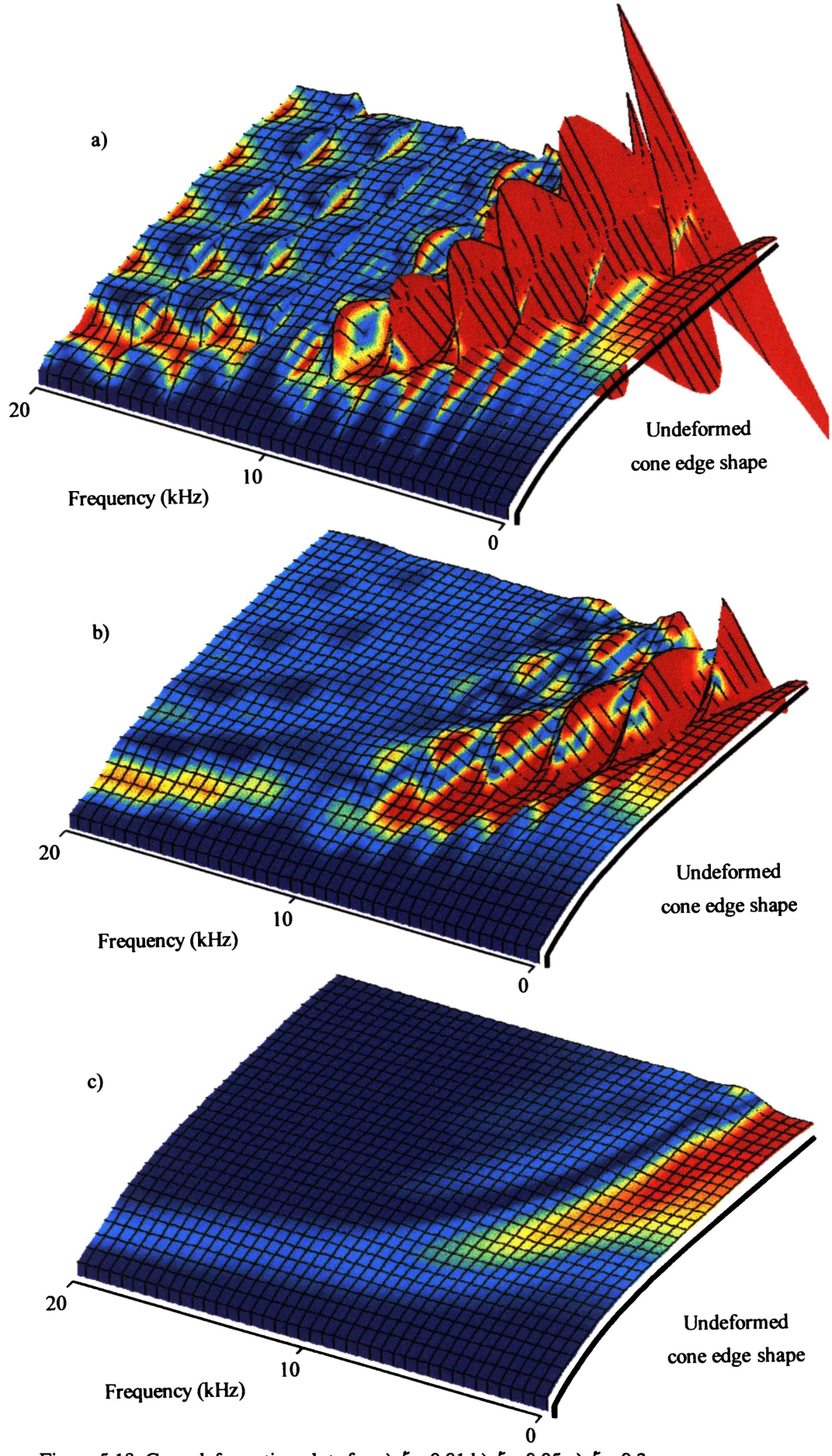

Figure 5.18. Cone deformation plots for a) $\xi = 0.01$ b) $\xi = 0.05$ c) $\xi = 0.3$

When the sound pressure response is plotted for ξ = 0.01, 0.05 and 0.3 (Figure 5.19), the effect of ξ on the smoothness of the sound pressure response is evident.

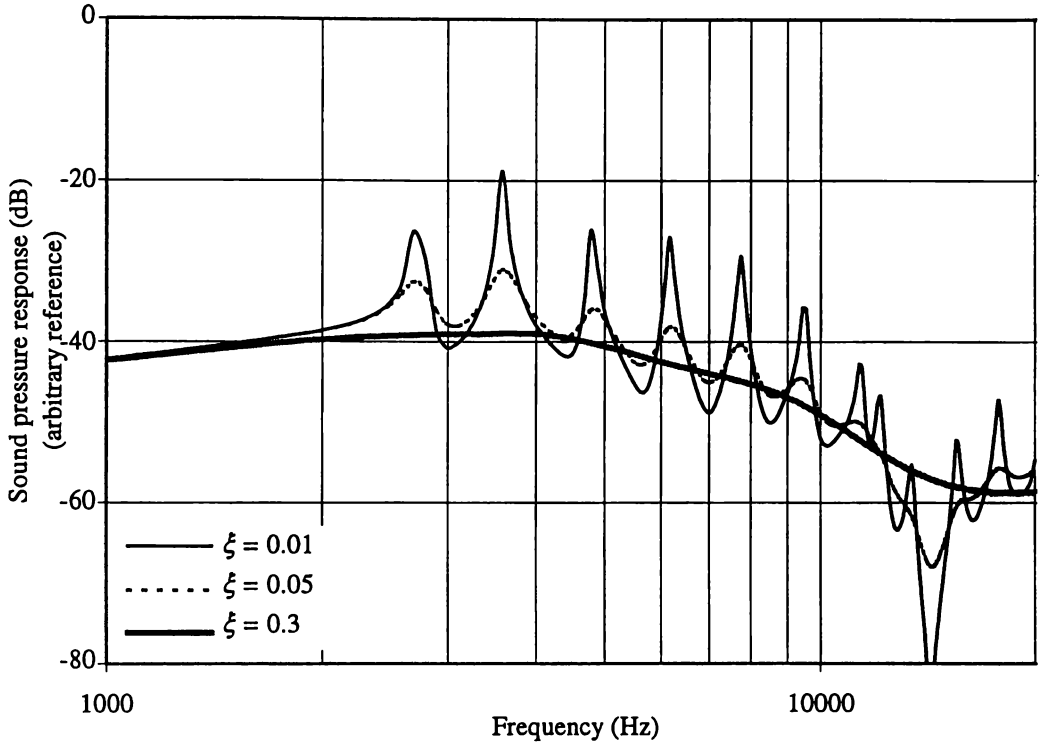

Figure 5.19. On-axis far-field sound pressure responses for ξ = 0.01, 0.05 and 0.3

Figure 5.19 confirms that increasing the damping ratio of the cone material has the desirable effect of smoothing the on axis sound pressure response. In general, when the damping ratio is $\geq$ 0.1, the sound pressure ripples caused by bending resonances disappear.

The off-axis sound pressure response is similarly affected by an increase in damping ratio, as shown in Figure 5.20. The polar sound pressure response plot of Figure 5.20b) is comparatively smooth, both on and off axis. When the loudspeaker is exhibiting very little flexure, the overall shape of the polar sound pressure response plot is primarily determined by the geometry of the cone, rather than cone break-up.

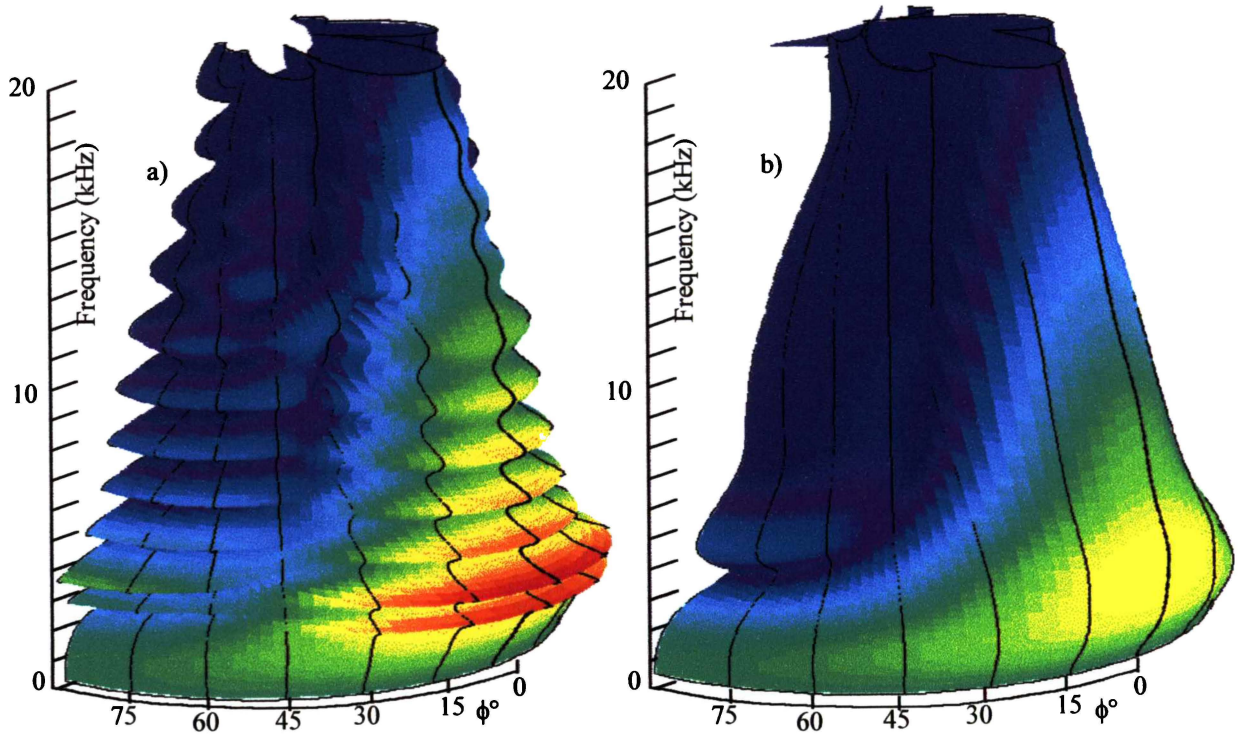

Figure 5.20. 3D Polar sound pressure response plot for a) $\xi = 0.05$ b) $\xi = 0.3$

While the damping ratio is essentially a property of the material itself, the damping qualities of polypropylene can be improved by "doping" the cone material with agents such as talc or mica. Doping the cone material with a damping agent may well also have an effect on other material properties such as Young's modulus and mass density.

Similarly, cones manufactured from stiff, light materials such as Kevlar can be coated with a substance that offers additional damping and helps to diminish the effect of the high frequency, high magnitude resonances of such materials.

Summary

Increasing the cone material damping ratio

- Diminishes the magnitude of bending modes and thereby smoothes the loudspeaker's sound pressure response.

5.3 EFFECT OF CONE THICKNESS GEOMETRY ON LOUDSPEAKER CHARACTERISTICS

The geometry of a loudspeaker cone (shape, size, thickness etc) has a considerable influence on the characteristics of the loudspeaker. The majority of published research considers the characteristics of straight-sided cones and draws general conclusions regarding the dependence of loudspeaker characteristics on cone geometry. In particular, Frankfort [6] considers the influence of the inner radius, outer radius, meridional length, thickness, and apex angle of a straight sided cone on its sound pressure, sound power and directivity characteristics. Frankfort's results are somewhat limited, as particular emphasis is placed on the dependence of longitudinal resonant behaviour on cone geometry, and bending mode behaviour is not considered in detail.

Geaves [30] applies an iterative design optimisation technique to design an optimal loudspeaker cone response, with the smoothness of the on-axis sound pressure response as the design criteria. This is achieved by repeatedly altering the cone geometry and thickness profile via an evolutionary process, until an optimal response is attained. In his particular case, the optimal response was achieved with a cone thickness that linearly varied between 0.277mm at the inside edge to 0.352mm at the outside edge of the cone.

In this section, the effect of the cone thickness and thickness profile on the resonant behaviour of cone C is further explored. Although the exact effect of other geometrical factors (cone shape etc) will not be considered here, further research in this area is required. In general, loudspeaker system manufacturers are only able to specify the size and thickness of loudspeaker cones when purchasing from cone suppliers. The cone shape (i.e. radii of curvature of convex cone) is usually predetermined by the supplier.

The loudspeaker cone's thickness and thickness profile (that is, variation of thickness between inner and outer edges) have an important influence on its natural frequencies. The loudspeakers considered in this thesis are vacuum-formed from sheet polypropylene to the specific shape defined in Section 4.3.1. The thickness of the polypropylene sheet used has a considerable effect on the measured Z_{mot} and sound pressure level characteristics of the loudspeaker. Further, even nominally identical loudspeakers, vacuum formed from the same polypropylene sheet, can exhibit different thickness profiles, and consequently possess a slightly different series of resonant frequencies.

In Section 5.3.1 the loudspeaker cone is assumed to have a constant thickness profile. By varying the thickness of the cone material, the thickness dependence of the natural resonances of the cone is demonstrated. Section 5.3.2 considers the behaviour of a loudspeaker with a non-uniform thickness profile, while Section 5.3.3 examines the effect of selectively changing the thickness of the elements making up the FE model of the loudspeaker cone.

5.3.1 THICKNESS

Assuming the thickness of a loudspeaker cone is constant, its effect on the Y_{ax} response can be determined. By varying the cone thickness t between 0.2mm – 0.5mm, the following 3D Y_{ax} versus t response was generated.

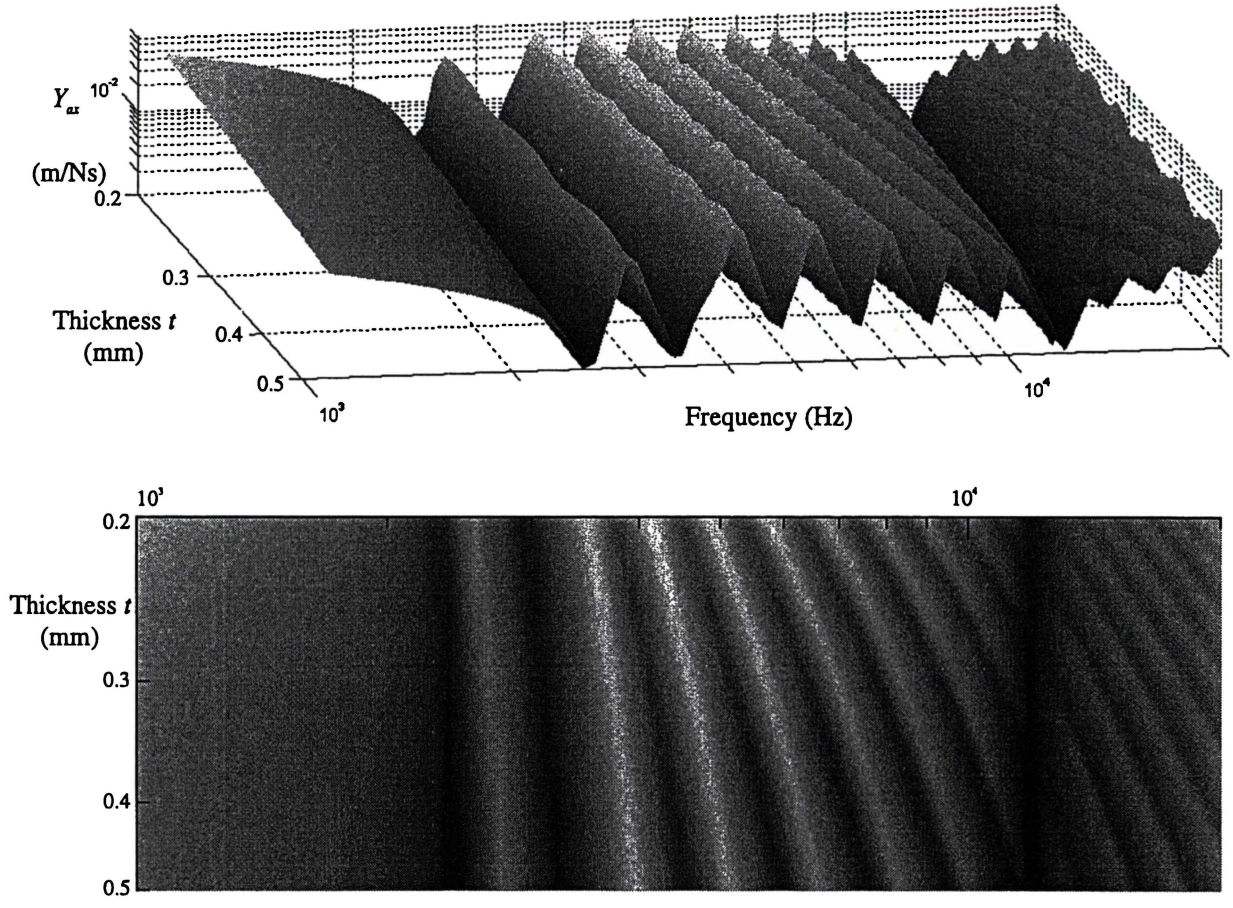

Figure 5.21. Calculated Y_{ax} frequency response of uniform thickness axisymmetric cone as cone thickness is varied from 0.2mm – 0.5mm.

Figure 5.21 demonstrates that the frequency of bending modes increases with increasing cone thickness, as the added thickness of cone material helps to resist the onset of cone break-up. The exact nature of the dependence of the bending mode frequencies on the thickness of the loudspeaker cone is not as simple as their dependence on the mass density, Young's modulus, or Poisson's ratio of the cone.

The magnitude of bending mode features on the Y_{ax} response also increases with increasing cone thickness, suggesting more pronounced ripple in the sound pressure response. Additionally, extra cone thickness results in higher total mass, lowering the mean value of the Y_{ax} response. This is shown in Figure 5.22, where the Y_{ax} responses for cone thickness = 0.2mm and 0.5mm are plotted.

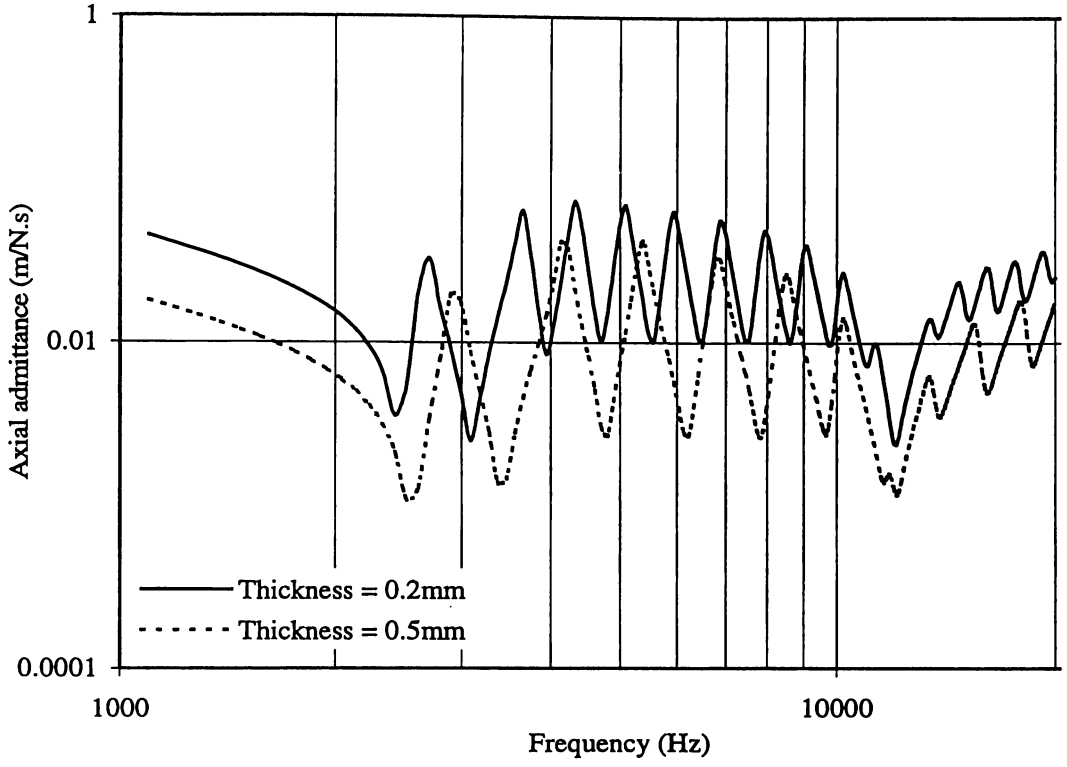

Figure 5.22. Modelled Y_{ax} response for cone thickness = 0.2mm, 0.5mm

The first longitudinal resonant frequency is unaffected by the thickness of the cone, implying that the upper limit of the sound pressure response is independent of cone thickness.

The cone deformation plots for cone thickness = 0.2mm and 0.5mm are shown in Figure 5.23, which illustrates that due to its lower total mass the thinner loudspeaker cone vibrates with greater amplitude in response to the 1N driving force. Furthermore, the nodal lines of each bending resonant mode of the loudspeaker move in towards the neck of the cone with increasing cone thickness, while the frequency and shape of the longitudinal antiresonance is unaffected.

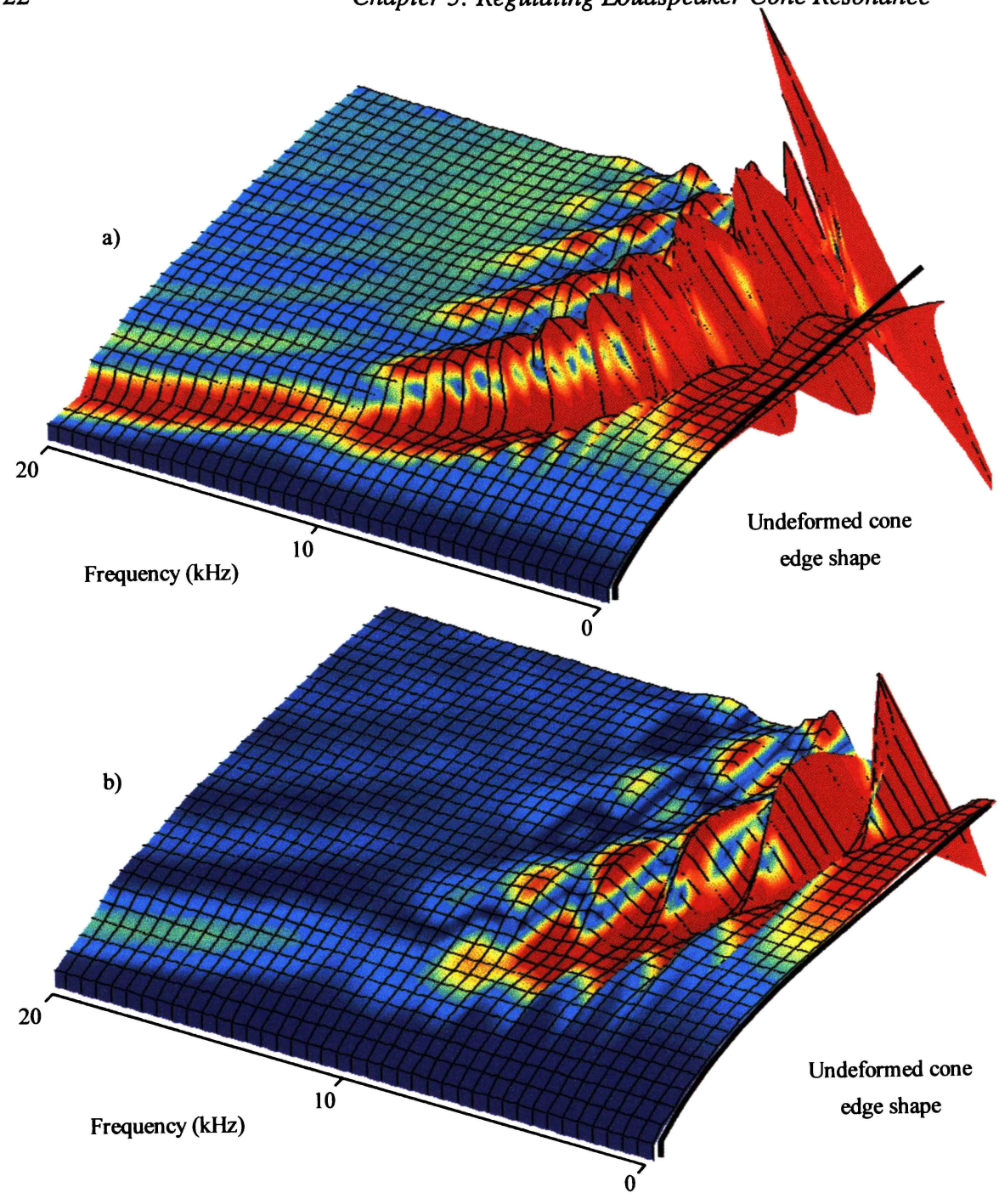

Figure 5.23. Cone deformation patterns for a) Cone thickness=0.2mm b) Cone thickness=0.5mm

The effect of cone thickness on the final sound pressure response of the loudspeaker is shown below:

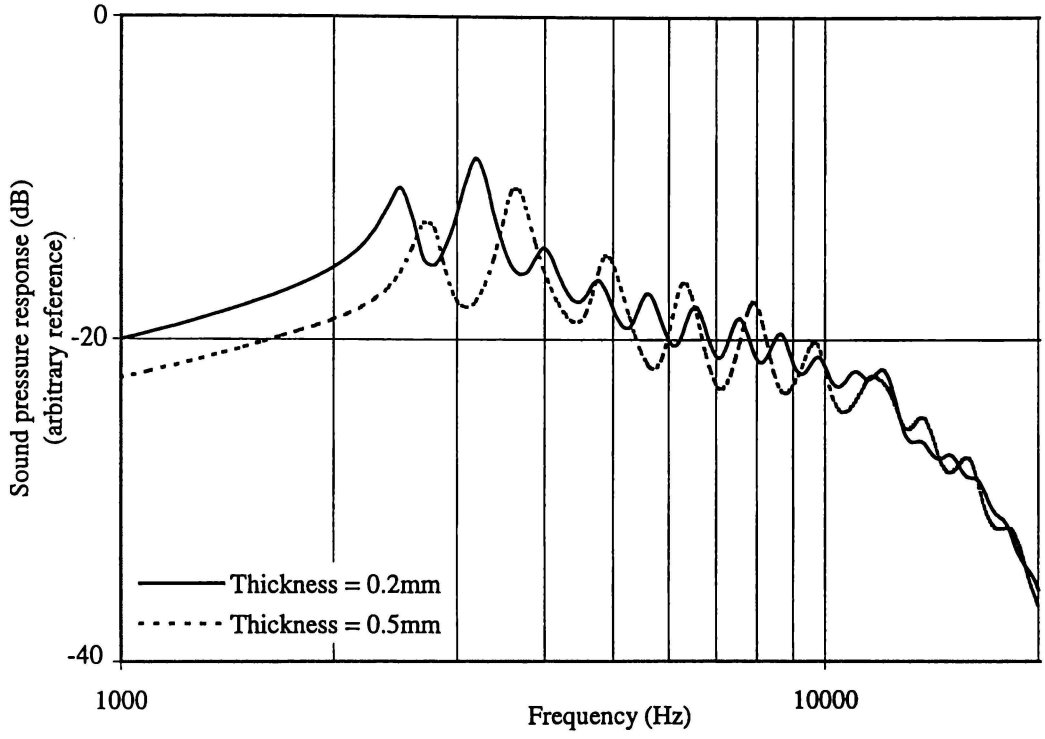

Figure 5.24. On-axis far-field sound pressure responses for cone thickness = 0.2mm, 0.5mm

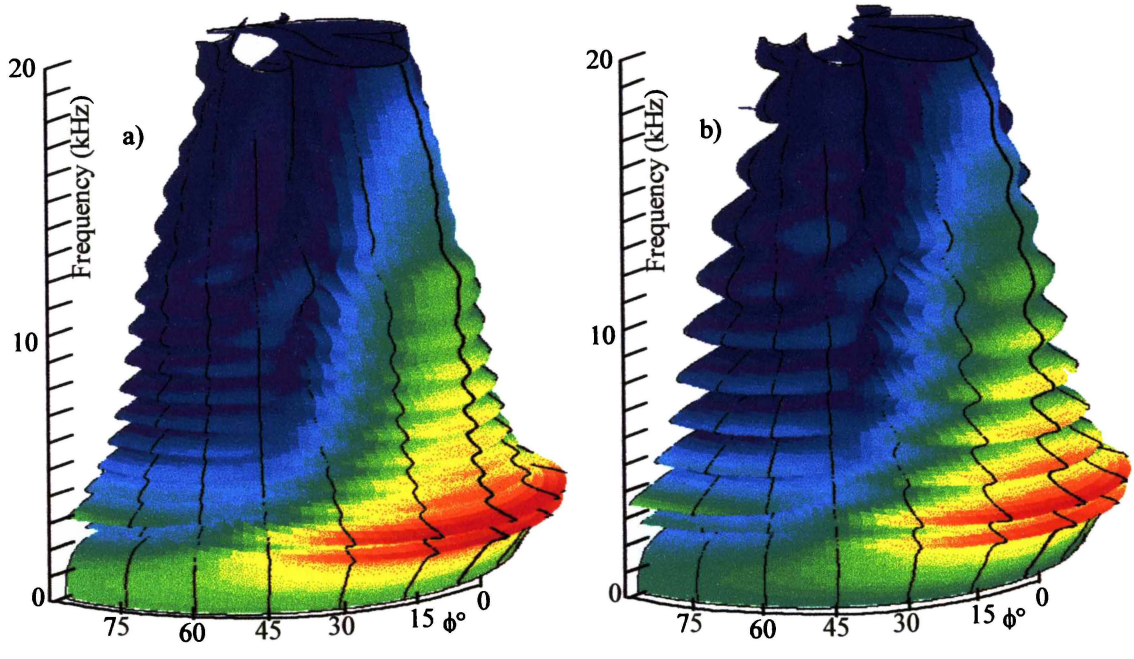

Figure 5.25. 3D Polar sound pressure response plot for a) thickness = 0.2mm b) thickness = 0.5mm

The mean developed sound pressure level generated by the thicker cone is lower than for the thin cone, corresponding to a lower efficiency. Although increasing the thickness of the loudspeaker cone results in a lower number of resonant features in the sound pressure response of the loudspeaker, the magnitude of the undesirable ripple caused by bending resonances is increased. The decrease of sound pressure at high frequency

caused by the onset of longitudinal antiresonance is unaffected by the cone thickness.

From the point of view of increased efficiency and lower sound pressure response ripple, a thinner cone is clearly preferable.

Summary

Increasing the cone thickness:

- Increases the frequency of bending modes, and thereby decreases the number of bending modes causing ripple in the sound pressure response.
- Increases the magnitude of sound pressure ripple caused by bending modes.
- Decreases the overall efficiency of the loudspeaker.
- Moves nodal and antinodal lines in towards the neck of the cone.
- Has no effect on the bandwidth of the loudspeaker.

5.3.2 THICKNESS PROFILE

Previously it was noted that the vacuum forming process produces a loudspeaker cone that has a characteristic variation in thickness from inner to outer edge. The variation in thickness has a strong effect on the shape of the axial admittance response of the loudspeaker as would be expected.

To investigate this effect, the inner edge thickness (t_i) of a speaker was held constant at 0.3mm, while the outer edge thickness (t_o) was varied between 0.1mm and 0.5mm. The thickness of the cone between inner and outer edges was described by a linear interpolation between these two extremes. The resulting axial admittance response profile is shown as a function of outer edge thickness in Figure 5.26.

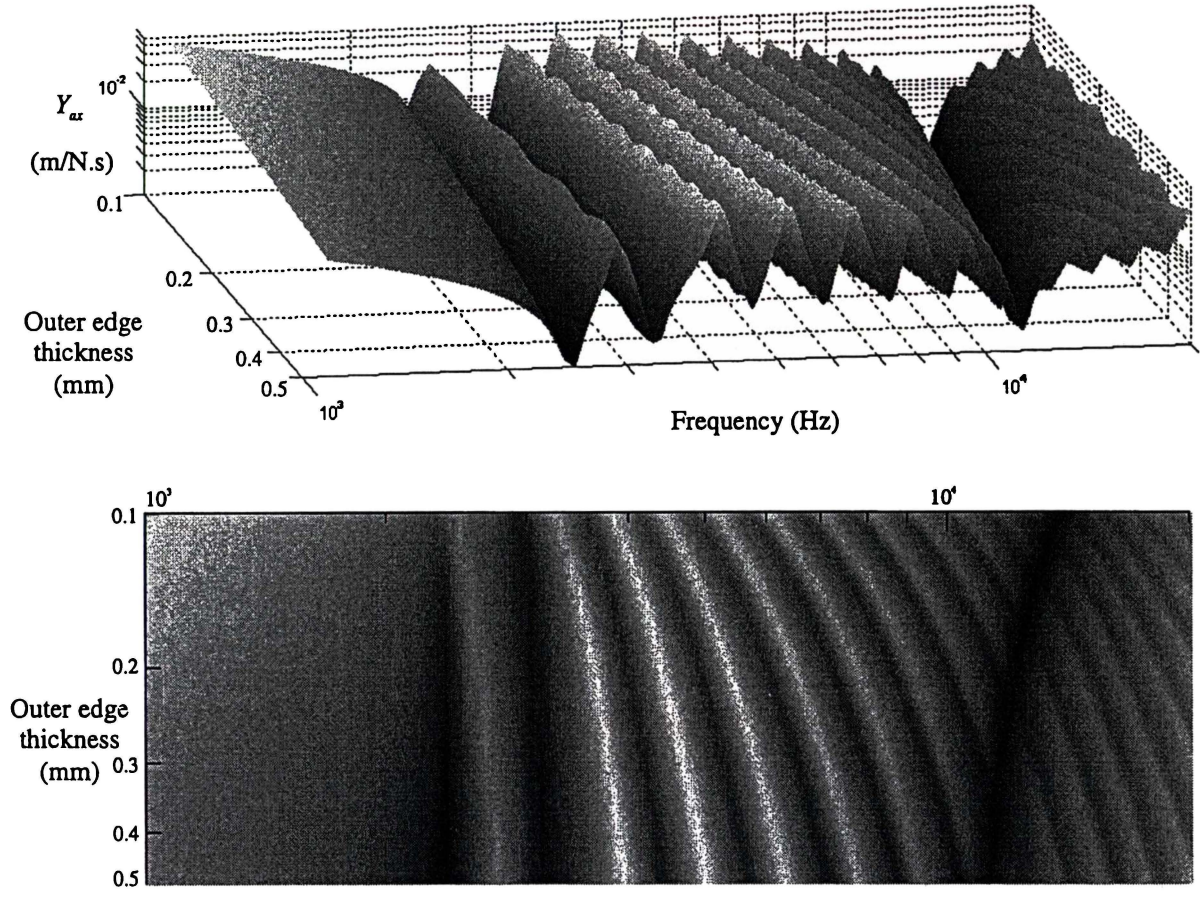

Figure 5.26. Calculated Y_{ax} frequency response of axisymmetric cone (inner edge thickness = 0.3mm) as cone outer edge thickness is varied from 0.1mm – 0.5mm. The cone thickness is varies linearly between inner and outer edges.

Figure 5.26 shows that the magnitude and frequency of all bending resonances increases with increasing t_o, higher order modes being more affected than lower order. This implies an increased number of ripples in the sound pressure response, while the decreased amplitude of each resonant feature suggests that the sound pressure response ripple will have a lower amplitude than for a cone with large t_o. Additionally, the first longitudinal antiresonance is decreased markedly in frequency with increased t_o.

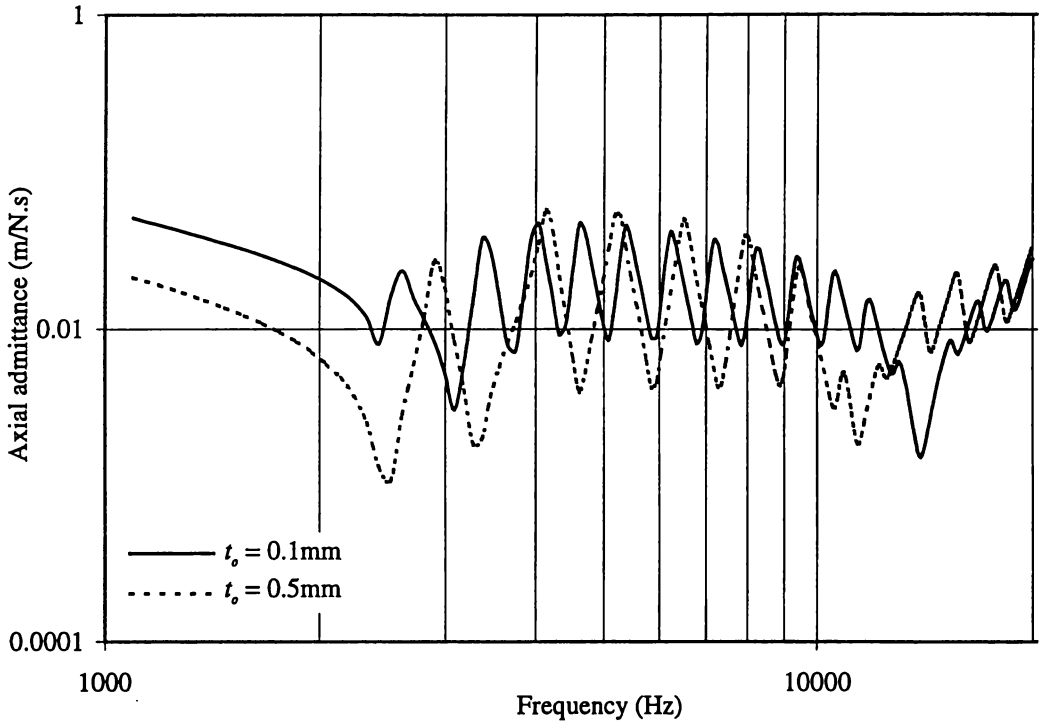

Figure 5.27. Modelled Y_{ax} response for t_0 = 0.1mm, 0.5mm

Figure 5.27 demonstrates the dependence of Y_{ax} responses on the cone outer edge thickness by comparing the Y_{ax} responses for t_o= 0.1mm and t_o = 0.5mm.

The mode shape, and cone displacement pattern is particularly affected by the thickness profile. The effect on mode shape is best displayed by viewing the cone displacement mode shapes across the frequency range 100Hz-20kHz for outer edge thicknesses of 0.5mm and 0.1mm respectively. These plots are shown in Figure 5.28.

Figure 5.28 confirms that the mode shapes are strongly affected by the cone thickness profile. Further, there is a large increase in the number of modes occurring before the onset of longitudinal antiresonance, when the cone has a thin outside edge. It is also evident that the nodal and antinodal lines for each mode are moved outwards with decreasing outer node thickness.

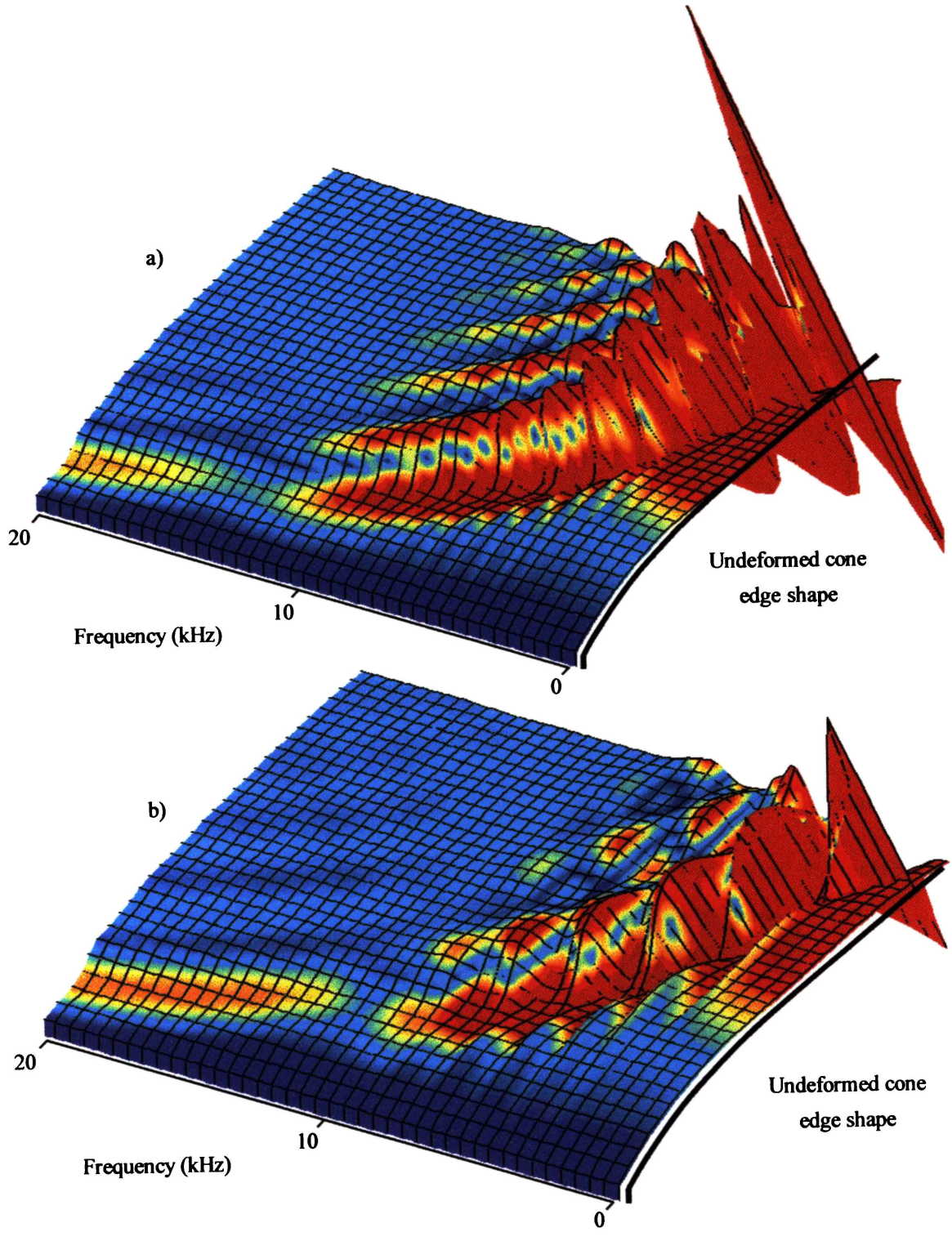

Figure 5.28. Cone deformation patterns for a) t_i = 0.3mm, t_o = 0.1mm b) t_i = 0.3mm, t_o = 0.5mm

The effect of cone thickness on the sound pressure response of the loudspeaker is shown in Figure 5.29 and Figure 5.30, where p_{ax} is shown for outer cone thickness = 0.1mm and 0.5mm. Although the cone with thinner outer edge possesses a much greater outer edge displacement, the overall sound pressure response of the cone is smoother. Further, the reduction of mass near the outer edge significantly diminishes the magnitude of the sound pressure peak caused by the first bending mode. This effect is considered further in the next section.

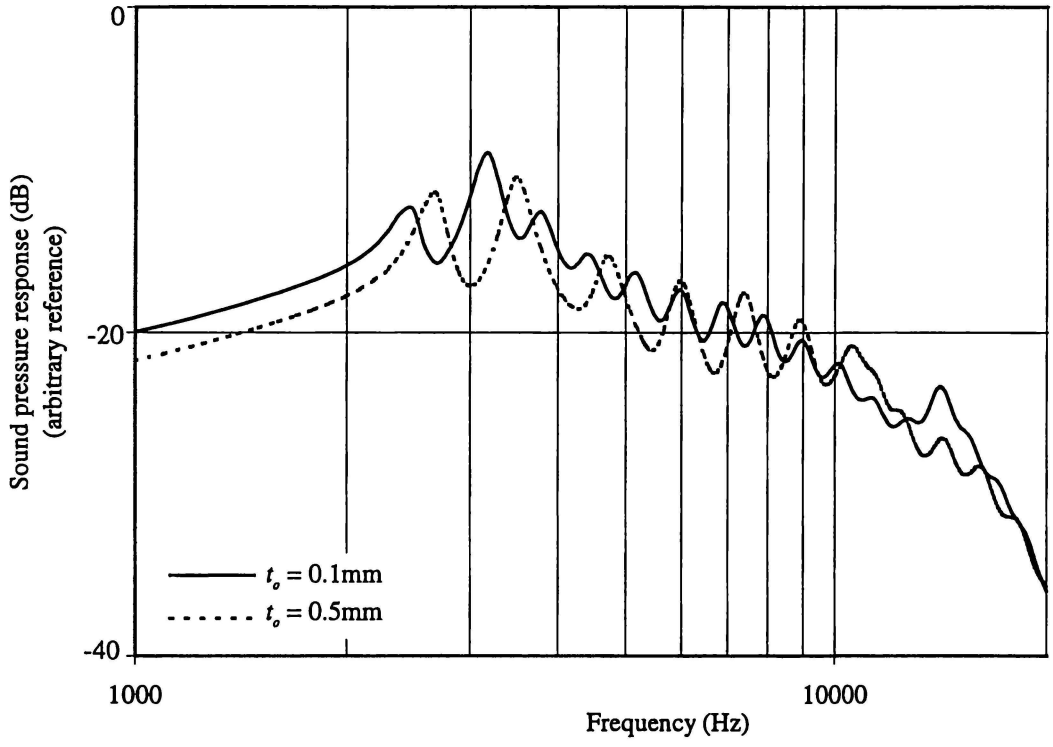

Figure 5.29. On-axis far-field sound pressure responses for t_o = 0.1mm, 0.5mm

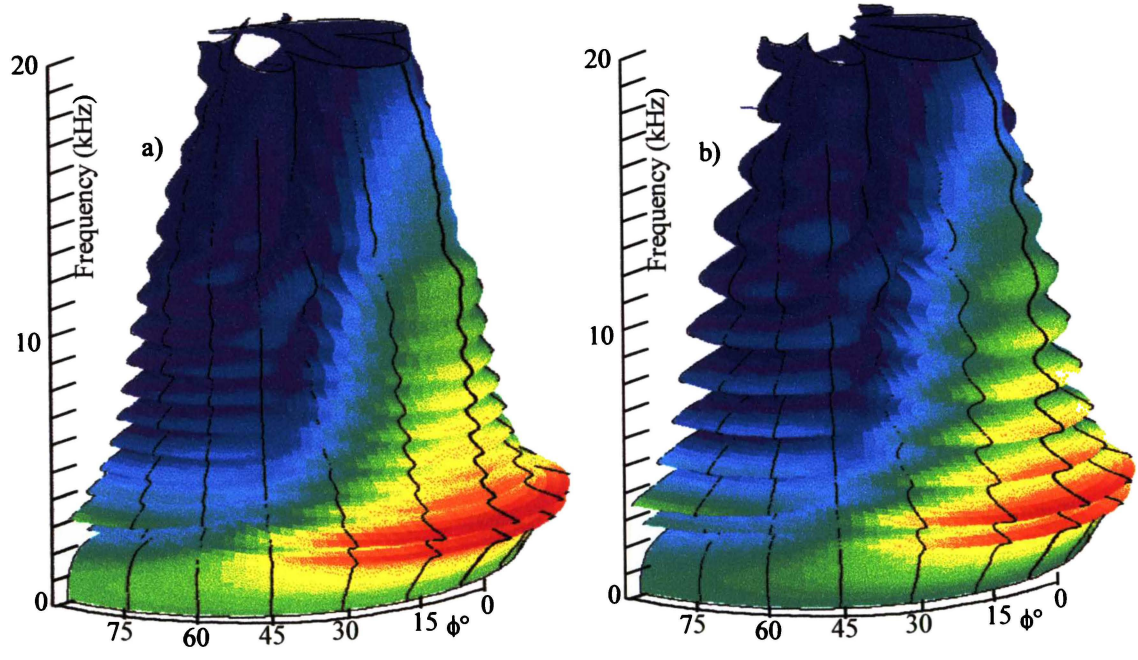

Figure 5.30. 3D Polar sound pressure response plot for a) t_o = 0.2mm b) t_o = 0.5mm

The cone thickness profile does not appear to cause any significant change in the overall shape of the polar sound pressure response plot.

Evidently, a cone with a thin outside edge possesses many more ripples in its sound pressure response profile, although these resonances are much less pronounced than for a cone with a thicker outside edge. The high frequency limit caused by the onset of longitudinal antiresonance is also increased with decreasing outer edge thickness.

Summary

Constructing a loudspeaker with a thinner outside edge

- Moves the first longitudinal antiresonance to higher frequency, thereby extending the bandwidth of the loudspeaker cone.
- Increases the number of ripples in the sound pressure response.
- Diminishes the amplitude of ripples in the sound pressure response.

5.3.3 CHANGING THE THICKNESS OF CONE ANNULI

Thinning one element

Section 5.3.2 demonstrated that the thickness profile of the loudspeaker cone has a strong influence on the frequencies and amplitudes of the natural modes of a loudspeaker cone. It was confirmed that a loudspeaker cone with a thinner outer edge has more sound pressure ripples, but overall possesses a smoother sound pressure response. This section examines the effect of individually thinning the annuli formed by elements 3 (near the inner edge) to 31 (at the outer edge) of an axisymmetric cone model.

Beginning with a 2D FE model of loudspeaker C, the thickness of each element was selectively reduced to 0.15mm, and the Y_{ax} response calculated. The resulting Y_{ax} responses are shown below. The *y*-axis (out of the page) represents the number of the thinned element. (refer Figure 4.5).

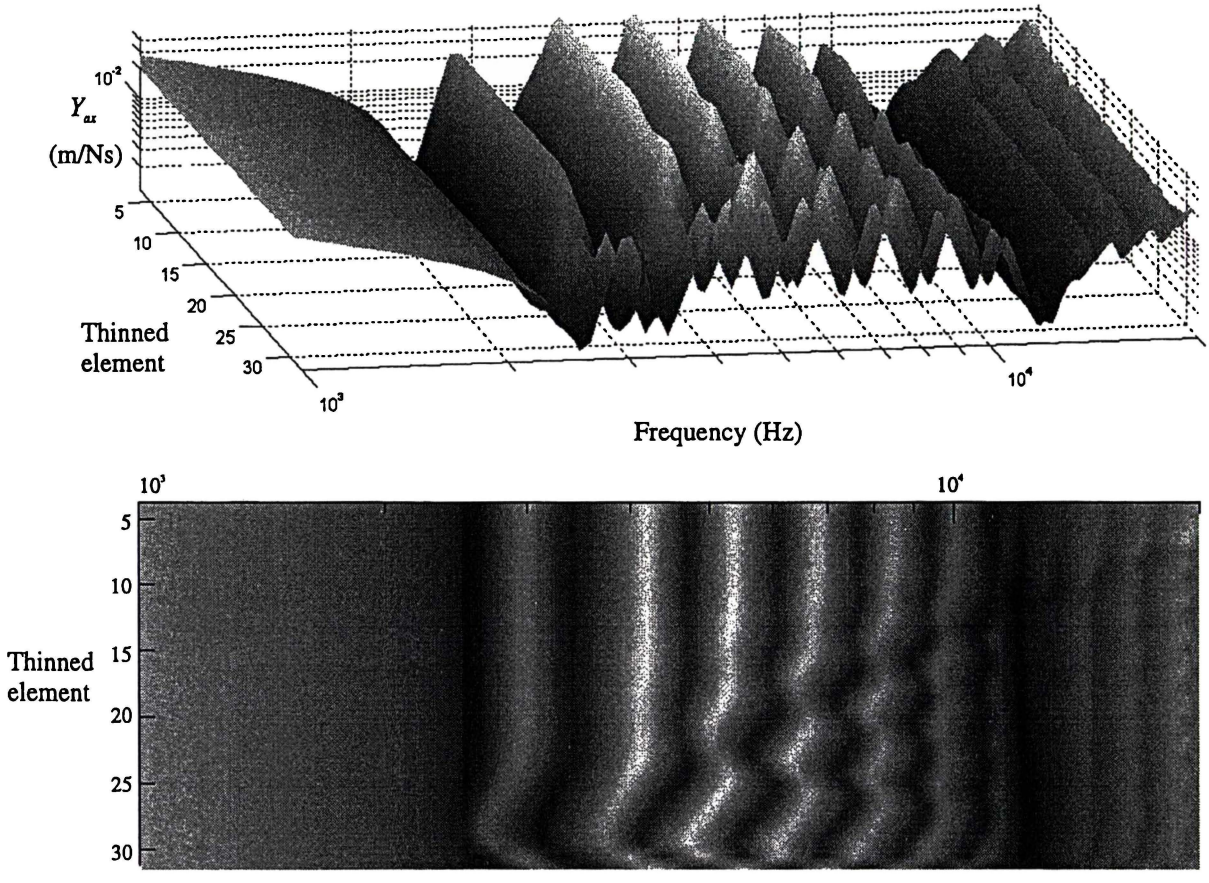

Figure 5.31. Calculated Y_{ax} frequency response of axisymmetric cone as the thickness of each element is selectively reduced to 0.15mm.

Figure 5.31 illustrates that thinning one of the thirty-one elements that make up the 2D FE model can have a considerable effect on the Y_{ax} response of the loudspeaker. The Y_{ax} response is almost unchanged when elements nearer the neck of the cone (e.g. element 3) are thinned, but thinning elements nearer the outer edge of the cone (element 31) results in a shift of the cone's resonant frequencies.

The characteristics displayed in Figure 5.31 can be explained by considering the deformation shape of a normal loudspeaker cone, as in Figure 4.15. Figure 4.15 can be partly summarised by determining the node of the FE model that vibrates with maximum displacement at any particular frequency, and plotting it as a function of frequency, as in Figure 5.32[6].

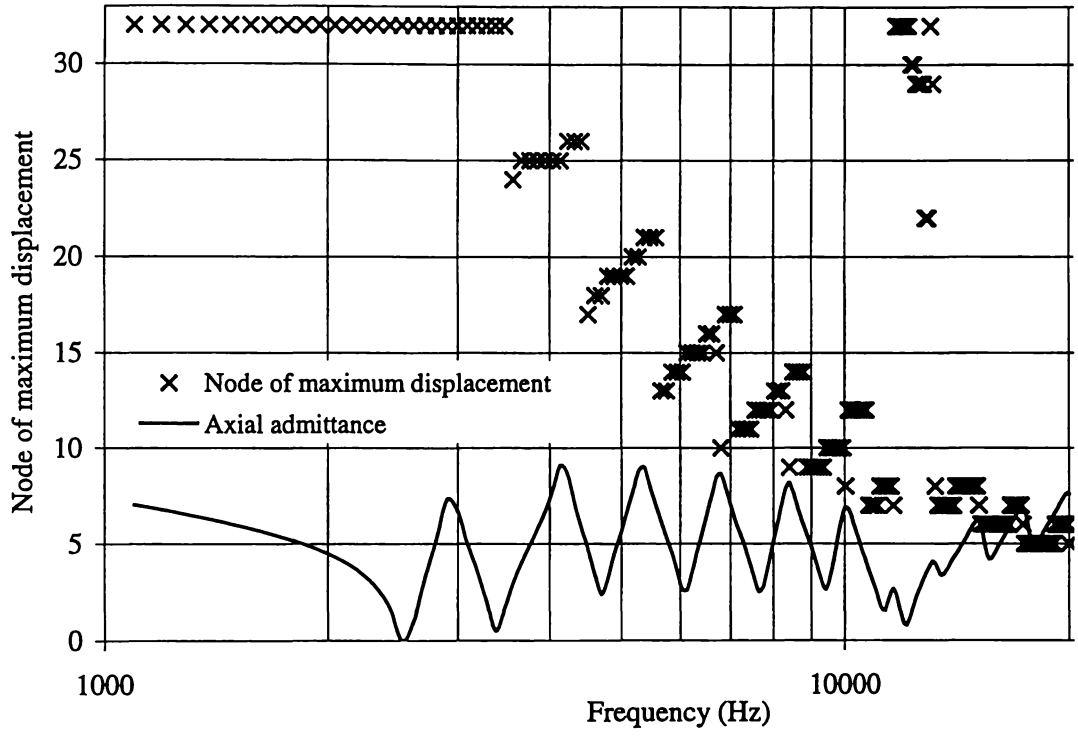

Figure 5.32. Node of maximum displacement and axial admittance versus frequency.

Figure 5.32 demonstrates that the outer edge of the cone (node 32) vibrates with maximum displacement until the driving frequency is slightly less than 3.4kHz. The point of maximum displacement displays an overall movement towards the centre of the cone (i.e. the node number decreases) with increasing frequency. In general, the point of maximum deformation corresponds to the position of the innermost bending antinode.

When an element is thinned, as in Figure 5.31, the resonant mode that excites the maximum displacement amplitude of that part of the cone is affected the most. Consequently, thinning the loudspeaker cone near the neck has no effect on the Y_{ax} response until high frequencies are reached, as it is only at high frequency that the innermost antinode reaches that part of the cone. Thus, by thinning the cone at a point corresponding to the innermost antinode of a resonant mode, that mode's frequency and amplitude can be "tuned."

The effect of thinning one element can be illustrated by considering two specific examples. Figure 5.32 indicates that when the third bending resonance is excited ($f \approx$

[6] The axial admittance response for Cone C is also reproduced, to allow the resonant modes to be identified.

5.2kHz), element 20 vibrates at maximum amplitude. Similarly, when the fifth bending resonance is excited ($f \approx$ 9.5kHz), element 10 vibrates with maximum amplitude. Consequently, thinning the loudspeaker cone at the position of element 20 will primarily affect the fifth bending resonance, and thinning the cone at element 10 will affect the third bending resonance.

This is demonstrated in Figure 5.33, which plots the Y_{ax} responses for FE models with elements 10 and 20 thinned individually. The Y_{ax} response for cone C is shown as a reference.

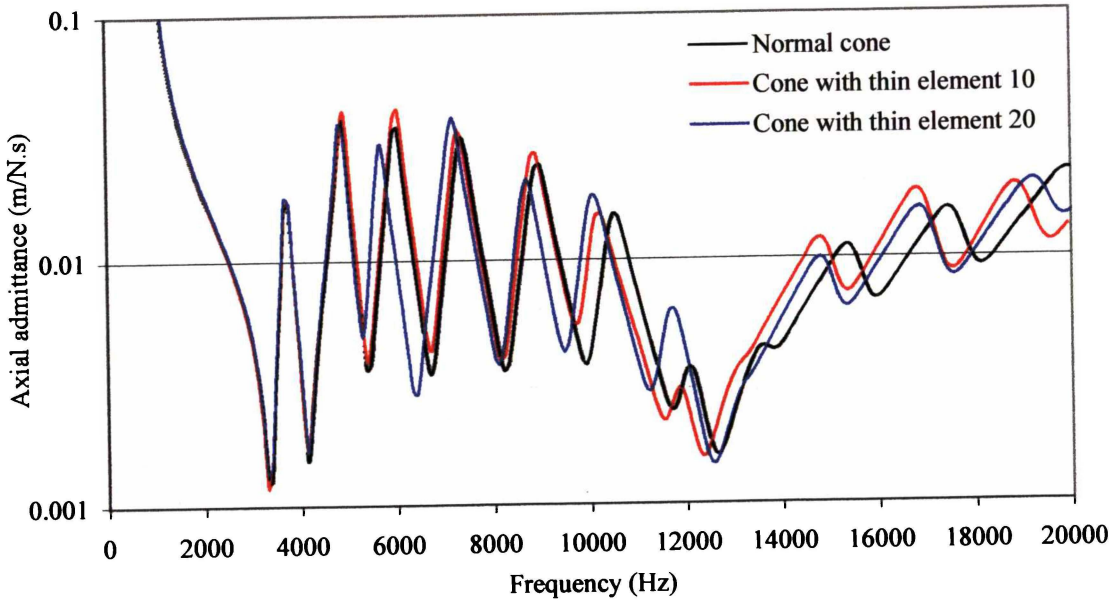

Figure 5.33. Y_{ax} responses for cone C; Element 10 thickness = 0.15mm; Element 20 thickness = 0.15mm

Figure 5.33 indicates that thinning element 10 has no effect on the Y_{ax} response until the fifth bending antiresonance is excited. The height of the ripple in the Y_{ax} curve is lowered near the fifth bending antiresonance, as is its frequency, and all subsequent modal frequencies. Similarly, Figure 5.33 indicates that thinning element 20 has a strong effect on the Y_{ax} response near the third resonance, decreasing the magnitude of ripple in the Y_{ax} curve near the second bending antiresonance and third bending resonance. Further, the second bending antiresonance and all subsequent bending modes are lowered in frequency.

The Y_{ax} response is plotted as a function of the thickness of elements 10 and 20 in Figure 5.34 and Figure 5.35 respectively. Figure 5.34 illustrates that the first five resonances are unaffected as element 10's thickness is decreased, while the sixth resonance (and subsequent resonances) are reduced in frequency as element 10 is thinned. Likewise, Figure 5.35 indicates that the first two resonant frequencies are unaffected by thinning element 20, but the third order mode is significantly lowered in frequency.

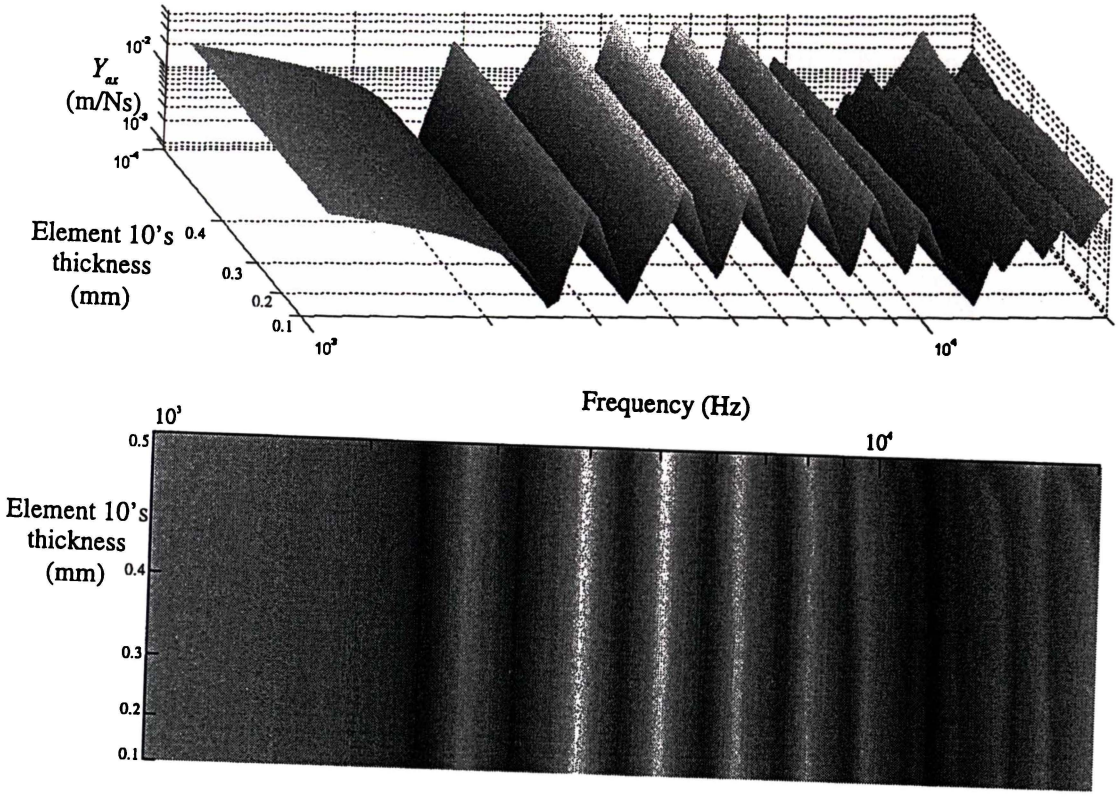

Figure 5.34. Y_{ax} response as the thickness of element 10 is varied from 0.1mm → 0.5mm

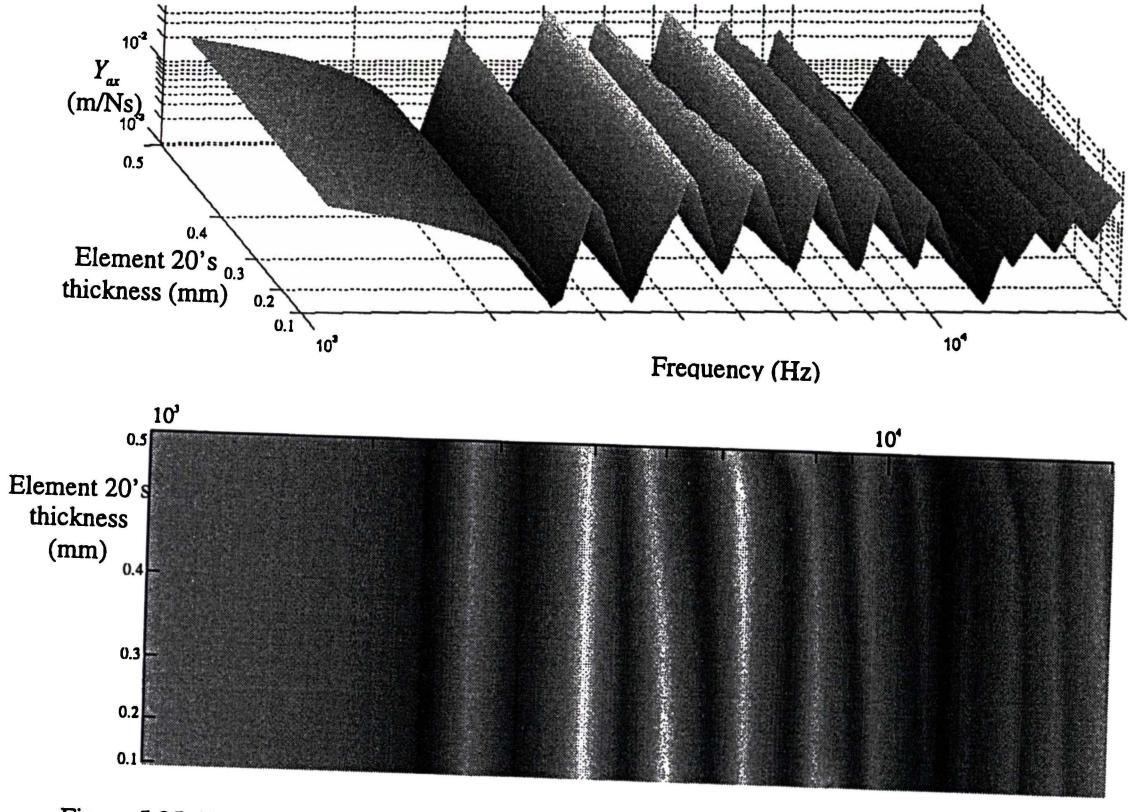

Figure 5.35. Y_{ax} response as the thickness of element 20 is varied from 0.1mm → 0.5mm

Thus, any resonant mode (and higher order modes) can be lowered in frequency and in magnitude by making the loudspeaker cone thinner at the point of maximum displacement for that mode.

This technique is similar to that often employed by bell manufacturers to tune the natural harmonics of bells into a consonant series. While this technique does allow the resonant frequencies of loudspeaker cones to be tuned, the overall smoothness of the sound pressure response is largely unaffected.

Thickening one element

It was shown in Section 4.5.4 that adding mass to the outside edge of the cone (in the form of a rubber ring overlapping the edge of the cone) moved the ring antiresonance to a significantly lower frequency. The other natural frequencies of the cone were also slightly lowered.

This effect can be explored in more detail if the thickness of each element is selectively increased. In Figure 5.36, the Y_{ax} response of cone C is plotted as the thickness of each element is selectively increased to 2.5mm. The y-axis (out of the page) represents the number of the thickened element.

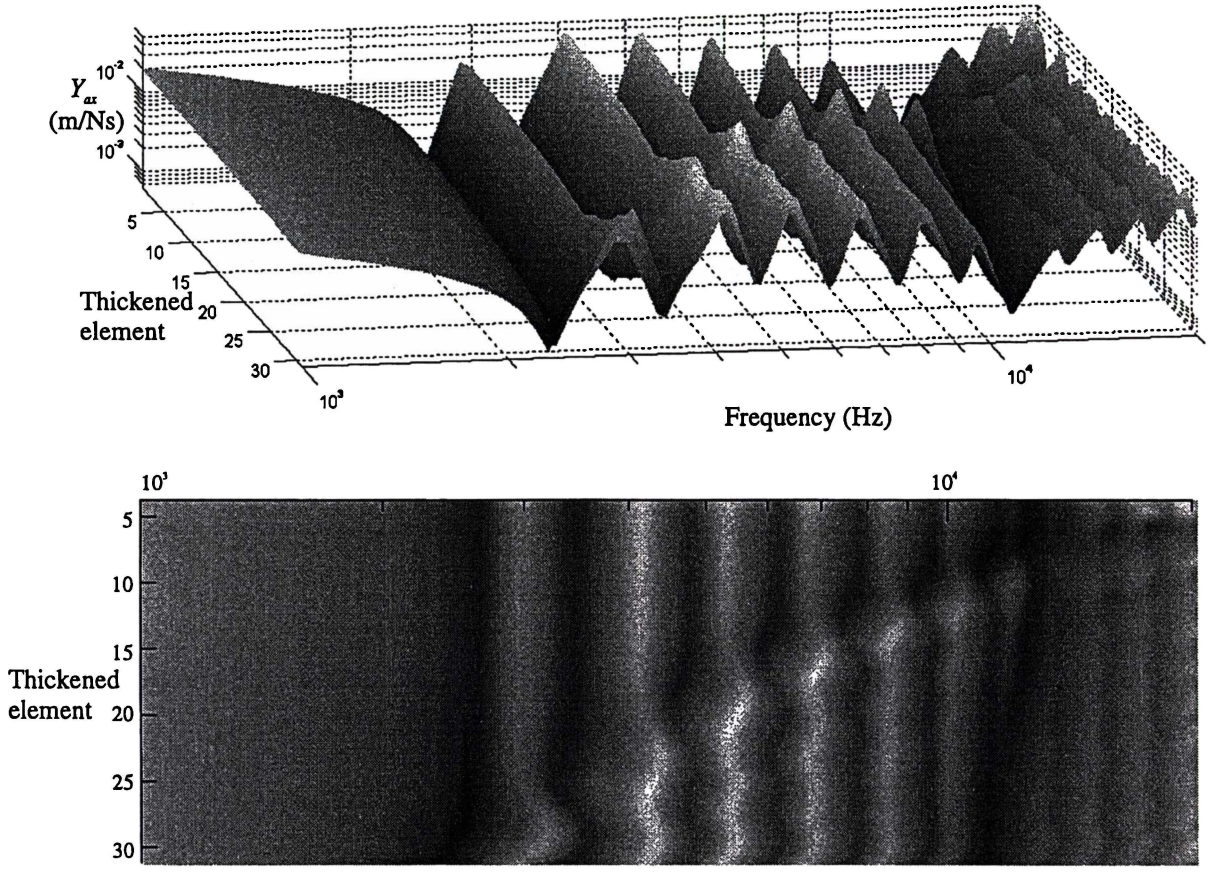

Figure 5.36. Calculated Y_{ax} frequency response of cone C as the thickness of an element is selectively increased to 2.5mm.

Figure 5.36 suggests that the modes most strongly affected by adding mass to a cone element are those with innermost antinode corresponding to the thickened part of the cone. In this case, the effect of adding mass is to accentuate the corresponding resonant feature in the Y_{ax} response, and move it to a slightly higher frequency, while lower order modes are diminished in amplitude. This is demonstrated in Figure 5.37 where the Y_{ax} response is shown for cone C with a) element 10 and b) element 20 individually

increased in thickness to 2.5mm.

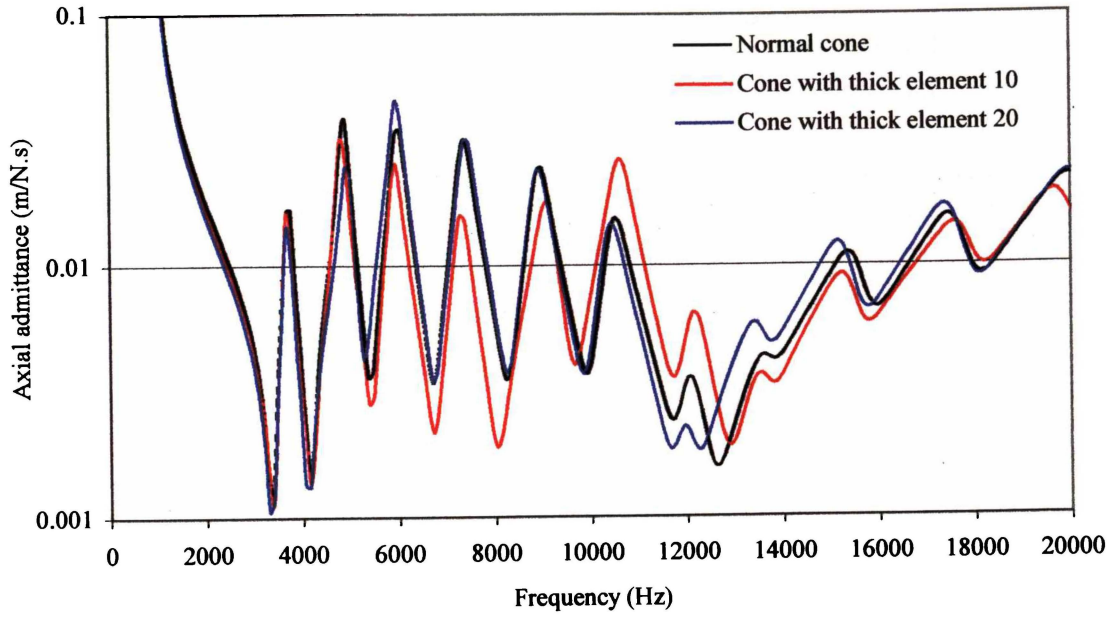

Figure 5.37. Y_{ax} response for cone C; Element 10 thickness=2.5mm; Element 20 thickness=2.5mm

Figure 5.37 illustrates that increasing the mass of element 10 has the effect of greatly accentuating the sixth bending resonance (the innermost antinode of the sixth bending resonance lies near element 10). The mean value of the axial admittance near the third, fourth and fifth bending resonances is lowered, although the height of the resonant peaks is unaffected. As the thickness of element 10 is increased (Figure 5.38), the height of the sixth resonance increases, and consequently begins to dominate the Y_{ax} response.

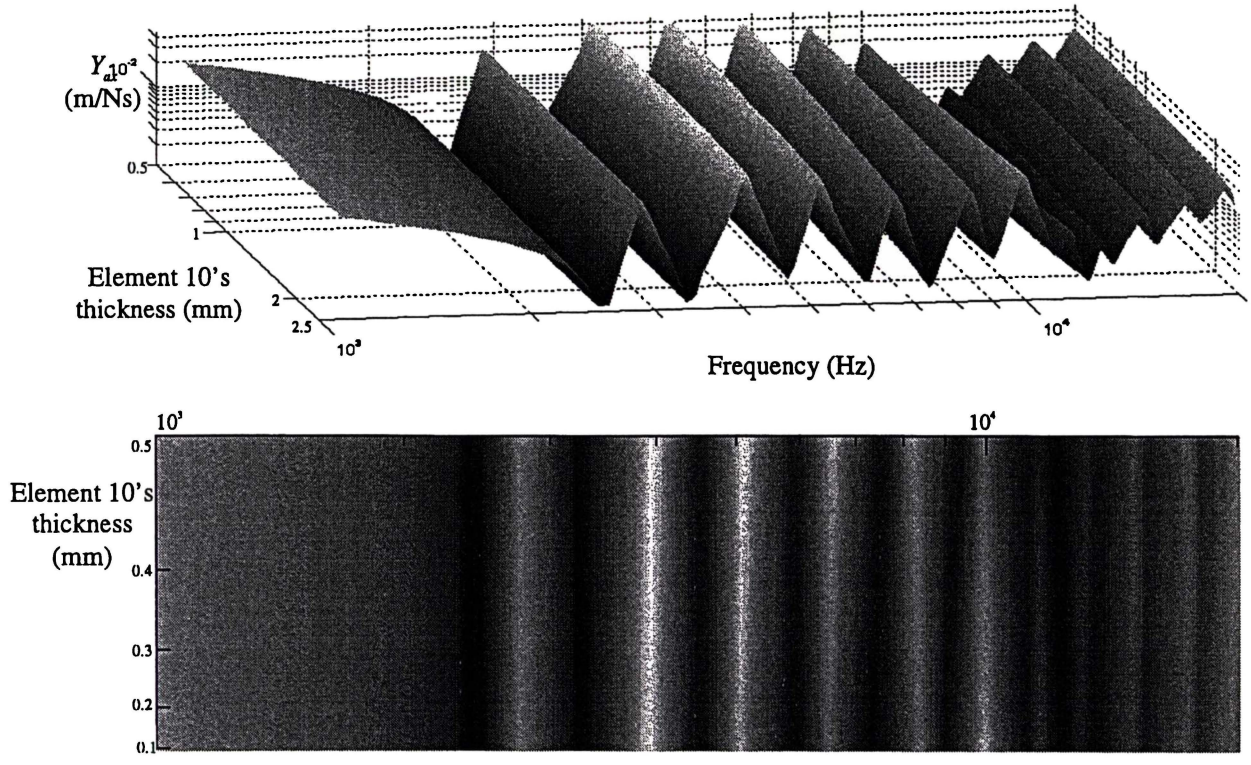

Figure 5.38. Y_{ax} response as the thickness of element 10 is varied from 0.5mm → 2.5mm

Figure 5.37 also indicates that adding mass to element 20 has the effect of accentuating the third bending resonance (the innermost antinode of the third bending resonance lies near element 20). The magnitude of the second resonance is also diminished; the third bending resonance dominates the Y_{ax} response.

The effect of adding or removing mass from an element of the FE model also has an effect on the mode shapes. Consider for example Figure 5.39, which shows the third resonant mode shape (innermost antinode ≈ element 20) as the thickness of element 20 is changed.

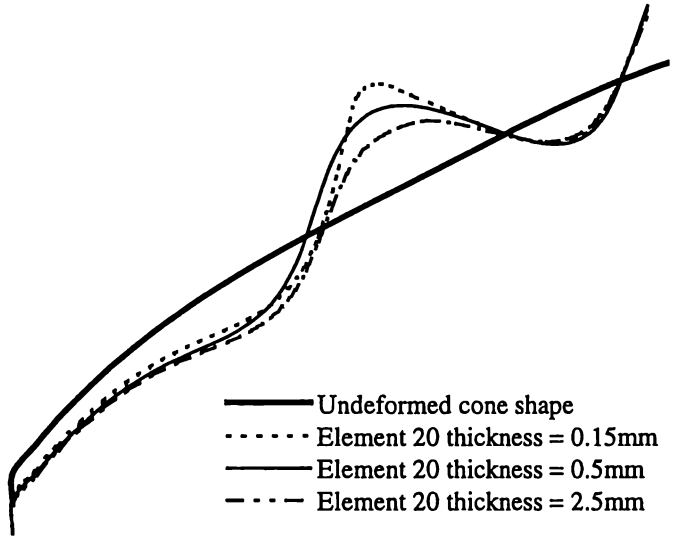

Figure 5.39. Third mode shape for element 20 thickness = 0.15mm, 0.5mm, 2.5mm

When the thickness of the innermost antinode is increased, the increased inertia of the antinode lowers its amplitude. However, the inner piston-like portion of the cone vibrates with lower amplitude than normal, resulting in a lower axial admittance for that mode.

Conversely, if the thickness of the cone is decreased at the innermost antinode of a resonant mode, the cone displacement will be increased at that point, due to the reduced inertia of the antinodal element. This results in the inner piston-like portion of the cone vibrating with greater amplitude than previously, implying an increased axial admittance and sound pressure for that resonant mode.

Summary

The effect of thinning the annulus formed by one axisymmetric element can be summarised as follows:

- All modes with innermost antinode closer to the outside edge of the cone than the thinned element are unaffected by the thinned element.

- All modes with innermost antinode closer to the centre of the cone than the thinned element are shifted to a lower frequency. The magnitude of the peaks and dips in the Y_{ax} response associated with such modes is diminished.

The effect of thickening the annulus formed by one axisymmetric element can be summarised as follows:

- The mode with innermost antinode corresponding to the thickened element will be accentuated on the Y_{ax} response.

- The lower order modes are diminished in amplitude

Using these guidelines, the relative magnitudes and frequencies of bending resonances and antiresonances can be "tuned" by lowering or increasing the thickness of certain parts of the loudspeaker cone.

Increasing the thickness of the loudspeaker cone at a particular element has a similar effect as simply adding mass to that part of the cone. This is most easily achieved by gluing a rubber ring to the rear surface of the driver. However, if the ring is made of highly damped material, similar to that used for the surround, the situation is somewhat more complicated. Rather than accentuating that resonant mode, the mode may be diminished by the additional damping offered by the rubber ring, as suggested by Heed [29].

While specific resonances can be accentuated or diminished through changing the thickness profile, the overall smoothness of the axial admittance/sound pressure response is not greatly affected. Nevertheless, if resonant modes measurably affect the sound pressure response of a loudspeaker design, this technique at least allows the designer some control over their frequency and amplitude.

5.4 CONCLUSION

This chapter has considered the effect of material properties and cone thickness on the resonant characteristics of a 6½-inch convex loudspeaker cone, without an outer surround attached. These results suggest the following conclusions:

Maximising bandwidth

The bandwidth of a loudspeaker of fixed shape and size is best extended by choosing light, stiff materials (i.e. with a high ratio of E/ρ). However, maximising E/ρ will also shift the bending resonances of the cone to a higher frequency, and increase the magnitude of ripple in the sound pressure response.

A high bandwidth can also be achieved through maximising Poisson's ratio.

Resonant frequencies.

The closeness of spacing of resonant frequencies can be minimised by reducing the cone thickness, which also results in lower magnitude sound pressure ripple. The relative spacing of bending resonant frequencies can also be altered by adjusting the cone thickness profile. Selectively thinning or thickening parts of the loudspeaker cone changes the shape of the Y_{ax} response, allowing specific resonant modes to be accentuated or diminished.

Minimising sound pressure ripple

The sound pressure ripple caused by resonant modes can be minimised by increasing the damping ratio of the cone material. This is commonly achieved by doping the cone material with a damping agent or coating the cone surface with a highly damped substance. (The damping contributed by the surround also has a very strong influence, as noted in Chapter 4.)

The amplitude of sound pressure ripple can also be minimised by decreasing the thickness of the cone, or by designing a cone with a thinner outside edge. This has the added benefit of increasing the efficiency of the cone, as the total moving mass is decreased.

CHAPTER 6

THE EFFECT OF CONE SLOTS ON LOUDSPEAKER RESONANCE

6.1 OVERVIEW

This chapter considers the effect of cutting narrow slots through the surface of a loudspeaker cone. The rationale for this research is outlined in Section 6.2, along with a brief description of the process followed to generate the modelled results considered in this chapter.

Section 6.3 considers the effect of radial cone slots (that is, slots lying along the meridional lines, between the inner and outer edges of the cone) on the resonant behaviour of the loudspeaker. The Y_{ax} response and mode shapes of a radially slotted cone are calculated and summarised. The effects of varying the length, number and position of the cone slots are also considered.

In Section 6.4, the slots are rotated so that they lie at an angle to the meridional lines of the cone. This changes both the shape of the Y_{ax} response and the nature of cone resonance. The effects of changing the length and angle of the angled slots are also determined.

Reducing the length and increasing the number of slots results in a "ring of slots", that can be used to "tune" any particular natural resonant mode of an axisymmetric cone. This method is briefly summarised in Section 6.5.

Finally, a cone design with three angled slots is implemented and measured in Section 6.6, confirming the predictions of the FE model. A technique of sealing over the cone slots with lightweight stickers is proposed and briefly investigated.

The cone slotting technique is summarised and conclusions are drawn in Section 6.7.

6.2 INTRODUCTION

It has long been understood that standing waves set up between the inner and outer edges of a loudspeaker cone are a fundamental cause of ripple in the loudspeaker's sound pressure response.

Consequently, cutting slots in a loudspeaker cone has been suggested as a means of precluding the formation of concentric standing waves on the cone, and thereby smoothing the sound pressure response of the loudspeaker. This theory is explored in this chapter by means of a full three-dimensional finite element model of a "slotted" loudspeaker cone.

A three-dimensional finite element model of a loudspeaker cone was initially designed and calibrated to loudspeaker cone C's material properties, as described in Chapter 4. This model was then used as a basis for experimenting with different slot designs.

Slots were introduced into the three-dimensional cone model by defining "forming" blocks that protruded through the surface of the cone. Subsequently, the blocks were subtracted from the cone shell using Boolean operations, leaving behind a "slotted" loudspeaker cone. Figure 6.1a) shows a view of a typical slotted cone with one of the forming blocks still in place.

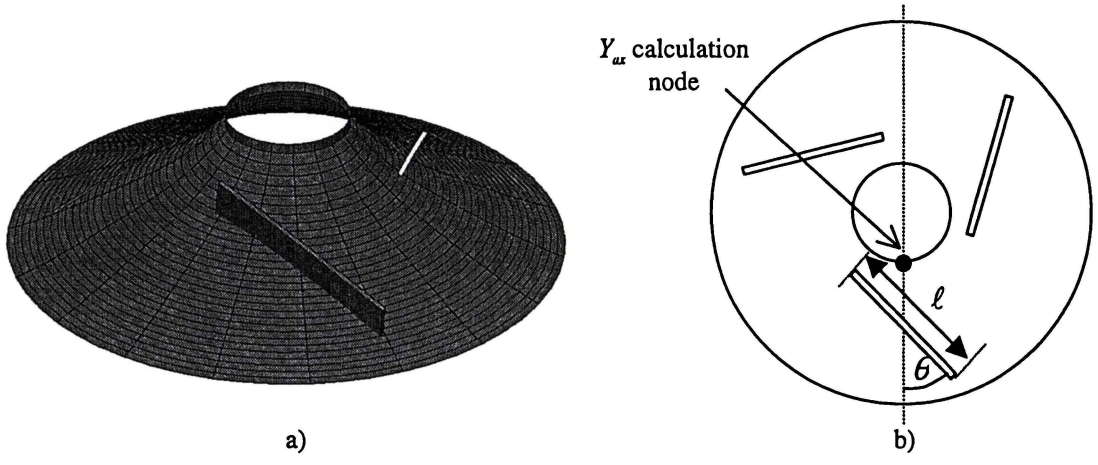

Figure 6.1. 3D cone model with three angled slots. a) The blocks used to create the slots protrude through the surface of the cone. b) Rear view of the loudspeaker cone, showing slot geometry.

Cone slots are defined in terms of their length ℓ, angle with the meridional line θ, and their position on the cone. All cone slots have a nominal width of 1mm, which is large enough to prevent the edges of the slot coming into contact with each other when the cone is vibrating. While it is likely that significantly increasing the width of the slot beyond 1mm would further alter the resonant behaviour of the loudspeaker cone, this investigation is restricted to describing the effect of narrow slots (length >> width), and thus the effect of slot width is not considered.

Prior to the subtraction of the forming blocks, a mesh density of 31 elements per meridonal line (as for a 2D model), and 36 elements per azimuthal line (10° angular element resolution) is specified. After the forming blocks are subtracted, the standard ANSYS auto-meshing algorithm is utilised to mesh the model using a combination of quadrilateral and triangular SHELL63 elements. The meshing algorithm automatically adjusts the element density and distribution during the meshing process, in order to meet the default ANSYS element size and aspect ratio criteria. In general, this process results in a rotationally symmetric element distribution (approximately 1500 elements and nodes) with a finer mesh density near the edges of the slots.

The innermost nodes of the cone were constrained to axial motion, with an axial force of magnitude of 1N, and the Y_{ax} response calculated for 100 linearly spaced frequencies in the range 100Hz -10kHz.

The vector displacement and colour contour plots of Section 6.3 demonstrate that for radial-slot models, the inner neck of the cone moves as a rigid body, with the nodes around the neck moving with almost equal amplitude and phase. Even in the worst-case radial slot model (9 44mm slots, Section 6.3.3), the variation in the displacement of innermost nodes was less than ±1% from the mean displacement. For angled slot models, the variation in inner-node displacement was up to ~10% particularly at higher frequencies, and when the inner end of the slot was close to the neck of the cone.

In each slot design considered, the chosen node was one that lay along the meridional line that passed through the centre of one of the cone slots, as shown in Figure 6.1b).

In previous sections, FE results were calculated for frequencies up to 20kHz. However, in order to reduce the total processing time, we restrict our examinations in this section to a bandwidth of 10kHz. This is appropriate, as the loudspeaker's sound pressure radiation is strongly rolled-off at high frequency by the mass of the voice coil, despite the resonant behaviour of the cone itself.

All calculations were performed on a WindowsNT 3.51 workstation (Pentium 133), which took approximately 6 minutes to find the finite element solutions for all nodes at each frequency considered. Thus, the total processing time required to solve one FE model for 100 frequencies is approximately 10 hours.

It was beyond existing monetary and processing constraints to calculate the sound pressure response radiated by any of the three dimensional cone designs. This is regrettable, but unavoidable, as the calculation time for even one frequency is of the order of hours.

However, the "smoothness" of the on-axis sound pressure response of a slotted cone can be estimated from the smoothness of its Y_{ax} response. This is certainly the case for axisymmetric cones, as the results of Chapters 4 and 5 show. The measured Z_{mot} and sound pressure responses presented in Section 6.6 vindicate the assumption that there is also a close relationship between Y_{ax} (and Z_{mot}) and sound pressure for a slotted

loudspeaker cone.

Admittedly, this assumption may not be valid for sound pressures not measured directly in front of the loudspeaker, and thus few conclusions can be made about the off-axis response of a slotted loudspeaker. This area warrants further research, particularly as the processing power of desktop computers increases to the extent that quickly solving the sound pressure response of such large models becomes more practical.

The results in this chapter are presented by means of the Y_{ax} response for 100Hz-10kHz and the mode shapes at significant resonant frequencies in this range. This allows the behaviour of slotted loudspeaker cones to be qualitatively understood, and allows their sound pressure responses to be predicted.

Hereinafter, the Y_{ax} response and mode shape results for loudspeaker cone C are often referred to as the "normal" results, as they are indicative of the characteristics of a typical axisymmetric loudspeaker. The normal resonances and antiresonances of cone C are referred to using the notation of Figure 4.10. By comparing the mode shapes of slotted cones with those of cone C, a qualitative description of slotted cone resonance is given.

6.3 RADIAL SLOTS

Radial slots correspond to the case where $\theta = 0$ and consequently lie along the meridional lines of the cone as shown in Figure 6.2.

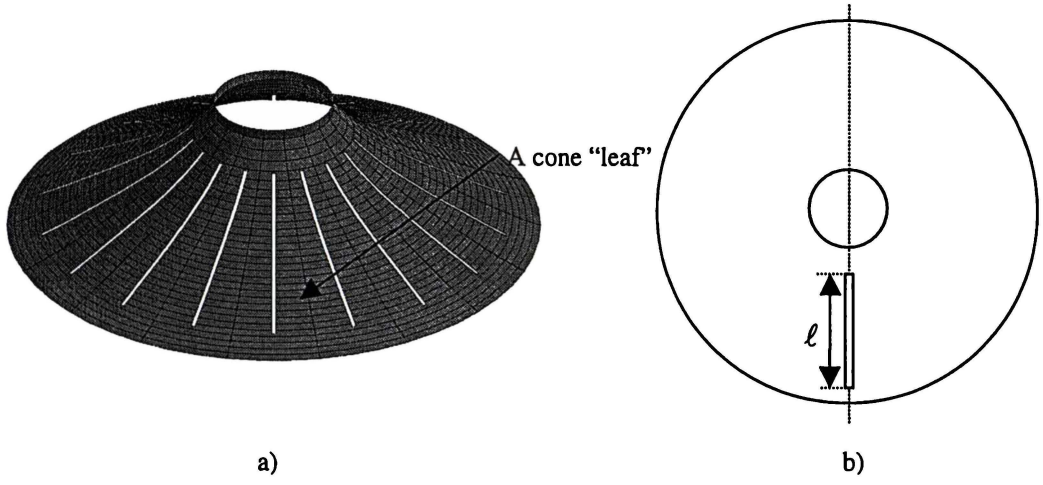

Figure 6.2. a) Cone FE model with 18 44mm slots. b) Slot geometry

By beginning with a FE model consisting of 18 radial slots, the resonant behaviour of a radially slotted cone is characterised in terms of its Y_{ax} response and mode shapes at significant modal frequencies. The effect of changing the length of the cone slots by moving the slot's inner and outer ends, and the effect of changing the number of slots is considered and summarised.

6.3.1 CHARACTERISING RADIAL SLOT RESONANCE

In order to characterise the effect of radial slots on the Y_{ax} response of cone C, eighteen 44mm long, 1mm wide slots were introduced into the three-dimensional cone model. The slots were cut from the middle of element four to the middle of element twenty-eight, as shown in Figure 6.2. Essentially, the loudspeaker cone model now consisted of an inner and outer annulus connected by eighteen relatively compliant "leaves" of cone material.

The axial admittance response of this design is shown in Figure 6.3 with the frequency axis drawn on a linear scale to enable the features of the Y_{ax} responses to be easily observed.

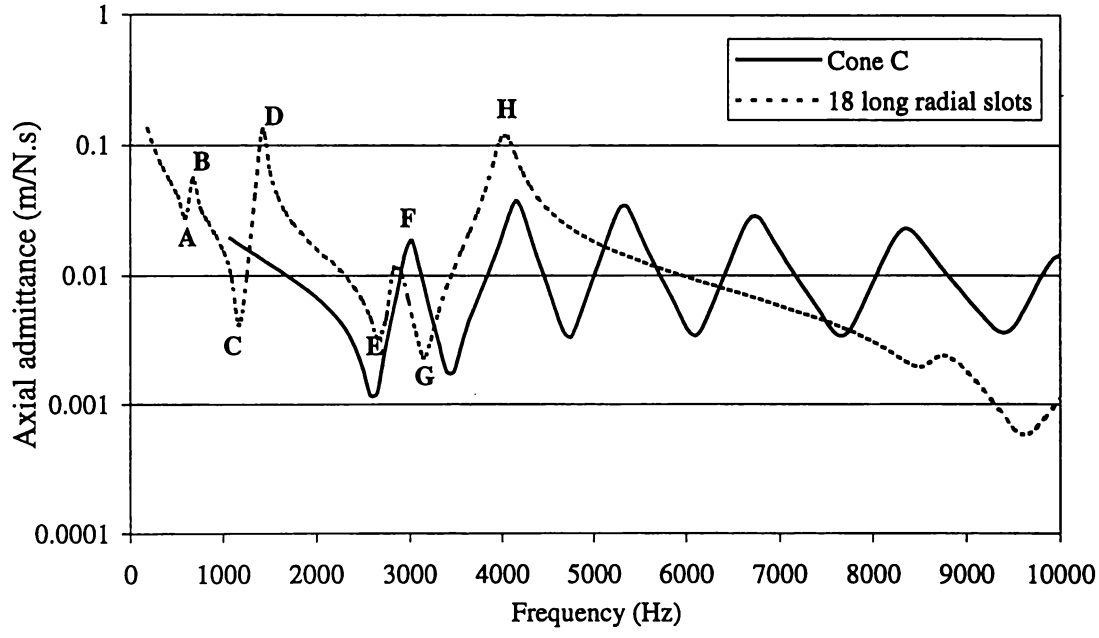

Figure 6.3. Y_{ax} response for cone with 18 44mm radial slots as in Figure 6.2

Figure 6.3 confirms that radial cone slots have a significant effect on the shape of the Y_{ax} response. The series of resonant frequencies that previously characterised the response of cone C are replaced with a different set of resonances and antiresonances.

For f < 4kHz, the radially slotted cone exhibits several modes not present in the Y_{ax} response of cone C. While the first bending antiresonance of cone C is not excited until $f \approx$ 2.6kHz, the model with radial cone slots exhibits resonant behaviour at frequencies as low as $f \approx$ 600Hz. For $f >$ 4kHz, cone C exhibits a number of higher order bending resonant modes which are absent from the response of the radially-slotted model, as the axial admittance decreases at a rate inversely proportional to frequency.

The exact nature of the resonance of a radially slotted loudspeaker cone can be outlined by considering the colour contour and vector displacement plots at the frequency of each Y_{ax} resonant feature. The resonant and antiresonant frequencies of the radially slotted loudspeaker are identified in Figure 6.3 by letters **A-G**. The plots for the first

two resonant features, denoted **A** and **B** on Figure 6.3 are shown in Figure 6.4.

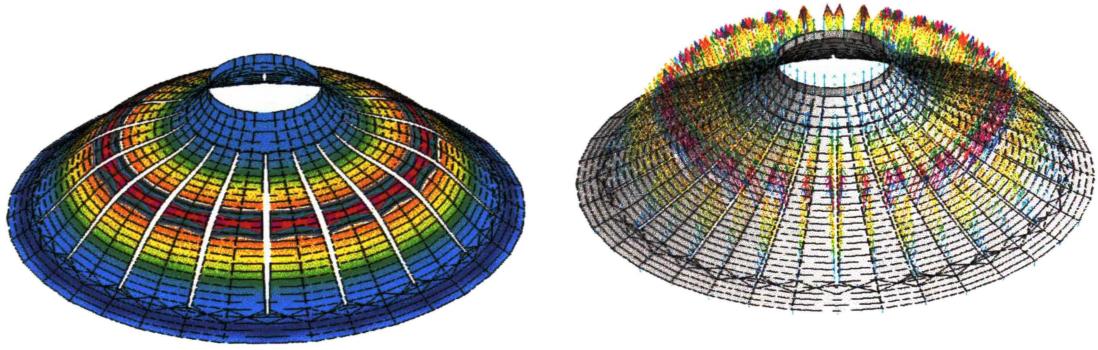

a) antiresonance **A** ≈ 600Hz

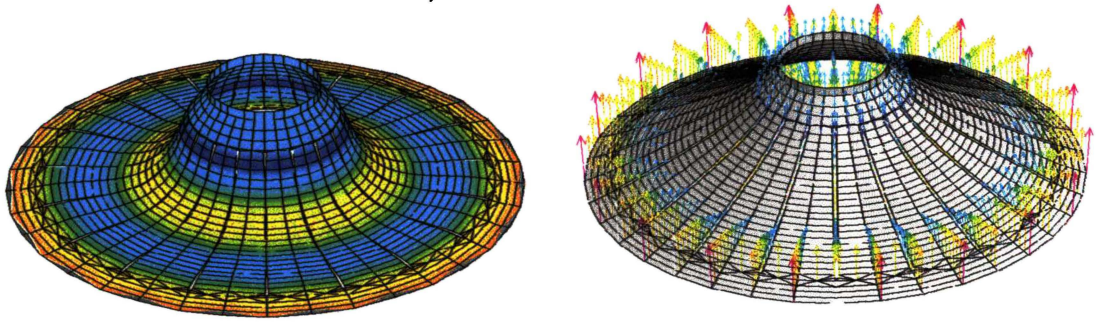

b) resonance **B** ≈ 680Hz

Figure 6.4. Colour contour and vector displacement plots for cone with 18 44mm slots at a) antiresonance **A** b) resonance **B**.

Figure 6.4 shows that antiresonance **A** is caused by a bending standing wave being excited in the cone leaves, with wavelength = 2ℓ. This mode can be thought of as the fundamental bending resonance of the cone leaves. At this quite low driving frequency, the loudspeaker has already significantly deviated from piston like behaviour.

At a slightly higher frequency, (Resonance **B**) the cone leaves begin to flex more, as a second order bending mode begins to be excited down the cone leaves. At approximately twice the frequency of the fundamental resonance of the cone leaves, resonant features **C** and **D** are excited. These modes correspond to the second bending cone-leaf resonant frequency, as shown in the colour-contour and vector displacement plots of Figure 6.5.

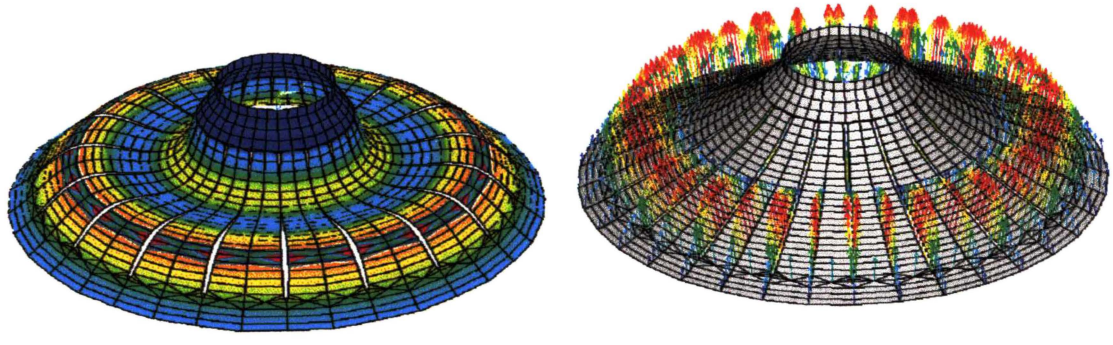

a) antiresonance **C** ≈ 1173Hz

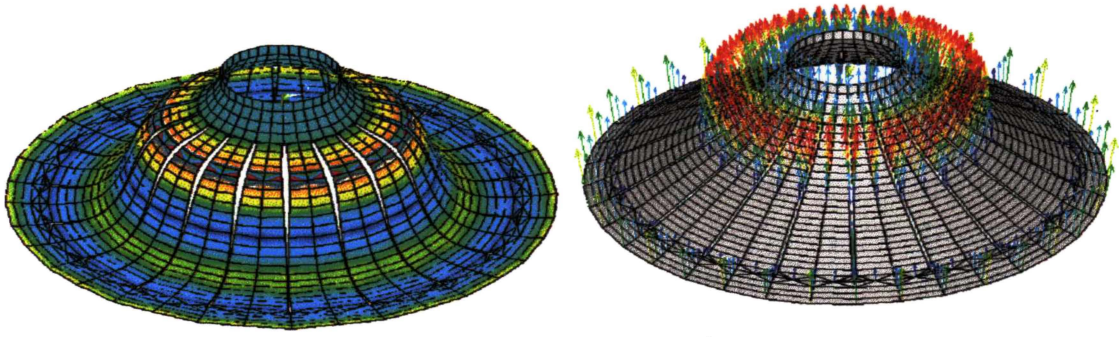

b) resonance **D** ≈ 1420 Hz

Figure 6.5. Colour contour and vector displacement plots for cone with 18 44mm slots at a) antiresonance **C** b) resonance **D**.

Figure 6.5 shows that features **C** and **D** are caused by the excitation of a bending mode in the cone leaves with one wavelength along each leaf length. At antiresonance **C**, the outer halves of the cone leaves vibrate with maximum amplitude, while at resonance **D**, the inner antinode shows higher displacement.

At $f \approx$ 2.7kHz, antiresonance **E** and subsequently resonance **F** are excited. These are shown in Figure 6.6.

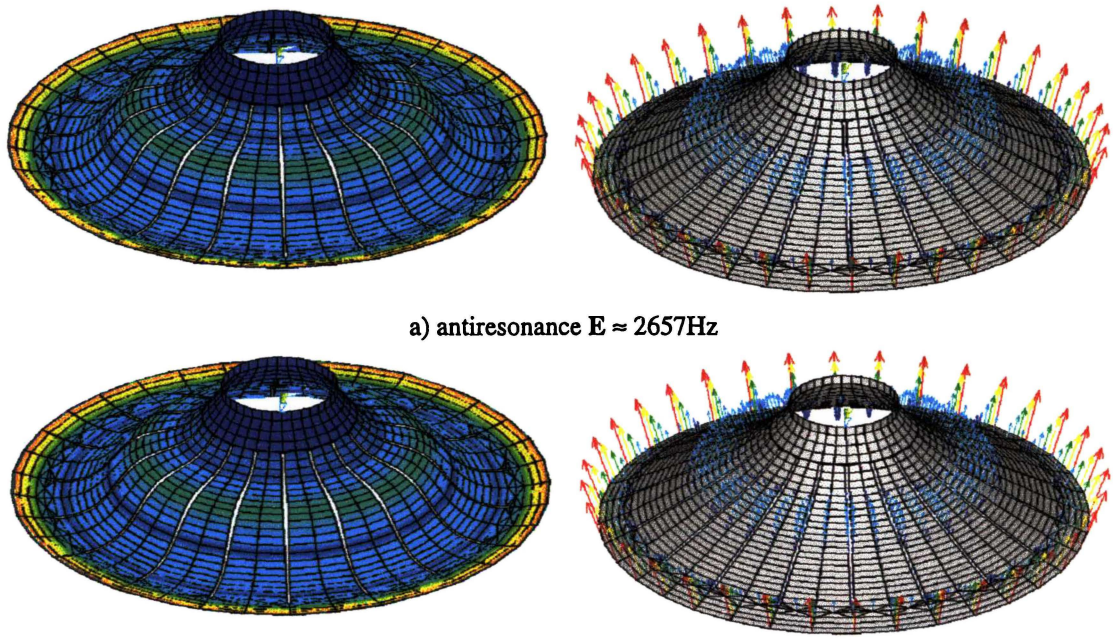

a) antiresonance **E** ≈ 2657Hz

b) resonance **F** ≈ 2823Hz

Figure 6.6. Colour contour and vector displacement plots for cone with 18 44mm slots at a) antiresonance **E** b) resonance **F**.

Modes **E** and **F** are a combination of the third order cone leaf resonance ($\lambda = 3\ell/2$) and the ring antiresonance shape of a normal cone. The outer edge of the cone moves with maximum transverse amplitude, as for f_{ra} (Figure 4.14a), which is combined with a bending wave motion near the middle of the leaves of the cone.

Since the azimuthal stress in the cone area between elements four and twenty-eight has been relieved by the cone slots, any cone bending motion is opposed largely by the

relatively low bending stiffness of the cone material. Thus, these first six cone leaf bending modes (**A-F**) appear at comparatively low frequency, and cause a significant change in axial admittance for $f < 4$kHz.

At $f \approx 3200$Hz, the axial admittance response reaches a local minimum (**G**), as an antiresonant frequency is excited, followed by a very significant resonance (**H**) at f ≈ 4kHz. These are shown in Figure 6.7.

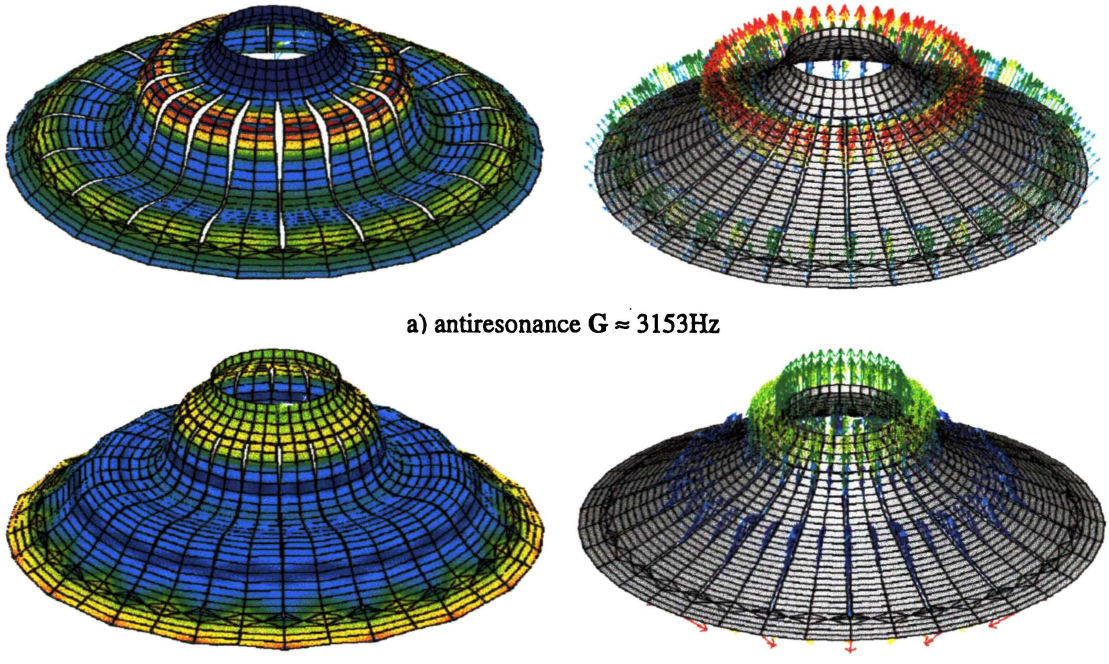

a) antiresonance **G** ≈ 3153Hz

b) resonance **H** ≈ 4060Hz

Figure 6.7. Colour contour and vector displacement plots for cone with 18 long slots at a) antiresonance **G** b) resonance **H**.

Antiresonance **G** is characterised by a bending standing wave down the leaves of the cone, with 1½ bending wavelengths between the inner annulus and the outer edge of the cone. Thus, this mode corresponds to the third natural frequency of the cone leaves. At this frequency, the axial displacement at the inner annulus is almost zero, while three antinodal lines form on the leaves of the cone. The maximum transverse displacement of the cone occurs at the innermost of these three antinodal lines.

Resonant frequency **H** (Figure 6.7b) is a combination of azimuthal stretching motion of the outer annulus, and a bending standing wave motion down the cone leaves. For this and higher frequencies, the outer circumference of the cone significantly expands and contracts with the driving force while a standing wave ($\lambda = \ell/2$) is set up along the length of the cone leaves.

Resonant frequency **H** marks a transition in the resonant behaviour of the cone. Above this frequency, the Y_{ax} response of the cone decreases at a rate approximately inversely proportional to frequency. The outer annulus of the cone continues to expand and contract, and some bending motion of the leaves still occurs while the inner annulus of the cone retains its piston-like motion.

6.3.2 CHANGING THE LENGTH OF RADIAL SLOTS

The characteristics of the resonant behaviour introduced by radial slots can be illustrated further by considering the effect of cone slots of various lengths on the loudspeaker's Y_{ax} response.

Firstly, the slot length was varied by holding the position of the outer edge of the cone slot fixed, and varying the position of the inner edge of the slot, as illustrated in Figure 6.8.

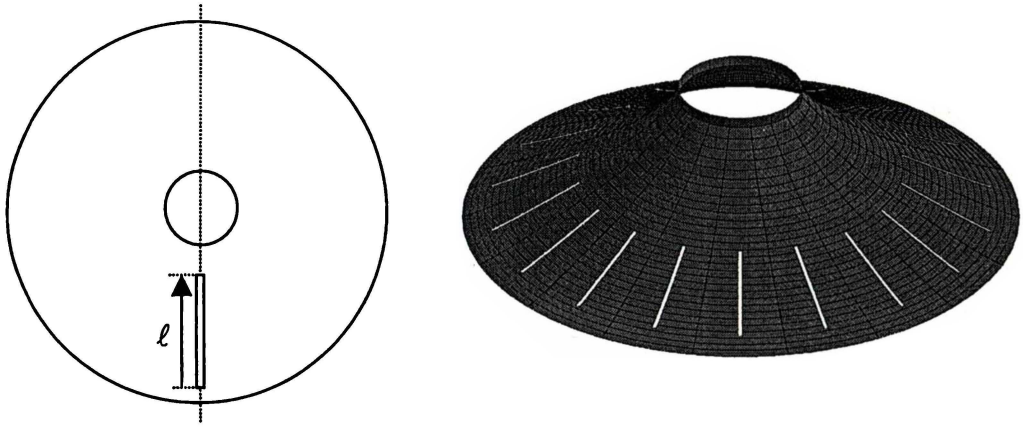

Figure 6.8. a) The position of the outer end of the slot is fixed; the length of the slot is changed from 0mm → 44mm. b) Example: cone slot length = 22mm.

The cone slot length was varied from 0mm (no slot) to 44mm in steps of 2mm, and the Y_{ax} response calculated for 100Hz < f < 10kHz. The calculated results are plotted in Figure 6.9. The bending modes associated with normal loudspeaker cone resonance are denoted on the lower plot of Figure 6.9 by their order (**1-5**), while the resonant frequencies caused by radial cone slots are denoted **A-H** as in Figure 6.3.

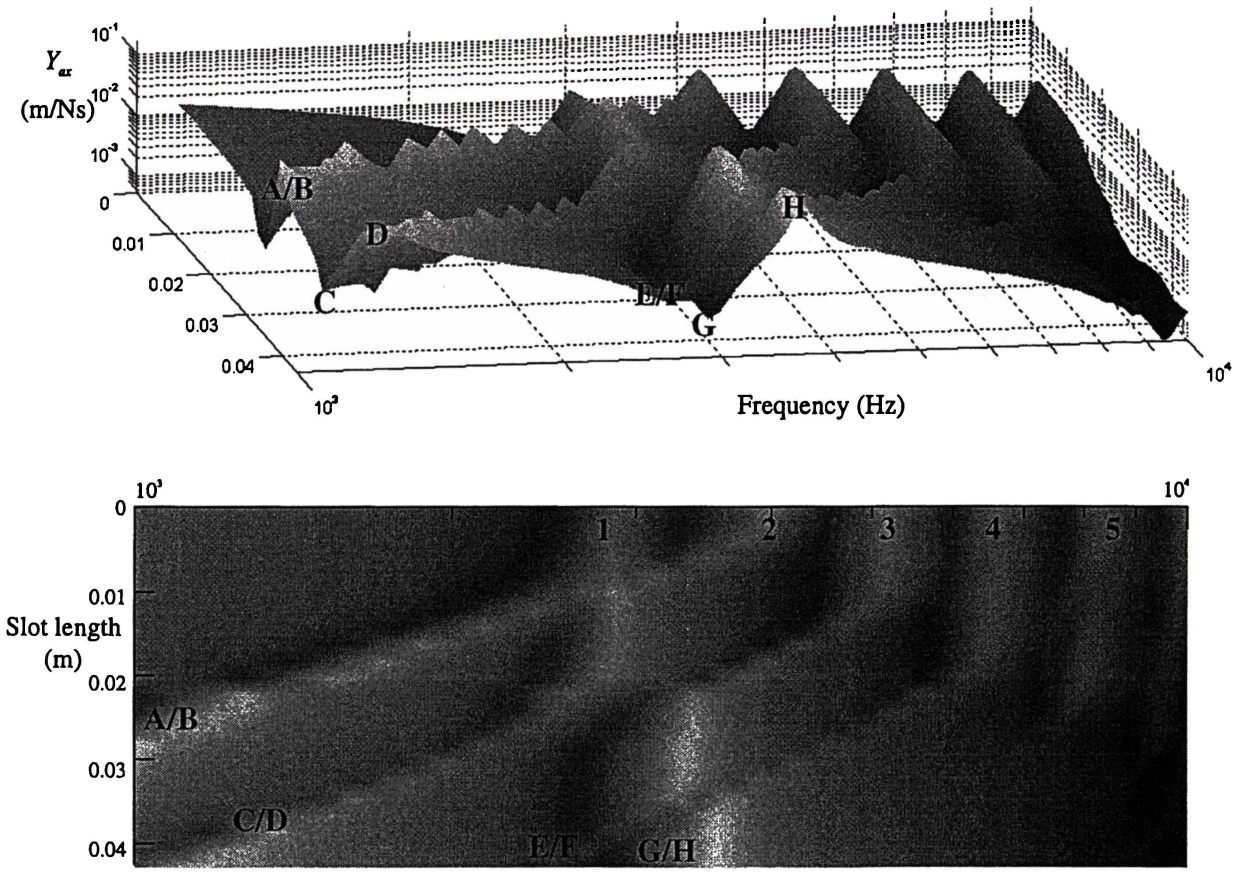

Figure 6.9. 3D plot of Y_{ax} response as cone slot length is varied from 0 → 44mm. The outer edge of the slot is fixed.

The modes that are associated with bending modes down the length of the cone leaves (**A-F**) are quite dependent on the length of the cone leaves, moving to lower frequency with increasing leaf length. In contrast, resonant features **G/H** move to slightly higher frequency with increasing cone leaf length.

Each normal loudspeaker mode disappears from the Y_{ax} response when the inner end of the slot lies near its innermost antinode. For example, the second bending resonance (**2**) is not affected by the cone slot until the innermost end of the slot lies near nodal line 25, the position of the innermost antinode of bending resonance two. This corresponds to a slot length of approximately 6mm.

Similarly, the third bending resonance (**3**) disappears from the Y_{ax} response when the cone slot length is approximately 12mm. A slot of 12mm length has its inner end at nodal line 21, which corresponds to the innermost antinode for mode 3.

When the cone slots are lengthened such that the inner end of the slots lies at nodal line 11 (corresponding to a slot length of 30mm), the first six normal bending resonances disappear from the Y_{ax} response and are replaced by the ring resonance (**G,H**) and the cone leaf resonances. This occurs because the innermost antinode for the 6th bending resonance lies at antinodal line 11.

The effect of cone slot length can also be illustrated by holding the position of the inner end of the slot fixed, and changing the position of the outer end of the slots, as shown in Figure 6.10.

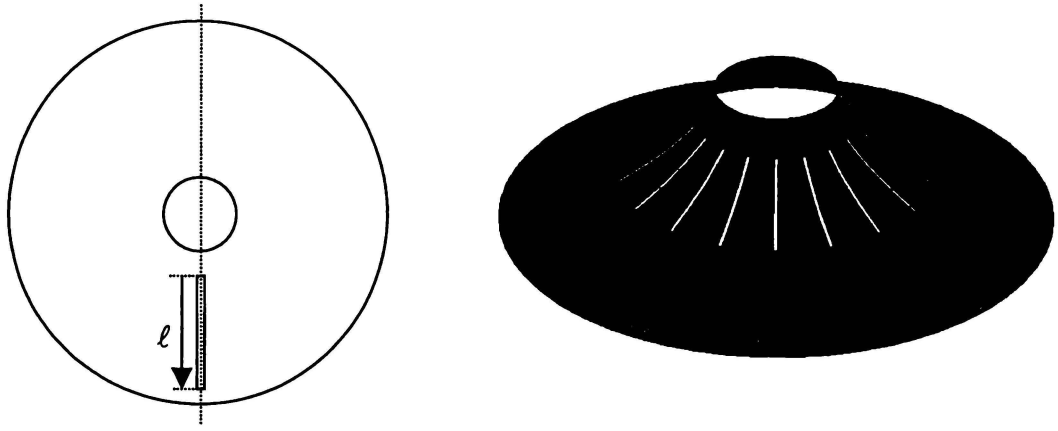

Figure 6.10. a) The position of the inner end of the slot is fixed; the length of the slot is changed from 0mm → 44mm. b) Example: cone slot length = 22mm.

The Y_{ax} response was calculated with cone slot lengths varying from 0 → 44mm in 2mm steps and is plotted as a function of cone slot length in Figure 6.11.

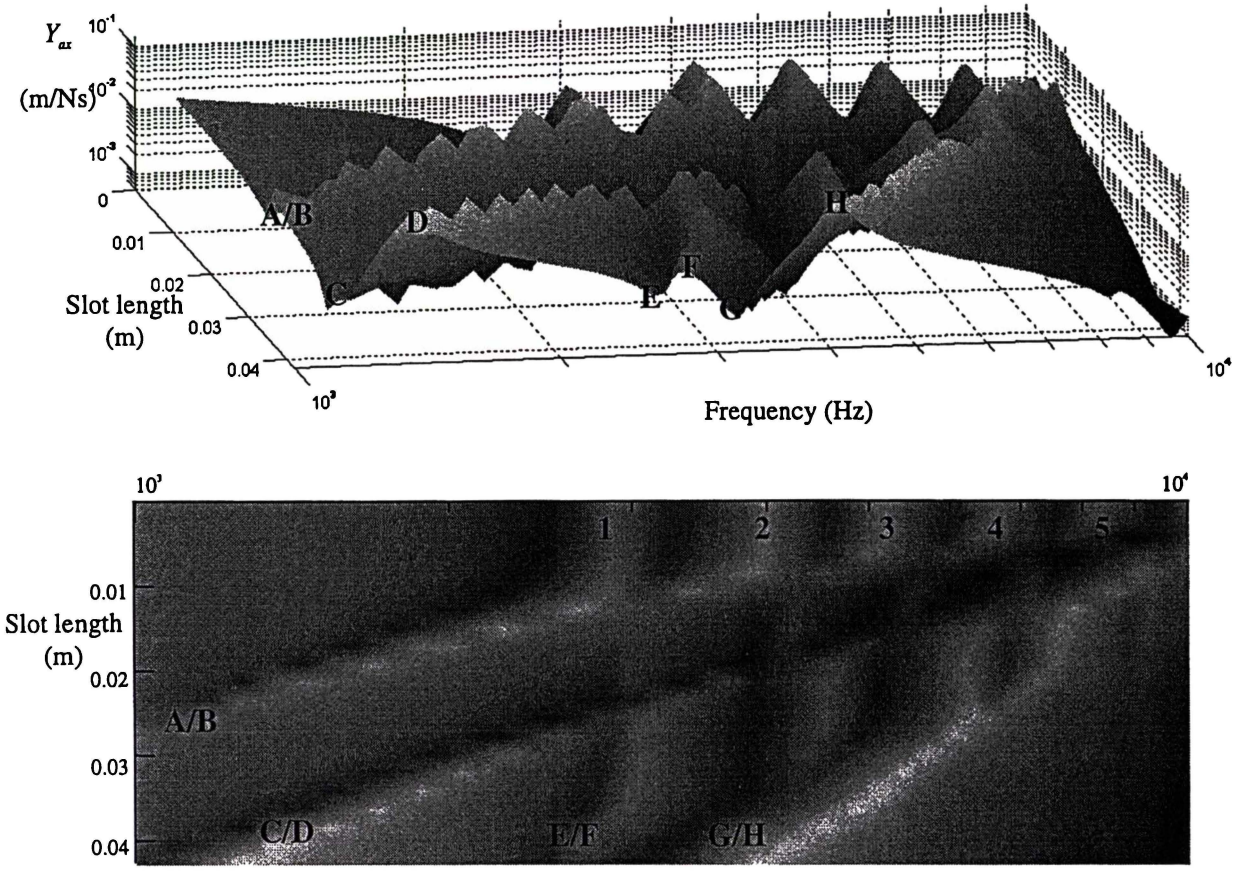

Figure 6.11. 3D plot of Y_{ax} response as cone slot length is varied from 0 → 44mm. The outer edge of the slot is fixed

As previously, the cone slots introduce bending standing waves down the slot leaves,

which are shifted to lower frequency with increasing slot length (modes **A-D**). The natural bending frequencies of the cone leaves are higher than previously, as the cone slots are closer to the centre of the cone, where the bending stiffness is greater.

As the cone slot is lengthened, the first natural bending frequency of the leaves is excited, perturbing the higher order modes first, as the cone slot moves outwards and approaches their innermost antinodes. However, the natural bending modes do not entirely disappear; rather, each natural mode re-emerges as the first and then second bending modes of the cone leaves become lower in frequency than the natural mode. The natural modes are not entirely removed until resonant modes **G** and **H** are excited.

The frequency of resonant features **G** and **H** is proportional to the length of the outer annulus of the cone. In Figure 6.9, the outer annulus stays the same size as the inner end of the slot is moved towards the centre of the cone, and consequently **G** and **H** are comparatively unaffected by increasing the slot length. In contrast, Figure 6.11 shows that resonant modes **G** and **H** move to lower frequency as the length of the outer cone annulus is decreased.

6.3.3 NUMBER OF SLOTS:

The designs considered in Sections 6.3.1 and 6.3.2 consisted of 18 radial slots. In this section, the influence of the number of slots on the frequency and shape of the resonant modes of the cone is briefly considered. In order to determine the influence of the number of radial slots, two further FE models were generated. The first of these models consisted of twelve radial slots of length 44mm, the second of nine radial slots of length 44mm. The Y_{ax} responses of both these models are shown in Figure 6.12.

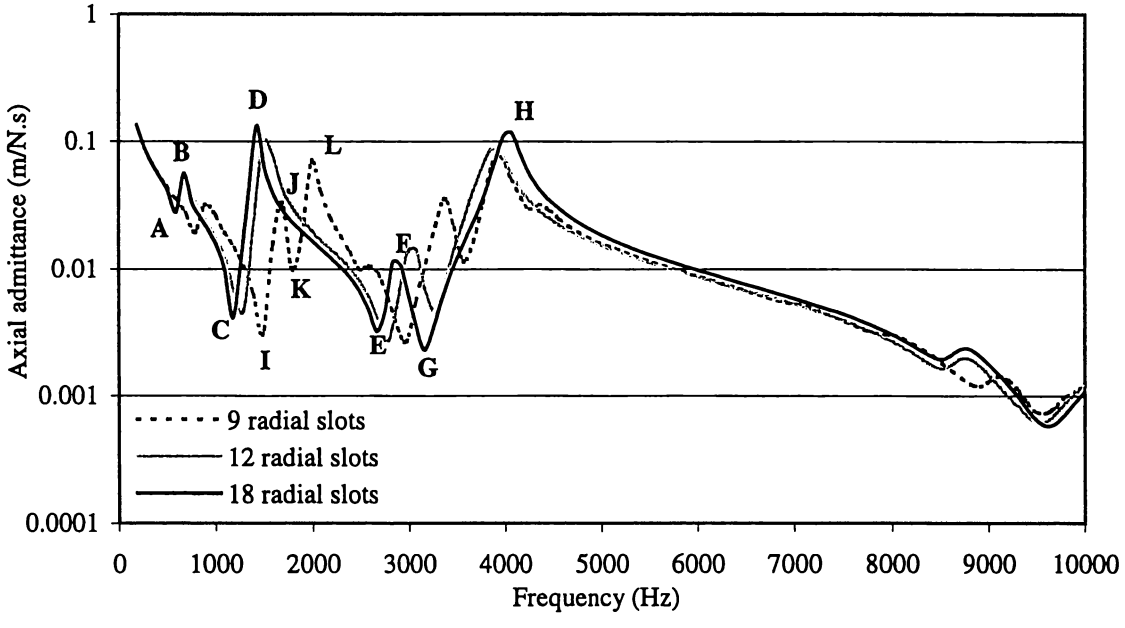

Figure 6.12. Y_{ax} response for cones with 9, 12, and 18 radial slots. Slot length = 44mm.

Figure 6.12 shows that the resonant features associated with standing waves down the length of the cone leaves (**A-F**) are all moved to higher frequencies as the number of

slots is decreased. Decreasing the number of radial slots in the cone has the effect of widening the cone leaves, thereby increasing the bending stiffness of the leaves, and lowering their natural frequencies. Antiresonance **G** and resonance **H** are slightly lowered in frequency as the number of slots is increased.

Decreasing the number of slots to nine also has the effect of dividing resonant features **C** and **D** into two separate pairs of resonances and antiresonances (**I, J, K, L**). These new modes arise because of the excitation of radial bending motion around the outer circumference of the loudspeaker. Figure 6.13 shows the mode shapes of features **I** and **K**.

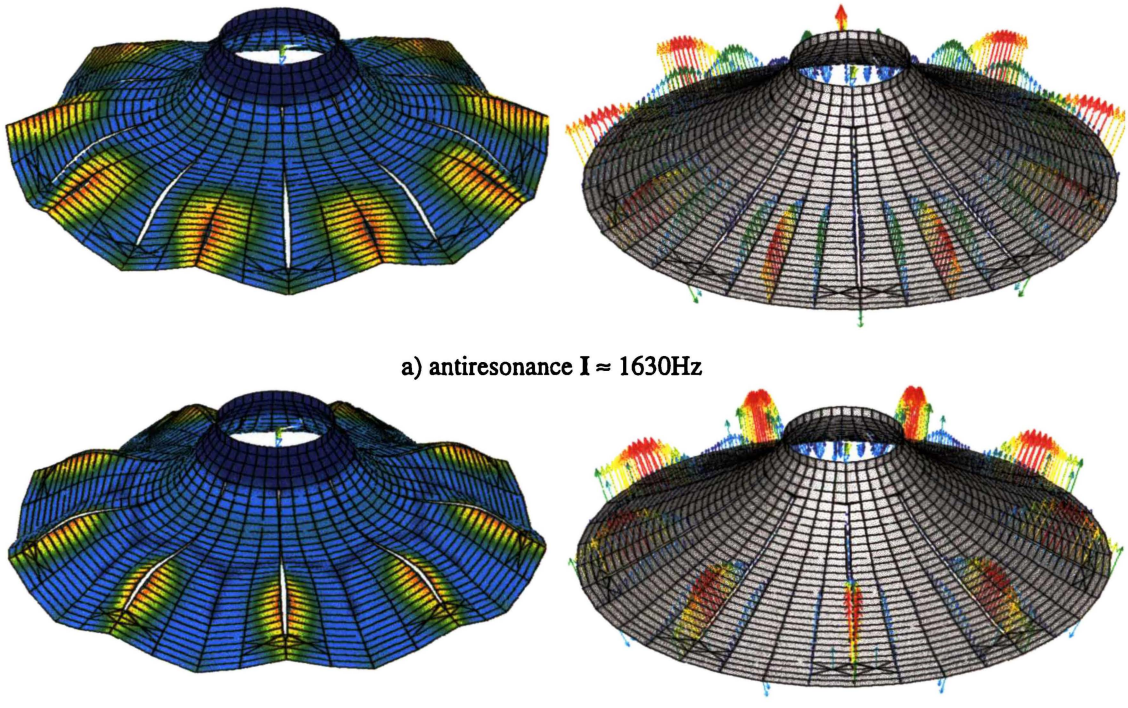

a) antiresonance **I** ≈ 1630Hz

b) antiresonance **K** ≈ 1900Hz

Figure 6.13. Colour contour and vector displacement plots for cone with 9 47mm long slots at a) antiresonance **I** b) antiresonance **K**.

Figure 6.13a indicates that when antiresonance **I** is excited, the loudspeaker cone moves with maximum displacement in the region between the cone slots near the outside edge of the cone. The mode shape of antiresonance **K** (Figure 6.13b), is similar to mode shape C for the cone with 18 radial slots (Figure 6.5a), particularly along the length of the slot. Although a bending wave is excited along the slot length, with $\lambda \approx \ell$, the portion in the middle of the cone leaves moves out of phase with the edges of the cone slot.

6.3.4 SUMMARY:

The effect of radial cone slots on the resonant behaviour of a normal loudspeaker cone can be summarised as follows:

- The n^{th} bending mode of a normal loudspeaker cone is affected when the cone slot's inner end lies closer to the centre of the cone than the innermost antinode for mode n.

- Bending standing waves along the cone "leaves" introduce new resonant features to the Y_{ax} response. These frequencies increase with decreasing slot length.

- The Y_{ax} response reaches an overall maximum at resonant frequency **H**, the frequency of which increases with the length of the outer annulus of the cone. This mode shape is characterised by the entire outer cone annulus stretching and shrinking in response to the driving force, combined with a bending wave motion down the cone leaves.

- If the n^{th} bending mode of a normal cone is of lower frequency than mode **H**, it is diminished, rather than removed by the cone slots.

- When the cone slots are long, the frequency of mode **H** is minimised. In this case, the natural resonances of the cone disappear from the Y_{ax} response, which decreases at a rate proportional to frequency.

- Decreasing the number of slots increases the frequency of standing waves down the cone leaves, and introduces radial modes around the outer edge of the cone.

Although radial slots have an interesting effect on cone motion, and greatly alter the Y_{ax} response and mode shape of a cone, they do not produce a smooth, uniform Y_{ax} response, particularly in the critical range $f < 4$kHz. In general, the on-axis sound pressure of a cone follows the same trend as its Y_{ax} response, and thus the sound pressure of a radially slotted cone would be far from desirable.

While the smooth decrease in Y_{ax} for $f > 4$kHz implies a smooth, desirable roll-off in sound pressure at these frequencies, this characteristic is more than off-set by the undesirably large peaks and dips in Y_{ax} caused by bending modes **A-F**.

6.4 ANGLED SLOTS

This section considers the effect of angled cone slots on the nature of loudspeaker cone resonance. The angled slot design is characterised by three or more 1mm wide slots of length ℓ placed at an angle θ to the meridional lines of the cone, as shown in Figure 6.14:

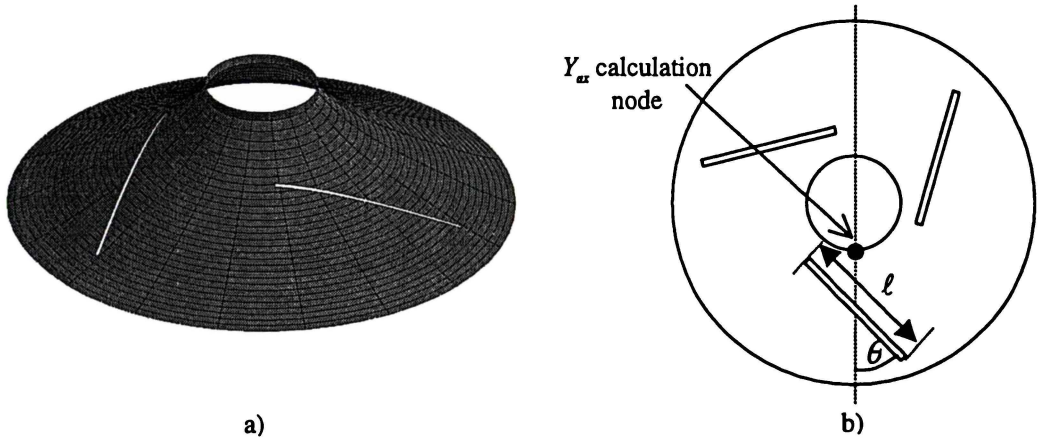

Figure 6.14. a) Cone model with three angled slots. b) Rear view of cone showing slot geometry.

Each slot is centred on a point midway between the inner and outer edges of the loudspeaker cone as seen from the front of the loudspeaker. In each slot design considered, the Y_{ax} response was calculated from a node lying along a meridional line passing through the centre of one of the cone slots, as shown in Figure 6.1b).

The effect of the angled slots on the modelled Y_{ax} response can be demonstrated by initially considering the calculated response of a cone with ℓ=47mm and θ = 45°, as shown in Figure 6.15.

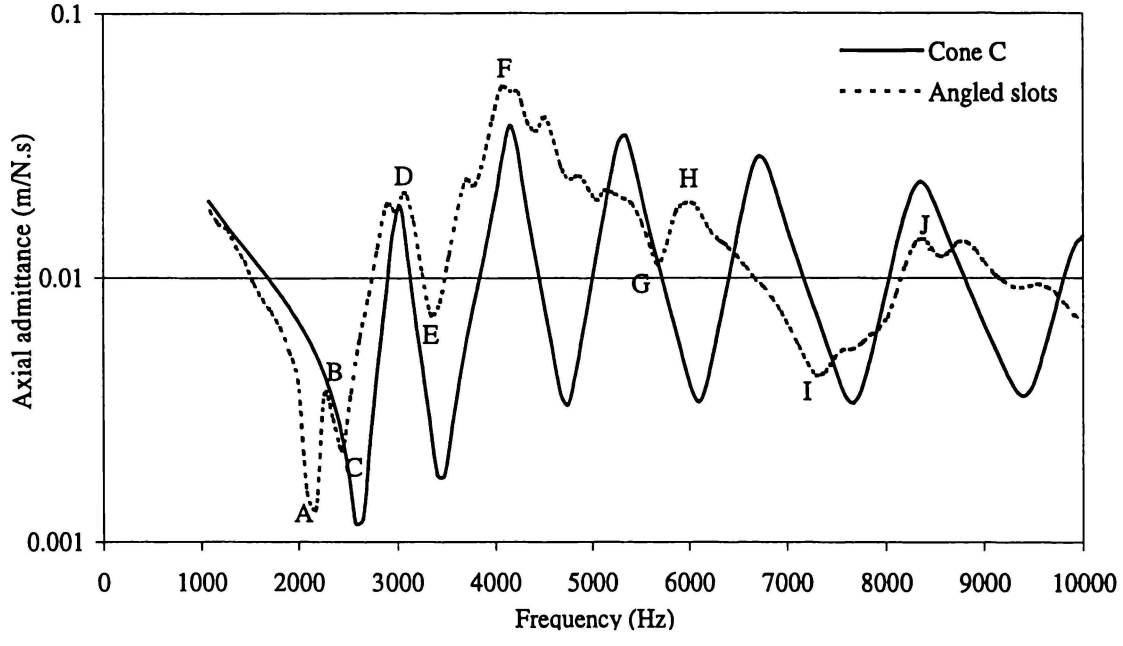

Figure 6.15. Y_{ax} response for cone C with and without angled slots (ℓ=47mm, θ = 45°)

The addition of cone slots significantly affects the shape of the Y_{ax} response, particularly for frequencies above the second bending resonance (f > 4kHz). The axial admittance response reaches an overall peak at f≈4kHz, and thereafter diminishes steadily. While the modelled Y_{ax} response is not completely flat, the magnitude of its ripple is significantly less than for a normal cone.

6.4.1 CHARACTERISING ANGLED SLOT CONE RESONANCE

Although angled cone slots result in cone motion that is often quite complicated, the resonant behaviour of the loudspeaker cone can described by considering the colour contour and vector displacement plots at the frequency of each Y_{ax} resonant feature. The plots for the first two resonant features, denoted **A** and **B** on Figure 6.15, are shown in Figure 6.16.

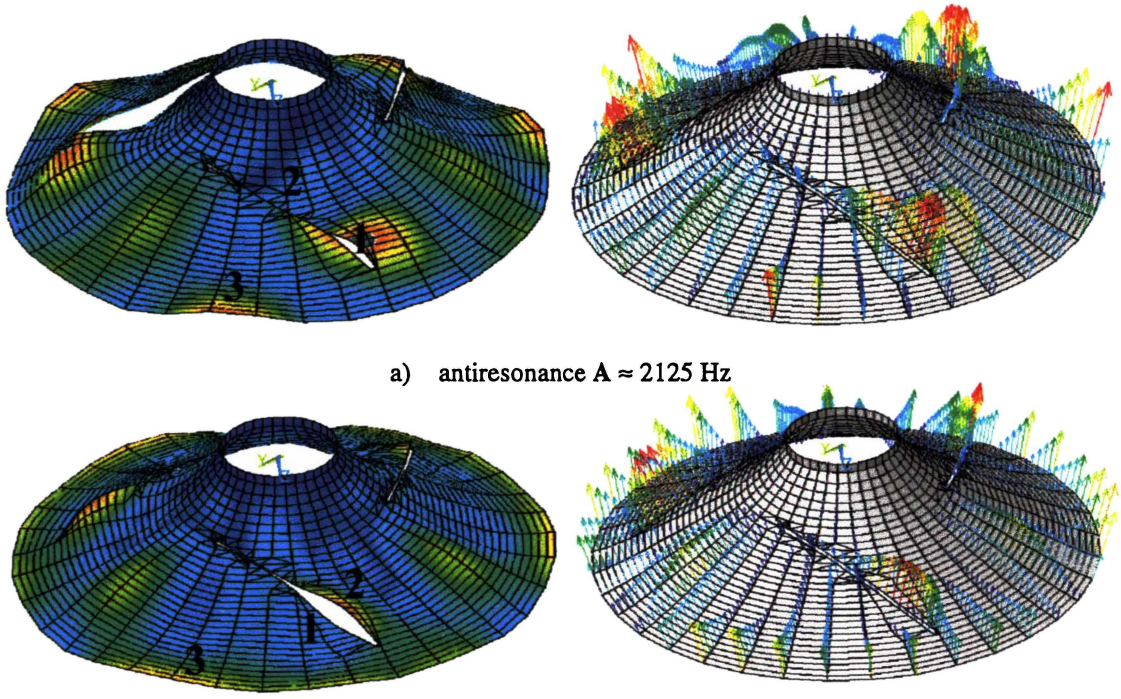

a) antiresonance **A** ≈ 2125 Hz

b) resonance **B** ≈ 2275 Hz

Figure 6.16. Colour contour and vector displacement plots for cone with 3 angled slots at a) antiresonance **A** b) resonance **B**.

A bending motion on the innermost edge of the cone slots creates the first antiresonance. Point **1** (at the inner side of the slots) marks the point of maximum cone displacement, which vibrates 180° out of phase with point **2**. A further antinode, denoted by point **3**, exists at the outer edge of the cone and vibrates in phase with point **1**.

At a slightly higher frequency, bending resonance (**B**) is excited, in which each side of the outermost half of the slot (points **1** & **2**) vibrates in opposite phase. Point **3** on the outer edge of the cone vibrates in phase with point **2**. The frequencies of both these first two modes are strongly related to the length of the slot, moving to lower frequency with increasing slot length. This is discussed in more detail in Section 6.4.2.

At $f \approx$ 2350Hz, antiresonance **C** is excited (refer Figure 6.17).

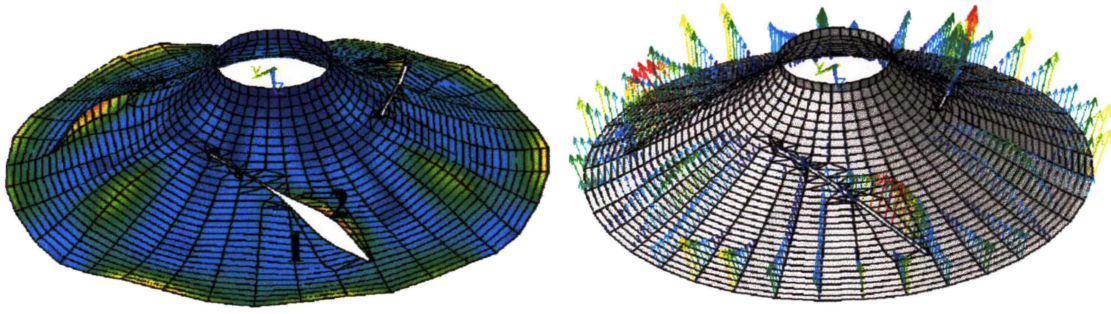

Figure 6.17. Colour contour and vector displacement plots for cone with 3 angled slots at antiresonance **C**.

The mode shape for antiresonance **C** is almost the same as resonance **B**. The outer edge of the cone vibrates with large amplitude, combined with a bending motion on the outer half of the cone slot. As with resonance **B**, points **1** and **2** vibrate out of phase with each other.

At $f \approx$2950Hz, resonance **D** is excited. This frequency approximately corresponds with f_{brl} for a normal cone, a mode with antinodes at the 23rd and 32nd nodal lines (refer Figure 4.14b). Figure 6.18 shows the contour and vector displacement plots for resonance **D**.

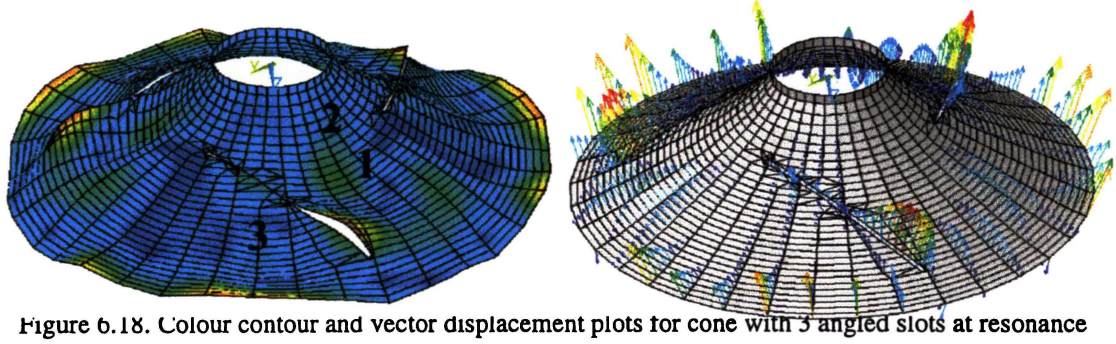

Figure 6.18. Colour contour and vector displacement plots for cone with 3 angled slots at resonance **D**.

While the antinodes of **D**'s mode shape (points 1 and 2) do coincide with nodal lines 23 and 32, the cone motion is far less uniform than at f_{brl} for a normal cone. Points **1** and **2** vibrate out of phase, with point **3** vibrating in phase with point **1**.

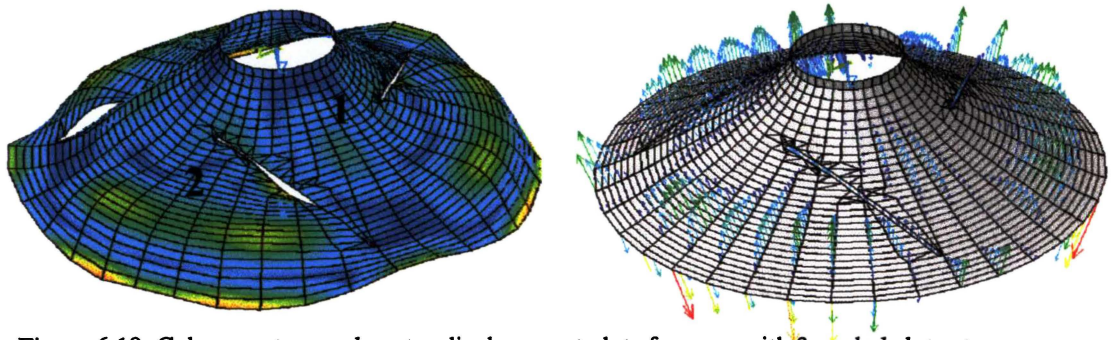

Figure 6.19. Colour contour and vector displacement plots for cone with 3 angled slots at antiresonance **E**.

Antiresonance **E** (Figure 6.19) has a very similar frequency and shape to f_{ba2} for a normal cone, with antinodes at nodal lines 23 and 32. The motion of the cone beyond the middle of the slot (point 2) is very similar to the normal f_{ba2} mode shape, while the cone vibration between the slots (point 1) is less so. Further, the dip in the Y_{ax} response at this frequency is diminished in comparison to a normal cone.

At 4kHz, a significant overall maximum in the Y_{ax} response is reached. This resonance (**F**) is characterised by the formation of a standing wave along the inner edge of the cone slots, with $\lambda \approx 2/3\,\ell$.

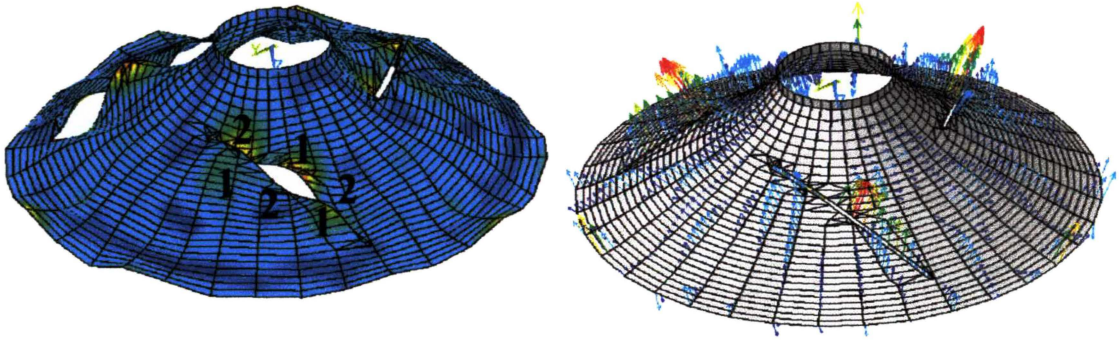

Figure 6.20. Colour contour and vector displacement plots for cone with 3 angled slots at resonance **F**.

At this mode, the inner portion of the cone moves approximately as a rigid body, while the adjacent edges of the cone slots vibrate antiphase. The regions of the cone denoted by **1** in Figure 6.20 vibrate antiphase with regions **2**.

When $f > 4$kHz, Y_{ax} decreases relatively smoothly with increasing frequency, as was the case when radial slots were used (Section 6.3).

The resonant features at points **G** (5575Hz) and **H** (5800Hz) are caused by resonant and antiresonant modes of a similar shape to the third bending resonance of a normal cone.

At $f \approx 7200$Hz, a significant antiresonance (**I**) occurs (refer Figure 6.21)

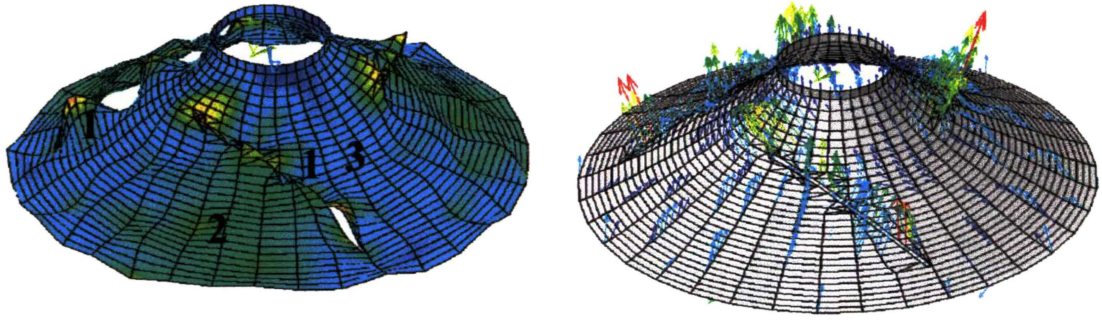

Figure 6.21. Colour contour and vector displacement plots for cone with 3 angled slots at antiresonance **I**.

This mode shape is a complicated combination of twisting and bending motion, coupled with some meridional displacement, as the outer circumference of the cone expands and contracts.

At this frequency, a bending wave (wavelength $\approx \frac{1}{2}\ell$) is formed along the inner edge of the cone slots (denoted by point 1). The region denoted by point **2** undergoes a translation in the meridional direction, coupled with slight transverse bending. The region between the slots, denoted by point **3**, is twisted slightly about the driving axis of the loudspeaker. As the cone is propelled forward, the outer circumference of the cone increases; propelling the cone backwards reduces the cone circumference.

Cone displacement is mostly parallel to the surface of the cone, and with very little transverse component. Thus, a significant minimum in radiated sound pressure is expected at this frequency.

Finally, a resonance (**J**) is excited at $f \approx 8700$Hz (refer Figure 6.22).

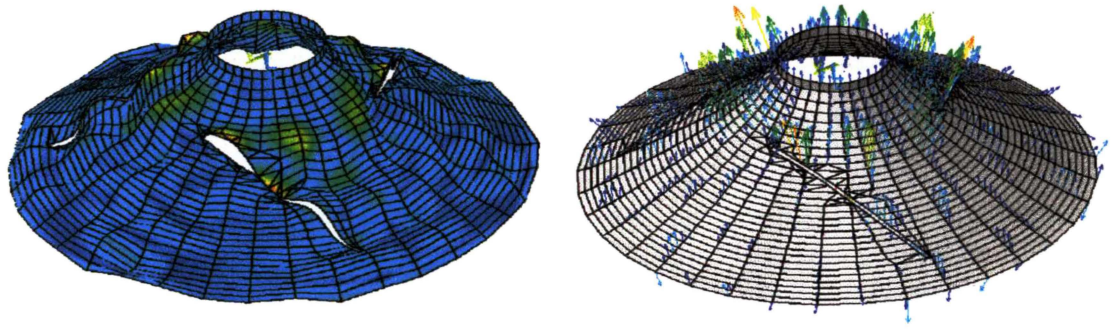

Figure 6.22. Colour contour and vector displacement plots for cone with 3 angled slots at resonance **J**.

This mode is similar in shape to the fifth bending resonance for a normal loudspeaker, and occurs at a similar frequency. The portion of the cone at the inside of the slots vibrates with maximum displacement with a bending wave length $\frac{1}{2}\ell$, while the portion between the slots vibrates with a bending wave motion reminiscent of the mode shape at f_{br5}. The Y_{ax} response diminishes with increasing frequency for $f > 8700$Hz.

6.4.2 SLOT LENGTH

With the cone slot set at an angle of 45° to the meridional lines, and the position of the inside end of the slot fixed, the length of the slot was varied between 22-55 mm, as shown in Figure 6.23.

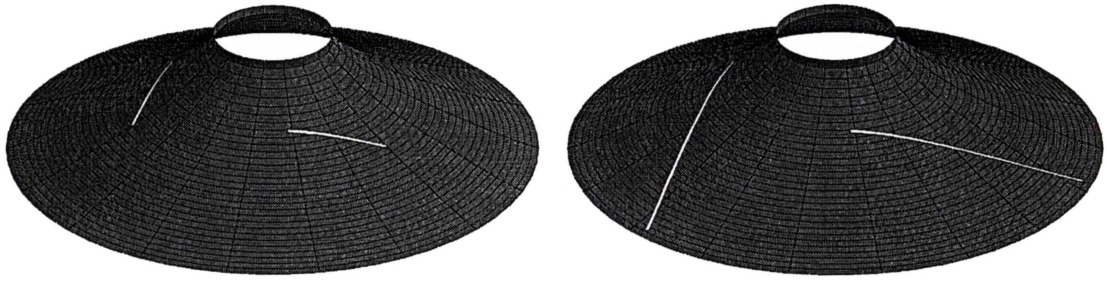

Figure 6.23. Angled slot cone model for a) ℓ =22mm, b) ℓ = 55mm

The outer end of the 22mm slot lies at the 15th nodal line, corresponding to the innermost antinode of the third bending resonance and antiresonance of a normal cone. The outer end of the 55mm slot lies at the 31st nodal line.

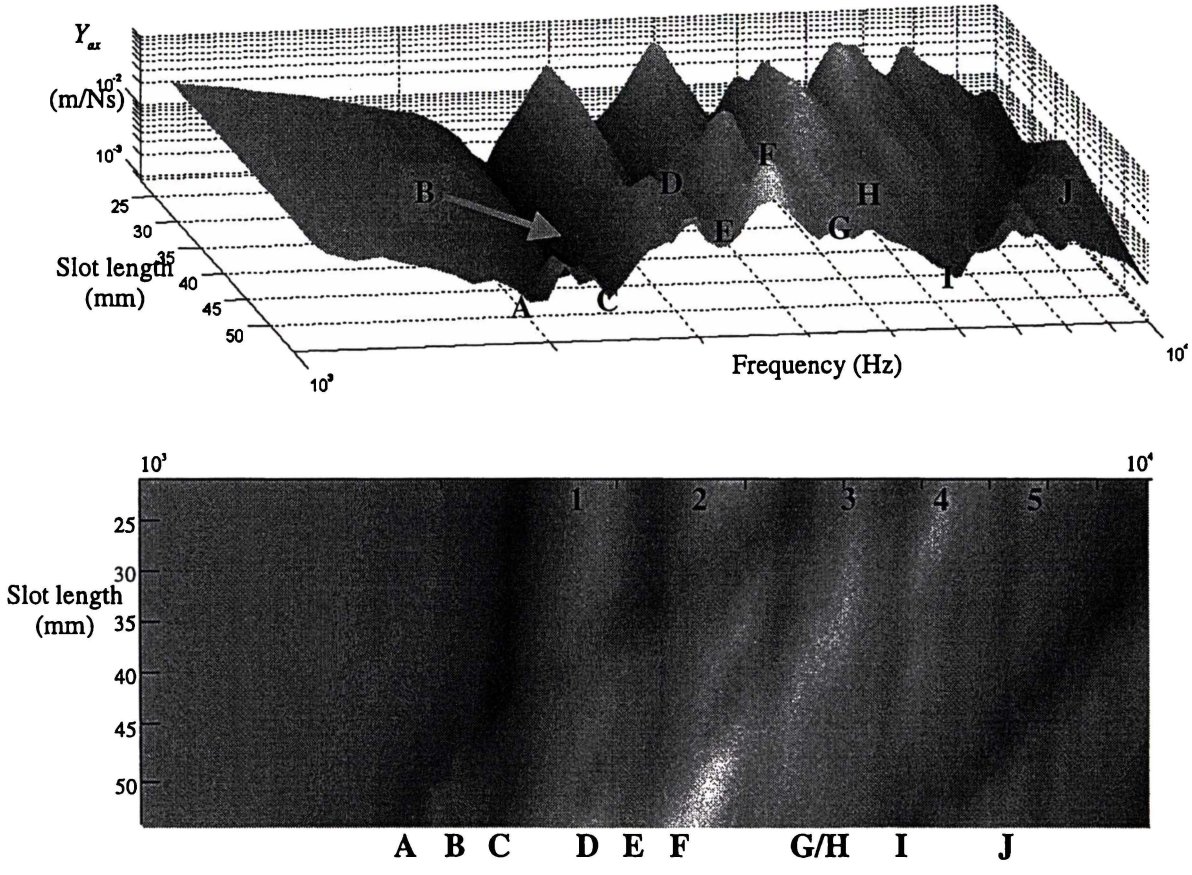

Figure 6.24. Modelled Y_{ax} response as slot length is varied from 22mm → 55mm. Slot angle is fixed at θ = 45°

In Figure 6.24, the normal resonant modes are denoted by numbers **1-5**, as previously.

The resonant characteristics caused by angled cone slots are also denoted by letters **A** to **J**, as in Figure 6.15.

As the length of the slot is increased all the natural bending resonances and antiresonances (**1-5**) are very slightly lowered in frequency, as was the case for radial slots (refer Figure 6.9, Figure 6.11).

As resonant modes **A**, **B**, **D**, **F**, **I** and **J** are associated with bending standing waves down the inner edge of the cone slots, their frequencies decrease with increasing slot length.

While normal bending modes 1-5 are not entirely removed by the cone slots, they are greatly obscured when the slot is sufficiently long. The cone slots have little effect on the Y_{ax} response until the driving frequency is such that the innermost antinode of the cone mode shape lies in the area in which the cone is slotted. Thus, modes 1 and 2 are not affected when the cone length is 22mm, as the inner most antinode for modes 1 and 2 lies closer to the outside edge of the cone than the slot.

6.4.3 SLOT ANGLE

In this section, the influence of the angle of the slots is explored. In order to derive these results, the cone slot length was held constant (44mm) and its angle with the meridional line (θ) varied from 0° to 90° in steps of 7.5°. The slot angle θ=0° corresponds to radial slots.

In all FE models considered in this section, a node that was adjacent to the centre of the cone slots was chosen as the node from which the Y_{ax} response was calculated. In practice, the innermost ring vibrates almost as a rigid body, with very little difference in displacement between any of the innermost nodes. Figure 6.25 shows the Y_{ax} response of a cone with three angled slots, as the slot angle is varied from $0° \leq \theta \leq 90°$.

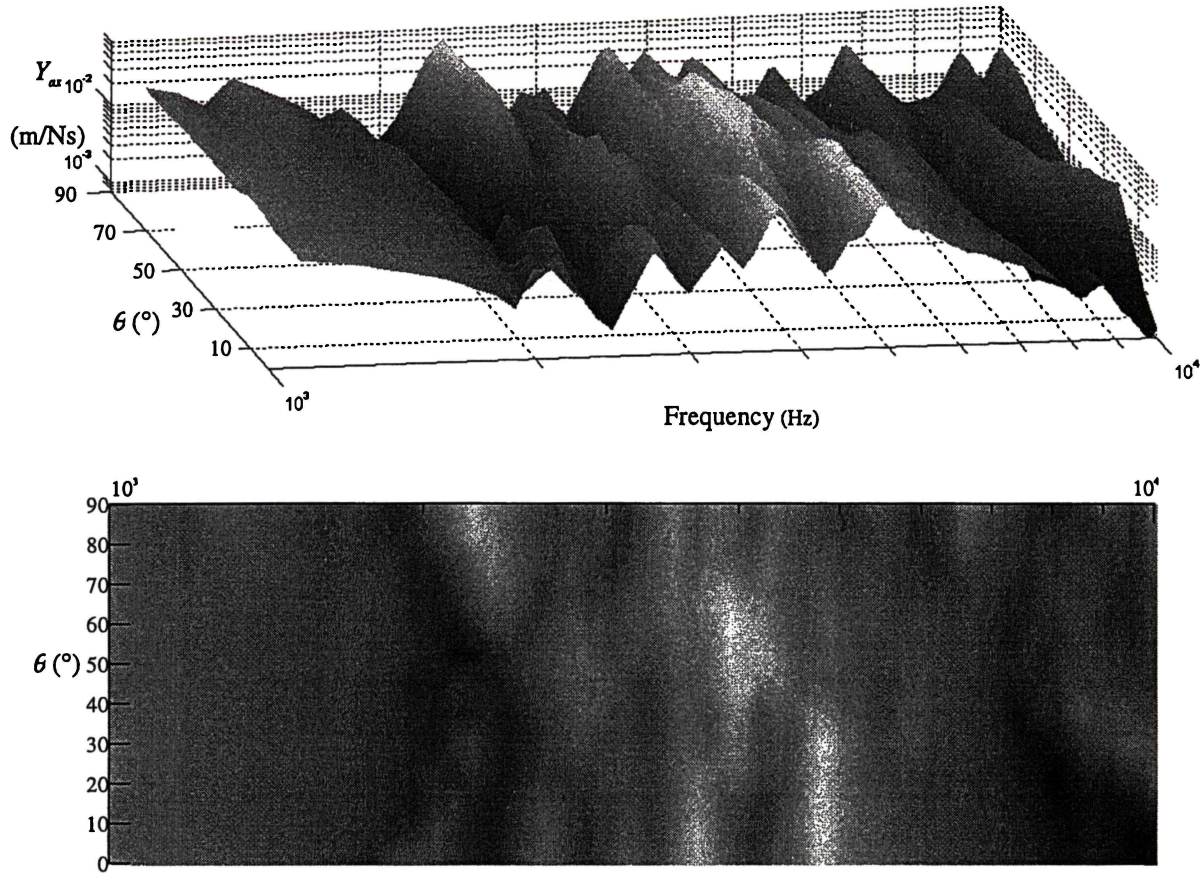

Figure 6.25. Modelled Y_{ax} response as slot angle θ is varied from 0°→ 90°. Slot length is fixed at ℓ = 44mm.

It is difficult to identify a clear relationship between the angle of the cone slots and the Y_{ax} characteristic of the cone, as changing the slot angle has a large effect on the types of standing waves formed. However, the following general observations can be made:

The extreme case of $\theta = 0°$ corresponds to a radial cone slot design, in this case with only three slots. The Y_{ax} characteristic for $\theta = 0°$ exhibits a smooth roll-off at high frequency ($f \geq 5$kHz), as was the case for a radially slotted cone. However, because there are only three radial slots, the natural bending modes of a normal cone are not completely removed from the Y_{ax} response. Consequently, the Y_{ax} response for $f \leq 5$kHz contains a higher number, but less pronounced resonances than when 9-18 radial slots are used. The resonant features on the Y_{ax} response are due to a combination of the natural bending modes of a normal cone, and bending waves that are excited down the edges of the cone slots.

At the other extreme of $\theta = 90°$, the cone slots are perpendicular to the meridional lines of the cone, and the Y_{ax} response contains many peaks and dips. In contrast to other slot designs, the mean value of Y_{ax} stays relatively constant over the frequency range 1-10kHz.

When $\theta = 45 \pm 7.5°$, the least amount of ripple is exhibited in the Y_{ax} response, as shown in Figure 6.26.

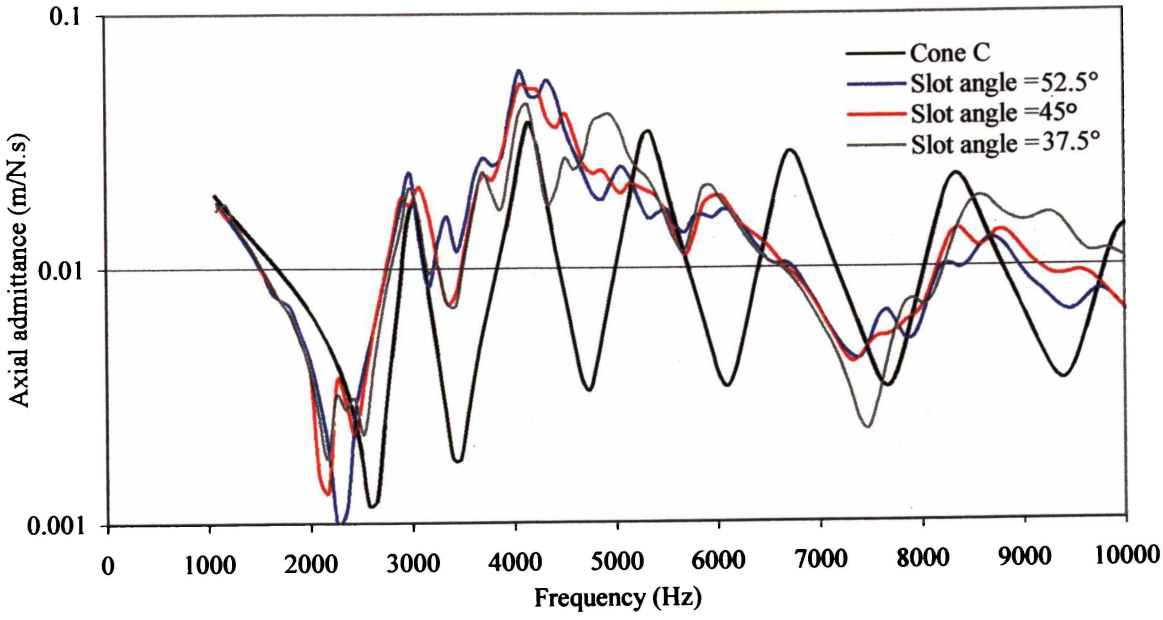

Figure 6.26. Y_{ax} responses for θ =37.5°, 45°, 52.5°

While there are a higher number of resonant features in the Y_{ax} response when angled slots are cut in the cone, the magnitude of Y_{ax} ripple is far less than for a normal cone. Generally, antiresonances are less pronounced than for a normal cone, and the Y_{ax} response decreases smoothly above 4kHz. This implies that the sound pressure response of a cone with angled slots will be smoother than a normal cone, and will decrease rapidly above 4kHz.

6.4.4 NUMBER OF SLOTS:

The effect of the number of angled slots on the shape of the Y_{ax} response is shown in Figure 6.27. The Y_{ax} response is shown for 3, 4, 5, and 6 slots.

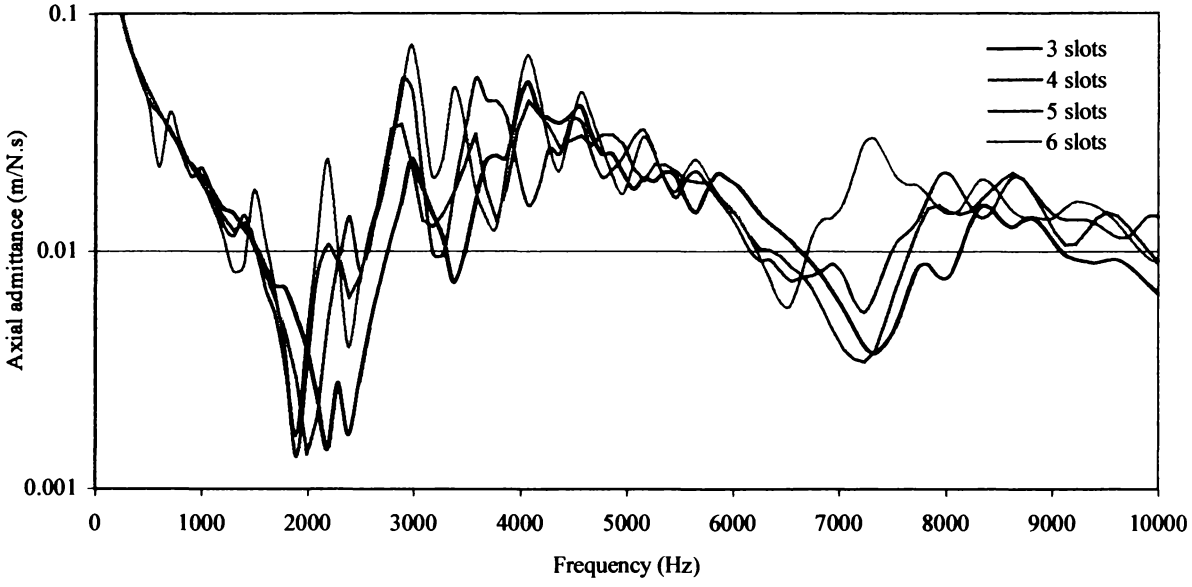

Figure 6.27. Y_{ax} response for cone with angled slots ($\theta = 45°$, $\ell = 47$mm) as the number of slots is varied from 3-6.

The main effect of increasing the number of angled slots is to decrease the frequency of resonant features **A/B**, and **I/J**. Furthermore, the amount of ripple in the Y_{ax} response increases when a higher number of slots is used.

Additionally, using a large number of radial slots can have the effect of encouraging torsional motion, where the portions of the loudspeaker cone turn about the driving axis, and the cone leaves set up a twisting motion.

6.4.5 SUMMARY

The effect of angled cone slots on the resonant behaviour of a normal loudspeaker cone can be summarised as follows:

- The natural bending resonances of a normal loudspeaker cone are almost entirely obscured by a new set of resonant modes. The new modes are bending standing waves, which form along the inside edge of the cone slots and introduce new resonant features to the Y_{ax} response. These frequencies increase with decreasing slot length.

- The n^{th} bending mode of a normal loudspeaker cone is removed when the cone slot's inner end lies closer to the centre of the cone than then innermost antinode for mode n.

- The Y_{ax} response reaches an overall maximum at resonant frequency **F**, the frequency of which increases with the length of the outer annulus of the cone. This mode shape is characterised by a bending standing wave down the inner edge of the cone slots.

- Increasing the number of slots lowers the frequency of modes **A/B** and **I/J** as well as slightly increasing the magnitude of ripple in the Y_{ax} response.

Thus, the response of a cone with angled slots is a compromise between the response of a normal cone, and that of a cone with radial slots. The radially slotted cone exhibits an overall decrease in Y_{ax} for frequencies above 4kHz, a characteristic shared with the angled-slot cone design. However, the peaks and dips in the Y_{ax} response created by radial slots for frequencies below 4kHz are less pronounced in the angled slot design.

Overall, the Y_{ax} response of a loudspeaker cone with angled slots is smoother than a normal cone, and exhibits a comparatively steady, smooth decrease in Y_{ax} for frequencies above 4kHz.

6.5 RINGS OF ANGLED SLOTS

This section examines the effect of cone slots when the cone slot length is kept very small, and the number of slots is greatly increased. Specifically, 32 slots of length 8mm were cut into the cone at an angle of 45° to the meridional lines. The cone slots were configured in a concentric ring as shown in Figure 6.28.

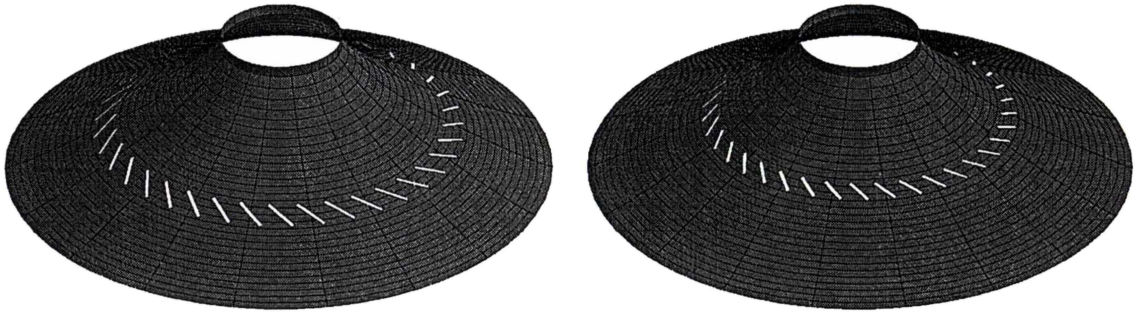

Figure 6.28. Cone designs with a ring of small angled slots. a) Slots lie at nodal lines 17-20 b) Slots lie at nodal lines 13-16.

The designs of Figure 6.28 have the cone slots deliberately placed at the position of the innermost antinode of the second and third bending antiresonances respectively. The length and angle of the slots is such that the slots run from node 13 to node 16. The effect of this type of cone slot configuration on the Y_{ax} response of a normal cone is illustrated in Figure 6.29.

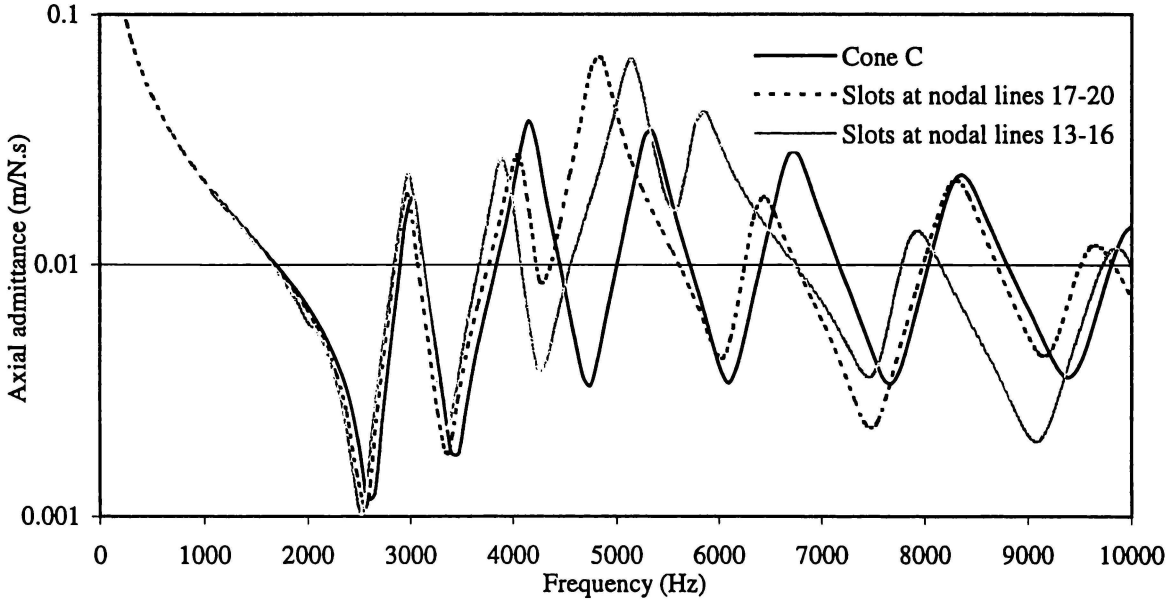

Figure 6.29. Y_{ax} response for the cone designs of Figure 6.28.

Placing the cone slots at nodal lines 17-20 has the effect of lowering the frequencies of the second bending antiresonance and the third bending resonance. Furthermore, the third bending resonance is accentuated in comparison to the other bending resonances of the cone. Similarly, cutting slots at nodal lines 13-16 has the greatest effect on the third bending antiresonance and fourth bending resonance as their frequencies are

lowered considerably, and their magnitudes increased. However, the third bending resonance is also lowered in frequency and increased in magnitude, since its innermost antinode lies close to the position of the cone slots.

In summary, cutting a ring of slots at a natural mode's innermost antinode has the effect of slightly lowering that mode, and accentuating its magnitude with respect to the other resonances of the cone.

6.6 SLOTTED CONE IMPLEMENTATION

When $\theta = 45°$ and $\ell = 47$mm, the Y_{ax} response of a cone with three angled slots exhibits considerably diminished ripple in comparison to a normal cone's response (Figure 6.15). Moreover, Y_{ax} decreases relatively smoothly above 4kHz, implying a desirably smooth roll-off in sound pressure at high frequency.

The Y_{ax} responses of Figure 6.15 were post-processed (assuming a voice coil mass of 10g) to yield the Z_{mot} response of a cone with and without three radial slots, and are plotted in Figure 6.30. The resonant features in the slotted cone response are identified after the notation of Figure 6.15.

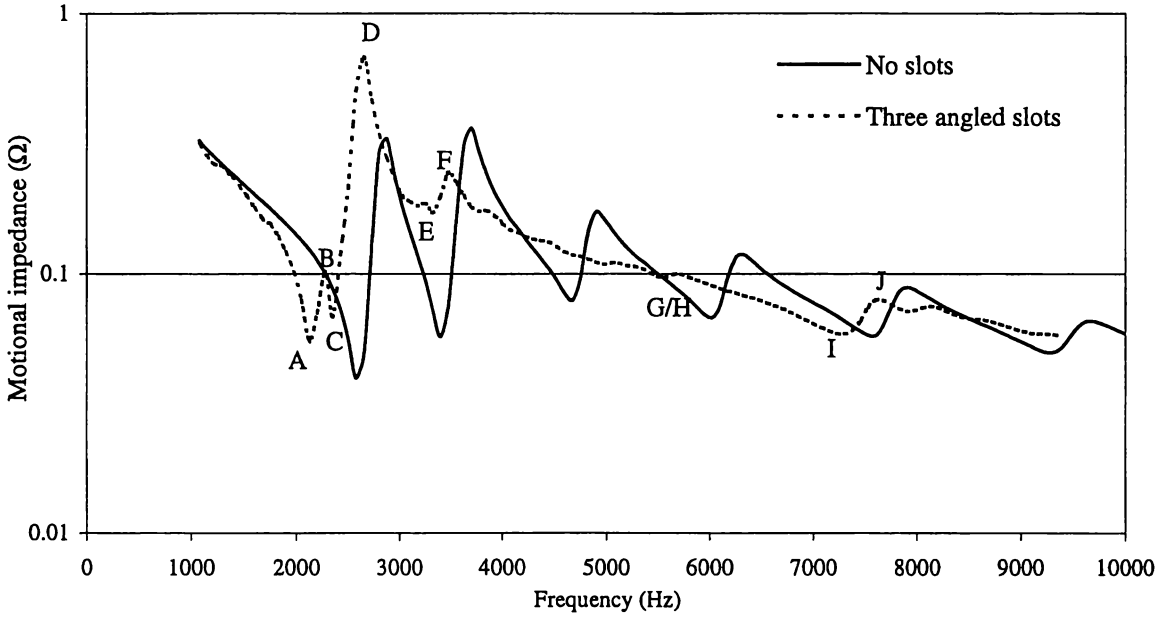

Figure 6.30. Modelled Z_{mot} responses of a loudspeaker cone with and without three angled slots ($\theta = 45°$, $\ell = 47$mm)

Figure 6.30 indicates that above $f \approx 3$kHz, the Z_{mot} response of a cone with three radial slots is considerably smoother than that of a normal loudspeaker cone. The peak at 2.5kHz (resonance **D**) is of greater magnitude than that caused by the first bending resonance of the normal cone. Above resonance **D**, the peaks and dips caused by bending resonances and antiresonances **2-4** are absent from the modelled Z_{mot} response of the slotted cone.

The resonant features at 7.5kHz (**I/J**) cause a similar magnitude of ripple as the fifth bending resonance that normally occurs at this frequency.

6.6.1 INITIAL MEASUREMENTS

A loudspeaker cone (cone D) was fabricated with three slots of $\theta = 45°$ and $\ell = 47$mm. Cone D's measured Z_{mot} response is shown in Figure 6.31 with its modelled Z_{mot} response[7].

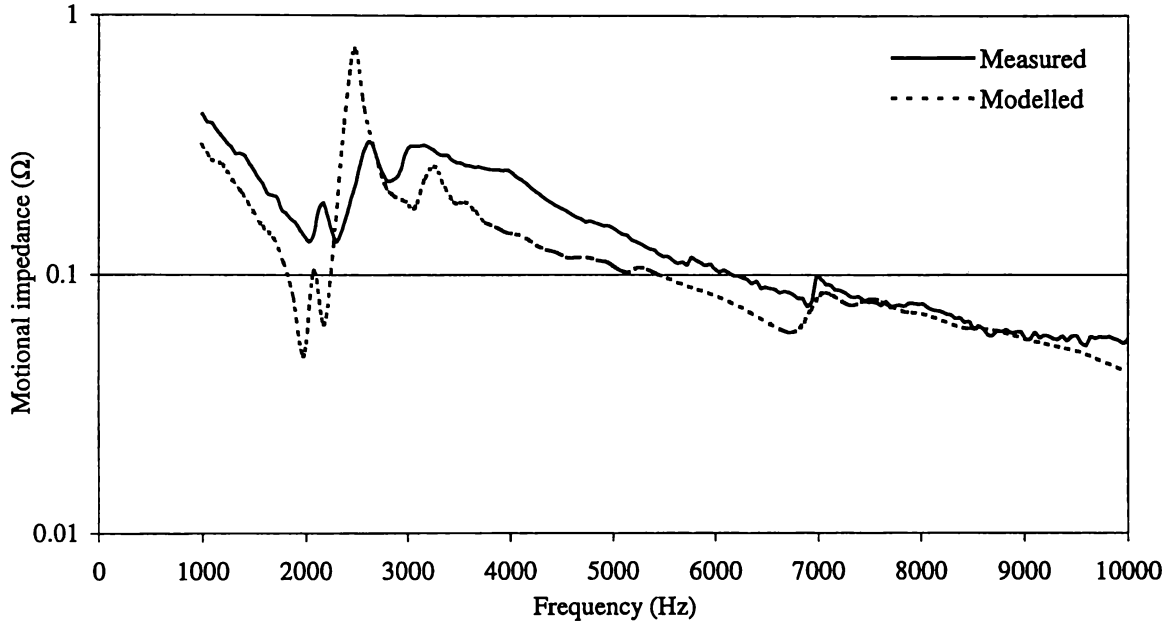

Figure 6.31. Measured and modelled Z_{mot} responses of cone D.

Figure 6.31 shows that similar resonant features appear in the modelled and measured Z_{mot} responses for cone D at similar frequencies. The same trends are also seen in both Z_{mot} responses, with a small discrepancy at $f \approx 2.5$kHz, where the measured curve does not rise to the magnitude predicted by the modelled curve. This discrepancy may be caused in part by inadequacies in the frequency dependent damping model used by ANSYS.

Above this frequency, the measured Z_{mot} response exhibits the expected steady decrease predicted by the modelled Z_{mot} response.

Figure 6.32 (over) compares the measured Z_{mot} response of cone D with that of cone C, a normal, unslotted cone. The ripples that are evident in the measured Z_{mot} response of cone C for frequencies greater than 3kHz are absent from the measured response of cone D, while the first two resonant features of cone C's response are replaced with a broader, smoother resonance. Furthermore, cone D's mean Z_{mot} response decreases at a higher rate than cone C's, for frequencies above 3kHz.

---

[7] Material properties for the FE model of cone D were identical to those used for cone C (Table 4.2) with the exception of the Young's modulus, which was slightly reduced to 6.2×10^9 N/m^2. This resulted in a better match between the measured and modelled Z_{mot} response near 7.5kHz, and can be attributed to the natural variation in material properties and cone thickness that often occurs between cones.

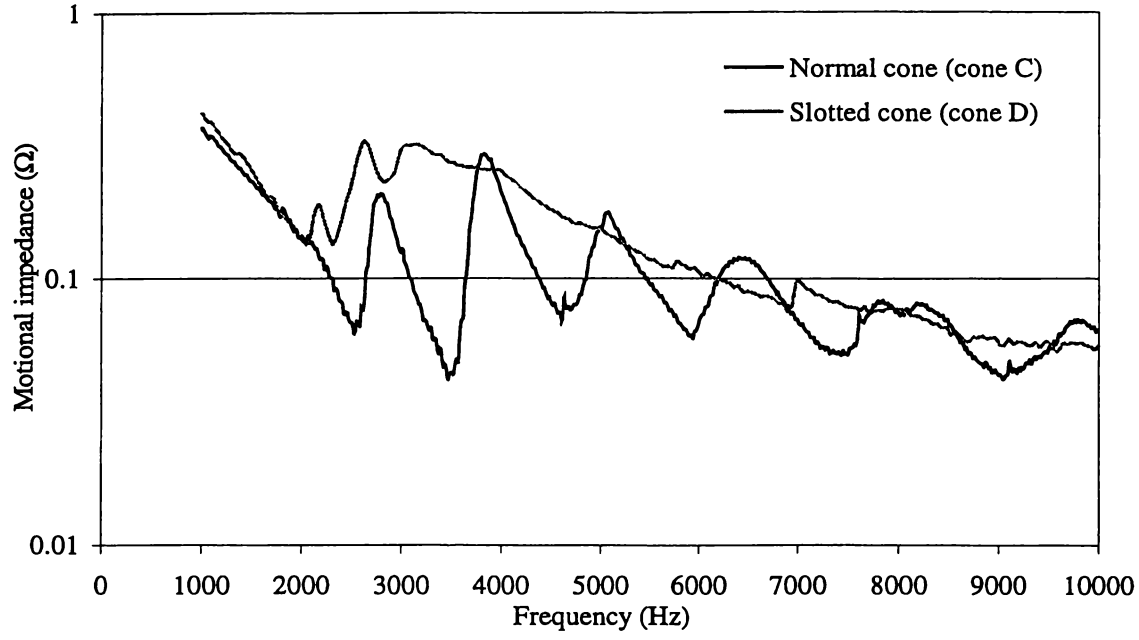

Figure 6.32. Measured motional impedance (Z_{mot}) responses of normal (cone C) and slotted (cone D) loudspeaker cones.

In general, the shape and smoothness of the on-axis sound pressure response (p_{ax}) of a loudspeaker shows a strong correlation with its motional impedance response. Thus, the radiated sound pressure response of cone D should be expected to compare favourably with that of cone C. This expectation is confirmed in Figure 6.33, where the measured sound pressure responses of cones C and D are compared.

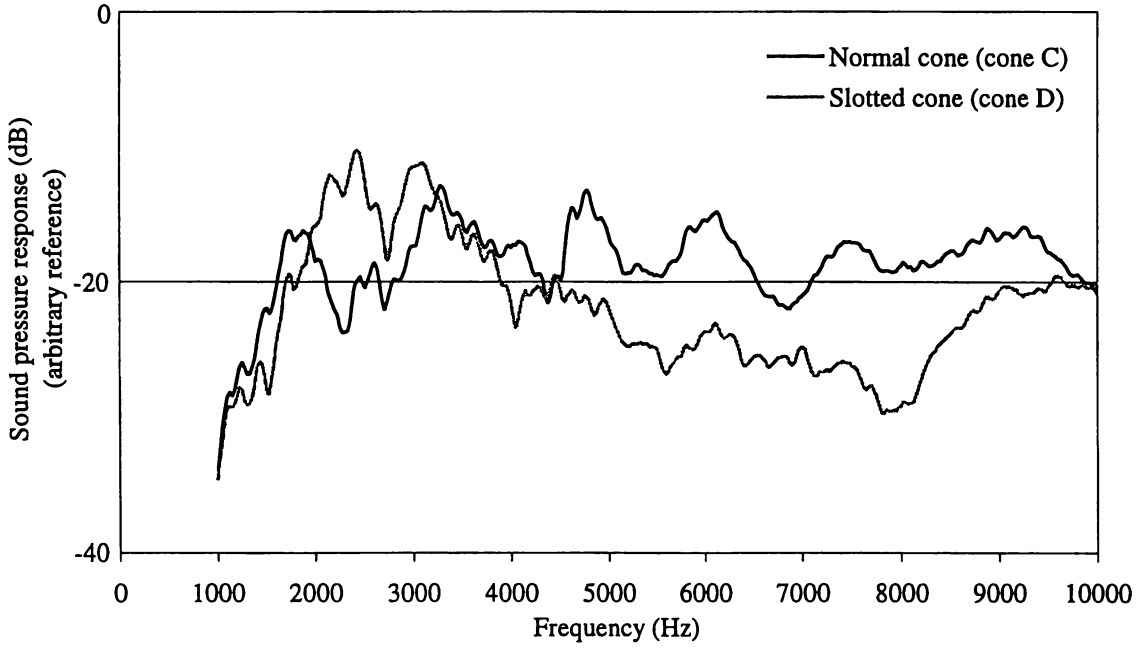

Figure 6.33. Measured on-axis sound pressure (p_{ax}) responses of normal (cone C) and slotted (cone D) loudspeaker cones.

Figure 6.33 verifies that the measured sound pressure responses of cones C and D

follow the same trends as their measured Z_{mot} responses in Figure 6.32. The variations in cone C's sound pressure for frequencies greater than 3kHz are absent from the measured response of cone D. Instead, cone D's response is characterised by a smooth, steady decrease in sound pressure for frequencies in the range 3-8kHz. At 8kHz, the sound pressure response of cone D begins to increase again, but does not reach the magnitude of cone C's response. An increase in the magnitude in sound pressure in the frequency range 2-3kHz is also evident in cone D's measured response.

Figures 6.32 and 6.33 both indicate that cutting three slots of $\theta = 45°$ and $\ell = 47$mm creates a loudspeaker cone with "mechanically filtered" characteristics. This slot design is particularly effective at disrupting the formation of the normal axisymmetric standing waves associated with cone break-up, and thereby minimising their adverse effect on the smoothness of the sound pressure reponse. In contrast to normal axisymmetric modes, the additional modes created by the introduction of these slots do not dominate the sound pressure response.

The decrease in p_{ax} with frequency for $f >$ 3kHz can also be advantageous, particularly if the loudspeaker is to be used in a configuration where it is to be "crossed-over" to a high frequency radiator at ~3-4kHz, as is often the case for a driver of this diameter.

6.6.2 SEALING OVER THE SLOTS

Cutting slots in the loudspeaker potentially allows a small amount of air to pass between the front and rear of the cone through the slots, particularly at low frequencies when the cone excursion is large. When the loudspeaker is mounted in a vented or sealed cabinet, the air leakage path offered by the cone slots is quite undesirable, as it alters the low-frequency effect of the cabinet, and potentially allows the air to "whistle" or "chuff" as it passes through the slots.

This difficulty can be simply alleviated by sealing over the cone slots with a light, compliant, yet non-porous material in order to provide an air seal. Ideally, the material used should not disrupt the resonant behaviour of the slotted cone.

To illustrate the potential of this technique, some lightweight[8] plastic stickers of length 50mm and width 5mm were placed over the slots of cone D, overlapping each side and end of the slots by a few millimetres and providing an air-tight seal. The effect of these stickers on the Z_{mot} response of the cone is shown in Figure 6.34

[8] The exact properties of the sticker material are not known.

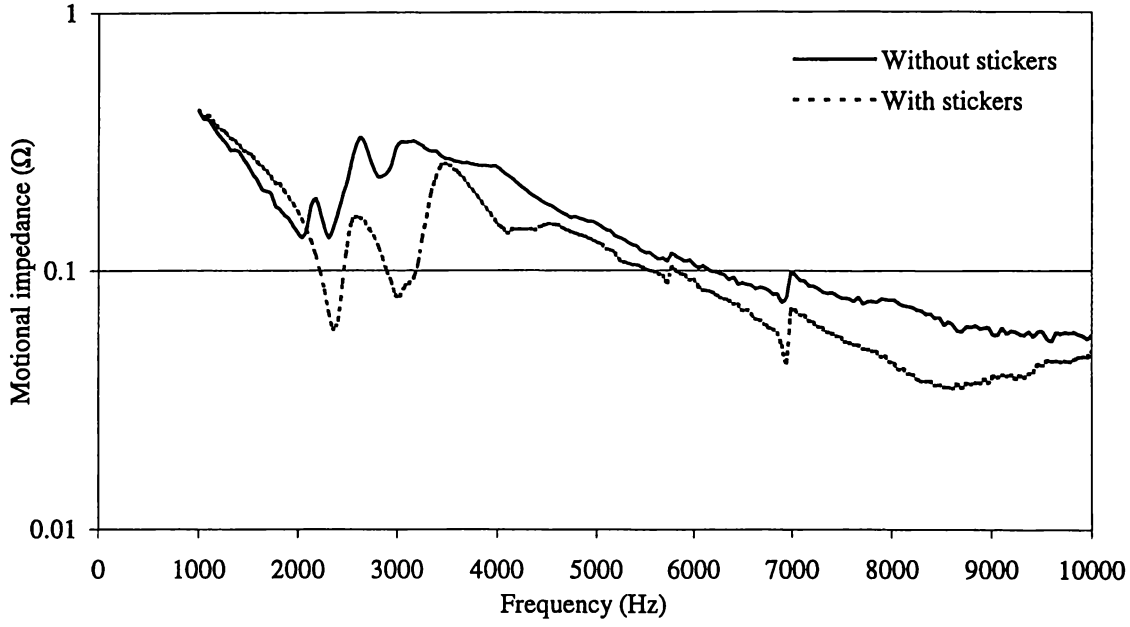

Figure 6.34. Z_{mot} response of cone D with and without plastic stickers sealing over the cone slots.

Figure 6.34 demonstrates that when the plastic stickers were placed over the slots, the first two bending modes shapes were excited as in a normal cone. However, for frequencies above 4kHz the response is similar to when no stickers are used.

The effect of the stickers on the measured p_{ax} response of a loudspeaker is shown in Figure 6.35 where the measured response of cones C (normal) and D (slotted, with and without stickers over the slots) are plotted.

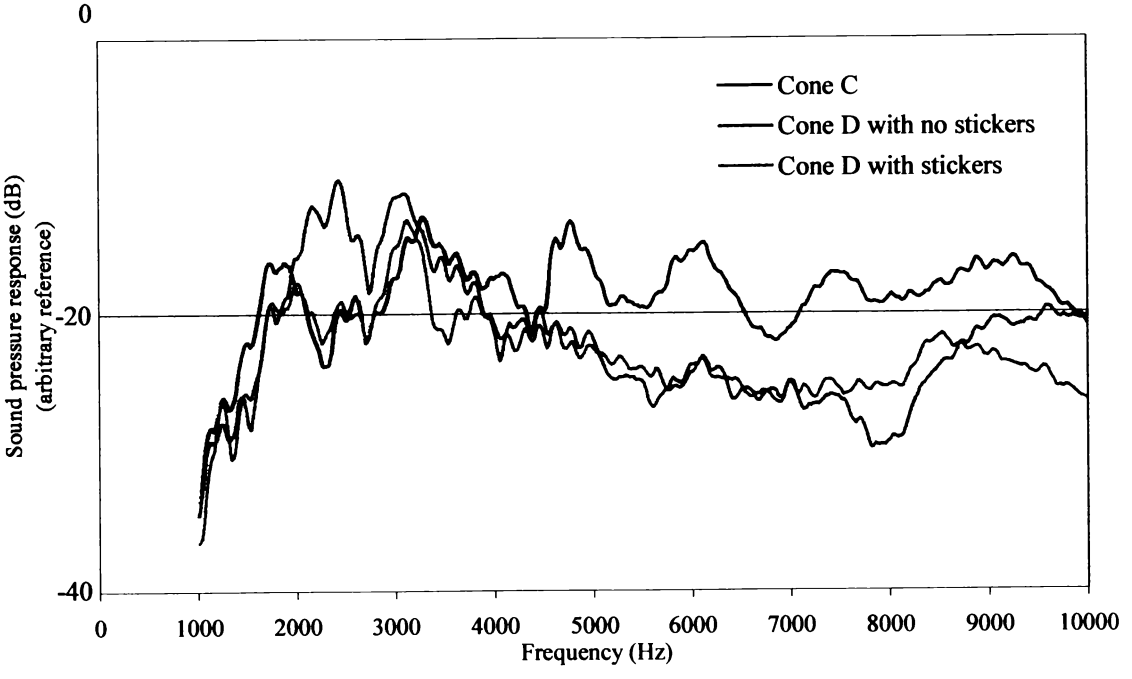

Figure 6.35. Measured on-axis sound pressure response (p_{ax}) for loudspeaker cones C and D.

Figure 6.35 indicates that the stickers do have a slight effect on the sound pressure

response of the cone. Sealing over the cone slots with these stickers re-introduces the first two sound pressure peaks of cone C in the frequency range 2-3kHz, while for frequencies above 3kHz the sound pressure response is similar to cone D when no stickers are used. Overall, the measured sound pressure response of cone D with stickers attached is still a significant improvement over that of cone C.

The effect of the material properties of the cone stickers on the behaviour of the "sealed-over" slotted cone has not been investigated, and is a potential area of further research. In particular, the FE model could be extended to include the effect of the slot stickers, and the dependence of the overall response of the slotted cone on the properties of the sticker investigated. A sticker of a material more compliant (yet still non-porous) than the plastic used in this case could potentially still provide the necessary air seal, without affecting the slotted-cone Z_{mot} response.

6.7 CONCLUSION

This chapter has illustrated that cutting slots in a loudspeaker cone has a profound effect on the Y_{ax} response, and consequently the Z_{mot} and p_{ax} responses of the loudspeaker.

It has been shown that the natural resonances of a normal cone, as characterised in Chapter 4, can be partially or completely obscured by a new class of resonant modes. These new resonant modes are identified by bending motions up the edges of the cone slots, and, in the case of angled slots, a small amount of axial twisting of the outer parts of the cone. The frequencies of these "new" modes are highly dependent on the length of the cone slots.

Any natural modes of a normal cone are removed or perturbed by cone slots when the slots fall in an area of the cone that corresponds to the innermost antinode of the natural mode.

Radial slots have the effect of greatly smoothing the Y_{ax} response of the cone for frequencies above 4kHz, but creating more peaks and dips below 4kHz. By using three angled slots, the natural resonances of the cone are obscured and partially replaced by new bending/twisting modes. This has the measurable effect of significantly smoothing the Y_{ax} and p_{ax} responses of the cone, and diminishing the output of the cone above 4kHz.

Finally, a technique for sealing over the cone slots with a sticker material has been proposed and briefly investigated. Placing stickers over the cone slots has a measurable effect on the resonant characteristics of the slotted cone below 3kHz, but preserves the slotted cone's characteristics above 3kHz, and allows the slotted cone loudspeaker to be used in a practical loudspeaker system.

This chapter has not considered the effect of cone slots on the distortion characteristics of the loudspeaker cone, nor has the off-axis response of the loudspeaker been considered. Both of these areas are worthy of further research and consideration, but are beyond the scope of this thesis.

CHAPTER 7

CONCLUSION

7.1 THESIS REVIEW AND DISCUSSION

Chapter 1 gave an overview of the history of electrodynamic loudspeaker cone modelling and stated the aims of this thesis:

1. To extensively examine and summarise the resonant behaviour of a mineral-doped polypropylene loudspeaker by using 2D and 3D FE models of the cone and surround.
2. To use 2D FE models to explore the dependence of the frequency and magnitude of natural cone resonant modes on the cone's material properties and thickness parameters.
3. To employ 3D FE models to examine the resonant behaviour of a 6½ inch polypropylene loudspeaker cone with narrow slots cut through its surface.

These goals were pursued and achieved as follows:

The electrodynamic loudspeaker theory outlined in chapter 2, and the mathematical and experimental methods described in Chapter 3, were used in Chapter 4 to develop and calibrate finite element and boundary element models of a loudspeaker cone. The calibrated two- and three-dimensional models were then utilised to produce a detailed description of the resonant characteristics of a axisymmetric 6½-inch polypropylene loudspeaker cone (cone C) in terms of its axial admittance, sound pressure response and resonant mode shapes.

These results showed that the cone standing waves that affect the smoothness of a loudspeaker's sound pressure response are primarily of a bending-wave type; that is,

cone displacement is mostly normal to the surface of the cone. The bending motion of the cone continues with increasing frequency until the first longitudinal antiresonance of the cone is excited. The onset of the first longitudinal antiresonance results in a large decrease in radiated sound pressure, as cone vibration becomes primarily longitudinal in nature, with very little bending motion.

Chapter 4 also showed that the surround has a major influence on the amplitude and frequency of cone standing waves. The "external half roll" surround employed by the speakers considered in this thesis has a two-fold effect on the resonances of the cone. Firstly, the ring antiresonance and first bending resonant frequency are significantly lowered by the additional inertia supplied by the mass of the surround where it attaches to the outer edge of the cone. Secondly, some of the wave energy in the cone is transmitted into and absorbed by the half roll of the surround, significantly reducing the amplitude of cone standing waves. Thus, the surround plays an important role in determining the frequencies and amplitudes of standing waves in the cone itself.

This thesis has not attempted to explore the relative virtues of different surround designs, and since little modelling seems to have been performed in this area, surround design is potentially an aspect for further research.

Chapter 5 explored the individual effects of varying the cone material parameters and cone thickness on the frequency, shape, and magnitude of cone standing waves. The effect of these parameters on the smoothness of the sound pressure response was also considered. These results illustrated how the natural modes of loudspeaker cones may be shifted to higher or lower frequency by adjusting the cone material properties, or cone thickness profile. The amplitudes of cone standing waves and their relative dominance of the axial admittance and sound pressure responses were also shown to be dependent on cone material properties and thickness profile.

It was shown that using materials that have a higher Young's modulus and/or lower mass density increases the frequencies of cone standing waves, and increases the bandwidth of the loudspeaker. However, choosing a lighter, stiffer material only delays the onset of cone break-up and actually increases the magnitude of ripple in the sound pressure response once break-up begins to occur.

The value of Poisson's ratio for the cone material has a strong influence on the frequency of the longitudinal antiresonance, but not on the frequency or amplitude of bending waves. Consequently, increasing the value of Poisson's ratio results in a cone with a higher bandwidth, and has very little effect on the smoothness of the sound pressure response.

The damping properties of the cone material have a very strong influence on the magnitude of cone standing waves, and thus on the smoothness of the loudspeaker's sound pressure response. A cone material of high damping ratio exhibits very little variation in its on-axis sound pressure response.

A thinner loudspeaker cone has a greater number of ripples in its sound pressure response, but each ripple is of a lower magnitude than for a thicker cone of the same shape and material. Furthermore, reducing the thickness of the cone towards its outside edge increases the number and reduces the magnitude of ripples in the sound pressure response and moves the first longitudinal antiresonance to higher frequency, thereby increasing the bandwidth of the cone.

If the outer-edge thickness of the cone were to be significantly reduced, the effect of the surround on cone resonance would be likely to be greater than for a normal constant thickness cone. Thus, to preserve a good mechanical impedance match between cone and surround, the thickness or mass density of the surround rim would need to be similarly reduced. This is an area that requires more extensive research.

The frequency and magnitude of individual cone resonances can be altered by increasing or reducing the thickness of the cone at the innermost antinode of a mode shape, as detailed in Section 5.3.3. While this technique is interesting, and certainly allows resonant modes to be altered in frequency and magnitude, the loudspeaker designer would normally be more interested in removing the effect of standing waves altogether, rather than just slightly adjusting their frequency and magnitude.

In Chapter 6, a calibrated 3D FE model was used to explore the effects of thin cone slots on the mode shapes and axial admittance characteristics of the loudspeaker cone. The cone slots were demonstrated to have a profound effect on the characteristics on the modelled cone, and variations in slot design were explored. In particular, the effect of slot angle, length and number of slots was considered.

It was shown that cutting slots in the loudspeaker cone introduces a new series of standing wave shapes, and disrupts the formation of the axisymmetric modes that dominate the sound pressure response of a normal cone. The FE model of a loudspeaker cone with three angled slots predicts the smoothest Y_{ax} response.

Consequently, a loudspeaker cone with three slots of $\theta = 45°$ and $\ell = 47\text{mm}$ was constructed, and its measured characteristics were shown to compare favourably with those predicted by the FE model. Many of the break-up resonances that dominated the response of a normal loudspeaker cone were very significantly removed by this particular slot design, and the slotted loudspeaker was demonstrated to possess a desirably smooth "roll-off" in response at high frequency.

The effect of the surround on the angled-slot cone design was not considered, but as predicted by Section 4.5.5, the surround would be likely to particularly affect the lower frequency mode shapes, and further decrease the amplitude of the cone's standing waves.

The potential of a method for sealing over the cone slots with plastic stickers was also demonstrated in Section 6.6. The stickers were shown to have an effect on the slotted cone's behaviour at low frequency, but little effect at high frequency.

7.2 FURTHER WORK

Chapter 4 has highlighted the need for more extensive research into the relative merits of various surround designs. This could be relatively easily performed using the 2D FE models used in this thesis. Although loudspeaker designers undoubtedly possess a great deal of empirical knowledge and experience in this area, there appears to be little published research on the subject.

While the measured and modelled axial admittance responses, and measured sound pressure response of the angled-slot cone are a great deal smoother than for a normal cone, there is a need for more experimental research into the effects of the cone slots on other characteristics of loudspeaker cones. In particular, the effects of cone slots on the distortion and cumulative spectral decay characteristics of the cone have not been considered. These parameters could be measured relatively easily but are more difficult to determine from FE and BE model results.

Furthermore, the off-axis sound pressure response of the cone is likely to be affected by the cone slots. Careful anechoic chamber measurements may be able to determine whether there are any variations in off-axis response caused by the non-axisymmetric wave types of a slotted cone. Ideally, a 3D BE model of slotted loudspeaker cone could be created, and the off-axis sound pressure response directly calculated.

The effect of the material properties of the stickers on the sound pressure response, particularly at low frequency, is also an area that justifies further research. This could be achieved by extending the 3D FE model of the cone.

This thesis has illustrated the potential of using 3D finite element models to predict the resonant behaviour of non-axisymmetric loudspeaker cones. These techniques could be similarly applied to other non-axisymmetric (e.g. oval) loudspeaker designs.

A further potential area for research is in time-domain modelling of loudspeakers. In particular, modelling the impulse response of a slotted loudspeaker cone would yield extra insight into the flow of energy through the cone, along and around the slots, and into the surround. ANSYS has the capabilities to model the time-domain response of structures to time varying forces, and so could be used to perform this research, although this would require the damping properties of the cone material to be represented using a more precise technique than a constant damping ratio.

7.3 CONCLUSION

This thesis has successfully utilised 2D and 3D structural vibration FE models and 2D BE sound radiation models of loudspeaker cones as research tools for exploring the resonant behaviour of loudspeaker cones of different designs and materials. In particular, these models have been used to extensively explore and detail the manner in which cone resonance can be adjusted and controlled by varying the material properties and thickness profile of loudspeaker cones.

Furthermore, in a novel approach, 3D FE models have been used to simulate the behaviour of loudspeaker cones with narrow slots cut into them. This has allowed a slotted loudspeaker with a very desirable sound pressure response to be modelled and constructed. The measured characteristics of the slotted loudspeaker have been shown to agree favourably with those predicted by the FE model.

APPENDIX A - LIST OF SYMBOLS

δ	3D Dirac function
ε	Strain
λ_i	Eigenvector of ith mode.
ν	Poisson's ratio
ϕ	Displacement phase shift
ρ	Mass density
ρ_{air}	Density of air
σ	Stress
ω	Angular frequency
ξ	Damping ratio
$\mathbf{B}$	Strain-displacement matrix
$B\ell$	Electromechanical coupling factor
c	Speed of sound in air
$\mathbf{C}$	Viscous damping matrix
C_{spider}	Compliance of spider
C_{tot}	Total compliance of loudspeaker
$\mathbf{D}$	Elasticity matrix
E	Young's modulus
f	Frequency
f_0	Free-air resonant frequency
F_{ax}	Axial force
f_{bax}	Frequency of bending antiresonance x
f_{brx}	Frequency of bending resonance x
f_c	Cut-off frequency of voice coil
f_{la}	Frequency of longitudinal antiresonance
F_n	Vector of nodal forces
f_{ra}	Frequency of ring antiresonance
G	Green's function
I	Voice coil current
j	$\sqrt{-1}$
$\mathbf{K}$	Stiffness matrix
k	Wavenumber
L_{coil}	Inductance of voice coil
$\mathbf{M}$	Mass matrix
M_{coil}	Mass of voice coil
M_{tot}	Total moving mass of loudspeaker
n	Number of nodes
$\mathbf{N}$	Shape function matrix
p	Sound pressure
p_{ax}	On-axis sound pressure
Q	Quality factor
r	Distance from centre of plate, cone etc

R_{coil}	DC resistance of voice coil
R_{spider}	Mechanical resistance of spider
R_{tot}	Total mechanical resistance of loudspeaker
S	Surface area of sphere
t	Time
t_i	Cone thickness at inner edge
t_o	Cone thickness at outer edge
u	Displacement
v_{axial}	Axial velocity of voice coil
V	Applied voltage
V_{mot}	Voltage due to test loudspeaker's motional impedance
V_{ref}	Voltage across reference loudspeaker
V_{test}	Voltage across test loudspeaker
Y_{ax}	Axial admittance
$Y_{tot(mech)}$	Total mechanical admittance of loudspeaker
Z_{coil}	Electrical impedance of voice coil
$Z_{elec(ref)}$	Electrical impedance of reference loudspeaker
$Z_{elec(test)}$	Electrical impedance of test loudspeaker
Z_{mot}	Motional impedance of loudspeaker
$Z_{mot(test)}$	Motional impedance of test loudspeaker
Z_{ref}	Total electrical impedance of reference loudspeaker
Z_{tot}	Total electrical impedance of loudspeaker
$Z_{tot(mech)}$	Total mechanical impedance of loudspeaker

APPENDIX B– CIRCUIT DIAGRAMS

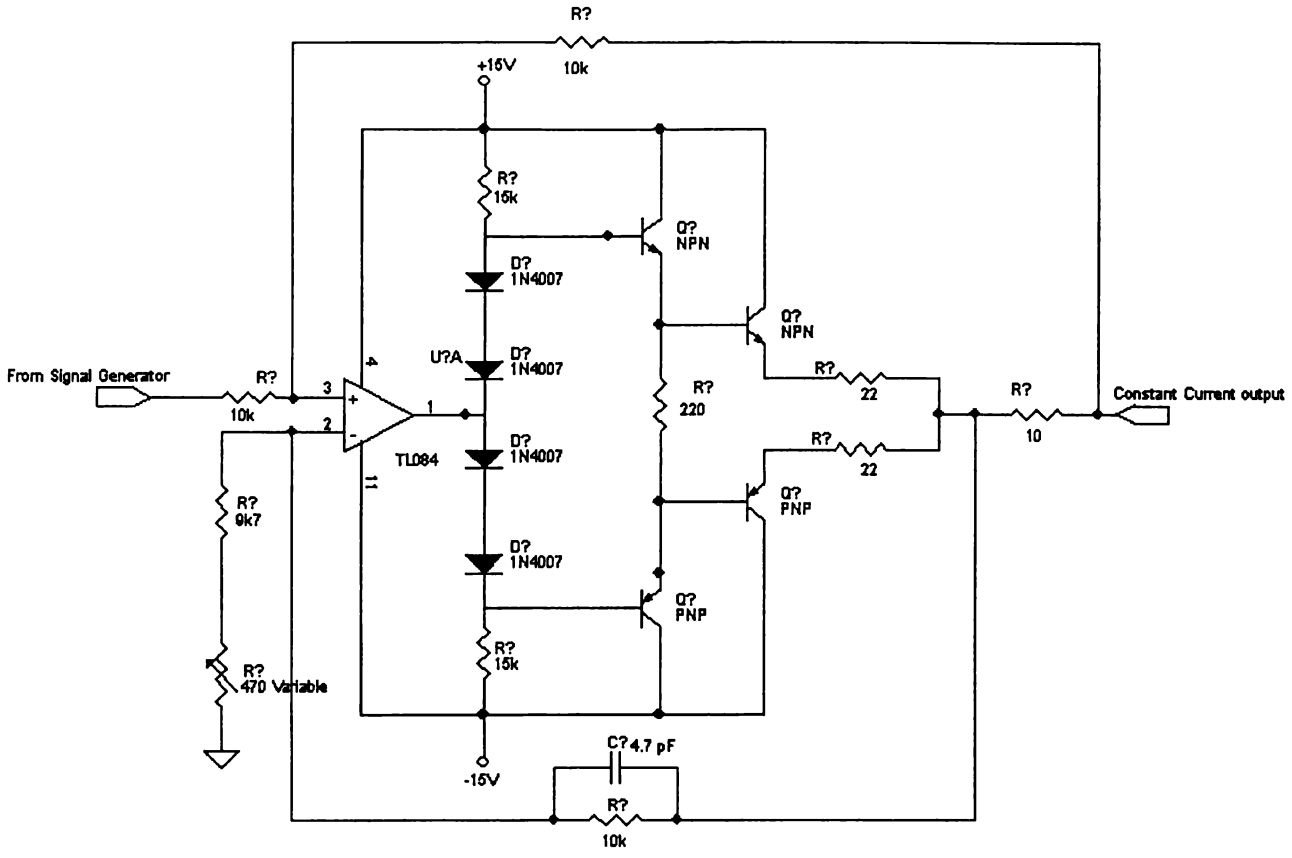

Figure B.1. Constant current amplifier circuit diagram

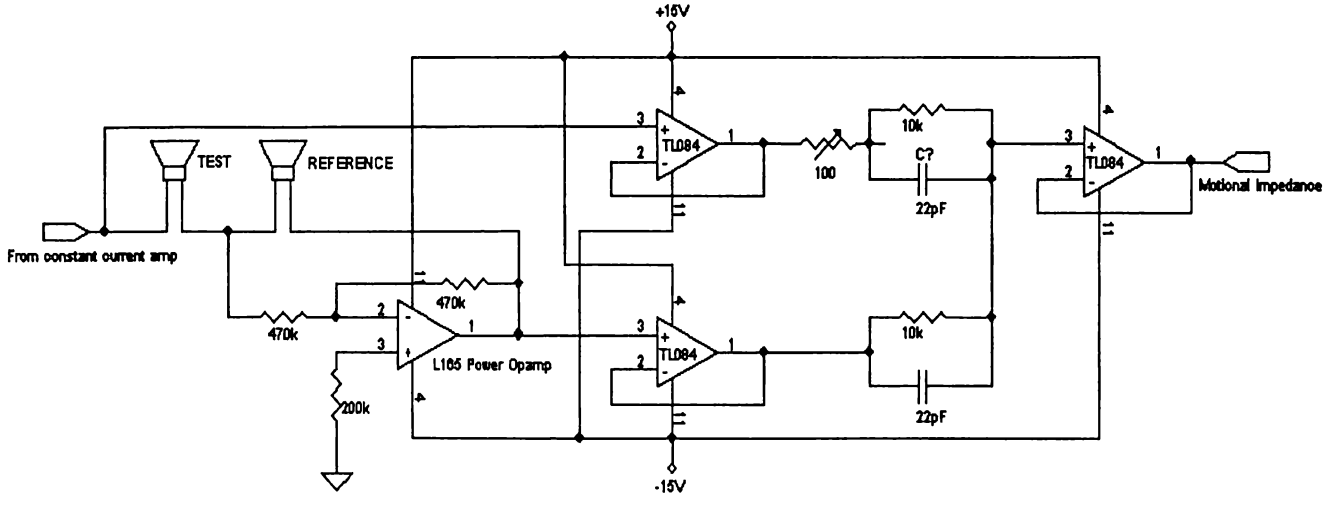

Figure B.2. Differential amplifier circuit diagram

REFERENCES

1. Rice, C.W., Kellog, E.W., "Notes on the development of a new type of hornless loudspeaker", reprinted *Journal of the Audio Engineering Society*, Vol. 30, No. 7/8, (July 1982).

2. Jordan, E.J., *Loudspeakers*, Focal Press, London, (1963).

3. Beranek, L., *Acoustics*, McGraw-Hill, New York (1954).

4. Goldberg, J.E., Bogdanoff, J.L., "On the calculation of the Axisymmetric Modes and Frequencies of Conical Shells," *Journal of the Acoustical Society of America*, Vol. 32, No. 6, p738, (June, 1960).

5. Kalnins, A., "Free Vibration of Rotationally Symmetric Shells," *Journal of the Acoustical Society of America*, Vol. 36, No.7, p1355, (July 1964).

6. Frankfort, F.J.M., "Vibration and Sound Radiation of Loudspeaker Cones", *Thesis*, Delft, (1975).

7. Frankfort, F.J.M., "Vibration Patterns and Radiation Behaviour of Loudspeaker Cones," *Journal of the Audio Engineering Society*, Vol. 26, pp. 609-622 (Sept 1978).

8. Bruneau, A.M., "Amplitude and Phase Measurements of Vibration of Radiating Surfaces in Order to Determine the Emitted Sound Field", *Journal of the Audio Engineering Society*, (December 1983).

9. Bruneau, A.M., Bruneau, M., "Electrodynamic Loudspeaker with Baffle," *Journal of the Audio Engineering Society*, Vol. 34, p. 970, (December 1986).

10. Shepherd, I.C., Alfredson, R.J., "An Improved Computer Model of Direct-Radiator Loudspeakers," *Journal of the Audio Engineering Society*, Vol. 33, p. 322, (May 1985).

11. Suzuki, K., Nomoto, I., "Computerized Analysis and Observation of the Vibration Modes of a Loudspeaker Cone," *Journal of the Audio Engineering Society*, Vol. 30, (1982).

12. Kagawa, Y., Yamabuchi, T., Sugihara, K., "A Finite Element Approach to a Coupled Structural-Acoustic Radiation System with Application to Loudspeaker Characteristic Calculation," *Journal of Sound and Vibration*, Vol. 69, No. 2, p. 229, (1980).

13. Kaiser, A.J.M, Leeuwestein, A., "Calculation of the Sound Radiation of a Nonrigid Loudspeaker Diaphragm Using the Finite Element Method," *Journal of the Audio Engineering Society*, Vol. 36, p. 539, (July/August 1988).

14. Kirkup, S. M., Jones, M.A., "Computational Methods for the Acoustic Modal Analysis of an Enclosed Fluid With Application to a Loudspeaker Cabinet",

Applied Acoustics, Vol. 48, No. 4, p. 275, (1996).

15. Yamamoto, T., Tsukagoshi, T., Tohma, T, Kimura, M., Tanaka, F., "High-Fidelity Loudspeakers with Boronized Titanium Diaphragms," *Journal of the Audio Engineering Society*, (December 1980).

16. Tsukagoshi, T., Yokozeki, S., Hagiwara, S., Yosino, T., Arai, Y., Yamamoto, T., "Polymer-Graphite Composite Loudspeaker Diaphragm," *Journal of the Audio Engineering Society*, (October 1981).

17. Niguchi, H., Yamamoto, O., Ieki, M., Shimizu, T., Sakamoto, N., "Reinforced Olefin Polymer Diaphragm for Loudspeakers," *Journal of the Audio Engineering Society*, (November 1981).

18. Takahashi, S., Katoh, T., Taguchi, S., Watanabe, T., "Glass-Fiber and Graphite-Flake Reinforced Polyimide Composite Diaphragm for Loudspeakers," *Journal of the Audio Engineering Society*, (October 1983).

19. Sakamoto, N., Satoh, K. Satoh, K., Atoji, N., "Loudspeaker with Honeycomb Disk Diaphragm," *Journal of the Audio Engineering Society*, (October 1981).

20. Matsuda, A., Kishigami, J., Nishimura, M., "Peripherally Reinforced Laminated Loudspeaker Diaphragm," *United States Patent # 4198550*, Sony Corporation, Tokyo, (April 1980).

21. Nakazono, J., Shimada, K., Tsuchiya, Y., Furukawa, T., Matsumoto, Y., "Coaxial Flat-Plane Loudspeaker with Polymer-Graphite Honeycomb Sandwich Plate Diaphragm," *Journal of the Audio Engineering Society*, (November 1981).

22. Taguchi, S., Watanabe, T., Takahashi, E, Takahashi, S., Tanaka, S., "Sandwich-Construction Loudspeaker Diaphragm with Foamed High-Polymer and Carbon Fibre," *Journal of the Audio Engineering Society*, Vol. 34, p. 895, (November 1986).

23. Geaves, G.P., "The Simulation of Midrange Loudspeakers using Numerical Methods," *Proceedings of the IEE Audio Engineering Colloquim*, London, (May 1995).

24. Murata, K., Takayama, S., Takewa, H., Suiki, S. Tanaka, T., "Diaphragm for loudspeaker," *United States Patent #4803242*, Matsushita Electric Industrial Co., Osaka, (Feb 1989).

25. Colloms, M., *High Performance Loudspeakers*, Wiley, New York, (1991).

26. Eargle, J.M., *The Loudspeaker Handbook*, Chapman and Hall, New York, (1997).

27. Schreiher, W.P., "Loudspeaker Driver Surrounding," *United States Patent #5418337*, Bose Corporation, Framington Mass., (May 1995).

28. Shindo, T., Yashima, O., Suzuki, H., "Effect of Voice-Coil and Surround on

Vibration and Sound Pressure Response of Loudspeaker Cones," *Journal of the Audio Engineering Society*, (July/August 1980).

29. Heed, T., "Minimising the Amplitudes of Transverse Modal Waves in Diaphragms," presented at the 101st Convention of the Audio Engineering Society, *Journal of the Audio Engineering Society (Abstracts)*, preprint no 4333, (November 1996).

30. Geaves, G.P., "Design and Validation of a System for Selecting Optimised Midrange Loudspeaker Diaphragm Profiles," *Journal of the Audio Engineering Society*, Vol. 44, No. 3, p. 107, (March 1996).

31. Struck, C.J., "Investigation of the Non-Rigid Behaviour of a Loudspeaker Diaphragm using Modal Analysis," *Journal of the Audio Engineering Society*, Vol. 38, p. 667, (September 1990).

32. Geaves, G.P., "An Investigation using the Boundary-Element Method into the Acoustic Field Resulting From Concave Loudspeaker-Type Structures," *Acoustics Letters*, Vol.18, No. 6, (1994).

33 . Vanderkooy, J., "A Model of Loudspeaker Driver Impedance Incorporating Eddy Currents in the Pole Structure," *Journal of the Audio Engineering Society*, Vol. 37, No.3, (March 1989).

34 . Wright, J. R., "An Empirical Model for Loudspeaker Motor Impedance", *Journal of the Audio Engineering Society*, Vol. 40 (January/February 1992).

35. Small, R. "Closed-Box Loudspeaker Systems. Part I: Analysis", *Journal of the Audio Engineering Society*, Vol. 20, No. 10, (December 1972).

36. Small, R. "Closed-Box Loudspeaker Systems. Part II: Synthesis", *Journal of the Audio Engineering Society*, Vol. 21, No. 1, (January/February 1973).

37 Jones, M.A., Binks, L.A., Henwood, D.J., "Finite Element Methods Applied to the Analysis of High-Fidelity Loudspeaker Transducers", *Computers and Structures*, Vol. 44, No. 4, p. 765, (1992).

38. Desai, C.S, Abel, J.F., *Introduction to the Finite Element Method*, Van Nostrand Reinhold, New York, (1972)

39. Hinton, E., Owen, D.R.J., *Finite Element Programming*, Academic Press Inc, London, (1977)

40. Zienkiewicz, *The Finite Element Method*, McGraw Hill, New York, (1977).

41. "ANSYS Users Manual Volume 4 – Theory", *Swanson Analysis Systems Inc.*, Houston, (1994).

42. "SYSNOISE Theoretical Manual Revision 5.1", *Numerical Integration Technologies,* N.V., Leuven, (1993).

43. Dobrucki, A., "Nontypical effects in an Electrodynamic Loudspeaker with a

Nonhomogeneous Magnetic Field in the Air Gap and Nonlinear Suspensions", *Journal of the Audio Engineering Society*, Vol.42, No. 7/8, (July/August 1994).